Modelling of Ar-CO_2 Thermal Plasma

By

THOMAS GORDON BEUTHE, B. Eng., M. Eng.

A Thesis
Submitted to the School of Graduate Studies
in Partial Fulfilment of the Requirements
for the Degree
Doctor of Philosophy

McMaster University

Modelling of Ar-CO_2 Thermal Plasma

DOCTOR OF PHILOSOPHY (1992) MCMASTER UNIVERSITY
(Engineering Physics) Hamilton, Ontario

TITLE: Modelling of Ar-CO_2 Thermal Plasma

AUTHOR: Thomas Gordon Beuthe, B. Eng., M. Eng.

SUPERVISOR: Dr. J.S. Chang

NUMBER OF PAGES: xxii, 300

Summary

A chemical kinetic model has been constructed to predict the pressure and gas and electron temperature dependency of the neutral and ionic species composition in Ar-CO_2 mixtures under thermal plasma conditions. Pure Ar and Ar-C models have also been constructed as a part of this investigation. The models include electron impact, thermal impact, ion-molecule, and recombination reactions as well as accounting for diffusion. Important metastable and excited states of species have been accounted for as well as the presence of neutral molecules, radicals, and atoms, positive and negatively charged atoms and molecular ions as well as electrons. All relevant electron temperature, gas temperature and pressure terms have been included, and primarily experimentally derived reaction rate constants were utilized.

Electron and gas temperature dependent species concentrations were obtained under both thermodynamic equilibrium and non-equilibrium conditions for gas temperatures from 300 to 15000 K, electron temperatures from 300 to 20000 K, and pressures from 1 Torr to 15200 Torr. Percentage mixtures of C and CO_2 in Ar were varied between 0.1 and 40%.

Results indicate that the neutral and excited species Ar, Ar^*, Ar^{**}, C, CO, CO_2, O, O_2 and O_3, positive ions Ar^+, Ar_2^+, C^+, $CArO^+$, CO^+, CO_2^+, CO_4^+, $C_2O_2^+$, O^+, O_2^+, C_4^+, and O_5^+ and negative ions CO_3^-, CO_4^-, O^-, O_2^-, and O_3^- and electrons are observed. Under thermodynamic equilibrium conditions, Ar, C, CO, CO_2, and O were found to be the dominant neutral species, C^+, CO_4^+, O^+, and O_2^+ the dominant positive ions, and O^- and electrons the dominant negatively charged species under certain gas temperature ranges.

The introduction of thermodynamic non-equilibrium conditions, changes in

gas pressure, and percentage mixture of C or CO_2 were observed to have a significant influence on the temperature dependent concentrations of these species.

The results were found to be in good agreement with previous experimental and theoretical results. Comparison of the present results with the results of the Saha equation seem to indicate that the simple Saha equation type approach may mispredict the plasma density of Ar, Ar-C, and Ar-CO_2 mixtures under thermal plasma conditions.

Acknowledgements

I would like to take this opportunity to express my sincere gratitude to Dr. Jen-Shih Chang for his supervision of this thesis. His broad overview of the subject, indefatigable willingness to lend a sympathetic ear, provide a push in the right direction and his rapid feedback proved invaluable.

Thanks are also due to the other members of my committee, Dr. Frank Chu, Dr. Gordon Irons, and Dr. W. Lu for their help and guidance.

My thanks to all of the researchers at the Musashi Institute of Technology in Tokyo including Prof. Teii, Prof. Matsumura, Dr. Ono, and all of the students of the Musashi group including Tsuruta-san and Miyamoto-san.

To all of the researchers in Dr. Chang's group whom I have had the pleasure of working with over the years, including Prof. Chang from Kunming, Prof. Wang from Beijing, and others too numerous to mention, I would like to express my gratitude for making these years an interesting, and enjoyable experience.

Finally, as always, my sincerest thanks are due to Sabine and Tatjana for their help and understanding, and just for being there.

Hab nun, ach, die Philosophei
Medizin und Juristerei
Und leider auch die Theologie
Durchaus studiert mit heißer Müh.
Da steh ich nun, ich armer Tor,
Und bin so klug als wie zuvor.
Heiße Doktor und Professor gar
Und ziehe schon an die zehen Jahr
Herauf, herab und quer und krumm
Meine Schüler an der Nas herum
Und seh daß wir nichts wissen können;
Das will mir schier das Herz verbrennen.

Der Urfaust
J. W. v. Goethe

Contents

Summary iii

Acknowledgements v

Table of Contents vii

List of Figures x

List of Tables xix

List of Symbols xxi

1 Introduction 1

1.1 Introduction 1

1.2 Review of Previous Work 2

1.2.1 Previous Experimental Work 3

1.2.2 Previous Modelling Work 5

1.3 LTE Models for the Determination of Neutral and Ionic Species . . . 6

1.3.1 Saha Equation 6

1.3.2 LTE Models 8

1.4 Statement of Problem 10

2 Environment of Thermal Plasma 12

2.1 Arc Plasmas 12

2.2 Plasma Jets 13

2.3 Flame Plasmas 17
2.4 Glow Discharges 25
2.5 Spark Discharges 27
2.6 Shock Wave Plasmas 30
2.7 Summary 30

3 Basic Equations and Numerical Procedures **35**
3.1 Basic Equations 35
3.2 Chemical Reactions 38
3.2.1 Neutral Reactions 39
3.2.2 Ionic Reactions 39
3.3 Numerical Procedures 42

4 Numerical Model of Ar Thermal Plasma **49**
4.1 Ar Thermal Plasmas 49
4.2 Chemical Reactions 51
4.3 Numerical Results 58
4.3.1 Gas Temperature Effects 58
4.3.2 Electron Temperature Effects 60
4.3.3 Gas Pressure Effects 62
4.4 Comparison with Previous Models 74
4.5 Comparison with Previous Experimental Results 78
4.6 Summary of Ar Thermal Plasmas 78

5 Numerical Model of Ar-C Thermal Plasma **81**
5.1 Ar-Atom Thermal Plasmas 81
5.2 Chemistry of Ar-C Mixture Plasmas 82
5.3 Numerical Results 87
5.3.1 Gas Temperature Effects 87
5.3.2 Electron Temperature Effects 89
5.3.3 Gas Pressure Effects 93
5.3.4 Carbon Percentage Mixture Effects 104

5.4 Comparison with Experimental Results 106
5.5 Summary of Ar-C Thermal Plasmas 106

6 Numerical Model of Ar-CO_2 Thermal Plasma **110**
6.1 Ar-Molecule Mixture Plasmas 110
6.2 Chemistry of Ar-CO_2 Mixture Plasmas 112
6.3 Numerical Results 136
6.3.1 Gas Temperature Effects 136
6.3.2 Electron Temperature Effects 147
6.3.3 Gas Pressure Effects 152
6.3.4 CO_2 Percentage Mixture Effects 167
6.4 Comparison with Previous Results 176
6.4.1 Previous Numerical Results 176
6.4.2 Previous Experimental Results 185
6.5 Summary of Ar-CO_2 Thermal Plasmas 188

7 Conclusion **190**

8 Recommendations for Future Work **194**

References **195**

Appendices **212**

A Ar-CO_2 Thermal Plasma Species Sources and Sinks **213**

B Rate Equations for Ar-CO_2 Thermal Plasma **241**

C Collision Cross Sections **247**

D Program Source Codes **258**
D.1 Ar Thermal Plasma 258
D.2 Ar-C Thermal Plasma 268
D.3 Common Subroutines 281

List of Figures

2.1 Calculated and measured isotherms of a free-burning argon arc (I = 200 A, p = 760 Torr)[47]. 14
2.2 Schematic diagram of (a) DC[48] and (b), (c) RF plasma torches[49]. 16
2.3 Spectroscopically measured radial temperature profiles downstream of the exit of a DC plasma torch[50]. 18
2.4 Axial temperature profiles downstream of the exit of a DC plasma torch as measured by an array of thermocouples by Beuthe et al.[5]. . 19
2.5 Radial temperature profiles downstream of the exit of a DC plasma torch as measured by an array of thermocouples in conjunction with an infrared thermal image processing system by Beuthe et al.[5] (plasma gas: argon, diam.: 25.4 mm, p = 760 Torr, power = 30 kW, plasma gas flow rate = 3.9 g/sec). 20
2.6 Temperature measured at the geometric centre of a plasma torch exit, 38 mm from the front face of the plasma torch for various different plasma gas flow patterns and flow rates as measured by Beuthe et al.[51]. 21
2.7 Temperature map in the exit jet of an induction plasma at different total plasma gas flow rates (gas: argon, diam.: 14 mm, f = 17 MHz, p = 760 Torr, power = 6 to 8 kW.[52]. 22
2.8 Downstream plasma jet electron temperatures for various system pressures (plasma gas: argon, flow rate: 5 l/min)[53][54]. 23
2.9 Downstream plasma jet electron densities for various system pressures (plasma gas: argon, flow rate: 5 l/min)[53][54]. 24

2.10 (a) Electrical conductivity and temperature in a hydrocarbon diffusion flame[55] (b) Ion density and temperature profile through a flame[56]. 26
2.11 Typical glow discharge. 1. Cathode sheath, 2. Crooks or cathode dark space, 3. Negative glow, 4. Faraday dark space, 5. Positive column, 6. Anode sheath[49]. 28
2.12 Typical spark discharge.[60]. 29
2.13 Conventional shock tube and pressure profiles at various time intervals[57]. 31
2.14 Range of electron and gas temperatures occurring in thermal plasmas. 33
2.15 Range of electron densities as a function of electron temperatures occurring in thermal plasmas. 34
3.1 Typical collision cross section σ and Maxwellian energy distribution $f(E)$ of particles in a thermal plasma. 47
3.2 Schematic of the calculation scheme used to solve the chemical kinetic model. 48
4.1 Temperature dependence of the values of the reaction rate constants for the chemical kinetic argon thermal plasma model. 56
4.2 Plasma chemistry for an Ar discharge including molecular ions, and thermal and electron impact reactions. 57
4.3 Ionized and neutral species concentrations as a function of gas temperature for argon with p = 760 Torr, and $T_e = T_g$. 61
4.4 Ionized and neutral species concentrations as a function of electron temperature for argon with T_g = 300 K, and p = 760 Torr. 63
4.5 Ionized and neutral species concentrations as a function of electron temperature for argon with T_g = 5000 K, and p = 760 Torr. 64
4.6 Ionized and neutral species concentrations as a function of electron temperature for argon with T_g = 300 K, and p = 10 Torr. 66
4.7 Ionized and neutral species concentrations as a function of electron temperature for argon with T_g = 5000 K, and p = 10 Torr. 67
4.8 Ionized and neutral species concentrations as a function of gas temperature for argon with p = 100 Torr, and $T_e = T_g$. 69

4.9 Ionized and neutral species concentrations as a function of gas temperature for argon with p = 10 Torr, and $T_e = T_g$. 70
4.10 Ionized and neutral species concentrations as a function of gas temperature for argon with p = 15200 Torr, and $T_e = T_g$. 72
4.11 Summary of the effect of changing pressure on the temperature dependent concentrations of Ar and e for a pure argon plasma. 73
4.12 Summary of the effect of changing pressure on the degree of ionization for a pure argon plasma. 75
4.13 Ionized and neutral species concentrations as a function of electron temperature. Comparison of the present results with those of Braun and Kunc[90][91]. 77
4.14 Comparison of the experimental and numerical results of Chang et al.[112] and the present chemical kinetic model. 79
5.1 Temperature dependence of the values of the reaction rate constants for the chemical kinetic Ar-C thermal plasma model. 84
5.2 Plasma chemistry for an Ar-C discharge including molecular ions, and thermal and electron impact reactions. 86
5.3 Ionized and neutral species concentrations as a function of gas temperature for an argon-1% carbon mixture with p = 760 Torr, and $T_e = T_g$. 90
5.4 Ionized and neutral species concentrations as a function of electron temperature for an argon-1% carbon mixture with T_g = 300 K, and p = 760 Torr. 91
5.5 Ionized and neutral species concentrations as a function of electron temperature for an argon-1% carbon mixture with T_g = 5000 K, and p = 760 Torr. 94
5.6 Ionized and neutral species concentrations as a function of electron temperature for an argon-1% carbon mixture with T_g = 300 K, and p = 10 Torr. 96
5.7 Ionized and neutral species concentrations as a function of electron temperature for an argon-1% carbon mixture with T_g = 5000 K, and p = 10 Torr. 97

5.8 Ionized and neutral species concentrations as a function of gas temperature for an argon-1% carbon mixture with p = 100 Torr and $T_e = T_g$. 98
5.9 Ionized and neutral species concentrations as a function of gas temperature for an argon-1% carbon mixture with p = 10 Torr, and $T_e = T_g$. 99
5.10 Ionized and neutral species concentrations as a function of gas temperature for an argon-1% carbon mixture with p = 15200 Torr, and $T_e = T_g$. 101
5.11 Summary of the effect of changing pressure on the temperature dependent concentrations of Ar, C, and e for an Ar-1%C mixture plasma. . 102
5.12 Summary of the effect of changing pressure on the degree of ionization for an Ar-1%C mixture plasma. 103
5.13 Ionized and neutral species concentrations as a function of gas temperature for an argon-10% carbon mixture with p = 760 Torr, and $T_e = T_g$. 105
5.14 Summary of the effect of changing percentage carbon on the temperature dependent concentrations of Ar, C, and e for an Ar-C mixture plasma. 107
5.15 Summary of the effect of changing percentage carbon on the degree of ionization for an Ar-C mixture plasma. 108
6.1 Neutral species chemistry for an Ar-CO_2 mixture gas. 123
6.2 Positive ion chemistry for an Ar-CO_2 mixture gas. 124
6.3 Negative ion chemistry for an Ar-CO_2 mixture gas. 125
6.4 Temperature dependence of the values of the reaction rate constants for important sources and sinks of all neutral species included in the chemical kinetic Ar-CO_2 thermal plasma model. 131
6.5 Temperature dependence of the values of the reaction rate constants for important sources and sinks of all positive ions included in the chemical kinetic Ar-CO_2 thermal plasma model. 132
6.6 Temperature dependence of the values of the reaction rate constants for important sources and sinks of all negative ions included in the chemical kinetic Ar-CO_2 thermal plasma model. 133

6.7 Neutral species concentrations as a function of gas temperature for an Ar-10%CO_2 mixture, with p = 760 Torr, and $T_e = T_g$. 138
6.8 Positive ion concentrations as a function of gas temperature for an Ar-10%CO_2 mixture, with p = 760 Torr, and $T_e = T_g$. 139
6.9 Negative ion concentrations as a function of gas temperature for an Ar-10%CO_2 mixture, with p = 760 Torr, and $T_e = T_g$. 140
6.10 Neutral species concentrations as a function of electron temperature for an Ar-10%CO_2 mixture with p = 760 Torr and T_g = 6000 K. . . . 148
6.11 Positive species concentrations as a function of electron temperature for an Ar-10%CO_2 mixture with p = 760 Torr, and T_g = 6000 K. . . 149
6.12 Negative species concentrations as a function of electron temperature for an Ar-10%CO_2 mixture with p = 760 Torr, and T_g = 6000 K. . . 150
6.13 Neutral species concentrations as a function of gas temperature for an Ar-10%CO_2 mixture with p = 100 Torr and $T_e = T_g$. 154
6.14 Positive ion concentrations as a function of gas temperature for an Ar-10%CO_2 mixture with p = 100 Torr and $T_e = T_g$. 155
6.15 Negative ion concentrations as a function of gas temperature for an Ar-10%CO_2 mixture with p = 100 Torr and $T_e = T_g$. 156
6.16 Neutral species concentrations as a function of gas temperature for an Ar-10%CO_2 mixture with p = 10 Torr, and $T_e = T_g$. 158
6.17 Positive ion concentrations as a function of gas temperature for an Ar-10%CO_2 mixture with p = 10 Torr, and $T_e = T_g$. 159
6.18 Negative ion concentrations as a function of gas temperature for an Ar-10%CO_2 mixture, with p = 10 Torr, and $T_e = T_g$. 160
6.19 Neutral species concentrations as a function of gas temperature for an Ar-10%CO_2 mixture with p = 15200 Torr, and $T_e = T_g$. 163
6.20 Positive ion concentrations as a function of gas temperature for an Ar-10%CO_2 mixture with p = 15200 Torr, and $T_e = T_g$. 164
6.21 Negative ion concentrations as a function of gas temperature for an Ar-10%CO_2 mixture with p = 15200 Torr, and $T_e = T_g$. 165

6.22 Summary of the effect of changing pressure on the temperature dependent concentrations of CO_2, CO, C, O, and electrons for an Ar-10%CO_2 mixture plasma. 166
6.23 Summary of the effect of changing pressure on the degree of ionization for an Ar-10%CO_2 mixture plasma. 168
6.24 Neutral species concentrations as a function of gas temperature for an Ar-1%CO_2 mixture with p = 760 Torr, and $T_e = T_g$. 169
6.25 Positive ion concentrations as a function of gas temperature for an Ar-1%CO_2 mixture with p = 760 Torr, and $T_e = T_g$. 170
6.26 Negative ion concentrations as a function of gas temperature for an Ar-1%CO_2 mixture with p = 760 Torr, and $T_e = T_g$. 171
6.27 Summary of the effect of changing percentage CO_2 on the temperature dependent concentrations of CO_2, CO, C, O, and electrons for an Ar-10%CO_2 mixture plasma. 177
6.28 Summary of the effect of changing percentage CO_2 on the degree of ionization for an Ar-10%CO_2 mixture plasma. 178
6.29 Comparison of the energy minimization model by Nishimura and Takenouchi[13] with the Ar-CO_2 chemical kinetic model. 180
6.30 Comparison of the local thermodynamic equilibrium model by Lapicque et al.[21] with the Ar-CO_2 chemical kinetic model. 181
6.31 Comparison of the local thermodynamic equilibrium model by Huczko[20] with the Ar-CO_2 chemical kinetic model. 183
6.32 Comparison of the local thermodynamic equilibrium model by Kapoun et al.[24] with the Ar-CO_2 chemical kinetic model. 184
6.33 Comparison of the experimental results of Honda et al.[18] and Huczko[20] with the Ar-CO_2 chemical kinetic model. 186
6.34 Comparison of the experimental results of Nishimura and Takenouchi[13] with the Ar-CO_2 chemical kinetic model. 187
A.1 Sources and sinks of Ar included in the chemical kinetic Ar-CO_2 thermal plasma model. 214

A.2 Sources and sinks of Ar^* included in the chemical kinetic Ar-CO_2 thermal plasma model. 215
A.3 Sources and sinks of Ar^{**} included in the chemical kinetic Ar-CO_2 thermal plasma model. 216
A.4 Sources and sinks of C included in the chemical kinetic Ar-CO_2 thermal plasma model. 217
A.5 Sources and sinks of CO included in the chemical kinetic Ar-CO_2 thermal plasma model. 218
A.6 Sources and sinks of CO_2 included in the chemical kinetic Ar-CO_2 thermal plasma model. 219
A.7 Sources and sinks of O included in the chemical kinetic Ar-CO_2 thermal plasma model. 220
A.8 Sources and sinks of O_2 included in the chemical kinetic Ar-CO_2 thermal plasma model. 221
A.9 Sources and sinks of O_3 included in the chemical kinetic Ar-CO_2 thermal plasma model. 222
A.10 Sources and sinks of Ar^+ included in the chemical kinetic Ar-CO_2 thermal plasma model. 223
A.11 Sources and sinks of Ar_2^+ included in the chemical kinetic Ar-CO_2 thermal plasma model. 224
A.12 Sources and sinks of C^+ included in the chemical kinetic Ar-CO_2 thermal plasma model. 225
A.13 Sources and sinks of $CArO^+$ included in the chemical kinetic Ar-CO_2 thermal plasma model. 226
A.14 Sources and sinks of CO^+ included in the chemical kinetic Ar-CO_2 thermal plasma model. 227
A.15 Sources and sinks of CO_2^+ included in the chemical kinetic Ar-CO_2 thermal plasma model. 228
A.16 Sources and sinks of CO_4^+ included in the chemical kinetic Ar-CO_2 thermal plasma model. 229

A.17 Sources and sinks of $C_2O_2^+$ included in the chemical kinetic Ar-CO_2 thermal plasma model. 230
A.18 Sources and sinks of O^+ included in the chemical kinetic Ar-CO_2 thermal plasma model. 231
A.19 Sources and sinks of O_2^+ included in the chemical kinetic Ar-CO_2 thermal plasma model. 232
A.20 Sources and sinks of O_4^+ included in the chemical kinetic Ar-CO_2 thermal plasma model. 233
A.21 Sources and sinks of O_5^+ included in the chemical kinetic Ar-CO_2 thermal plasma model. 234
A.22 Sources and sinks of CO_3^- included in the chemical kinetic Ar-CO_2 thermal plasma model. 235
A.23 Sources and sinks of CO_4^- included in the chemical kinetic Ar-CO_2 thermal plasma model. 236
A.24 Sources and sinks of electrons e included in the chemical kinetic Ar-CO_2 thermal plasma model. 237
A.25 Sources and sinks of O^- included in the chemical kinetic Ar-CO_2 thermal plasma model. 238
A.26 Sources and sinks of O_2^- included in the chemical kinetic Ar-CO_2 thermal plasma model. 239
A.27 Sources and sinks of O_3^- included in the chemical kinetic Ar-CO_2 thermal plasma model. 240
C.1 Collision cross-section for the Ar + e $\xrightarrow{k_{Ar3}}$ Ar^+ + e + e reaction[95]. . 249
C.2 Collision cross-section for the Ar + e $\xrightarrow{k_{Ar4}}$ Ar^{**} + e reaction[96]. . . . 250
C.3 Collision cross-section for the Ar^{**} + e $\xrightarrow{k_{Ar5}}$ Ar^+ + e + e reaction[97]. 251
C.4 Collision cross-section for the C + e $\xrightarrow{k_{C2}}$ C^+ + e + e reaction[95]. . . 252
C.5 Collision cross-section for the CO + e $\xrightarrow{k_{11}}$ Products reaction[132]. . . 253
C.6 Collision cross-section for the CO_2 + e $\xrightarrow{k_{12}}$ Products reaction[132]. . 254
C.7 Collision cross-section for the O + e $\xrightarrow{k_{14}}$ O^+ + e + e reaction[132]. . 255
C.8 Collision cross-section for the O_2 + e $\xrightarrow{k_{15}}$ Products reaction[132]. . . 256

C.9 Collision cross-section for the $O_3 + e \xrightarrow{k_{16,1}} O_2^+ + O + e + e$ and $O_3 + e \xrightarrow{k_{16,2}} O^+ + O^- + O + e + e$ reactions[136]. 257

List of Tables

1.1 Previous studies of the behaviour of Ar-CO_2 mixtures under thermal plasma conditions. 4
4.1 Reactions for the argon system. 52
4.2 Diffusion constants for the argon system at 1 Torr, 300 K. 53
5.1 Reactions for the argon-carbon system. 85
5.2 Diffusion constants for the argon-carbon system at 1 Torr, 300 K. . . 85
6.1 Ionization reactions for the Ar-CO_2 system. 113
6.2 Attachment reactions for the Ar-CO_2 system. 114
6.3 Dissociation reactions for the Ar-CO_2 system. 114
6.4 Recombination reactions for the Ar-CO_2 system. 115
6.5 Ion-molecule reactions for the Ar-CO_2 system (positive ions). 116
6.6 Ion-molecule reactions for the Ar-CO_2 system continued (negative ions). 117
6.7 Neutral reactions for the Ar-CO_2 system. 118
6.8 Important sources and sinks of all neutral species included in the chemical kinetic Ar-CO_2 thermal plasma model. 120
6.9 Important sources and sinks of all positive ions included in the chemical kinetic Ar-CO_2 thermal plasma model. 121
6.10 Important sources and sinks of all negative ions included in the chemical kinetic Ar-CO_2 thermal plasma model. 122
6.11 Diffusion constants for the Ar-CO_2 system at 1 Torr, 300 K. 126
6.12 Summary of the values of the reaction rate constants for important sources and sinks of all neutral species included in the chemical kinetic Ar-CO_2 thermal plasma model. 128

6.13 Summary of the values of the reaction rate constants for important sources and sinks of all positive ions included in the chemical kinetic Ar-CO_2 thermal plasma model. 129
6.14 Summary of the values of the reaction rate constants for important sources and sinks of all negative ions included in the chemical kinetic Ar-CO_2 thermal plasma model. 130
6.15 Temperature ranges in the Ar-10%CO_2 model, p = 760 Torr, $T_e = T_g$. 137
6.16 Dominant positive ions in the Ar-10%CO_2 model, $T_e = T_g$, p = 760 Torr. 142
6.17 Temperature ranges in the Ar-10%CO_2 model, p = 100 Torr, $T_e = T_g$. 153
6.18 Dominant positive ions in the Ar-10%CO_2 model, $T_e = T_g$, p = 100 Torr. 153
6.19 Temperature ranges in the Ar-10%CO_2 model, p = 10 Torr, $T_e = T_g$. 157
6.20 Dominant positive ions in the Ar-10%CO_2 model, $T_e = T_g$, p = 10 Torr. 157
6.21 Temperature ranges in the Ar-10%CO_2 model, p = 15200 Torr, $T_e = T_g$. 161
6.22 Dominant positive ions in the Ar-10%CO_2 model, $T_e = T_g$, p = 15200 Torr. 161
6.23 Temperature ranges in the Ar-1%CO_2 model, p = 760 Torr, $T_e = T_g$. 172
6.24 Dominant positive ions in the Ar-1%CO_2 model, $T_e = T_g$, p = 760 Torr. 173

List of Symbols

Roman

a = polynomial coefficient

B = fractional proportion

C = linear slope of the collision cross section in the threshold region

D = diffusion coefficient

E = applied electric field

E_i = first ionization energy

$f(\ )$ = function

G = thermophoresis coefficient

h = Planck's constant

$h\nu$ = photon energy

J = particle flux density

k = Boltzmann constant, or reaction rate constant

m = mass

N = density of gas/ions/electrons

p = pressure

q = constant = $\sqrt{2.405}$

Q = partition function

R = universal gas constant, radius

T = temperature

U = partition function

x = mole fraction

A, B, C, D, E, F, G = reacting species or products
M = third body or collision partner

Greek

α = degree of ionization
μ = mobility
π = pi (= 3.1415...)
ν_s, ν_{si} = stoichiometric coefficients

Subscripts

a = atoms
c = charged particles
$coll$ = collision
e = electrons
i = ions
int = internal
IG = ideal gas
$spin$ = spin
th = threshold
TOT= total
tr = translational
i, j, l, m, s = running variables

Superscripts

+ = positive ion
- = negative ion
* = excited species
** = metastable species

Chapter 1

Introduction

1.1 Introduction

Carbon dioxide is one of the most abundant chemicals found in nature[1]. Mixed with argon, its behaviour at elevated temperatures represents a topic of interest in the chemical, metallurgical and welding industries.

In welding or cutting, Ar and Ar-CO_2 mixtures are commonly used as shielding gases to displace air from the arc region. In this case, the Ar-CO_2 mixtures are directly exposed to the arc itself, and fundamentally affect the stability of the arc, its electrical characteristics, and its temperature. The choice of shielding gas mixture also affects the efficiency of the overall process and the integrity of the weld which is produced through the complex chemical interaction of the gas mixture with the weld material under thermal plasma conditions[2]. This type of welding or cutting gas is normally used for the construction and decommissioning of nuclear power plants. Thus, the study of Ar and Ar-CO_2 mixtures under thermal plasma conditions represents a subject of fundamental interest and importance to welding technology.

In the metallurgical industry, carbon monoxide is used as a reducing gas to convert iron ore into iron. Here, the production of carbon monoxide from carbon dioxide via high temperature thermal plasma processes represents a topic of interest. Sharpened environmental regulations, the rising cost of fossil fuels relative to the cost of electricity, and aging in-place coke ovens have created a favourable climate for

the investigation of the use of thermal plasmas for the production of carbon monoxide from carbon dioxide[3]. In blast furnaces, both CO and H_2 represent important gases in the production of iron from iron ore[4]. Beuthe et al.[5][6] have investigated the simultaneous production of CO and H_2 via coal and steam injection into a thermal plasma environment. Such considerations could potentially help to decrease the dependence on coke, decrease environmental emissions, and increase the operating efficiency and stability of blast furnaces. Beuthe et al.[5][6] have also proposed to use this type of process for nuclear iron making using CANDU type nuclear power plants, since, unlike high temperature gas-cooled reactors, CANDU power plants generate up to 380 K steam. Hence, nuclear electricity in the form of a thermal plasma could be combined with nuclear steam and coal powder for this type of process.

In the chemical industry, many chemicals involve the use of carbon monoxide in the production process. Large quantities of carbon monoxide are used in the production of synthetic fuels[7], and in organic synthesis[8]. In some industrial manufacturing applications, the combination of long term contracts for the supply of carbon monoxide via pipeline and fluctuating demand for the products made from the carbon monoxide can produce unexpected increases in unit costs. In such cases, the use of Ar-CO_2 thermal plasmas for the production of carbon monoxide represents a potentially attractive process[9].

Under the conditions outlined in the above processes, CO_2 can be dissociated into simpler molecules and its atomic components. These components and the argon atoms in the mixture can be ionized to form a thermal plasma, a complex mixture of neutral and ionic species with both high gas and electron temperatures. An understanding of the fundamental physical and chemical processes taking place within such a thermal plasma is of importance to the investigation and development of these processes.

1.2 Review of Previous Work

The behaviour of carbon dioxide under thermal plasma conditions has stimulated an ongoing research interest. A summary of previous experimental studies and

models of Ar-CO_2 under thermal plasma conditions is shown in Table 1.1. The studies included for discussion have been restricted to those investigations which have examined the thermal and chemical behaviour of Ar-CO_2 mixtures under thermal plasma conditions generated via electrical discharges or in furnaces.

1.2.1 Previous Experimental Work

Experimental investigations have examined a number of different thermal plasma conditions experimentally including RF, microwave, and arc discharges. Blanchet et al.[10], Huczko and Szymański[17][19], Huczko[20], Honda et al.[18], Szymański and Huczko[22], Sekiguchi et al.[26], and Pustogarov et al.[27] have investigated the decomposition of Ar-CO_2 mixtures in thermal plasmas generated using non-transferred DC plasma torches operated at atmospheric pressure. Gas compositions from Ar-6.7%CO_2 to 100%CO_2 were passed through different nozzle and electrode geometries, and the product gases were examined for the presence of CO_2, CO and O_2. The plasma temperatures measured in these experiments ranged from 1000 to 11000 K, and fractional conversions of CO_2 between 3% and 80% have been achieved.

Lapicque et al.[21] have investigated the use of a furnace for the dissociation of CO_2 in an Ar-CO_2 mixture at atmospheric pressure. The results indicate that under the gas temperatures attainable in the furnace (1500–4000 K), between 2–6% of the CO_2 can be dissociated into products such as CO, O_2 and O.

Brown and Bell[11] have examined the used of capacitively coupled RF discharges, Nishimura et al.[13], Hirotsu[15], and Hayashi et al.[29] have examined the use of induction coupled RF discharges, Baiterekov et al.[23][25] and Chan and Venugopalan[28] have investigated the use of microwave discharges for the dissociation of CO_2. The pressures under which these investigations were carried out ranged from 0.03 Torr to atmospheric pressure, and the gas mixtures ranged from Ar-4.4%CO_2 to 100%CO_2. The measured plasma gas temperature ranged from T_g = 300–12000 K. Reported conversion efficiencies of CO_2 ranged from less than 1% to 70%. In all cases, only neutral end-products such as CO_2, CO, O_2, O, and C were measured.

It should be noted that none of the above experimental investigations have attempted to measure the electron temperature T_e, the electron concentration N_e,

Table 1.1: Previous studies of the behaviour of Ar-CO_2 mixtures under thermal plasma conditions.

Author	Discharge Plasma	Pressure	Plasma Gas
Blanchet et al. (1969) [10]	DC (Arc)	760 Torr	Ar-10%CO_2
Brown and Bell (1974) [11]	RF (13.56 MHz)	2–32 Torr	100%CO_2
Brown and Bell (1974) [12]	Model	2–32 Torr	100%CO_2
Nishimura and Takenouchi (1976) [13]	RF (4 MHz), Model	760 Torr	Ar-4.4%CO_2
Butylkin et al. (1977) [14]	Model	760 Torr	100%CO_2
Hirotsu (1981) [15]	RF (13.56 MHz)	0.03–0.1 Torr	100%CO_2
Lietzke and Mullins (1981) [16]	Model	10^{-5}–100 atm	100%CO_2
Huczko and Szymański (1982) [17]	DC (Arc), Model	760 Torr	Ar-18.5–65%CO_2
Honda et al. (1983) [18]	DC (Arc), Model	760 Torr	Ar-6.7%CO_2
Huczko and Szymański (1984) [19]	DC (Arc), Model	760 Torr	Ar-18.5–65%CO_2
Huczko (1984) [20]	DC (Arc), Model	760 Torr	Ar-18.5–65%CO_2
Lapicque et al. (1984) [21]	Furnace, Model	760 Torr	Ar-?%CO_2
Szymański and Huczko (1984) [22]	DC (Arc)	760 Torr	Ar-18.5–65%CO_2
Baiterekov et al. (1985) [23]	Microwave (2.4 GHz)	40–100 Torr	100%CO_2
Kapoun et al. (1985) [24]	Model	760 Torr	100%CO_2
Baiterekov et al. (1987) [25]	Microwave (2.4 GHz)	5–13 kPa	100%CO_2
Sekiguchi et al. (1987) [26]	DC (Arc), Model	760 Torr	Ar-50%CO_2
Pustogarov et al. (1988) [27]	DC (Arc)	150–400 kPa	100%CO_2
Chan and Venugopalan (1991) [28]	Microwave (2.4 GHz)	0.03–3 Torr	100%CO_2
Hayashi et al. (1992) [29]	RF (27.12 MHz)	0.52–5.1 Torr	Ar-5%CO_2

or the concentration of any positively or negatively charged ionized species. In most cases where DC arc plasmas or high pressure discharges were being used, tacit assumptions were made that the gas and electron temperatures were in an equilibrium state $T_e = T_g$.

1.2.2 Previous Modelling Work

Although many experimental studies have been carried out as shown in Table 1.1, the modelling efforts to predict the plasma parameters, ion and neutral species in Ar-CO_2 mixtures under thermal plasma conditions are not as well developed. The theory which accompanies investigations of thermal plasmas most often relies on local thermodynamic equilibrium (LTE) models. A discussion of the theoretical principles of LTE models will be undertaken in Section 1.3.2.

Lietzke et al.[16], Huczko and Szymański[17][19], Huczko[20], and Lapicque et al.[21] use simple energy minimization LTE models which consider only two or at most three chemical equilibria to predict the species composition of CO_2 over a temperature range of T_g = 100–6000 K. Species include CO_2, CO, O_2, O, and in some cases C. Nishimura and Takenouchi[13] use the same approach to investigate the temperature dependent concentrations of 8 species (CO_2, CO, O_2, O, C, C_2, C_3, and C_2O) over a wider temperature range (T_g = 2500–10000 K). Kapoun et al.[24] further extend this approach and consider 19 species, including positive and negative ions (CO_2, CO, O, O_2, C, C_2, C_3, C_4, C_5, O^+, O_2^+, C^+, C_2^+, CO^+, CO_2^+, O^-, O_2^-, C_2^-, e) over a temperature range of T_g = 3000–20000 K. The results concentrate primarily on neutral species concentrations and the concentration of C^+, O^+, and e.

Chemical kinetic approaches have been taken by Honda et al.[18] and Sekiguchi et al.[26]. Both of these efforts use a simplified LTE formalism however, considering only the presence of CO_2, CO, O_2, and O using 6 chemical equations (derived from the same three chemical equilibria of the LTE models as those used by Lietzke, Huczko, and Lapicque above) over a temperature range of T_g = 1000–4000 K. Brown and Bell[12] and Butylkin et al.[14] consider more complex chemical kinetic models (15 and 53 chemical reactions respectively), over temperature ranges of T_g = 400–1200 K and T_g = 2500–10000 K respectively. Brown and Bell consider the presence of CO_2,

CO, O_3, O_2, and O, and Butylkin et al. consider the presence of CO_2, CO, O_3, O_2, O, C, C_2, C_2O, C_2O_3, O^-, and e.

Maezono and Chang[30] modified the combustion gas model of Chang[31] to examine the possible chemical reaction channels which can occur in an Ar-CO_2 mixture under corona discharge conditions. These investigations suggest that ion-molecule reactions, recombination reactions, and electron impact dissociation and ionization reactions play an important role in the processes, but no thermal impact dissociation or ionization reactions were included since the gas temperature range considered was below 600 K. No numerical results were obtained, but efforts were made to identify the potential neutral and ionic species as well as major reaction channels which can occur. The results of this study tend to indicate that the dominant neutral species are O, C, CO, CO_2, O_3, C_2O. The dominant positive ions are Ar^+, Ar_2^+, O^+, O_2^+, O_5^+, C^+, CO^+, CO_2^+, CO_4^+, $C_2O_2^+$, and $CArO^+$, and the negative ions are O^-, O_2^-, O_3^-, O_4^-, C^-, CO_2^-, CO_3^-, and CO_4^-.

In summary, the previous efforts to model the behaviour of Ar-CO_2 mixtures at high temperatures have concentrated primarily on the use of LTE models to predict the neutral species concentrations. Some chemical kinetic models have been attempted, but these have also focused primarily on the concentration of neutral species. None of the models have considered the detailed reactions leading to the generation of ions. In particular, no consideration is given to thermal impact ionization, electron impact ionization, dissociative recombination and ion-molecule reactions, and the same formalism was used to calculate the temperature dependent species concentrations regardless of the concentration of Ar in the system.

1.3 LTE Models for the Determination of Neutral and Ionic Species

1.3.1 Saha Equation

The Saha equation represents the simplest and by far most widely used method to determine the concentration of ionized species in a thermal plasma. Developed

originally to explain the ionization in the solar chromosphere[32], the Saha equation assumes that the charged particles in a plasma are generated by a variety of processes, all of which can be conceived as elementary reactions of the following type:

$$Z \rightleftharpoons Z^+ + e \tag{1.1}$$

where Z is a neutral monatomic atom, Z^+ represents a singly ionized atom, and e an electron.

Assuming reaction 1.1 is reversible, and occurs in a system which is in perfect thermodynamic and chemical equilibrium, the Law of Mass Action can be derived from the principles of statistical mechanics in the following form[33][34]:

$$\frac{N_{Z^+} N_e}{N_Z} = \frac{Q_{Z^+} Q_e}{Q_Z} \exp(-E_i/kT) \tag{1.2}$$

where N_Z, N_{Z^+}, and N_e represent the density of atoms Z, ions Z^+ and electrons e respectively, Q_Z, Q_{Z^+}, and Q_e represent the partition functions of the neutral species Z, its first ionized state Z^+ and electrons e respectively, k is the Boltzmann constant, and T is the temperature.

The partition functions Q can be written

$$Q_e = Q_{e,tr} \prod_{int} Q_{e,int} \tag{1.3}$$

$$Q_{Z^+} = Q_{Z^+,tr} \prod_{int} Q_{Z^+,int} \tag{1.4}$$

$$Q_Z = Q_{Z,tr} \prod_{int} Q_{Z,int} \tag{1.5}$$

where the subscripts tr and int are used to denote the components of the partition functions which are due to the translational and internal energy of the species respectively.

The only possible internal energies which an electron can have are those associated with its spin. Since the spin of an electron can only exist in two possible quantum energy states, both of which lie in a single ground level degeneracy 2, the internal component of the partition function can be expressed as

$$\prod_{int} Q_{e,int} = Q_{e,spin} = 2 \tag{1.6}$$

The translational partition function of the electron can be expressed as

$$Q_{e,tr} = \left(\frac{2\pi m_e kT}{h^2}\right)^{3/2} \tag{1.7}$$

where m_e is the mass of the electron and h is Planck's constant.

Since the masses of the ion Z^+ and the neutral particle Z differ only by the, in comparison, relatively small mass of the electron m_e, it is possible to state that, to a good approximation $Q_{Z^+,tr} = Q_{Z,tr}$. Thus, the final form of the Saha equation can be written as follows[35]:

$$\frac{N_e N_i}{N_a} = 2\frac{U_i(T)}{U_a(T)}\frac{(2\pi m_e)^{\frac{3}{2}}(kT)^{\frac{3}{2}}}{h^3}\exp(-E_i/kT) \tag{1.8}$$

where N_e, N_i, and N_a are the density of electrons, ions, and atoms respectively, U_a and U_i represent the internal energy partition functions $Q_{Z,int}$ and $Q_{Z^+,int}$ respectively. Assuming quasi-neutrality in the generated plasma, $N_e \approx N_i$, equation 1.8 can be used to calculate the electron or atomic ion density in the plasma.

The Saha equation neglects to account for the detailed mechanisms within the plasma which lead to ionization however. The presence of long-lived metastable excited states, the possible existence of molecular ions, and the chemical reactions relating these species to the gaseous and ionized states of the plasma are not considered. Throughout the present investigation, the results predicted by the Saha equation will be used as a comparative reference.

1.3.2 LTE Models

A more sophisticated approach to the problem of calculating temperature dependent concentrations of the species which can occur within a thermal plasma involves the use of a Local Thermodynamic Equilibrium (LTE) model. As the name implies, this model assumes that the system is in both thermodynamic and chemical equilibrium. The object is to determine the equilibrium mole fractions x_i of n chemical species made up of m elemental constituents which occur in the fractional proportions B_j where

$$\sum_{j=1}^{n} B_j = 0 \tag{1.9}$$

The complete set of relations needed to describe the chemical equilibrium concentrations of all species within the system are as follows[36]:

1) one equation expressing Dalton's Law:

$$\sum_{i=1}^{n} x_i = 1 \tag{1.10}$$

2) $j = 1, 2, 3, \ldots, m-1$ mass balance relationships of the form:

$$\frac{b_j}{\sum_{l=1}^{m} b_l} = B_j \tag{1.11}$$

where

$$b_j = \sum_{i=1}^{n} a_{ij} x_i, \quad b_l = \sum_{i=1}^{n} a_{il} x_i \tag{1.12}$$

and a_{ij} represents the number of atoms of element j in species i, and a_{il} represents the number of atoms of element l in species i.

3) $s = 1, 2, 3, \ldots, n-m$ equations of the Law of Mass Action as derived from $n-m$ chemical equilibria:

$$\prod_{i=1}^{n} (x_i)^{\nu_{si}} = K_s(T) P^{-\nu_s} \tag{1.13}$$

where

$$\nu_s = \sum_{i=1}^{n} \nu_{si} \tag{1.14}$$

where ν_{si} represents the stoichiometric coefficient of species i in the s^{th} chemical equilibrium relationship, and $K_s(T)$ is the constant of chemical equilibrium for the s^{th} reaction. The temperature dependent chemical equilibrium constants $K_s(T)$ can be obtained directly from experimental results, or can be derived from thermochemical tables[37]. The solution of the n linear equations 1.10, 1.11, and 1.13 in n unknowns yields the concentration of the constituents x_i[38].

LTE models are relatively easy to calculate, and are therefore quite popular, however, this method has several significant disadvantages when used to model thermal plasmas. Thermal plasmas represent a complex mixture of neutral and ionized

species undergoing a large number of chemical reactions as will be outlined in Section 3.2. As mentioned above, LTE models tend to assume that the plasma under consideration can be described by a simplified set of $n - m$ chemical equilibria which tend to disregard the more complex interactions in the plasma. LTE models also explicitly assume that the plasma is in local thermodynamic equilibrium. It is well known however that the condition of local thermodynamic equilibrium is often not satisfied in thermal plasmas. Especially under reduced pressure conditions, the temperature of the electrons in the plasma is not equal to the temperature of the neutral and ionic species. Finally, it is not possible to include physical parameters such as diffusion or time dependent effects into LTE models, thus reducing their usefulness for comparison with experimental results.

1.4 Statement of Problem

In this study, an attempt is made to assemble a comprehensive chemical kinetic model which takes into account electronic, ionic and neutral processes which occur in Ar-CO_2 plasmas. The model will be built up by first examining a pure Ar plasma, then adding carbon to form an Ar-C model, and finally constructing an Ar-CO_2 model. The numerical model separates the gas temperature T_g from the electron temperature T_e to allow for non-local thermodynamic equilibrium conditions. In addition, the model accounts for ambipolar diffusion and all relevant pressure terms in an attempt to make the final form applicable over a wide a range of plasma conditions. Gas temperature ranges of T_g = 300–15000 K, electron temperature ranges of T_e = 300–20000 K, pressure ranges of 1 Torr to 15200 Torr and percentage mixtures of C and CO_2 between 0.1 and 40% will be examined.

Chapter 2 will outline the types of plasma environments which can be expected in thermal plasmas generated in arc plasmas, plasma jets, flame plasmas, glow discharges, spark discharges and shock waves.

Chapter 3 will outline in detail the basic equations, chemical reactions, and numerical procedures used to model thermal plasmas in the present study.

Chapters 4, 5, and 6 contain detailed chemical kinetic models for pure Ar,

Ar-C mixtures, and Ar-CO_2 mixtures respectively. Results are calculated under the assumption of steady state ($dn/dt = 0$) and thermodynamic equilibrium and non-equilibrium under constant pressure and constant volume assumptions. Results of the present model will be compared with those of previous investigators as well as the Saha equation.

Appendix A includes a full summary of the sources and sinks of all species considered in the Ar-CO_2 chemical kinetic thermal plasma model of Chapter 6.

Appendix B provides a summary of the coupled rate equations used in the Ar-CO_2 model of Chapter 6.

Appendix C illustrates all collision cross sections which were used to derive the reaction rate constants used in the Ar, Ar-C and Ar-CO_2 models of Chapters 4, 5, and 6 respectively.

Appendix D provides a listing of relevant FORTRAN programs which were used in this study.

Chapter 2

Environment of Thermal Plasma

Although relatively abundant in the universe, plasma, the ionized state of matter, is not often found on the earth's surface. It was only 113 years ago that William Crooks[39] first suggested the idea that the ionized state of gases should be considered a fourth state of matter. The term "plasma" was first used in the open literature by Langmuir in 1929[40] to describe the state of gases in discharge tubes. Since then, thermal plasmas have become increasingly important for various industrial applications since they are the source of highest continuously maintainable temperature. The object of this chapter is to provide a brief overview of the more common sources of thermal plasmas, and briefly outline the salient features of each. However, due to the scope of the present work, thermonuclear fusion plasmas, atmospheric plasmas and other low temperature plasmas will not be discussed here.

2.1 Arc Plasmas

Arc plasmas represent the first continuous source of high temperature thermal plasma known to man[41] and constitute by far the most important industrial source of high temperature thermal plasmas today. As the name implies, arc plasmas are generated in an electrical arc struck between two electrodes. It is generally agreed that the arc should be defined only in terms of its current and voltage drops. Arc currents typically extend from a lower limit in the order of 0.1 to 1 A to a very large

($\geq$ 10000 A) but unspecified upper limit. The voltage drop between the electrodes is typically in the range of a few volts to a few tens of volts. The applied voltage can be direct, alternating (typically 50–60 Hz), or transient[42].

The electrons emitted from the cathode region of the arc are accelerated toward the anode under the influence of the applied electric field. In the process, they transfer their kinetic energy through collisions with the intervening gaseous atoms and molecules. The arc plasma is formed primarily through electron impact ionizations and through thermal impact ionization reactions of the gaseous atoms and molecules with each other.

Although arcs can be struck at high pressures ($p \geq 7600$ Torr or 10 atm), low pressures ($p \leq 10$ Torr), or even under vacuum conditions ($p \leq 10^{-3}$ Torr), most practical applications utilize arcs operated under atmospheric or reduced pressure conditions (p = 10–760 Torr). In many cases, the arc plasma is assumed to be at close to local thermodynamic equilibrium conditions ($T_e = T_g$). Although there may be some validity to this assumption in the case of high pressure[43], or high current[44] arcs, recent studies seem to indicate that thermal arc plasmas are not in thermal equilibrium under reduced pressures and low currents[45] or even at atmospheric pressure conditions[46]. Typical temperature profiles observed in a free-burning arc[47] are shown in Figure 2.1. As can be seen from this figure, the hottest temperature occurs at the centre of the discharge, close to the cathode tip. The point-to-plane geometry shown in Figure 2.1 is typically used in welding applications and metallurgical furnaces and is referred to as a transferred arc since the anode is also the piece which is heated by the action of the arc. Gas and electron temperatures in a plasma arc can be as high as 25000 K and electron densities typically in the range of 10^{15}–10^{17} cm^{-3} as summarized in Figures 2.14 and 2.15.

2.2 Plasma Jets

A plasma jet is an extended arc plasma which is formed downstream of an electrical discharge by passing a steady stream of gas through the discharge. The discharge is typically confined in a cylindrical geometry to ensure that as much of

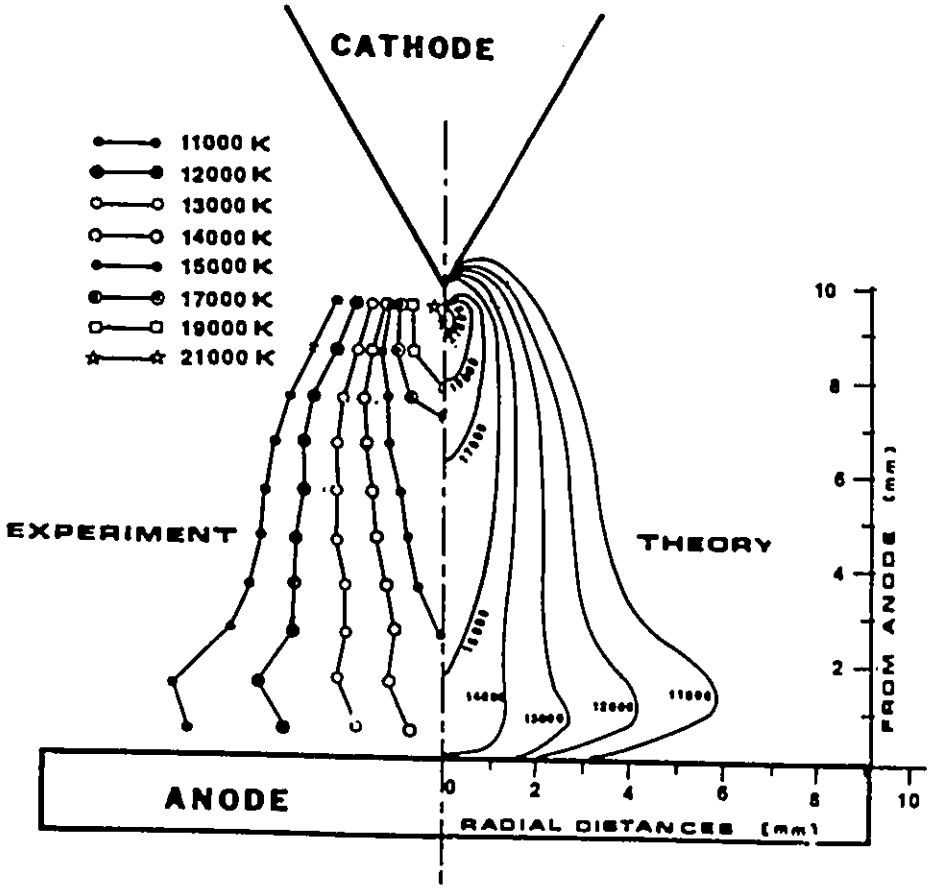

Figure 2.1: Calculated and measured isotherms of a free-burning argon arc (I = 200 A, p = 760 Torr)[47].

the gas passes through the discharge as possible. Devices which generate plasma jets are commonly referred to as plasma torches. Typical configurations of DC[48] and RF[49] plasma torches are shown in Figure 2.2.

In the case of the DC arc plasma torch (Figure 2.2a), the arc is struck between an anode and a cathode as described in Section 2.1. In this case however, both the cathode and the anode are water-cooled. The plasma jet formed downstream can be used for cutting or heating gases, solids or powders which do not form an integral part of the anode itself. For this reason, the arc which is struck inside of a DC plasma torch is referred to as a non-transferred arc.

In the RF plasma torch, a high voltage RF signal is applied to the torch electrodes which excites and ionizes the gas inside the tube. The electrodes can be arranged in such a way that either inductive (Figure 2.2b) or capacitive (Figure 2.2c) coupling takes place within the gas inside the tube. RF plasma torches have the advantage that the electrodes can be arranged in such a way that they are not physically in contact with the generated plasma as shown in Figures 2.2b, and 2.2c. Thus, no impurities can be introduced into the plasma from ablating electrode material. For this reason, RF discharges are often referred to as "electrodeless" discharges.

Unlike the arc, the plasma jet does not constitute a part of the current carrying component of the plasma. Typical temperatures and electron densities in such plasmas can be as high as those found in free-burning arcs due to the presence of the restricting walls and the expansion nozzles which are often used to additionally compress the thermal plasma jet prior to its emission from the plasma torch. Spectroscopically measured temperature profiles show that the temperature at the exit of the plasma torch is 7500 K, and drops to 6000 K at a distance of 2 cm from the exit of the torch as shown in Figure 2.3[50]. On emission from the plasma torch, the plasma jet temperature drops rapidly as the jet intermixes turbulently with the atmosphere. Figures 2.4, and 2.5 illustrate the rapidity with which the plasma quenches and spreads out in the axial and radial direction respectively as measured by Beuthe et al.[5] using an array of thermocouples and an infrared thermal image processing system. As shown, only 20 cm from the exit of the plasma torch, the temperature drops to less than 700 K. The variables Z and R refer to the axial distance from the

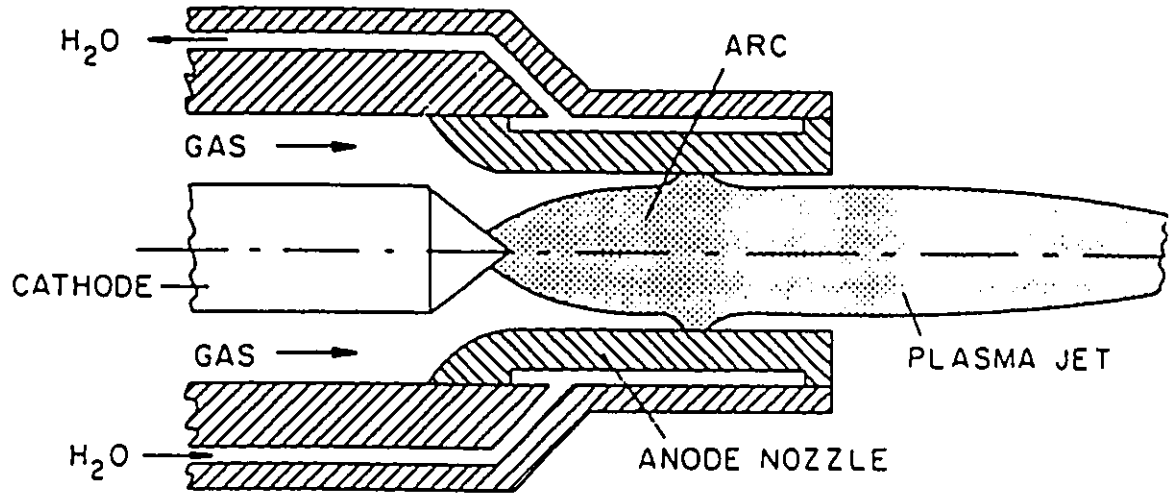

a)

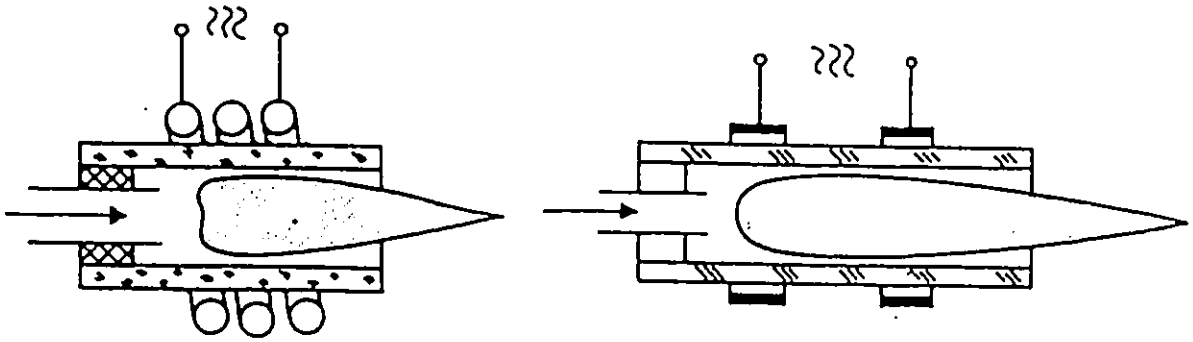

b) c)

Figure 2.2: Schematic diagram of (a) DC[48] and (b), (c) RF plasma torches[49].

exit of the plasma torch and the radial distance from the plasma torch centerline respectively. Further studies by Beuthe et al.[51] have shown that the downstream plasma jet temperature profiles can also be significantly affected by the flow pattern of the plasma gas within the plasma torch as shown in Figure 2.6.

Temperature profiles are shown in Figure 2.7[52] for a thermal plasma generated by an RF inductively coupled plasma torch under atmospheric pressure conditions. In this case, the temperature distribution at the exit of the plasma torch exhibits a bimodal distribution for reasons which will be discussed in Section 2.4. As indicated in Figure 2.7, the plasma jet generated via an RF plasma torch also quenches rapidly on emission from the plasma torch. Similar to the results for a DC plasma torch jet shown in Figure 2.4 increases in plasma gas flow tend to increase downstream temperatures, most likely due to the increased convective heat transport in the axial direction[6].

Measured plasma jet temperatures as high as 15000 K have been recorded and electron densities of 10^{16} cm^{-3} are not uncommon in the plasma jets of commercial and experimental RF and DC plasma torches as summarized in Figures 2.14 and 2.15. As with DC arc discharges, thermal plasma jets are often assumed to be in local thermodynamic equilibrium ($T_e = T_g$). Recent studies made by Ono et al.[53][54] tend to indicate that this may not be the case however. As shown in Figure 2.8, the measured values of electron temperature have been found to be well above the gas temperature in thermal plasma jets generated by a DC plasma torch, even at pressures as high as 365 Torr. Figure 2.9 shows that high electron densities can be expected more than 5 cm from the exit of the plasma torch.

2.3 Flame Plasmas

Combustion of material can generate flames with gas temperatures as high as a few thousand degrees Kelvin which can yield thermal plasmas in the luminous combustion zone as illustrated in Figure 2.10[55][56]. Flames produced by fast exothermic gas-phase chemical reactions are the most common source of low-temperature thermal plasmas. The presence of electrons and ionized species in flame plasmas is considered

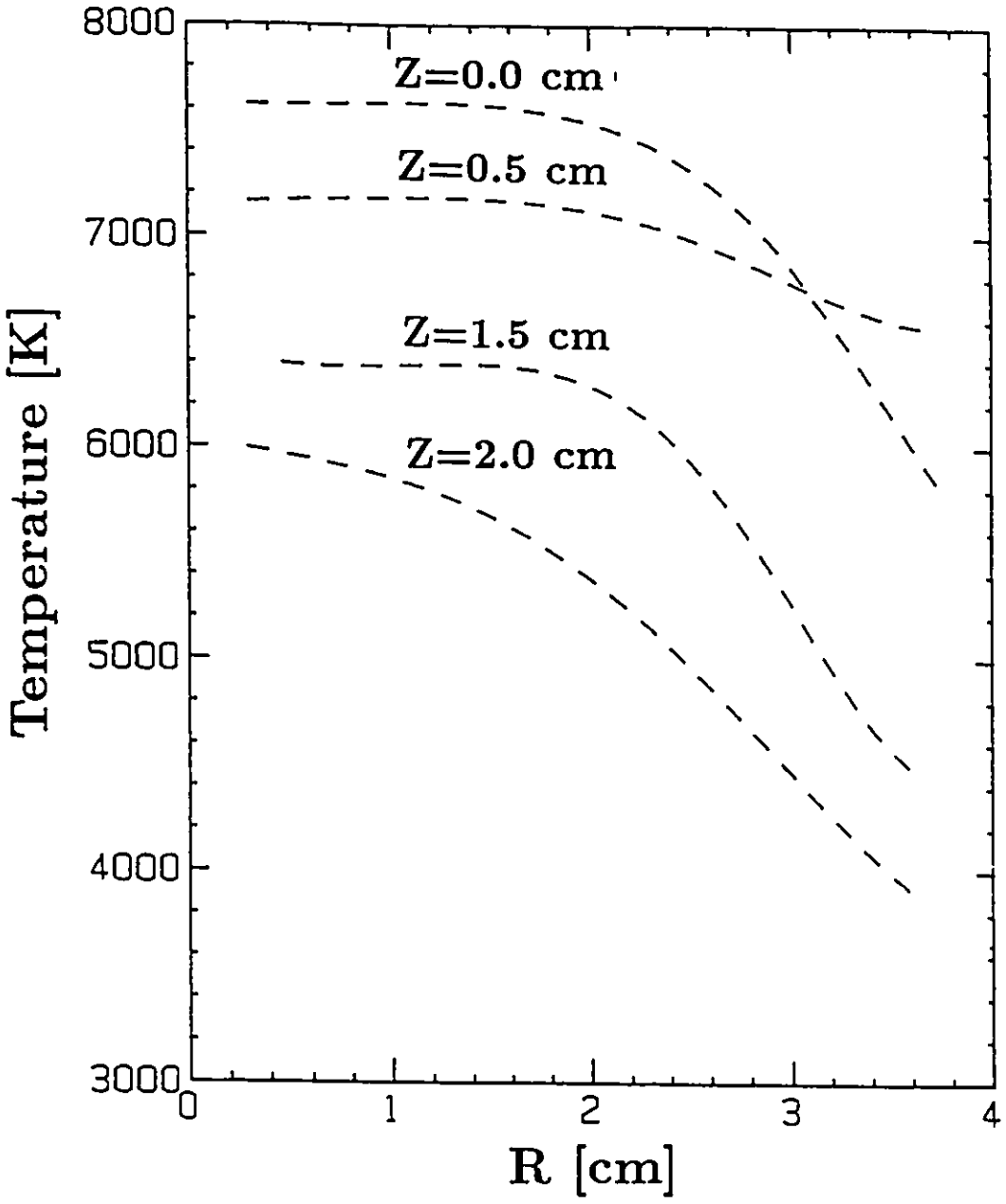

Figure 2.3: Spectroscopically measured radial temperature profiles downstream of the exit of a DC plasma torch[50].

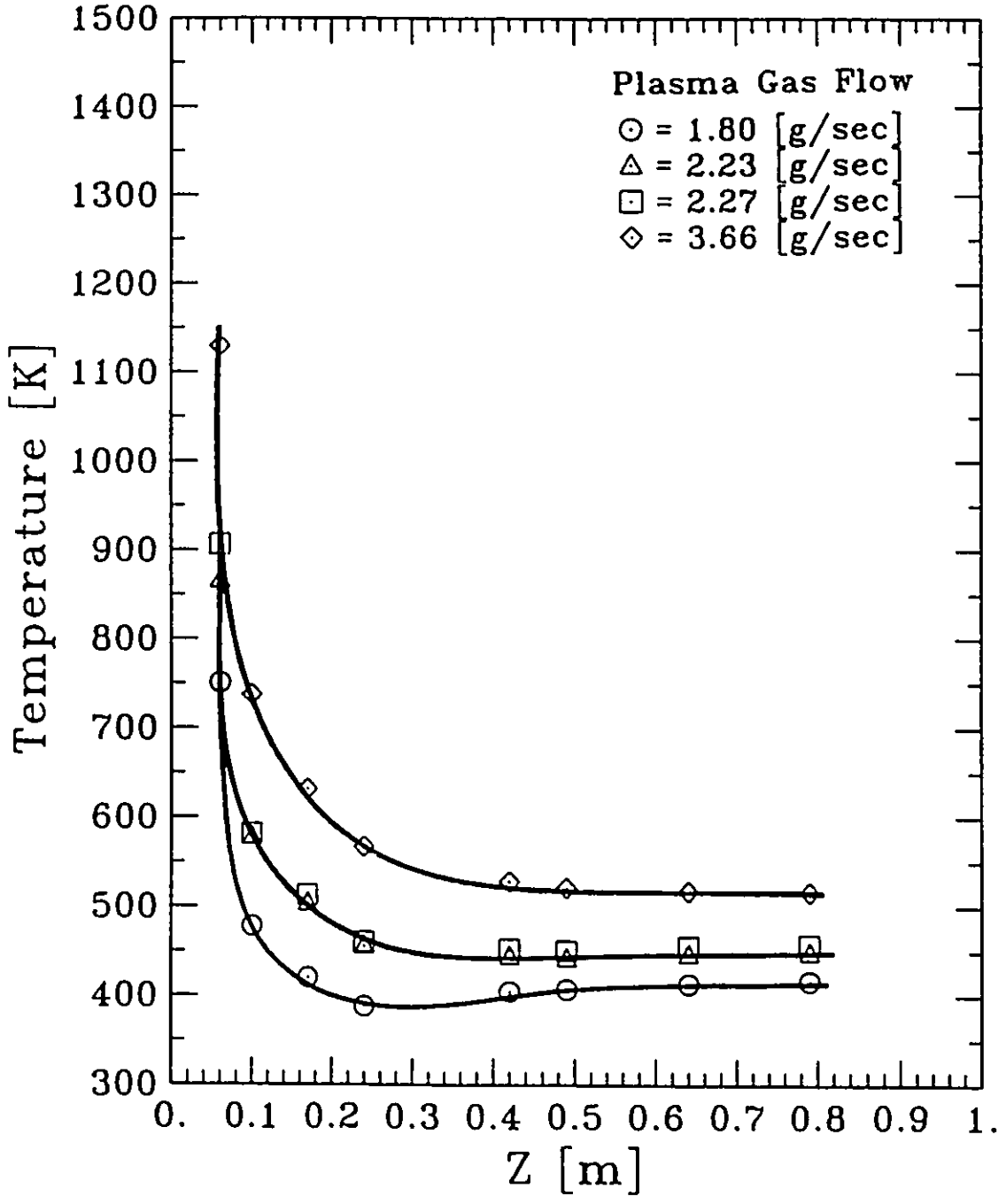

Figure 2.4: Axial temperature profiles downstream of the exit of a DC plasma torch as measured by an array of thermocouples by Beuthe et al.[5].

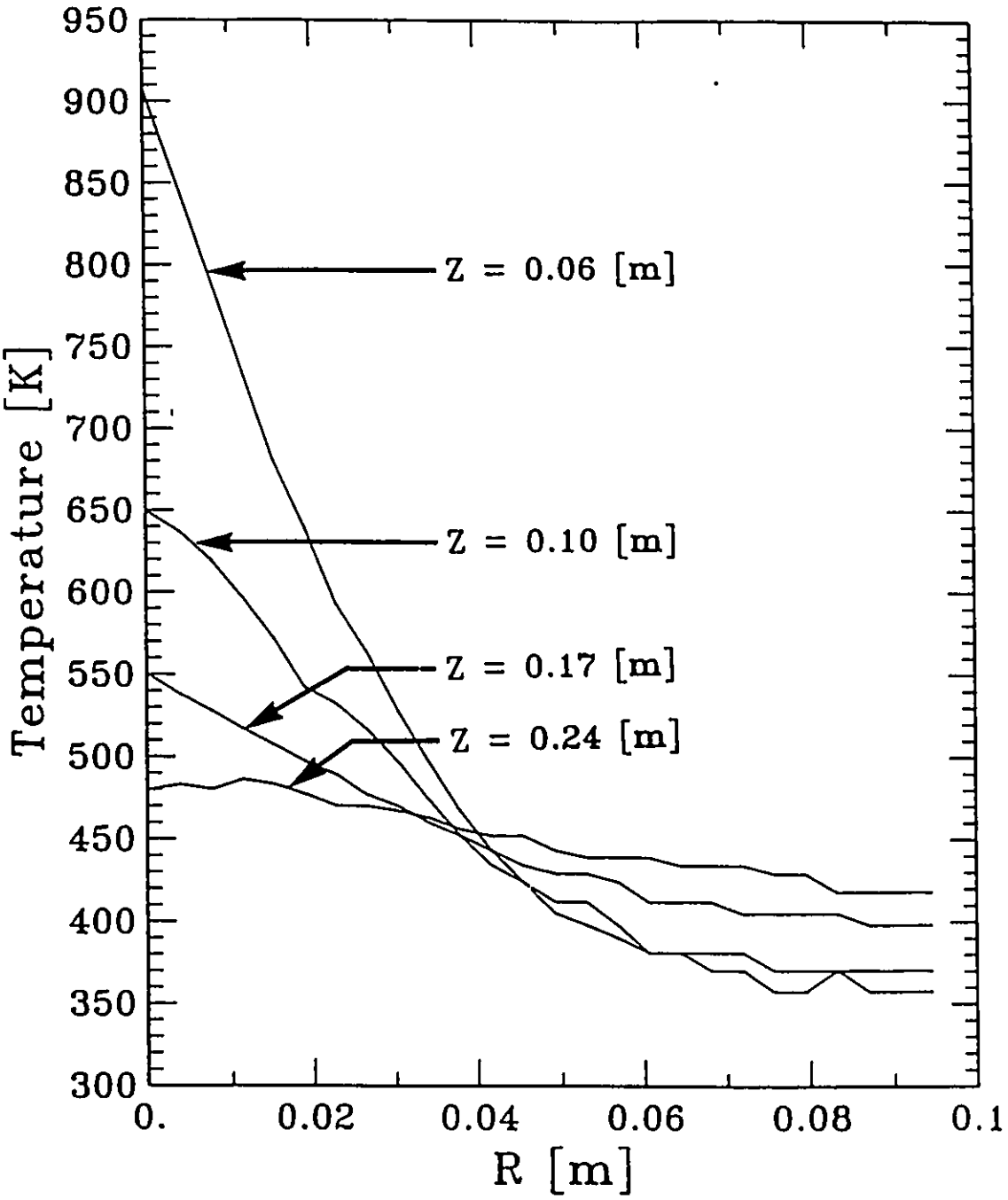

Figure 2.5: Radial temperature profiles downstream of the exit of a DC plasma torch as measured by an array of thermocouples in conjunction with an infrared thermal image processing system by Beuthe et al.[5] (plasma gas: argon, diam.: 25.4 mm, p = 760 Torr, power = 30 kW, plasma gas flow rate = 3.9 g/sec).

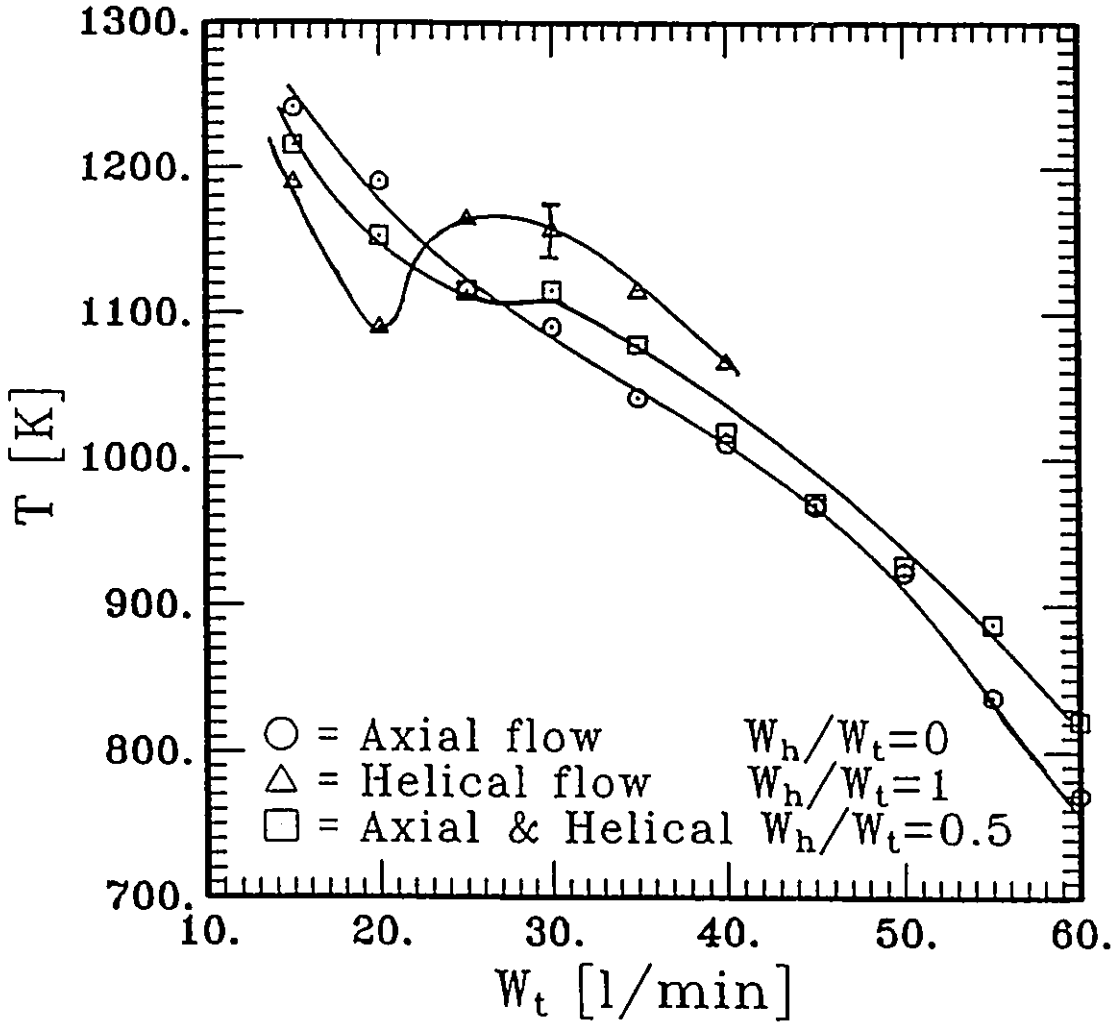

Figure 2.6: Temperature measured at the geometric centre of a plasma torch exit, 38 mm from the front face of the plasma torch for various different plasma gas flow patterns and flow rates as measured by Beuthe et al.[51].

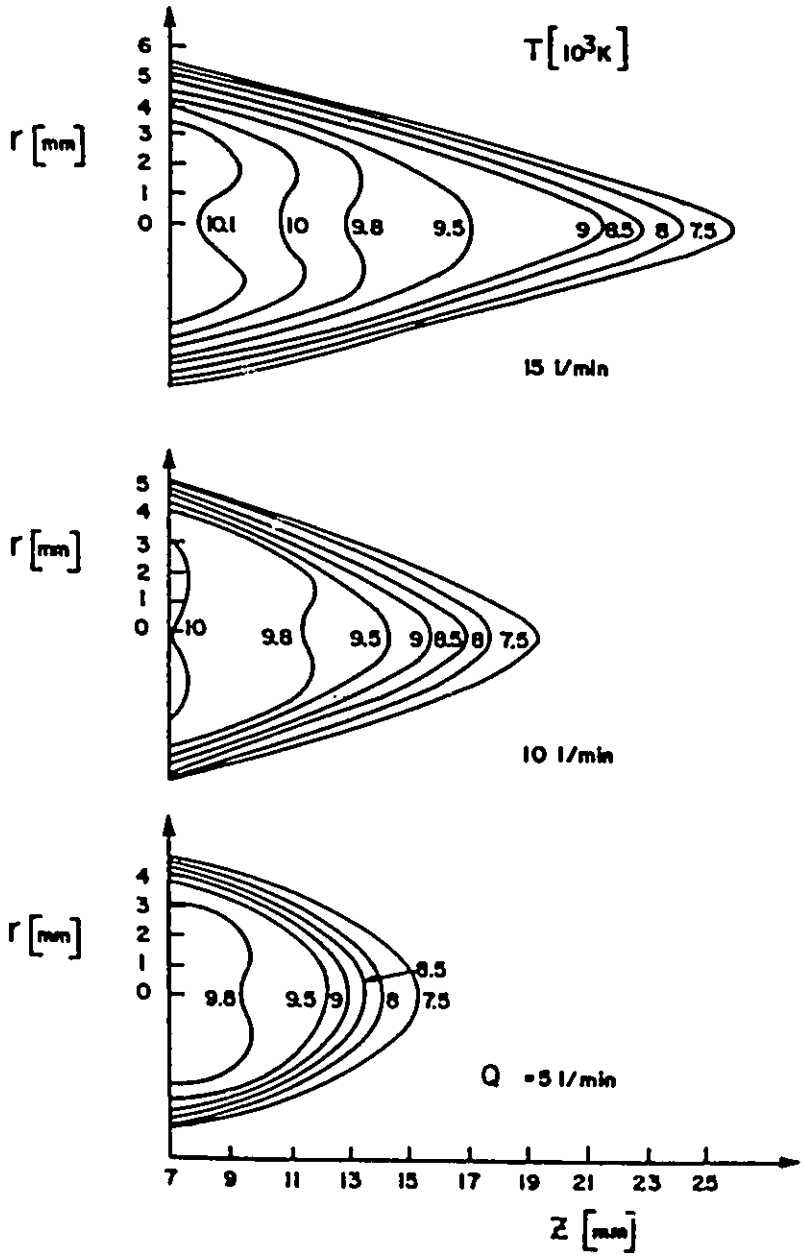

Figure 2.7: Temperature map in the exit jet of an induction plasma at different total plasma gas flow rates (gas: argon, diam.: 14 mm, f = 17 MHz, p = 760 Torr, power = 6 to 8 kW.[52].

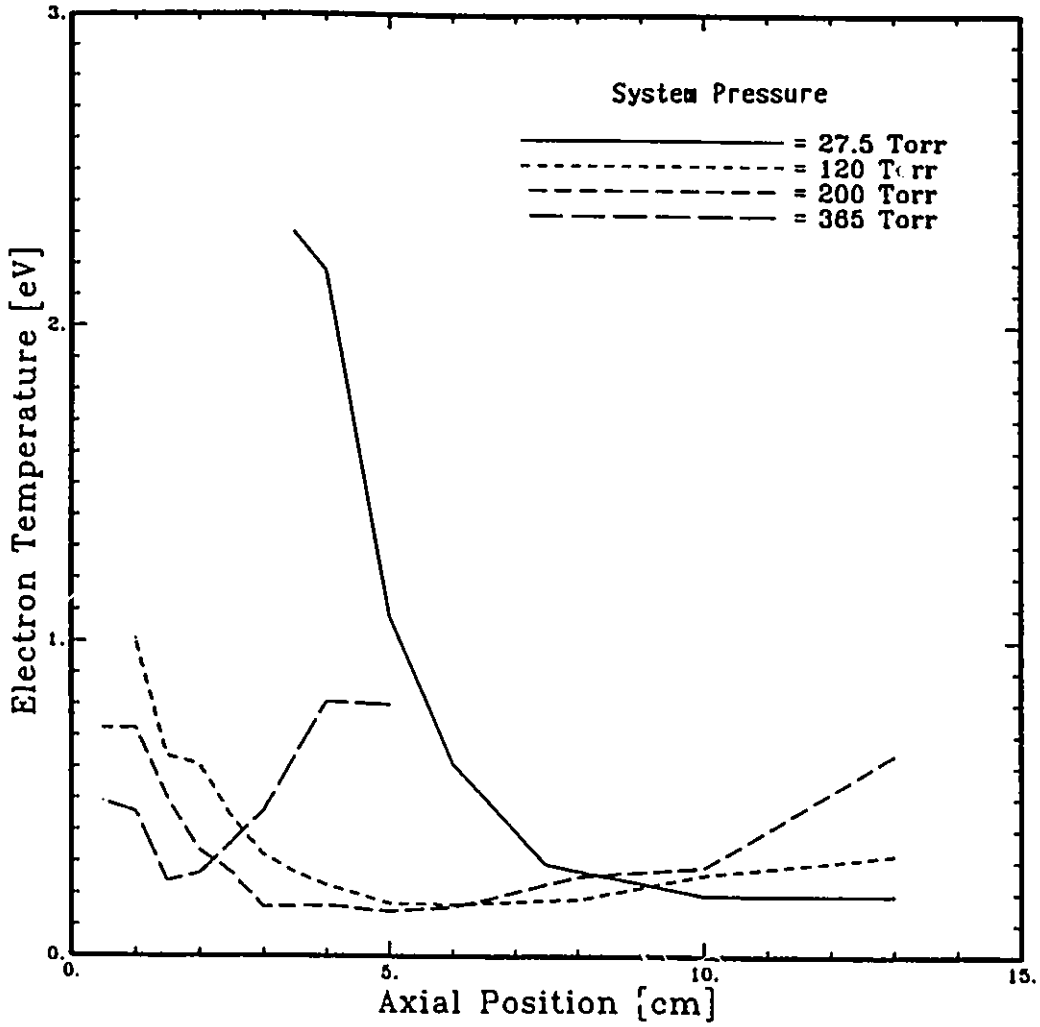

Figure 2.8: Downstream plasma jet electron temperatures for various system pressures (plasma gas: argon, flow rate: 5 l/min)[53][54].

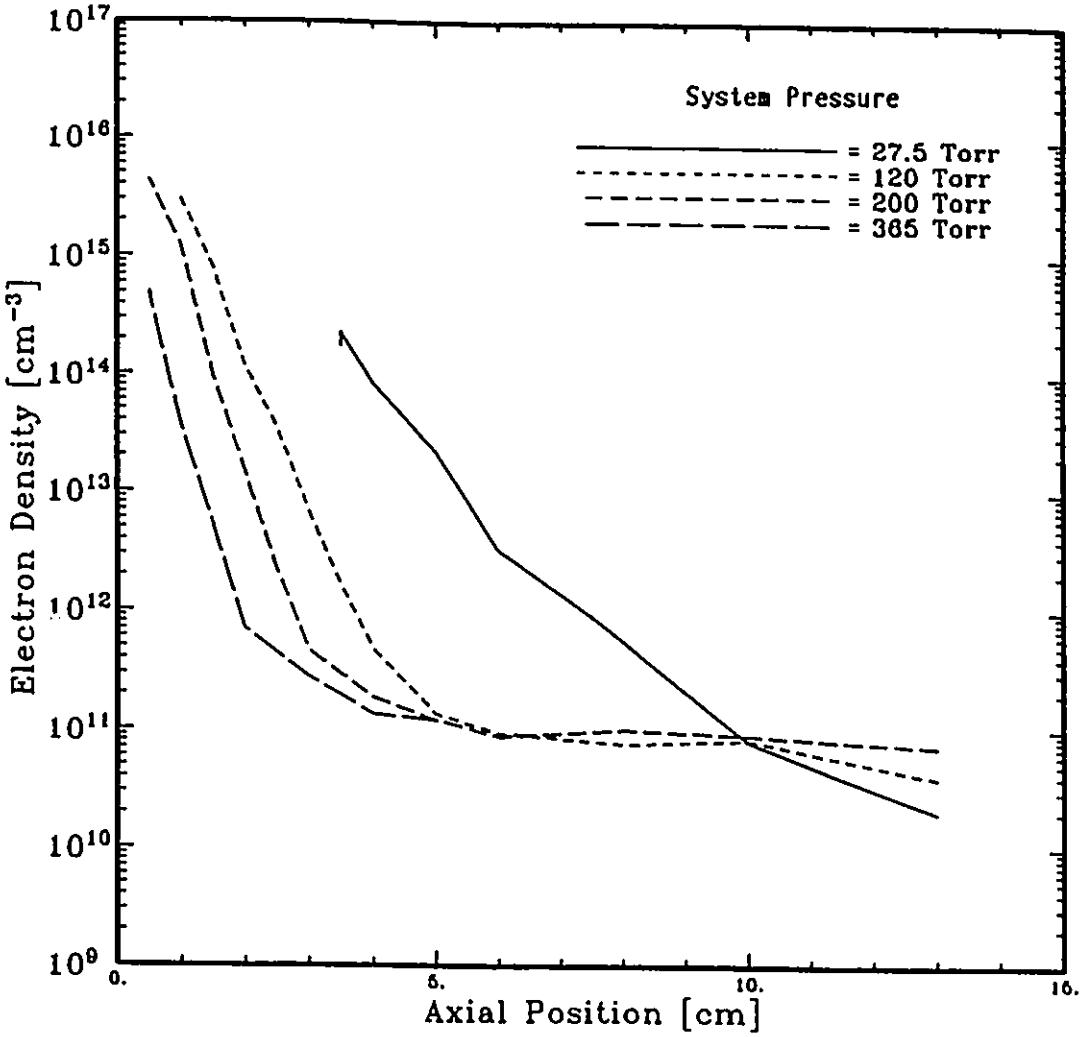

Figure 2.9: Downstream plasma jet electron densities for various system pressures (plasma gas: argon, flow rate: 5 l/min)[53][54].

to occur primarily through the collision of molecules or radicals. The mechanism may be primarily through thermal ionization as a result of combustion and the rearrangement of chemical bonds within molecules. It has also been suggested that electron impact collisions may contribute to the presence of ionized species in a flame plasma[57]. Temperatures in flame plasmas may be as high as 3500 K with electron densities up to 10^{10} cm^{-3} as summarized in Figures 2.14 and 2.15. It is generally assumed that thermal plasmas generated by combustion processes are in local thermodynamic equilibrium ($T_e = T_g$).

2.4 Glow Discharges

Glow discharges occur under medium gas pressure conditions (typically 10^{-3}–75 Torr) and distinguish themselves from arc discharges primarily by their relatively small discharge currents (0.1–100 mA) and high applied voltages (typically 0.5–20 kV).

Glow discharges can be produced by high voltage DC, RF or microwave applied electric fields. The electric field applies a force to the electrons in the gas (which are either emitted by the cathode in the case of the DC discharge, or can be initially injected by a starter electrode typically through the use of a tesla coil in an RF discharge), and if the ratio of the electric field to the pressure in the system E/p is high enough, the electrons will be able to gain enough energy between collisions to ionize the gas molecules.

A typical DC glow discharge in a tube with plane electrodes, a large electrode gap and a relatively small diameter is shown in Figure 2.11[49]. As indicated, the DC glow discharge is characterised by several diffuse luminous zones. The relative sizes of these zones varies with pressure and inter-electrode distance. Increasing the pressure tends to decrease the length of the negative glow and the Faraday dark space and increase the size of the positive column. Increasing the inter-electrode distance tends to increase the length of the positive column, but does not significantly affect the length of the negative glow and the Faraday dark space. The potential drop across the cathode often makes up the major part of the applied voltage as shown. Aside

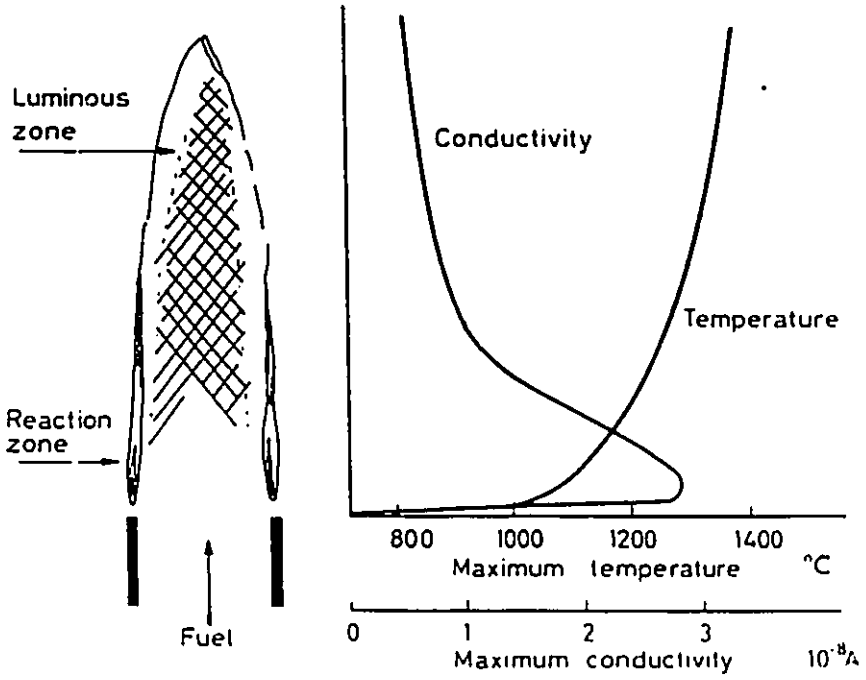

a)

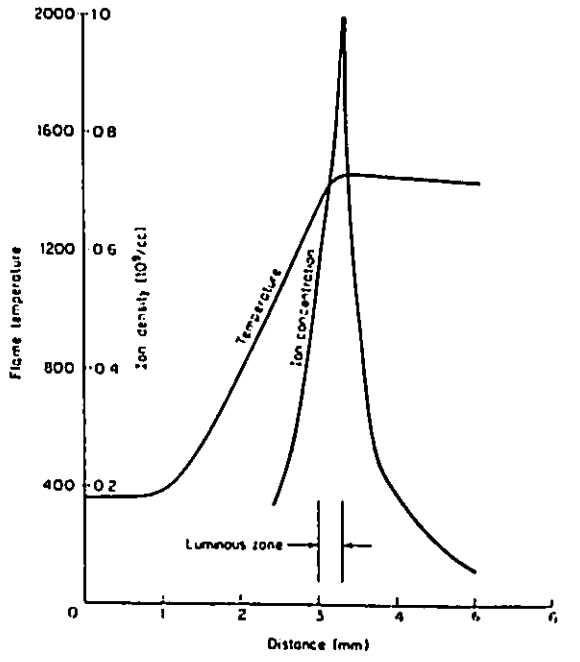

b)

Figure 2.10: (a) Electrical conductivity and temperature in a hydrocarbon diffusion flame[55] (b) Ion density and temperature profile through a flame[56].

from the cathode region, the space charge is essentially zero over the entire length of the discharge and the gas is in the form of a plasma[49].

When a high voltage, high frequency RF or microwave electric field is used to produce a glow discharge, the electrons tend to oscillate in the applied field and ionize the gas molecules via electron impact ionization. In this case, the high frequency applied electric field can only penetrate to a certain depth into the plasma gas. As a result, the temperature profiles an RF or microwave discharge can have off-axis maxima as shown previously in Figure 2.7.

Unlike arc discharges in which both the gas and electron temperatures are high, glow discharges typically have high electron temperatures (1–5 eV) and low gas temperatures (300–500 K). The generated electrons tend to cause a relatively low degree of ionization ($\sim 10^{-6}$ is typical) in the gas, and the charged particle density is typically of the order of 10^{6}–10^{13} cm^{-3} as summarized in Figures 2.14 and 2.15.

2.5 Spark Discharges

The continuity of arc or glow discharges is guaranteed by the presence of an adequate source of current or high voltage. If the total energy available for a discharge is limited, for example by the presence of a large capacitor, the electrical discharge tends to manifest itself in the form of rapid impulse-type filament discharges known as sparks as shown in Figure 2.12 at pressures above atmospheric pressure. The time and space dependent development of such a discharge represents a complex physical phenomenon which depends on numerous parameters such as pressure (if above atmospheric), electrode geometry, and electrode gap.

Sparks tend to generate non-LTE plasmas in which the gas temperatures can be as high as 1000 K, but the electron temperature can be orders of magnitude larger. The electron density is estimated to be 10^{10}–10^{13} cm^{-3}[58].

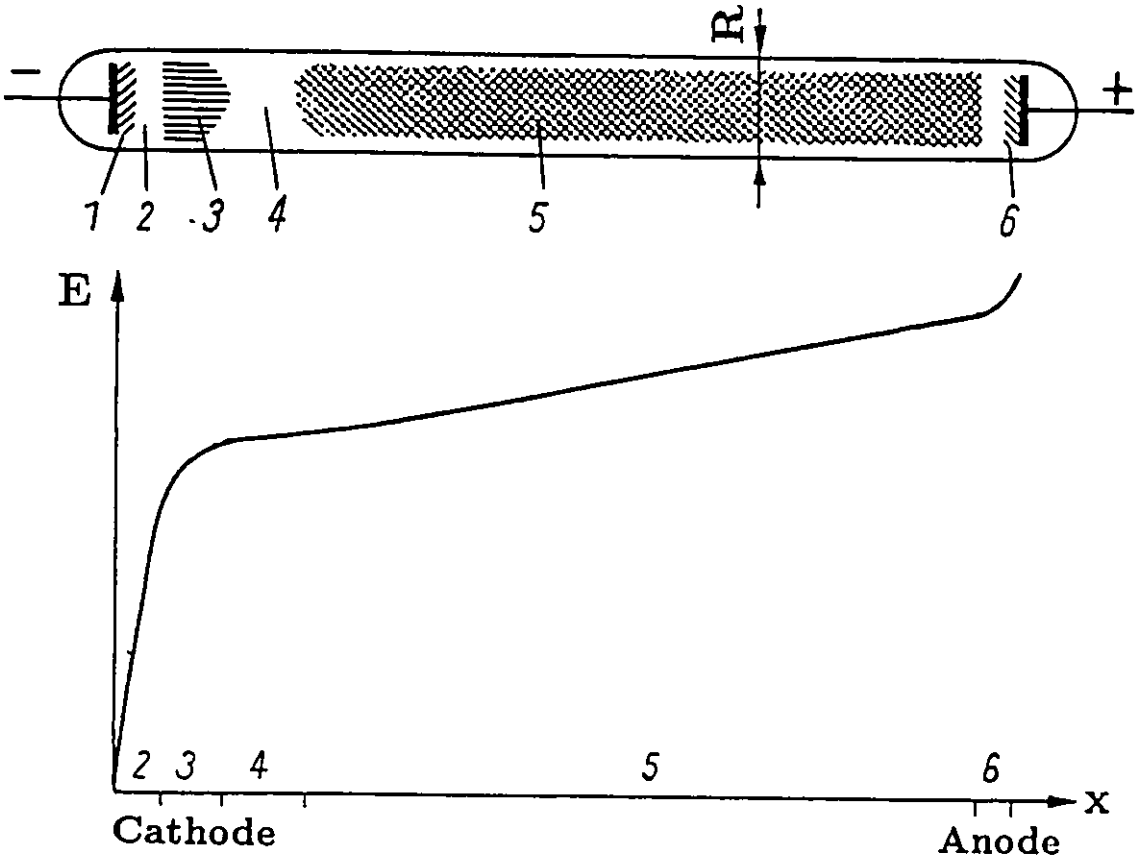

Figure 2.11: Typical glow discharge. 1. Cathode sheath, 2. Crooks or cathode dark space, 3. Negative glow, 4. Faraday dark space, 5. Positive column, 6. Anode sheath[49].

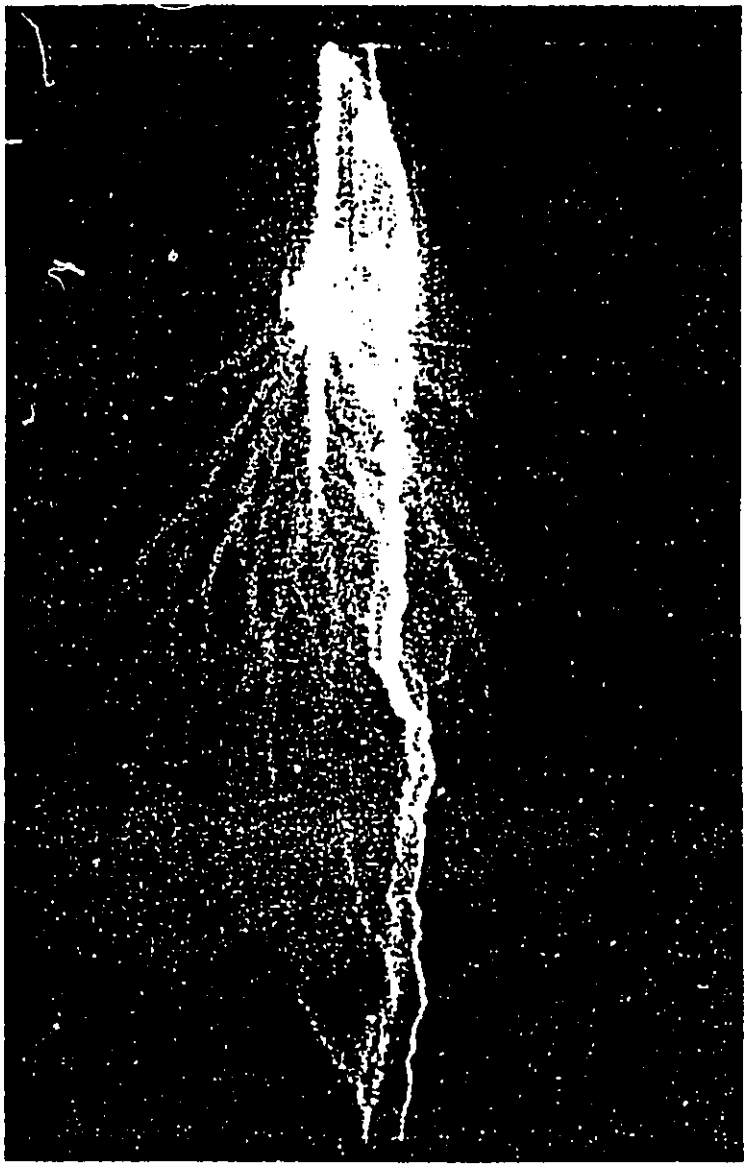

Figure 2.12: Typical spark discharge.[60].

2.6 Shock Wave Plasmas

A shock tube can be thought of as a system by which a sample of gas can be raised from a low temperature to a high temperature and kept at this temperature long enough to carry out detailed physical and chemical experiments. A conventional shock tube typically consists of two straight lengths of tubing with uniform cross-section separated by a thin diaphragm as shown in Figure 2.13.

The gas in a shock tube is initially at a low pressure, normally a few Torr or less. A driver section containing a gas at high pressure is separated from the evacuated section by a diaphragm. When the diaphragm ruptures, a shock wave S of typically 1–10 atmospheres pressure is passed over this gas as shown in Figure 2.13, and in doing so raises the temperature of the gas high enough for thermal ionization to occur. The maximum attainable thermal temperature by this method depends on the strength of the shock[59]. The mechanism of this rapid increase in thermal energy of the gas can be explained via the Hugonoit equations[60].

Typical experiments which have used shock tubes to study the ionization mechanisms of gases have attained temperatures of up to 20000 K and generated electron densities in excess of 10^{17} cm^{-3}[61]. As such, the shock waves are capable of generating plasmas with temperatures comparable to those found in thermal plasma arcs or jets. A summary of the temperatures and electron densities attainable in shock tubes has been summarized in Figures 2.14 and 2.15.

2.7 Summary

A summary of the typical gas and electron temperatures which can be expected in the thermal plasmas discussed above has been outlined in Figure 2.14. As shown here, flame plasmas constitute the lowest temperature thermal plasmas with temperatures up to 3200 K. Arc, jet, and shock all cover approximately the same electron and gas temperature region. Although arc plasmas and plasma jets can be generated intermittently, they are generally used as a continuous discharge. Shock and spark plasmas are intermittent by nature however. Glow discharges tend to

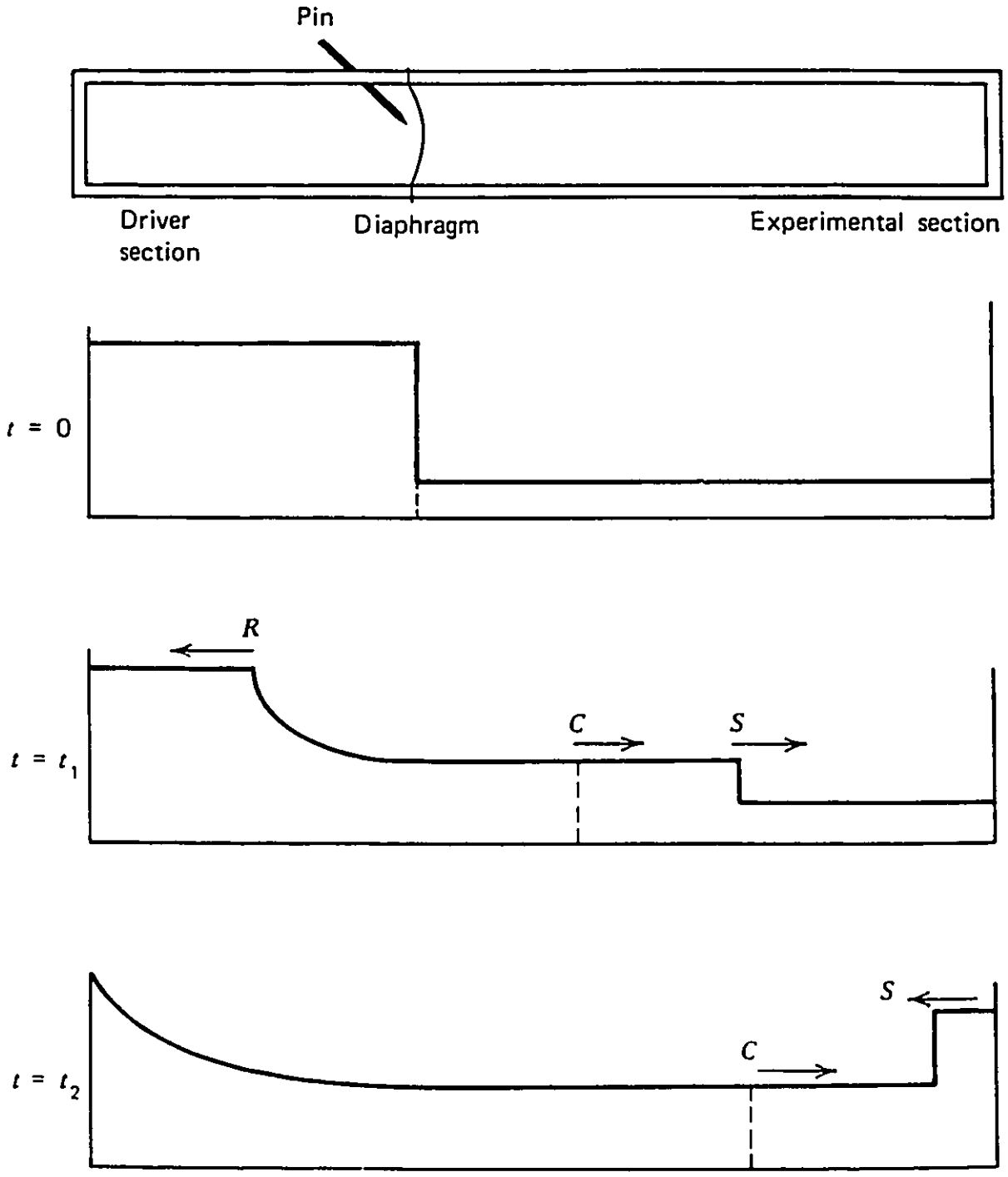

Figure 2.13: Conventional shock tube and pressure profiles at various time intervals[57].

have gas temperatures which range from room temperature to no more than a few hundred degrees above room temperature. Their electron temperatures are generally much higher then those generated by the other plasma generation mechanisms shown here.

Figure 2.15 illustrates the observed electron density as a function of electron temperature for thermal plasmas generated by various methods. As shown in Figure 2.15, arc, shock and jet plasmas have the highest electron density. These discharges normally operate at atmospheric or reduced pressures, and the degree of ionization which can occur in arc or shock generated plasmas can approach unity. Glow discharges operate under reduced pressure conditions which cause the electron density to be lower than that seen under arc, shock or plasma jet conditions. The degree of ionization is also much lower. Flame plasmas occur at temperatures significantly lower than those found in all other plasmas shown in Figure 2.15. The electron densities found in flame plasmas are also much smaller.

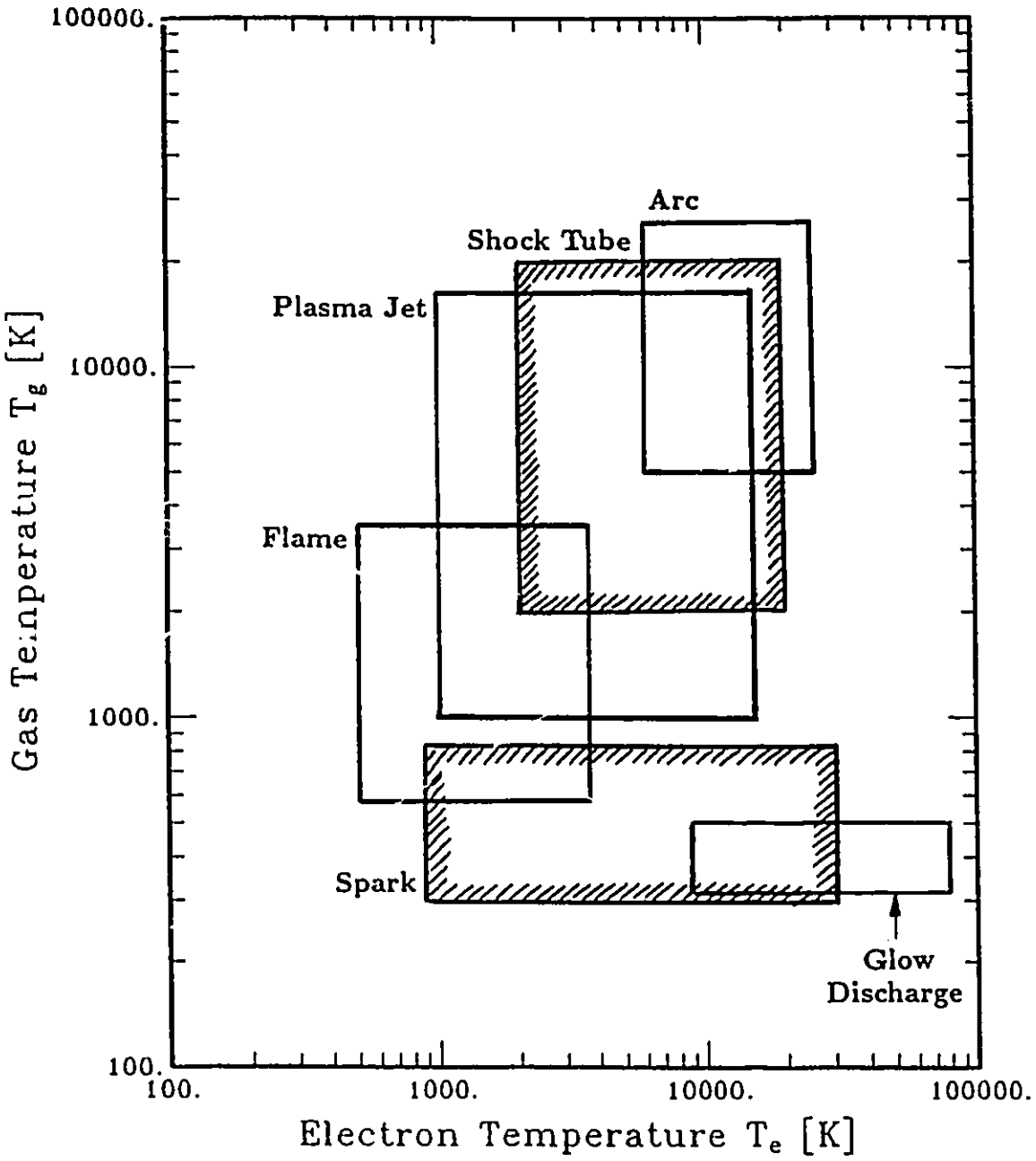

Figure 2.14: Range of electron and gas temperatures occurring in thermal plasmas.

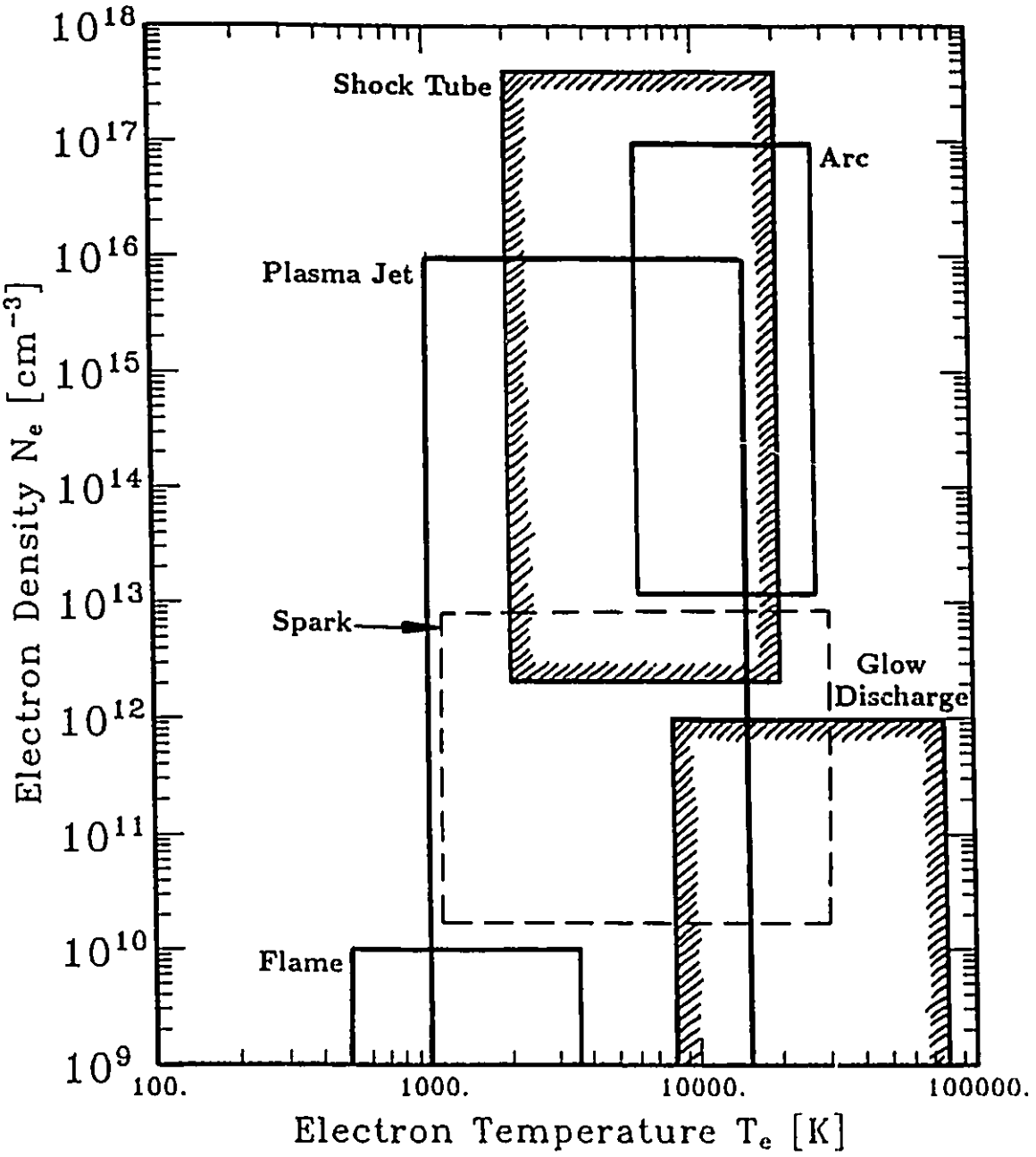

Figure 2.15: Range of electron densities as a function of electron temperatures occurring in thermal plasmas.

Chapter 3

Basic Equations and Numerical Procedures

3.1 Basic Equations

A thermal plasma represents a complex mixture of neutral and charged particles. In order to identify which species will occur in such a mixture and calculate their concentrations as a function of temperature and pressure, it is necessary to solve the continuity equation in conjunction with the charged particle transport equation[62]. The continuity equation states[63]

$$\nabla \cdot \mathbf{J} = -\frac{d[N]}{dt} + (\text{source}) - (\text{sink}) \tag{3.1}$$

and the charged particle transport equation can be written[64]

$$\mathbf{J} = N\mathbf{U} \pm \mu N\mathbf{E} - D\nabla N - GN\nabla T \tag{3.2}$$

where $\mathbf{J}$ is the particle flux density, N is the particle density, $\mathbf{E}$ is the electric field, D is the diffusion coefficient, $\mathbf{U}$ is the velocity, μ is the mobility, G is the thermophoresis coefficient, and T is the temperature. The sign of the mobility term is determined by the charge of the particle in question, + for positively charged particles, − for negatively charged particles. In equation 3.1, $\nabla \cdot \mathbf{J}$ represents the net flow across a control volume, $\frac{d[N]}{dt}$ represents the accumulation of the species within the control

volume, and sources and sinks are caused by the chemical reactions occurring within the control volume. In equation 3.2, $N\mathbf{U}$ represents the particle flux due to charged particles transported by the convection of gas, $\mu N\mathbf{E}$ represents the flux due to the drift motion of charged particles under the influence of an electric field, $D\nabla N$ represents the flux caused by diffusion, and $GN\nabla T$ represents the thermophoresis flux caused by spatial temperature inhomogeneities.

Taking the scalar product $\nabla\cdot$ of each side of equation 3.2, the transport equation becomes

$$\nabla \cdot \mathbf{J} = N\nabla \cdot \mathbf{U} \pm \mu N\nabla \cdot \mathbf{E} - D\nabla^2 N - GN\nabla^2 T \tag{3.3}$$

Substituting equation 3.1 into 3.3, the transport equation becomes

$$\frac{d[N]}{dt} = (\text{source}) - (\text{sink}) + N\nabla \cdot \mathbf{U} \pm \mu N\nabla \cdot \mathbf{E} - D\nabla^2 N - GN\nabla^2 T \tag{3.4}$$

Assuming the plasma under examination has no net velocity, there is no applied electric field, and the temperature of the system is uniform, it is possible to simplify equation 3.4 to yield

$$\frac{d[N]}{dt} = (\text{source}) - (\text{sink}) + D\nabla^2 N \tag{3.5}$$

Assuming the system under examination has a cylindrical geometry, and using a zero order Bessel function to approximate the radial density of the various species[65], the diffusion term in equation 3.5 can be reformulated in the following manner

$$D\nabla^2 N \approx \frac{Dq^2 N}{R^2} \tag{3.6}$$

where $q^2 = 2.405$ and R is the radius of the cylinder.

Substituting equation 3.6 into 3.5, the transport equation becomes

$$\frac{d[N]}{dt} = (\text{source}) - (\text{sink}) + D\frac{q^2 N}{R^2} \tag{3.7}$$

As mentioned previously, the source and sink terms of species referred to in equation 3.7 are determined by the rate of the chemical reactions occurring within the thermal plasma. In general, such reactions can take the form of two- or three-body collision reactions. In the case of two-body collision reactions

$$\mathrm{A} + \mathrm{B} \xrightarrow{k_2} \mathrm{C} + \mathrm{D}(+\mathrm{E} + \mathrm{F}) \tag{3.8}$$

the rate of decrease of concentration of species A and B can be expressed as

$$\frac{d[X]}{dt} = -k_2[A][B] \tag{3.9}$$

and the rate of increase of species C and D (as well as E and F) can be expressed as

$$\frac{d[X]}{dt} = k_2[A][B] \tag{3.10}$$

where [X] represents the concentration of A or B in equation 3.9 and the concentration of C, D, E, or F in equation 3.10, and k_2 represents the two-body reaction rate coefficient with units of cm^{-3}/s.

In the case of three-body collision reactions

$$A + B + M \xrightarrow{k_3} C + D(+E + F) + M \tag{3.11}$$

M acts as an intermediary to facilitate the reaction. The rate of decrease of concentration of species A and B can be expressed as

$$\frac{d[X]}{dt} = -k_3[A][B][M] \tag{3.12}$$

and the rate of increase of species C and D (as well as E and F) can be expressed as

$$\frac{d[X]}{dt} = k_3[A][B][M] \tag{3.13}$$

where [X] has the same meaning as in equations 3.9 and 3.10 and k_3 represents the three-body reaction rate coefficient with units of cm^{-6}/s. Details of the classes of reactions which can occur in thermal plasmas will be discussed in Section 3.2.

Assuming a steady state plasma, the transport equation becomes

$$(\text{source}) - (\text{sink}) + D\frac{q^2 N}{R^2} = 0 \tag{3.14}$$

Such an equation can be written for each species in the thermal plasma. The diffusion coefficient D is equal to the gaseous diffusion coefficient D_g for neutral particles

$$D = D_g \tag{3.15}$$

and the ambipolar diffusion D_a coefficient for ionized species

$$D = D_a = (1 + \frac{T_e}{T_i})D_i \tag{3.16}$$

where T_e is the electron temperature, T_i is the ion temperature, and D_i is the ionic diffusion coefficient. In this work, $T_i = T_g$ was assumed.

Diffusion coefficients are normally tabulated for room temperature (300 K) and 1 Torr pressure $D_{300K,1Torr}$. Diffusion coefficients are a function of pressure and temperature however. The temperature dependence of diffusion coefficients may be calculated via the following relationship[62]

$$D = D_{300K,1Torr}\left(\frac{1}{p}\right)\left(\frac{T_g}{300}\right)^{\frac{1}{2}} \tag{3.17}$$

where p is the pressure in Torr.

In order to calculate the total density of the species in the model, the ideal gas law can be used in the form

$$N_{TOT} = \frac{p}{R_{IG}T_g} \tag{3.18}$$

where N_{TOT} is the overall volumetric density in cm^{-3} of a gas under pressure p and at temperature T_g, and R_{IG} is the ideal gas constant. Over the temperature and pressure range considered in the present model (T_g = 300–15000 K, p = 1–15200 Torr) the ideal gas law represents an excellent relation for the calculation of the density of a gas[66][67][68].

3.2 Chemical Reactions

Thermal plasmas represent a system in which a large number of elementary processes involving the exchange and transmission of energy and particles between electrons, ions (both positive and negative), atoms, and molecules (including radicals) take place. The objective of this section is to give a brief overview of the possible collision processes which can act as potential sources and sinks of species in equation 3.14 under the thermal plasma conditions of interest in this study (T_g = 300–15000 K, T_e = 300–20000 K, p = 1–15200 Torr).

3.2.1 Neutral Reactions

Neutral reactions between atomic and molecular species play an important role in the determination of neutral species densities. Atomic and molecular collisions tend to dominate the behaviour of the plasma in the lower temperature ranges. In the present study, the reactions of interest include:

(a) Excitation

$A + B \longrightarrow A^* + B$ (thermal)

(b) Dissociation

$AB + M \longrightarrow A + B + M$ (diatomic thermal)

$ABC + M \longrightarrow AB + C + M$ (triatomic thermal)

(c) Recombination

$A + B \longrightarrow AB + h\nu$ (radiative)

$A + B + M \longrightarrow AB + M$ (diatomic molecular)

$A + BC + M \longrightarrow ABC + M$ (triatomic molecular)

(d) Exchange reactions

$A + BC \longrightarrow AB + C$

(e) De-excitation by collision with wall

$A^* + \text{wall} \longrightarrow A + \text{wall}$ (atomic)

3.2.2 Ionic Reactions

Ionic reactions tend to dominate the chemical kinetics of a thermal plasma at higher temperatures. However, as will be seen later, significant concentrations of ionic species can also occur in the lower temperature regions.

In general, the charged species can consist of atomic ions A^+, A^-, molecular ions AB^+, AB^-, ABC^+, ABC^-, etc., and electrons e. Ionic chemical reactions can be broadly classified into (I) those which act as sources of ions, (II) those which convert ions from one form into another, (III) those in which electrons act as intermediaries, and (IV) those which act as sinks of ions.

(I) Sources of Ions

(a) Ionization

(i) electron impact ionization

$e + A \longrightarrow A^+ + e + e$ (direct, atomic)

$e + A^* \longrightarrow A^+ + e + e$ (from excited state)

$e + AB \longrightarrow AB^+ + e + e$ (direct, molecular)

$\longrightarrow A^+ + B + e + e$ (dissociative)

$e + AB^* \longrightarrow A^+ + B + e + e$ (dissociative, from excited state)

(ii) thermal impact ionization

$A + B \longrightarrow A^+ + B + e$ (from the ground state)

$A^* + B \longrightarrow A^+ + B + e$ (from an excited state)

(iii) ionization by metastable particles

$A^{**} + B \longrightarrow A^+ + B + e$ (Penning ionization)

$\longrightarrow (AB^*) \longrightarrow AB^+ + e$ (associative ionization)

$A^{**} + B^{**} \longrightarrow (AB^*) \longrightarrow A^+ + B + e$ (metastable-metastable)

$\longrightarrow (AB^*) \longrightarrow AB^+ + e$

(b) Attachment

$e + A \longrightarrow A^- + h\nu$ (radiative, atomic)

$e + A \longrightarrow (A^{-*}) \longrightarrow A^- + h\nu$ (dielectronic)

$e + AB \longrightarrow AB^- + h\nu$ (radiative, molecular)

$\longrightarrow A^- + B$ (dissociative)

$\longrightarrow (AB^-)^* \xrightarrow{M} AB^-$ (collisional stabilization)

$e + A + M \longrightarrow A^- + M$ (three body, atomic)

$e + A + e \longrightarrow A^- + e$ (three body, atomic, via electron)

$e + AB + M \longrightarrow AB^- + M$ (three body, molecular)

(II) Ion Interconversion Processes

(a) Charge transfer

$A^\pm + B \longrightarrow B^\pm + A$ (atom-atom)

$A^\pm + B^* \longrightarrow B^\pm + A$

$A^\pm + BC \longrightarrow BC^\pm + A$ (atom-molecule)

$A^\pm + BC \longrightarrow B^\pm + A + C$ (dissociative)

$AB^{\pm} + C \longrightarrow C^{\pm} + A + B$ (dissociative)

(b) Clustering reaction

$A^{\pm} + B + M \longrightarrow AB^{\pm} + M$

(c) Ion-atom interchange

$A^{\pm} + BC \longrightarrow AB^{\pm} + C$

$A^{\pm} + BC \longrightarrow AB + C^{\pm}$

(d) switching reaction

$A^{\pm}{\cdot}B + C \longrightarrow A^{\pm}{\cdot}C + B$

(III) Electrons as Intermediaries

$e + A \longrightarrow A^{*} + e$ (electron impact, excited)

$\longrightarrow A^{**} + e$ (electron impact, metastable)

$e + AB \longrightarrow e + A + B$ (electron impact dissociation)

$e + ABC \longrightarrow e + AB + C$ (electron impact dissociation)

(IV) Sinks of Ions

(a) Volume recombination

$A^{+} + e \longrightarrow A + h\nu$ (radiative)

$\longrightarrow (A^{**}) \longrightarrow A^{*} + h\nu$ (dielectronic)

$A^{+} + e + M \longrightarrow A + M$ (three-body, atomic)

$A^{+} + e + e \longrightarrow A + e$ (three-body, electronic)

$AB^{+} + e \longrightarrow A^{*} + B$ (dissociative)

$AB^{+} + e + M \longrightarrow A + B + M$ (dissociative, three-body)

$AB^{+} + e + e \longrightarrow A + B + e$ (dissociative, three-body)

$A^{+} + B^{-} \longrightarrow A + B^{*}$ (mutual neutralization)

$A^{+} + B^{-} \longrightarrow AB + h\nu$ (mutual neutralization, radiative)

$A^{+} + B^{-} + M \longrightarrow AB + M$ (mutual neutralization, three-body)

$AB^{+} + C^{-} \longrightarrow A + B + C$ (dissociative neutralization)

$A^{+} + BC^{-} \longrightarrow A + B + C$ (dissociative neutralization)

$AB^{+} + C^{-} \longrightarrow A + BC$ (neutralization, switching)

$AB^{+} + C^{-} + M \longrightarrow A + BC + M$ (neutralization, switching, three-body)

(b) Detachment

$A^{-} + B \longrightarrow A + B + e$ (collisional)

$\longrightarrow$ AB + e (associative)

$AB^- + M \longrightarrow AB + e + M$ (molecular)

$A^- + e \longrightarrow A + e + e$ (electron)

$A^- + B^* \longrightarrow A + B + e$ (via metastable)

$A^+ + B^- \longrightarrow A^+ + B + e$

$A^- + B^- \longrightarrow A + B^- + e$

(c) neutralization by collision with wall

$AB^+ + e + wall \longrightarrow AB + wall$

$AB^+ + CD^- + wall \longrightarrow AB + CD + wall$

3.3 Numerical Procedures

Unlike the equilibrium models outlined in Chapter 1, the chemical kinetic approach to modelling thermal plasmas has the flexibility to consider thermodynamic equilibrium ($T_e = T_g$) as well as non-equilibrium ($T_e \neq T_g$) conditions. The formalisms which were introduced in Section 3.1 make the chemical kinetic model approach not only a more comprehensive examination of the processes occurring within a thermal plasma, but can also be included as part of a time dependent model. Unfortunately however, chemical kinetic models represent highly coupled, non-linear numerical systems which are relatively intractable to numerical solution and very sensitive to their input parameters. As a consequence, past research efforts have tended to prefer using LTE models since they tend to be somewhat more amenable to numerical solution.

Assuming there are n unknown species x_i in the thermal plasma to be examined, n different continuity equations can be written of the form of equation 3.14. In general, these equations take the form of a polynomial with a maximum degree of three as follows:

$$\begin{aligned} a_{1,1}x_1^3 + a_{1,2}x_1^2 + a_{1,3}x_1 + a_{1,4} &= 0 \\ a_{2,1}x_2^3 + a_{2,2}x_2^2 + a_{2,3}x_2 + a_{2,4} &= 0 \\ &\vdots \end{aligned} \tag{3.19}$$

$$a_{n,1}x_n^3 + a_{n,2}x_n^2 + a_{n,3}x_n + a_{n,4} = 0$$

Since the factors $a_{i,j}$ where $j = 1 \ldots 4$ can also potentially contain all other values of x_k such that $k = 1 \ldots i-1, i+1, \ldots n$, equations 3.19 represent a highly coupled set of equations which must be solved numerically. Each polynomial must be solved individually, and an iterative approach must be utilized to solve the n simultaneous polynomial equations. If $a_{i,1} = a_{i,2} = 0$ the polynomial equation is linear, and can be solved directly using the relation

$$x_i = -\frac{a_{i,4}}{a_{i,3}} \tag{3.20}$$

If only $a_{i,1} = 0$, the polynomial is quadratic, and can also be solved directly. A word of warning is in order at this point however. The use of the classical solution of the quadratic equation

$$x_i = \frac{-a_{i,3} \pm \sqrt{a_{i,3}^2 - 4a_{i,2}a_{i,4}}}{2a_{i,2}} \tag{3.21}$$

can lead to numerical error, in particular to the loss of accuracy which can be incurred if a real subtraction takes place between $-a_{i,3}$ and $\sqrt{a_{i,3}^2 - 4a_{i,2}a_{i,4}}$[69]. For this reason, if $a_{i,3}$ is negative, the first root $x_{i,1}$ of the polynomial should be calculated via the equation[70]

$$x_{i,1} = \frac{-a_{i,3} + \sqrt{a_{i,3}^2 - 4a_{i,2}a_{i,4}}}{2a_{i,2}} \tag{3.22}$$

If $a_{i,3}$ is positive, the first root should be calculated via the equation

$$x_{i,1} = \frac{-a_{i,3} - \sqrt{a_{i,3}^2 - 4a_{i,2}a_{i,4}}}{2a_{i,2}} \tag{3.23}$$

The second root $x_{i,2}$ can then be calculated using the value of $x_{i,1}$ via the relationship

$$x_{i,2} = \frac{-a_{i,4}}{a_{i,2}x_{i,1}} \tag{3.24}$$

Both roots should be calculated and the physically most appropriate value chosen as the species concentration. Complex roots are not allowed, and one of the roots is normally negative and therefore represents a non-physical solution.

In the case where $a_{i,1} \neq 0$, the first root of the polynomial must be calculated iteratively since algebraic solutions to third degree polynomials are not available. In this case, Newton's method, which converges quadratically with the number of iterations can be applied[69]. Newton's method states that the root x for a continuously differentiable function $f(x)$ of the form

$$f(x) = 0 \tag{3.25}$$

can be found iteratively as follows

$$x_{k+1} = x_k - \frac{f(x_k)}{f'(x_k)} \tag{3.26}$$

where $f'(x)$ represents the first derivative of f in x and k represents the k^{th} iterative step.

Given a typical 3$^{\text{rd}}$ degree polynomial

$$f(x_i) = a_{i,1}x_i^3 + a_{i,2}x_i^2 + a_{i,3}x_i + a_{i,4} \tag{3.27}$$

the first derivative is

$$f'(x_i) = 3a_{i,1}x_i^2 + 2a_{i,2}x_i + a_{i,3} \tag{3.28}$$

Thus, Newton's method reduces to

$$x_{k+1,i} = \frac{2a_{i,1}x_{k,i}^3 + a_{i,2}x_{k,i}^2 - a_{i,4}}{3a_{i,1}x_{k,i}^2 + 2a_{i,2}x_{k,i} + a_{i,3}} \tag{3.29}$$

but for calculation purposes, the nested form is better

$$x_{k+1,i} = \frac{((2a_{i,1}x_{k,i} + a_{i,2})x_{k,i} * x_{k,i}) - a_{i,4}}{(3a_{i,1}x_{k,i} + 2a_{i,2})x_{k,i} + a_{i,3}} \tag{3.30}$$

However, due to the large values of x which occur in chemical kinetic models, it was found that the following modified form was numerically more robust against overflow and underflow

$$x_{k+1,i} = \left(\left(\frac{2a_{i,1}x_{k,i} + a_{i,2}}{(3a_{i,1}x_{k,i} + 2a_{i,2})x_{k,i} + a_{i,3}}\right)x_{k,i}\right)x_{k,i} - \left(\frac{a_{i,4}}{(3a_{i,1}x_{k,i} + 2a_{i,2})x_{k,i} + a_{i,3}}\right) \tag{3.31}$$

After this iteration has converged with the desired accuracy, the calculated value of the root can be back-substituted into the original polynomial to reduce it to a quadratic polynomial which can be solved algebraically via equations 3.22, 3.23 and 3.24. All three calculated roots should be examined for their applicability as solutions. Under normal conditions, all three values are real, and two are typically negative, and therefore non-physical, which simplifies the choice. Complex results can also be ruled out as viable solutions.

A polynomial equation can be derived and solved to yield the concentration of each of the components of the thermal plasma including neutral species, positive ions, negative ions and electrons. Solving this set of continuity equations alone however would simply lead to the numerically consistent, but physically meaningless zero solution for each constituent species. In order to calculate a physically meaningful solution, the ideal gas law, as described in Section 3.1 must also be introduced as a constraint in the model. In gases containing m elemental atomic species, this can be done by replacing the m continuity equations which calculate the concentration of the largest constituent atomic or molecular species containing these elements with mass balances. This condition assures that the total mass in the system is dictated by the ideal gas law.

The concentration of electrons in the system can be calculated via the assumption of quasi-neutrality which states that

$$[e] = [\text{positive ions}] - [\text{negative ions}] \tag{3.32}$$

As indicated in Section 3.1 the values of the reaction rate coefficients k are normally tabulated directly in units of cm^3/s for two-body reactions and in units of cm^6/s for three-body reactions. In some cases however, only the collision cross-sections are available. In this case, the value of the reaction rate coefficients can be derived from the collision cross-sections. Assuming a Maxwellian energy distribution in the plasma particles and assuming that the reaction cross-section σ can be approximated by a linear function $C(E - E_{th})$ as shown in Figure 3.1, the reaction rate coefficient can be calculated from the collision cross-section as follows[62]

$$k = C\left(\frac{8e}{\pi m_{coll}}\right)^{\frac{1}{2}} E_{th}^{\frac{3}{2}} \left(\frac{kT_{coll}}{eE_{th}}\right)\left(\frac{1+2kT_{coll}}{eE_{th}}\right)\exp\left(\frac{-eE_{th}}{kT_{coll}}\right) \tag{3.33}$$

where C is the linear slope of the collision cross section in the threshold region as shown in Figure 3.1 in cm^2/eV, E_{th} is the threshold energy of the collision cross-section as shown in Figure 3.1 in eV, e is the electron charge (1.602×10^{-19} C), k is Boltzmann's constant (8.6184×10^{-5} eV/K), m_{coll} is the mass of the colliding species in kg, and T_{coll} is the temperature of the colliding species in eV. All collision cross-sections which were used in this study have been included in Appendix C.

A schematic of the overall calculation scheme has been outlined in Figure 3.2. After initializing all necessary variables, the system pressure, electron and gas temperatures, and choosing whether the calculation will be using a constant pressure or a constant volume assumption in the ideal gas law, the first approximate species concentrations are calculated via the transport equation and the mass balance relationships. These values are compared to the previous values, and a fixed point iteration is implemented until the calculated concentrations converge. On convergence, the calculated values are saved in an array, the next desired physical condition (T_g, T_e, and p) is chosen and the process is repeated. The values for the fixed point iteration are now initialized to the values which have just been calculated. Since they represent a good approximation for the next fixed point iteration, the choice of these initial values tends to stabilize and accelerate the calculations. In circumstances where small changes in T_e or T_g cause rapid changes in the species concentrations, it may be necessary to implement a feedback routine which changes the incremental temperature value based upon the number of iterations necessary for the fixed point iteration to reach stable values, as indicated in Figure 3.2. Similarly, the choice of the order in which the species concentrations are calculated in can significantly affect the stability and speed of the computation.

Programs used to calculated the chemical kinetic models in the present study have been included in Appendix D. All programs were written in ANSI standard FORTRAN 77 on a VAX 8600 using a VMS operating system. Since the compiler used 32-bit arithmetic by default, all codes were written in double precision with extended precision exponents (VAX G-floating compiler option) and checks for both arithmetic overflow and underflow were made. This high degree of precision is essential for the proper execution of the code.

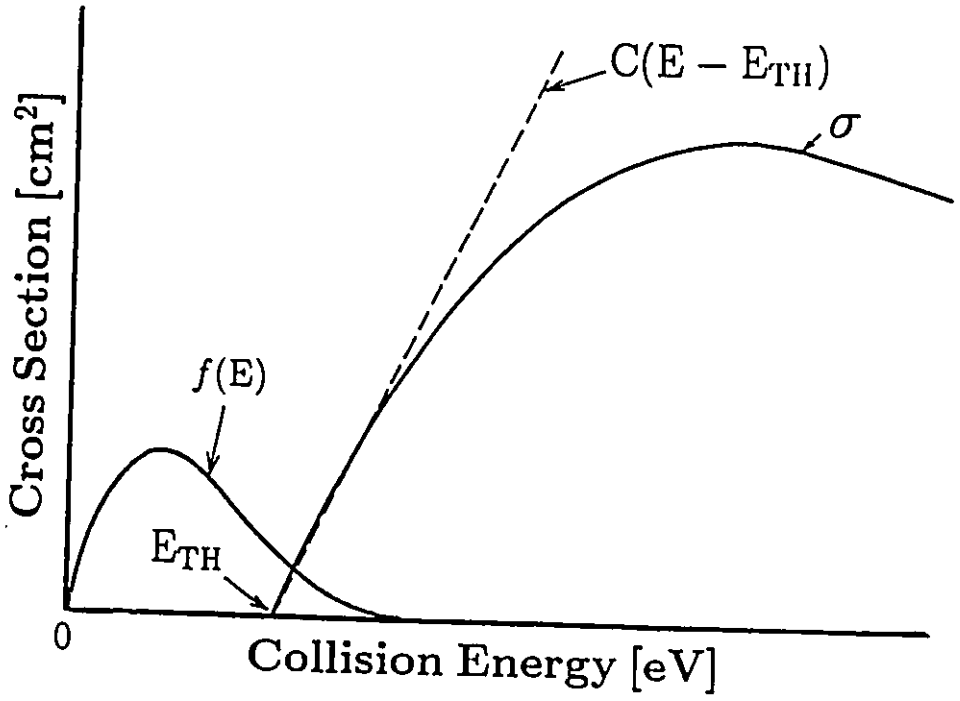

Figure 3.1: Typical collision cross section σ and Maxwellian energy distribution $f(E)$ of particles in a thermal plasma.

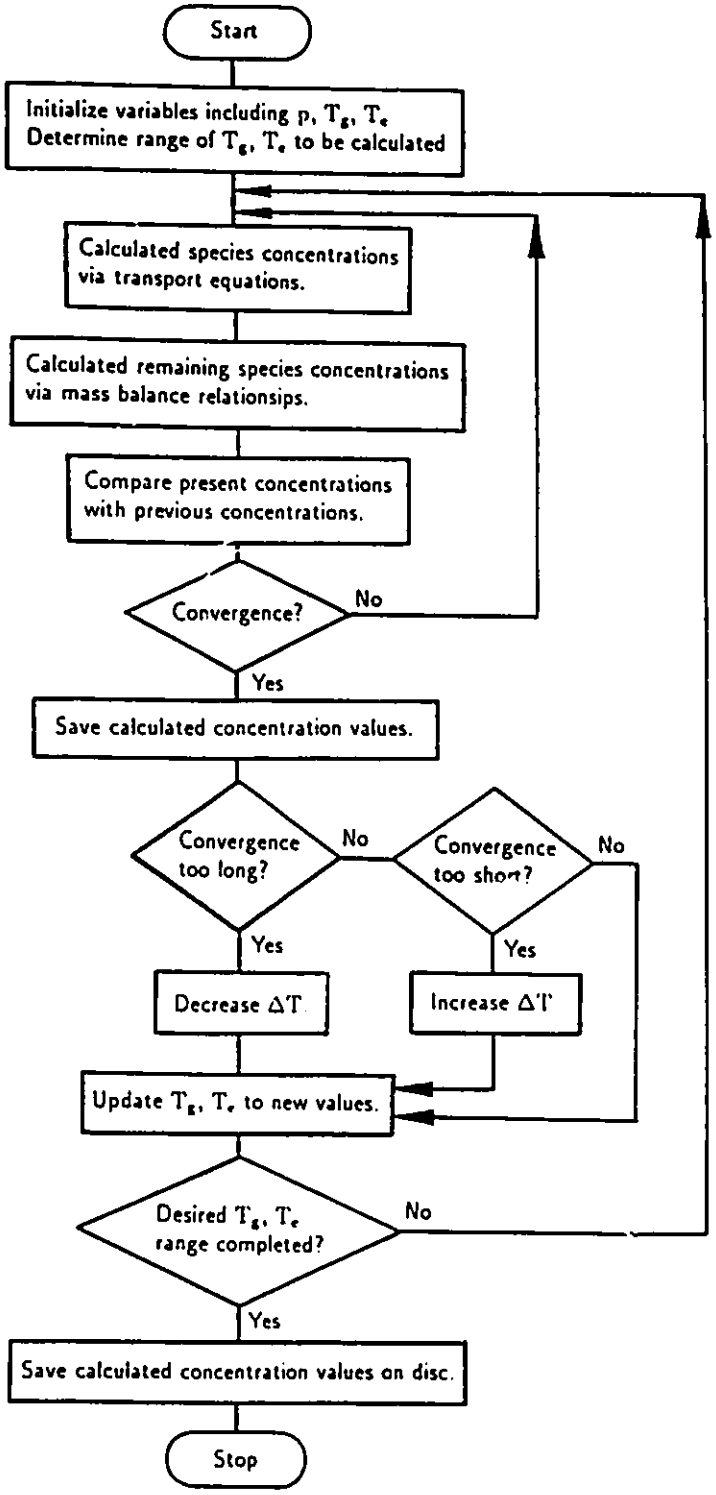

Figure 3.2: Schematic of the calculation scheme used to solve the chemical kinetic model.

Chapter 4

Numerical Model of Ar Thermal Plasma

4.1 Ar Thermal Plasmas

Argon is frequently the gas of choice in situations where an inert monatomic gas is needed. Its thermodynamic and fluid mechanical properties are well known over a wide range of temperatures and pressures[68][71], and it can be obtained in large quantities in ultra-pure form at a reasonable cost.

Electrical discharge experiments often utilize argon as a plasma gas to minimize electrode wear and to take advantage of its inert properties and relatively low breakdown voltage. Under these conditions, it is often of interest to calculate the chemical composition of argon in the discharge region.

In a thermal plasma, the most commonly accepted method of modelling the behaviour of argon is to assume that the argon gas is in a state of equilibrium with its first ionized state[72]. Under this condition, the Law of Mass Action in the form of the Saha equation, as discussed in Chapter 1, can be used to calculate the relative degree of ionization in the plasma. The first ionization energy of argon is $E_{i,Ar} = 15.769$ eV. Over the temperature ranges considered in this work the ratio of the partition functions $U_{i,Ar}/U_{a,Ar} = 6$ for argon[35]. Assuming quasi-neutrality in the generated plasma, $N_e \approx N_i$, the Saha equation can be used to calculate the electron or

argon ion density. The Saha equation neglects to account for the detailed mechanisms within the argon plasma which lead to ionization however as discussed in Chapter 1. The presence of long-lived metastable excited states, the existence of molecular ions, and the chemical reactions relating these species with the gaseous and ionized states of argon cannot be considered.

Numerous models have been assembled which account for a large number of collisional and radiative processes occurring in argon plasmas[73]-[82]. Notable examples of extensive models include those of Bacri and Gomez[81] and Vlček[82] who include 20 and 65 electronic levels respectively in their argon models as well as diffusion, three body reactions and thermal reactions. This type of model is useful in cases where it is desirable to predict the population of various electronically excited levels in argon, particularly in low pressure, high electron temperature plasmas. Surprisingly, none of these models account for the presence of molecular ions however, in spite of the fact that the importance of molecular ions in discharges of this type has been well established for quite some time[83]-[87].

Although these extensive collisional radiative models have commonly been used to model thermal plasma discharges, the differentiation between dozens of different closely spaced electronic levels is unnecessary for the prediction of the degree of ionization and the concentration of ionic species. In particular, considering the range of temperatures under consideration ($T \leq 20000$ K), and the large energy gap between the argon ground level and the first excited state (11.684 eV), the sum of all electrons which exist in the excited states constitutes less than 0.1% of the total number of electrons in the system[81]. For this reason, other investigators have chosen simplified argon models which account for 3 or 4 levels including the ground state, one or two excited states, and the ionized state[88]-[92]. A recent study by Repetti et al.[93] which compares a 10-level model with a 4-level model shows that there are no significant differences between the two models under the typical conditions encountered in medium to atmospheric pressure argon thermal plasmas.

In the following model, an attempt will be made to assemble a simple, yet useful chemical kinetic model which:

- Takes into account both thermal and electron impact reactions

- Includes ion-molecule reactions, and diffusive and recombinative effects
- Considers all important metastable, excited states and molecular ions
- Relies primarily on experimentally derived reaction rate constants
- Can account for electron temperature and gas temperature non-equilibrium and pressure effects.

The objective is to create a model which is extensive enough to be applicable under a wide variety of discharge conditions including arc discharges, glow discharges and plasma jets, yet simple enough to be effective as a building block toward more complex, multi-component chemical kinetic models. The present model, which uses a 4-level approach is substantially different from previous models in its almost exclusive use of experimentally derived reaction rates, and the inclusion of the Ar_2^+ molecular ion.

4.2 Chemical Reactions

A detailed list of reactions considered in the present model and their rate constants k have been outlined in Table 4.1. The species considered include neutral argon Ar, excited argon Ar*, and metastable argon Ar**, and the ionized species Ar^+ and Ar_2^+. T_g and T. represent the neutral gas and electron temperatures respectively and the neutral gas temperature is assumed to be equal to the temperatures of the excited and ionized species.

The main sources of Ar^+ are the two step processes of thermal ionization

$$Ar + Ar \xrightarrow{k_{Ar1}} Ar^* + Ar$$

$$Ar^* + Ar \xrightarrow{k_{Ar2}} Ar^+ + e + Ar$$

and electron impact ionization

$$Ar + e \xrightarrow{k_{Ar4}} Ar^{**} + e$$

Table 4.1: Reactions for the argon system.

Reactions	Reaction Rate Constants $[cm^3/s]$,$[cm^6/s]$[1]		T_g, T_e Dependence [K]	Ref.
$Ar + Ar \xrightarrow{k_{Ar1}} Ar^* + Ar$ $Ar^* + Ar \xrightarrow{k_{Ar2}} Ar^+ + e + Ar$	k_{Ar1} k_{Ar2}	$10^{(-78.67+14.89\log_{10}(T_g))}$ $10^{(-36.83+6.11\log_{10}(T_g))}$	$7000 \leq T_g \leq 12000$ $7000 \leq T_g \leq 12000$	[94] [94]
$Ar + e \xrightarrow{k_{Ar3}} Ar^+ + e + e$	k_{Ar3}	$2.0 \times 10^{-10} T_e^{1/2}(1 + 1.1 \times 10^{-5} T_e)$* $\exp(-1.8 \times 10^5/T_e)$	Cross Section	[62][95]
$Ar + e \xrightarrow{k_{Ar4}} Ar^{**} + e$ $Ar^{**} + e \xrightarrow{k_{Ar5}} Ar^+ + e + e$	k_{Ar4} k_{Ar5}	$3.3 \times 10^{-11} T_e^{1/2}(1 + 1.5 \times 10^{-5} T_e)$* $\exp(-1.4 \times 10^5/T_e)$ $3.0 \times 10^{-10} T_e^{1/2}(1 + 4.5 \times 10^{-5} T_e)$* $\exp(-4.5 \times 10^4/T_e)$	Cross Section Cross Section	[96] [97][98]
$Ar^{**} + Ar^{**} \xrightarrow{f_{Ar6} k_{Ar6}} Ar^+ + Ar + e$ $Ar^{**} + Ar^{**} \xrightarrow{(1-f_{Ar6}) k_{Ar6}} Ar_2^+ + e$	k_{Ar6} f_{Ar6}	6.12×10^{-10} 0.5		[99]
$Ar^+ + Ar + Ar \xrightarrow{k_{Ar7}} Ar_2^+ + Ar$	k_{Ar7}	$2.3 \times 10^{-31}(T_g/300)^{-0.75}$	Theory	[100][101]
$Ar^+ + e \xrightarrow{k_{Ar8}} Ar + h\nu$	k_{Ar8}	$6.3 \times 10^{-10}(300/T_e)^{0.5}$	Theory	[102][62]
$Ar^+ + e + e \xrightarrow{k_{Ar9}} Ar + e$	k_{Ar9}^1	$10^{\left(\sum_{i=0}^{3}\sum_{j=0}^{2} A_{i,j}(\log_{10}(\frac{T_e}{15.75}))^i (\frac{1000}{T_e})^j\right)}$	$300 \leq T_e \leq 16000$	[103][104]
$Ar_2^+ + e \xrightarrow{k_{Ar10}} Ar + Ar$	k_{Ar10}	$7.5 \times 10^{-7}(300/T_e)^{0.67}$ $4.38 \times 10^{-7}(670/T_g)^{1.5}$ $4.38 \times 10^{-7}(670/T_g)^{1.5}(T_g/T_e)^{0.60}$	$300 \leq T_e \leq 670$, $T_g \leq 670$ $T_g \geq 670$, $T_g \geq T_e$ $T_g \geq 670$, $T_g \leq T_e$	[102] [105][106]

[1] $[cm^3/s]$ for two-body reactions and $[cm^6/s]$ for three-body reactions.

[2] where $A_{0,0} = -13.319$ $A_{0,1} = 3.9654$ $A_{0,2} = -0.554716$
$A_{1,0} = -0.30894$ $A_{1,1} = 1.4089$ $A_{1,2} = -0.24503$
$A_{2,0} = -0.10322$ $A_{2,1} = 0.73602$ $A_{2,2} = -0.55010$
$A_{3,0} = 0.028512$ $A_{3,1} = -0.1206$ $A_{3,2} = 0.055961$

Table 4.2: Diffusion constants for the argon system at 1 Torr, 300 K.

Diffusion Species	D_g [cm^{2}Torr/s][a]	Ref.
Ar^*-Ar	49	[62]
Ar^{**}-Ar	49	
Diffusion Species	D_i [cm^{2}Torr/s][b]	Ref.
Ar^+-Ar	75	[62]
Ar_2^+-Ar	34.5	

[a] The values of the gaseous diffusion coefficients D_{Ar^*-Ar} and $D_{Ar^{**}-Ar}$ used in equations 4.1 and 4.2 were calculated as follows:

$$D = \left(\frac{D_g}{p}\right)\left(\frac{T_g}{300}\right)$$

[b] The values of ambipolar diffusion coefficients D_{Ar^+-Ar} and $D_{Ar_2^+-Ar}$ used in equations 4.3 and 4.4 were calculated as follows:

$$D = \left(\frac{D_i}{p}\right)\left(\frac{T_g}{300}\right)\left(1 + \frac{T_e}{T_g}\right)$$

where p is the system pressure in Torr.

$$Ar^{**} + e \xrightarrow{k_{Ar3}} Ar^{+} + e + e$$

via excited (*) or metastable (**) intermediaries. In this case, Ar* is assumed to be in the first excited state as described by McLaren and Hobson[94] and Ar** represents the sum of the 4^3P_2 and 4^3P_0 states as determined by Vriens[96]. The main source of Ar_2^+ is the three-body conversion process

$$Ar^{+} + Ar + Ar \xrightarrow{k_{Ar7}} Ar_2^{+} + Ar$$

Three-body recombination

$$Ar^{+} + e + e \xrightarrow{k_{Ar9}} Ar + e$$

and dissociative recombination

$$Ar_2^{+} + e \xrightarrow{k_{Ar10}} Ar + Ar$$

are the dominant plasma loss processes. Reaction rate constants k_{Ar1} and k_{Ar2} were derived by fitting the data obtained by McLaren and Hobson[94]. The reaction rate constants for k_{Ar3}, k_{Ar4}, and k_{Ar5} were derived by assuming the colliding species have a Maxwellian energy distribution and by using a linear approximation of the collision cross section of Vriens[96] and Ton-That[98] in the threshold region as described in Chapter 3. These cross sections can be found in Appendix C. In order to illustrate the relative importance of these reactions at various temperatures, Figure 4.1 shows the gas and electron temperature dependencies of reaction rate constants k_{Ar1}-k_{Ar10} as well as the equivalent "k" values of the diffusion reactions included in the model. As a caveat, it should be noted that the possible error of values of the reaction rate constants shown in Table 4.1 and Figure 4.1 can vary between 10-100%. This is also true of the reaction rate constants shown in Chapters 5 and 6 for the Ar-C and Ar-CO_2 models. As such, the temperature dependent concentrations of the species in a thermal plasma predicted by the present models can be considered to be accurate to within one order of magnitude. A summary of the chemical kinetics of the Ar system has been outlined in Figure 4.2, where Ar1-Ar10 refer to the reactions outlined in Table 4.1.

Argon dimers Ar_2, excimers Ar_2^*, excited excimers Ar_2^{**} and trimers Ar_3 have not been included due to the relative uncertainty of the reactions associated with their formation and their low relative concentrations in thermal plasmas[92][107].

The coupled rate equations for the different species at the centre of a cylindrical discharge tube can be written as follows:

$$\frac{d[Ar^*]}{dt} = k_{Ar1}[Ar]^2 - k_{Ar2}[Ar^*][Ar] - \frac{q^2 D_{Ar^*-Ar}[Ar^*]}{R^2} \quad (4.1)$$

$$\frac{d[Ar^{**}]}{dt} = k_{Ar4}[Ar][e] - k_{Ar5}[Ar^{**}][e] - 2k_{Ar6}[Ar^{**}]^2 - \frac{q^2 D_{Ar^{**}-Ar}[Ar^{**}]}{R^2} \quad (4.2)$$

$$\frac{d[Ar^+]}{dt} = k_{Ar2}[Ar^*][Ar] + k_{Ar3}[Ar][e] + k_{Ar5}[Ar^{**}][e] + f_{Ar6}k_{Ar6}[Ar^{**}]^2 \quad (4.3)$$
$$-k_{Ar7}[Ar^+][Ar]^2 - k_{Ar8}[Ar^+][e] - k_{Ar9}[Ar^+][e]^2 - \frac{q^2 D_{Ar^+-Ar}[Ar^+]}{R^2}$$

$$\frac{d[Ar_2^+]}{dt} = (1 - f_{Ar6})k_{Ar6}[Ar^{**}]^2 + k_{Ar7}[Ar^+][Ar]^2 \quad (4.4)$$
$$-k_{Ar10}[Ar_2^+][e] - \frac{q^2 D_{Ar_2^+-Ar}[Ar_2^+]}{R^2}$$

where $[X]$ represents the volume concentration of species X, R is the radius of the cylindrical system, and $[e]$ represents the concentration of electrons. A zero order Bessel function has been used to approximate radial density profiles of the various species in order to calculate the loss by radial diffusion in a cylindrical tube[108] as described in Chapter 3. In the model, the radius R of the system and the pressure conditions were chosen to be representative of the particular discharge under consideration. For arc discharges, thermal equilibrium ($T_e = T_g$) and constant pressure assumptions were made. A radius of 0.01 m was chosen in this case as arc discharges tend to be confined to smaller dimensions. To model glow or RF discharge conditions, a larger radius of 0.05 m was chosen to reflect the typically larger plasma dimensions associated with these discharge conditions, and a constant volume assumption was made. Since glow or RF discharges typically occur under reduced pressure conditions, a temperature non-equilibrium was assumed ($T_e \neq T_g$) in which T_g is constant and T_e is variable.

The diffusion coefficients used in the model are listed in Table 4.2. Assuming the system is in steady state ($d[X]/dt = 0$), and grouping terms, equations 4.1–4.4

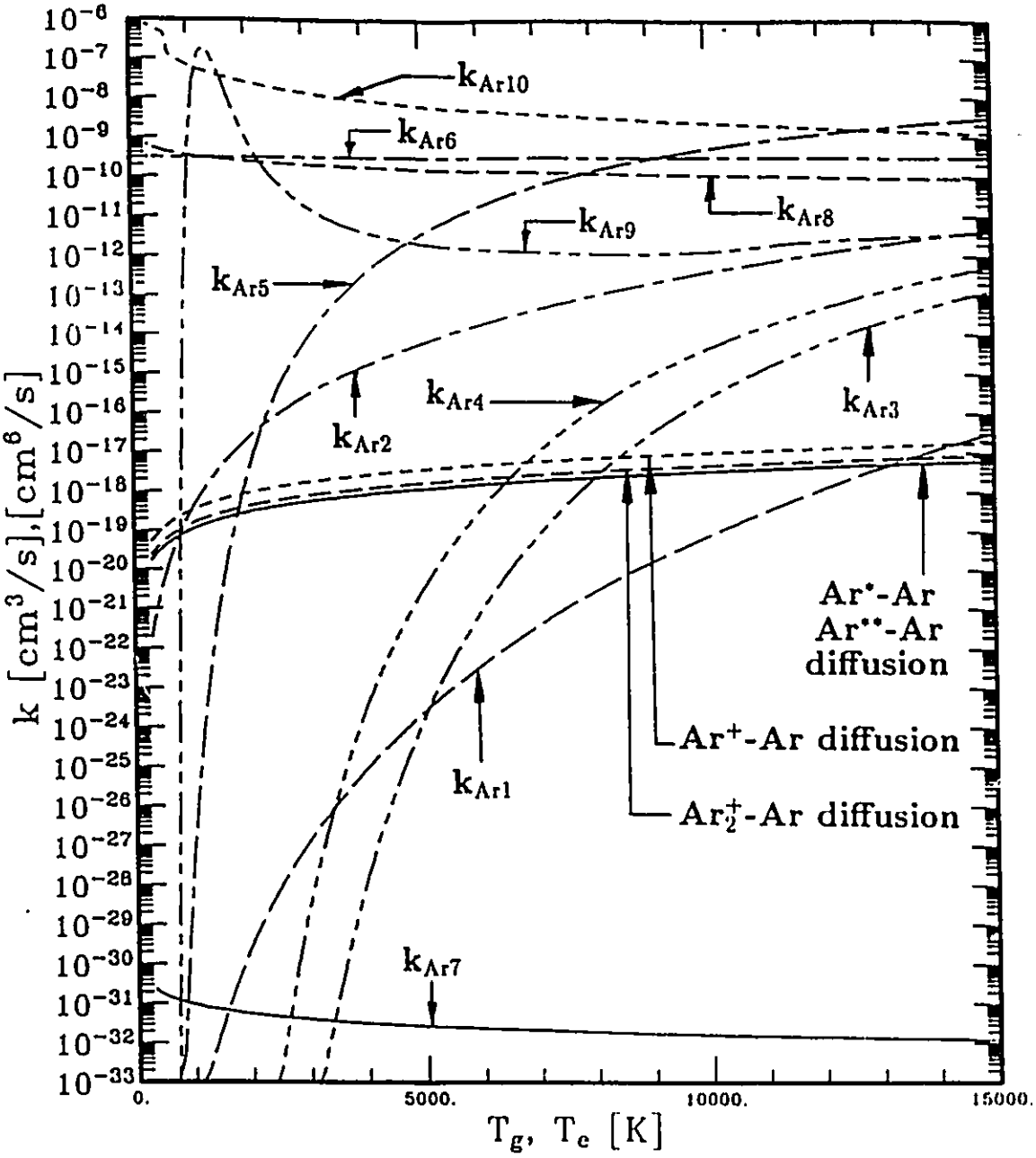

Figure 4.1: Temperature dependence of the values of the reaction rate constants for the chemical kinetic argon thermal plasma model.

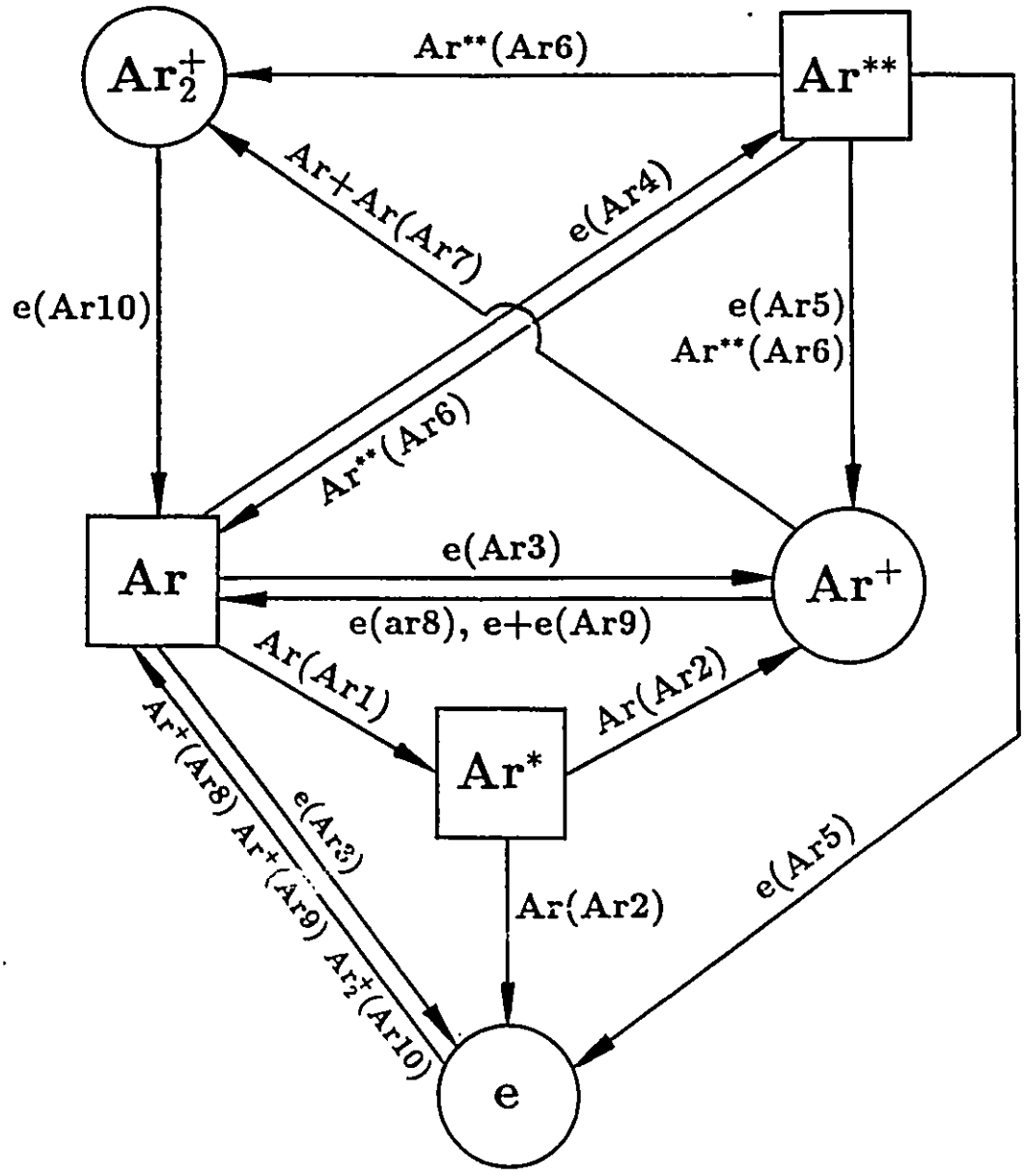

Figure 4.2: Plasma chemistry for an Ar discharge including molecular ions, and thermal and electron impact reactions.

reduce to a series of coupled polynomial equations which can be solved numerically as described in Chapter 3.

Over the range of temperatures considered in this model, the initial concentration of argon in the system can be derived with minimal error using the ideal gas law (see Chapter 3). Significant depletions of the original argon gas concentration can be corrected by using a mass balance as follows:

$$[Ar] = [Ar]_{IG} - [Ar^*] - [Ar^{**}] - [Ar^+] - [Ar_2^+] \tag{4.5}$$

where $[Ar]_{IG}$ represents the concentration of argon as calculated by the ideal gas law. Assuming the existence of a quasi-neutral plasma, the electron concentration can be calculated using a charged particle balance:

$$[e] = [Ar^+] + [Ar_2^+] \tag{4.6}$$

4.3 Numerical Results

4.3.1 Gas Temperature Effects

The concentration of ion and neutral species as a function of gas temperature under thermodynamic equilibrium conditions ($T_e = T_g$) as predicted by the chemical kinetic model are shown in Figure 4.3 for p = 760 Torr. The plasma density predicted by the Saha equation is also shown for comparison.

As shown in Figure 4.3, the concentrations of excited argon Ar^* and metastable argon Ar^{**} increase with increasing gas temperature through thermal and electron impact excitation respectively. At temperatures less than $T_g = 5500$ K where thermal ionization reactions have the greatest influence on the Ar^+ concentration, the Ar^* concentration is larger than the Ar^{**} concentration. At temperatures greater than $T_g = 5500$ K, the Ar^{**} concentration exceeds that of the Ar^*, tending to reflect the increased importance of electron impact ionization reactions to the generation of Ar^+.

Figure 4.3 shows that the electron density increases with increasing gas temperature, as expected from the Saha equation. However, the results tend to indicate

that the Saha equation may underestimate the plasma density at temperatures less than $T_g = 3800$ K and overestimate the plasma density at temperatures greater than $T_g = 4000$ K when compared with the chemical kinetic model. The discrepancies between the two models are particularly apparent in the $T_g = 5000$–10000 K temperature range. Here the Saha equation predicts an electron density which is two to three orders of magnitude greater than that calculated by the chemical kinetic model. This discrepancy may be due to a plasma loss via the dissociative recombination process of Ar_2^+

$$Ar_2^+ + e \xrightarrow{k_{Ar10}} Ar + Ar$$

which is not considered in the Saha model. At temperatures greater than $T_g = 10000$ K, where Ar^+ and electron impact phenomena dominate in the chemical kinetic model, the plasma concentration is also less than that predicted by the Saha equation, but the gas temperature dependence is proportional to the concentration predicted by the Saha equation. Sensitivity analysis indicates that both radiative recombination,

$$Ar^+ + e \xrightarrow{k_{Ar8}} Ar + h\nu$$

as well as three-body recombination

$$Ar^+ + e + e \xrightarrow{k_{Ar9}} Ar + e$$

have a significant effect on the Ar^+ density in this temperature range. The Saha equation cannot account for three-body recombination, which may explain its overestimation of the plasma density above $T_g = 10000$ K. It is also interesting to note that below $T_g = 9000$ K the chemical kinetic model predicts that Ar_2^+ forms the dominant ionized species, a fact which the Saha equation is unable to predict by its very nature. The dominant Ar_2^+ generation and loss processes, three body conversion

$$Ar^+ + Ar + Ar \xrightarrow{k_{Ar7}} Ar_2^+ + Ar$$

and dissociative recombination

$$Ar_2^+ + e \xrightarrow{k_{Ar10}} Ar + Ar$$

constitute a different physical mechanism than that underlying the Saha equation. Such being the case, it is not surprising that the temperature dependence of the Ar_2^+ concentration is not proportional to the ion density predicted by the Saha equation in this temperature range. In fact, the two cross over between $3800 \leq T_g \leq 4000$ K.

4.3.2 Electron Temperature Effects

In order to outline the effect of electron temperature non-equilibrium with gas temperature on the system, the chemical kinetic model was used to predict the temperature dependent species concentrations using a constant gas temperature, and an electron temperature which varied between $T_e = 300$–20000 K.

Figure 4.4 illustrates the ion and neutral species concentrations as a function of electron temperature at p = 760 Torr with $T_g = 300$ K. As shown in Figure 4.4, the concentrations of Ar^+, Ar_2^+, and Ar^{**} increase with increasing electron temperature and the metastable atom density Ar^{**} can be much larger than the plasma density.

At temperatures less than $T_e = 6000$ K the physical conditions are such that the plasma cannot sustain itself. This fact manifests itself in a steep decline in the plasma density below $T_e = 6000$ K. This temperature will be referred to as the plasma "onset" temperature from here on in. Similar to Figure 4.3, Ar_2^+ is the dominant ion at temperatures less than $T_e = 17000$ K, most likely due to the fact that the three-body reaction

$$Ar^+ + Ar + Ar \xrightarrow{k_{Ar7}} Ar_2^+ + Ar$$

converts a large fraction of the generated Ar^+ to Ar_2^+. At temperatures greater than $T_e = 12500$ K, the electron impact ionization reactions

$$Ar + e \xrightarrow{k_{Ar3}} Ar^+ + e + e$$

$$Ar + e \xrightarrow{k_{Ar4}} Ar^{**} + e$$

$$Ar^{**} + e \xrightarrow{k_{Ar5}} Ar^+ + e + e$$

are large enough to cause Ar^+ to become the dominant ion.

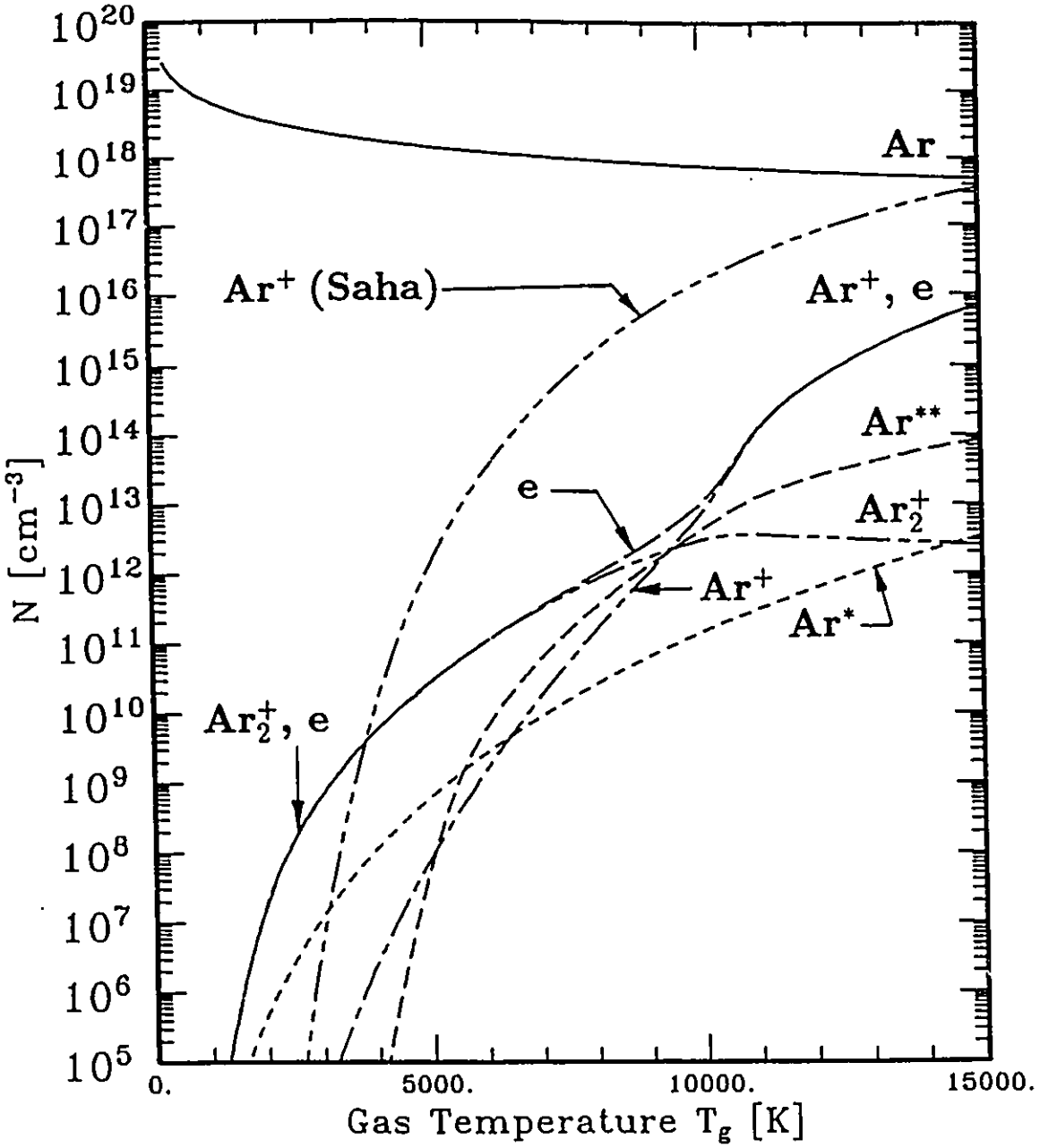

Figure 4.3: Ionized and neutral species concentrations as a function of gas temperature for argon with p = 760 Torr, and $T_e = T_g$.

Ion and neutral concentrations are shown as a function of electron temperature with T_g = 5000 K and p = 760 Torr in Figure 4.5. Increasing the gas temperature to T_g = 5000 K may have the effect of increasing the Ar^+ concentration due to generation by thermal impact ionization reactions

$$Ar + Ar \xrightarrow{k_{Ar1}} Ar^* + Ar$$

$$Ar^* + Ar \xrightarrow{k_{Ar3}} Ar^+ + e + Ar$$

This causes the plasma to sustain at constant values below T_e = 8000 K with Ar_2^+ as the dominant ion most likely due to the effect of the three-body reaction

$$Ar^+ + Ar + Ar \xrightarrow{k_{Ar7}} Ar_2^+ + Ar$$

The concentration of Ar^* remains at a constant value most likely due to the fact that the generation and loss mechanisms of this species depends only on the gas temperature, which is a constant in this case. The Saha equation also appears as a horizontal line in Figure 4.5 for the same reason since it assumes by definition that the system is in local thermodynamic equilibrium and cannot be modified to account for temperature non-equilibria.

A comparison of Figure 4.5 with Figure 4.4 shows that the electron temperature below which Ar_2^+ becomes the dominant ion decreases with increasing gas temperature. This may be due to the fact that the increase in gas temperature causes additional generation of Ar^+ ions through the thermal ionization reactions

$$Ar + Ar \xrightarrow{k_{Ar1}} Ar^* + Ar$$

$$Ar^* + Ar \xrightarrow{k_{Ar3}} Ar^+ + e + Ar$$

4.3.3 Gas Pressure Effects

Figure 4.6 illustrates the ion and neutral species concentrations as a function of electron temperature at p = 10 Torr, and T_g = 300 K. A comparison with Figure 4.4, in which p = 760 Torr and T_g = 300 K, shows that the decrease in pressure has

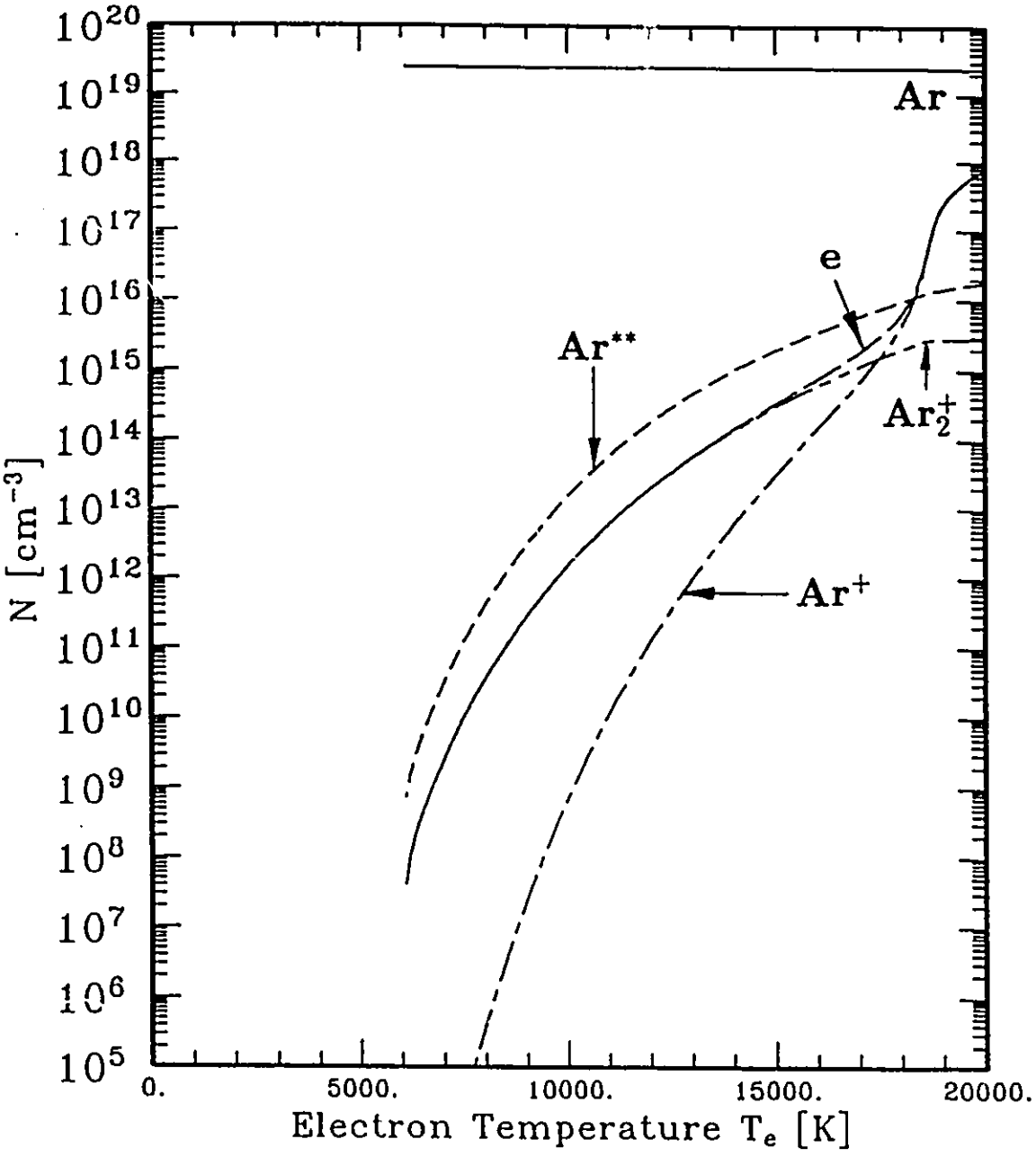

Figure 4.4: Ionized and neutral species concentrations as a function of electron temperature for argon with T_g = 300 K, and p = 760 Torr.

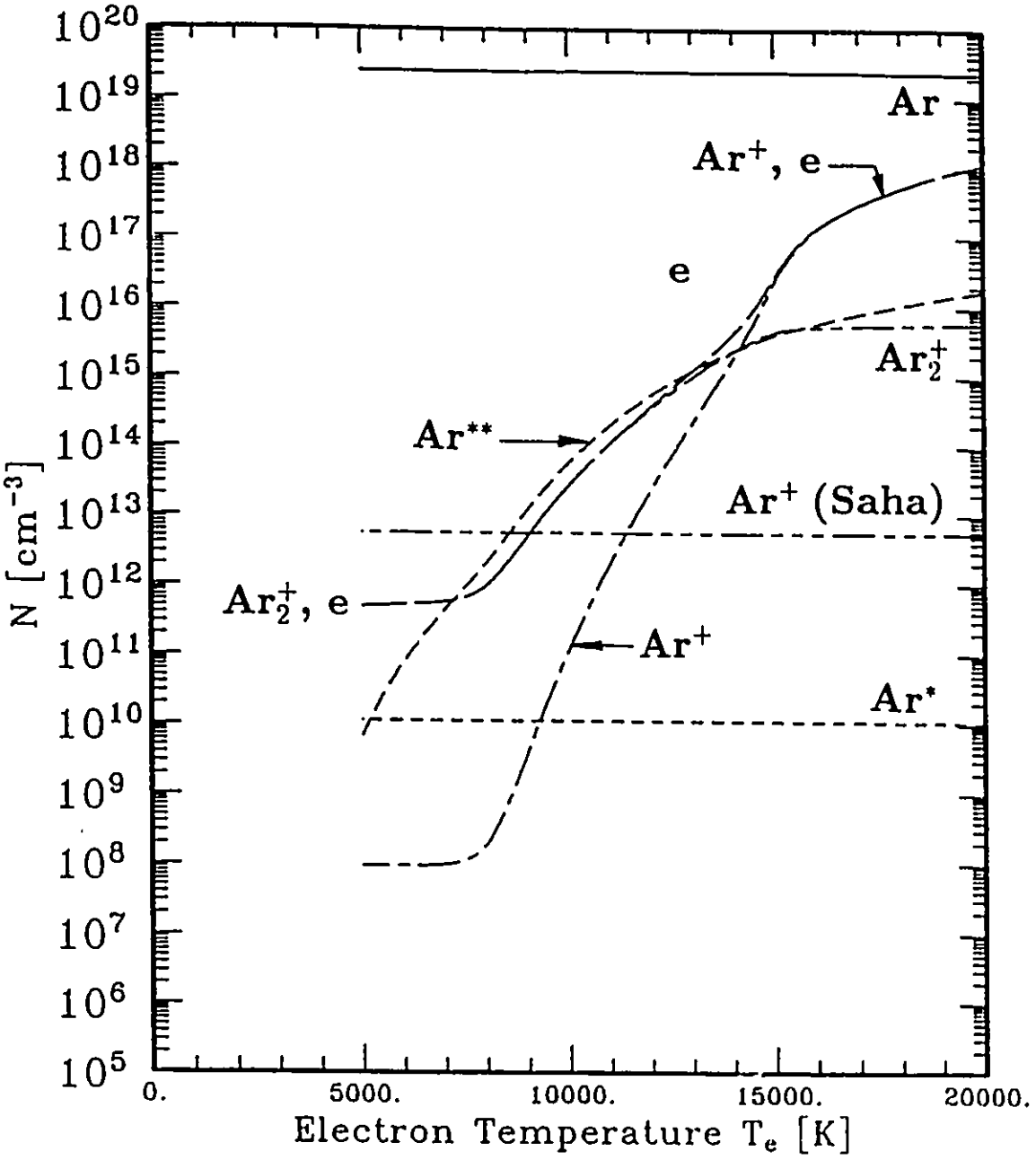

Figure 4.5: Ionized and neutral species concentrations as a function of electron temperature for argon with T_g = 5000 K, and p = 760 Torr.

caused a decrease in the temperature below which Ar_2^+ dominates the ionized species to T_e = 12500 K, and the plasma "onset" temperature has increased to T_e = 8000 K. At temperatures greater than T_e = 12500 K, Ar^+ is the dominant ion, and the Ar_2^+ concentration is virtually unaffected by the electron temperature.

Similar to the case in which p = 760 Torr and the gas temperature is increased to T_g = 5000 K shown in Figure 4.5, increasing the gas temperature to T_g = 5000 K at p = 10 Torr causes the ionized species to reach constant values at temperatures below T_e = 8000 K as shown in Figure 4.7, most likely due to thermal ionization reactions.

Figures 4.8, 4.9, and 4.10 illustrate the ionic and neutral species concentrations as a function of gas temperature for $T_e = T_g$ at p = 100 Torr, 10 Torr and 15200 Torr respectively.

(i) 100 Torr Pressure

In Figure 4.8, the general features shown in Figure 4.3 at p = 760 Torr have been retained, but significant differences are apparent due to the reduction in pressure to p = 100 Torr. Ar_2^+ is still the dominant ionized species at lower temperatures, but the temperature at which Ar^+ becomes the dominant ion is now T_g = 7500 K, as compared to 9000 K at p = 760 Torr. This reduction in gas temperature at which the Ar_2^+ to Ar^+ dominant switch-over point occurs is possibly due to the reduction of the overall Ar density caused by the lower pressure in the system which may reduce the influence of the three-body Ar_2^+ generation reaction

$$Ar^+ + Ar + Ar \xrightarrow{k_{Ar7}} Ar_2^+ + Ar$$

The difference between the Ar^+ concentration predicted by the Saha equation and the chemical kinetic model in the electron impact ionization dominated region ($T_g \geq$ 10000 K) is somewhat larger at p = 100 Torr than at p = 760 Torr. This relative reduction in the plasma density may have been caused by a reduction in the effectiveness of the thermal ionization reactions

$$Ar + Ar \xrightarrow{k_{Ar1}} Ar^* + Ar$$

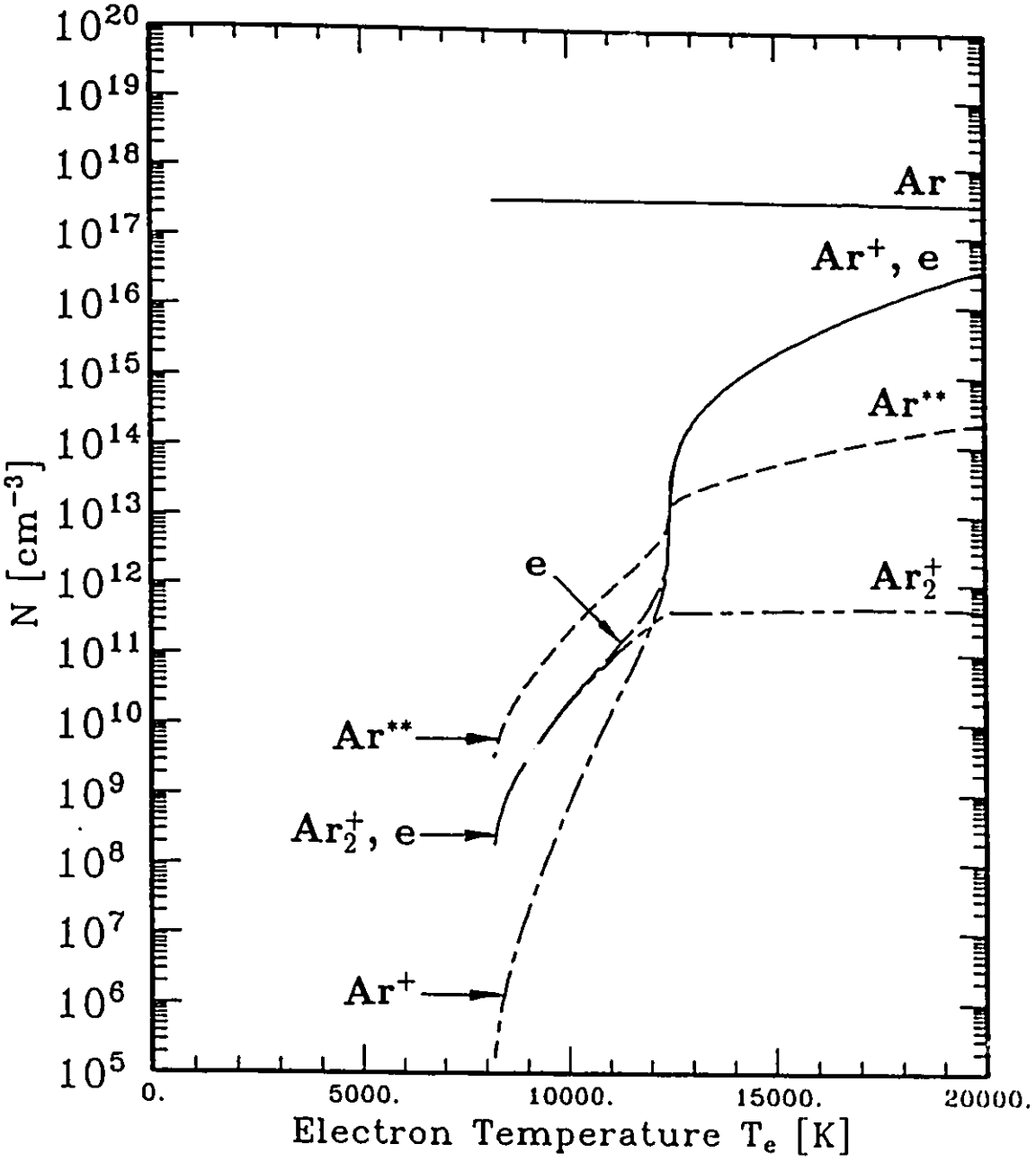

Figure 4.6: Ionized and neutral species concentrations as a function of electron temperature for argon with T_g = 300 K, and p = 10 Torr.

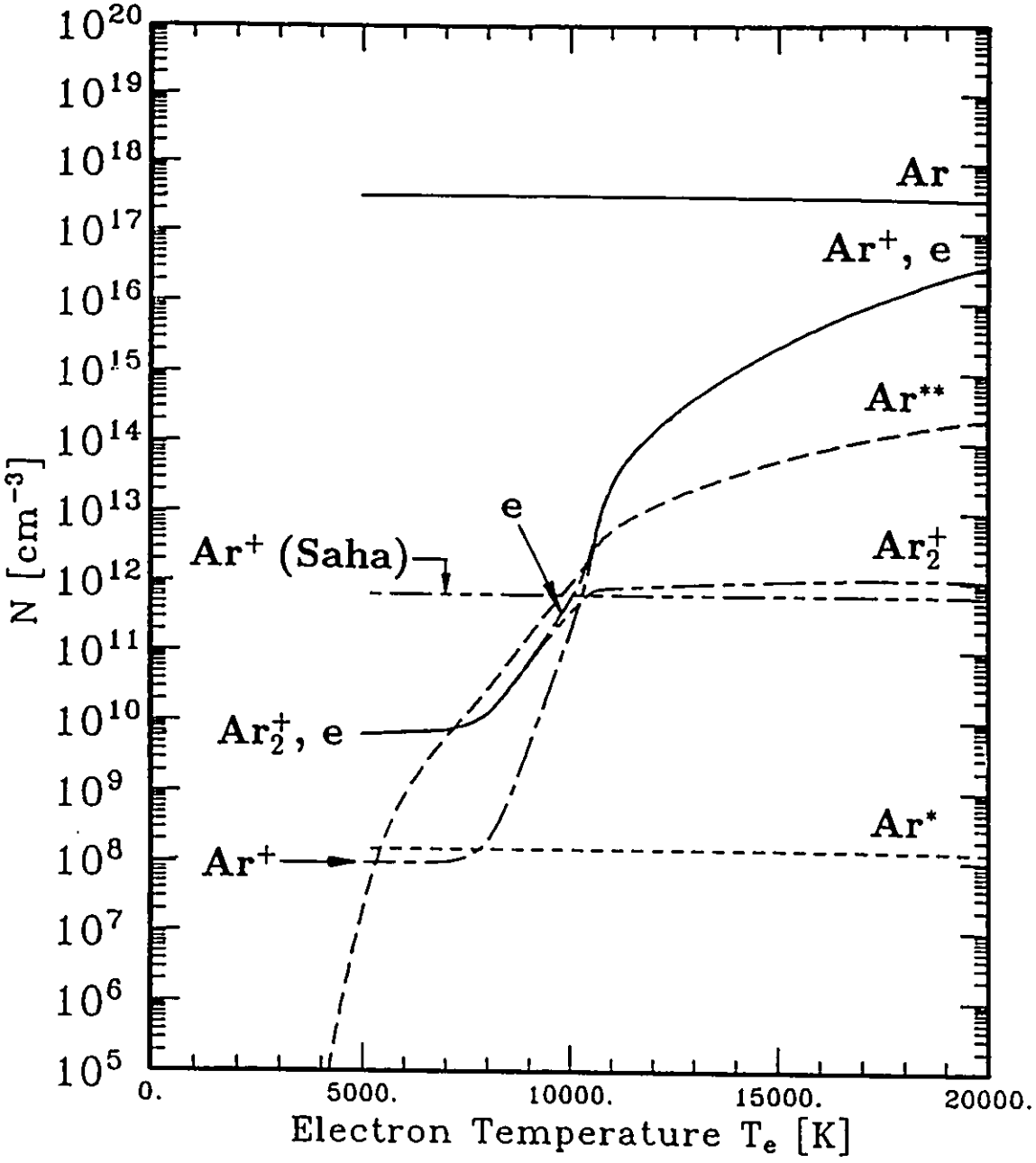

Figure 4.7: Ionized and neutral species concentrations as a function of electron temperature for argon with T_g = 5000 K, and p = 10 Torr.

$$Ar^* + Ar \xrightarrow{k_{Ar3}} Ar^+ + e + Ar$$

which are particulary sensitive to the Ar density. At $T_g = 15000$ K, the Saha equation now predicts full ionization of the argon while the chemical kinetic model still predicts a lower degree of ionization due to the combined effects of diffusion, and the radiative and three-body recombination reactions. The Saha equation includes neither diffusion nor three-body recombination however.

(ii) 10 Torr Pressure

When the pressure is reduced to 10 Torr as shown in Figure 4.9, the plasma density predicted by the Saha equation is invariably greater than that predicted by the present model, and Ar^+ is now the dominant ion over the entire temperature range under consideration. Both of these effects may have been caused by the significant influence of loss of ionized species by diffusion at this reduced pressure. The loss of generated Ar^+ ions is large enough to cause the plasma density to be smaller than that predicted by the Saha equation due to the reduction of thermal ionization as described in the previous section. This reduction in Ar^+ density may be significant enough to affect the three-body conversion reaction

$$Ar^+ + Ar + Ar \xrightarrow{k_{Ar7}} Ar_2^+ + Ar$$

and cause the density of Ar_2^+ to become at least one order of magnitude smaller than that of Ar^+. The predicted Ar_2^+ concentration now exhibits a local maximum at $T_g = 12000$ K as opposed to the broader maxima exhibited in Figures 4.3 and 4.8 at $T_g = 10000$ K and 9000 K respectively. Sensitivity analysis indicates that this local maximum is most likely caused by metastable-metastable collision generated Ar_2^+ via the Ar6 reaction

$$Ar^{**} + Ar^{**} \xrightarrow{f_{Ar6}k_{Ar6}} Ar^+ + Ar + e$$

in the $T_g = 10000$–12000 K temperature range.

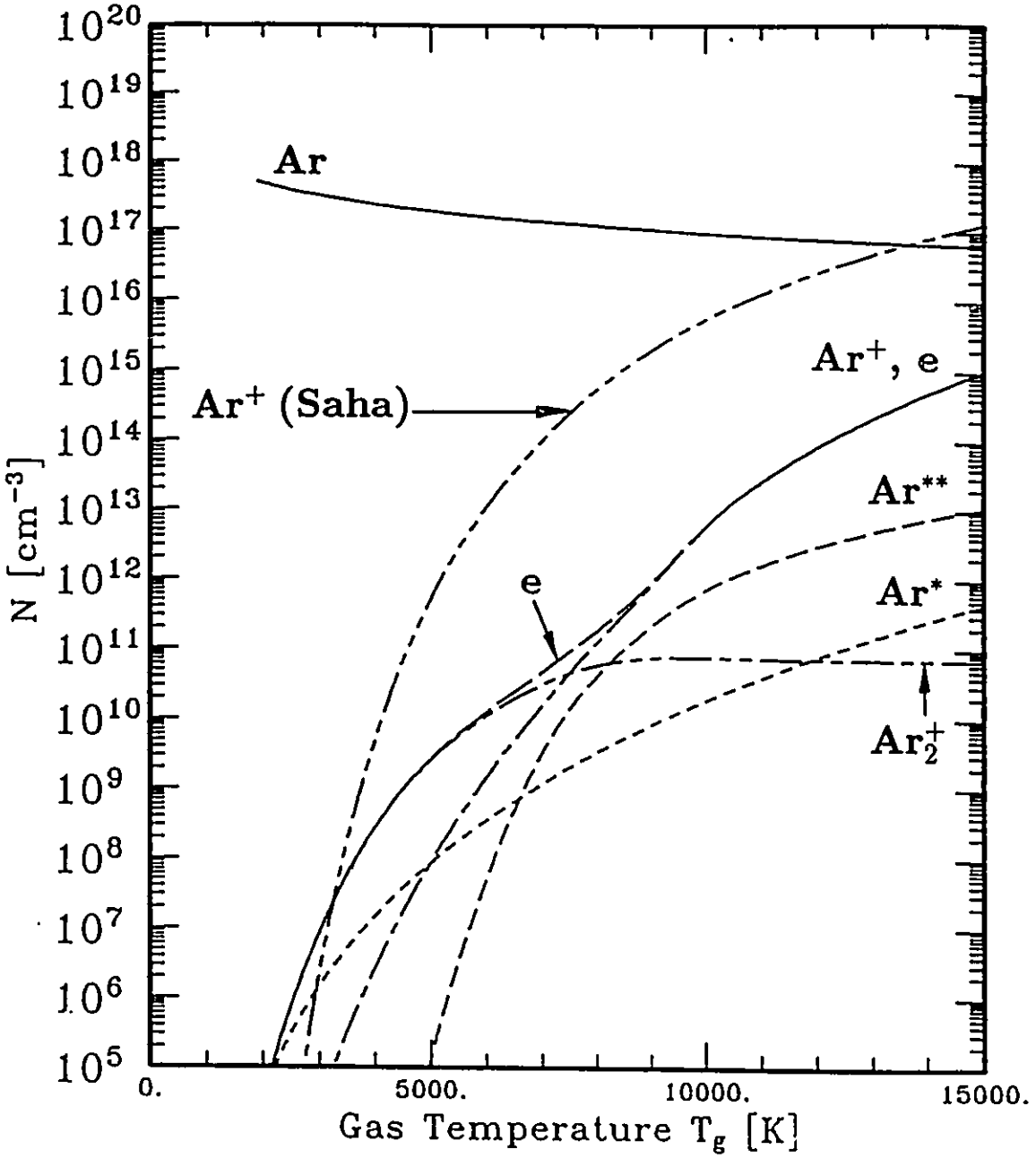

Figure 4.8: Ionized and neutral species concentrations as a function of gas temperature for argon with p = 100 Torr, and $T_e = T_g$.

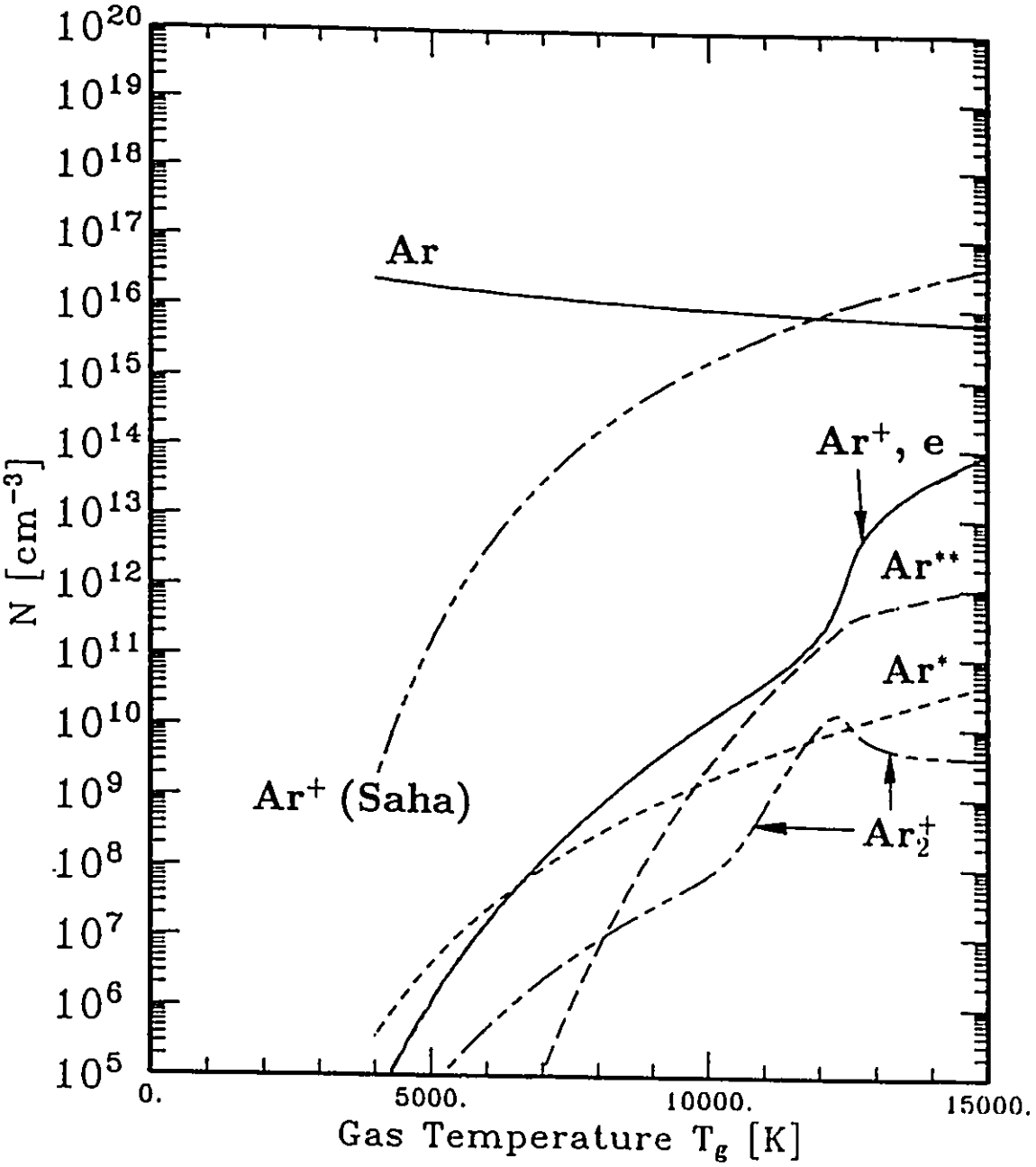

Figure 4.9: Ionized and neutral species concentrations as a function of gas temperature for argon with p = 10 Torr, and $T_e = T_g$.

(iii) 15200 Torr Pressure

Arc discharges are operated not only at atmospheric or reduced pressures. In some cases, wall stabilized arcs are operated at extremely high pressures[43][109]. Considerations of the pressures produced in confined arcs in plasma torches show that high pressures (7600–15200 Torr) can also be expected within the arc itself under this condition. Figure 4.10 shows the temperature dependent ion and neutral compositions at p = 15200 Torr. After accounting for the increase in gas density due to the increase in gas pressure, comparison with Figure 4.3 indicates that the importance of the three body Ar^+ loss processes through the conversion reaction

$$Ar^+ + Ar + Ar \xrightarrow{k_{Ar7}} Ar_2^+ + Ar$$

and the recombination reaction

$$Ar^+ + e + e \xrightarrow{k_{Ar8}} Ar + e$$

may have caused a relative decrease in the level of Ar^+ and a relative increase in the concentration of Ar_2^+. As a result, the Ar_2^+ to Ar^+ dominance transition occurs at a gas temperature of T_g = 12000 K at p = 15200 Torr as opposed to T_g = 10000 K at 760 Torr.

(iv) Summary of Pressure Effects

The gas temperature dependent concentrations of argon and the plasma density (as represented by the electron concentration) for pressures between 1 Torr and 15200 Torr have been summarized in Figure 4.11. The concentrations of Ar^*, Ar^{**}, Ar^+, and Ar_2^+ have been omitted for the sake of clarity. Figure 4.11 illustrates the increases of absolute plasma density which occur with increasing pressure. As shown, the largest increases occur at the lowest pressures, most likely due to the stronger effects of diffusion at these pressures. The Ar_2^+ to Ar^+ dominance transition gas temperatures have also been shown on the temperature dependent electron densities shown in Figure 4.11 to give an indication of the manner in which this temperature increases with increasing pressure. At lower gas pressures (p $\leq$ 10 Torr), Ar^+ forms the dominant ion over the entire temperature and density range under investigation.

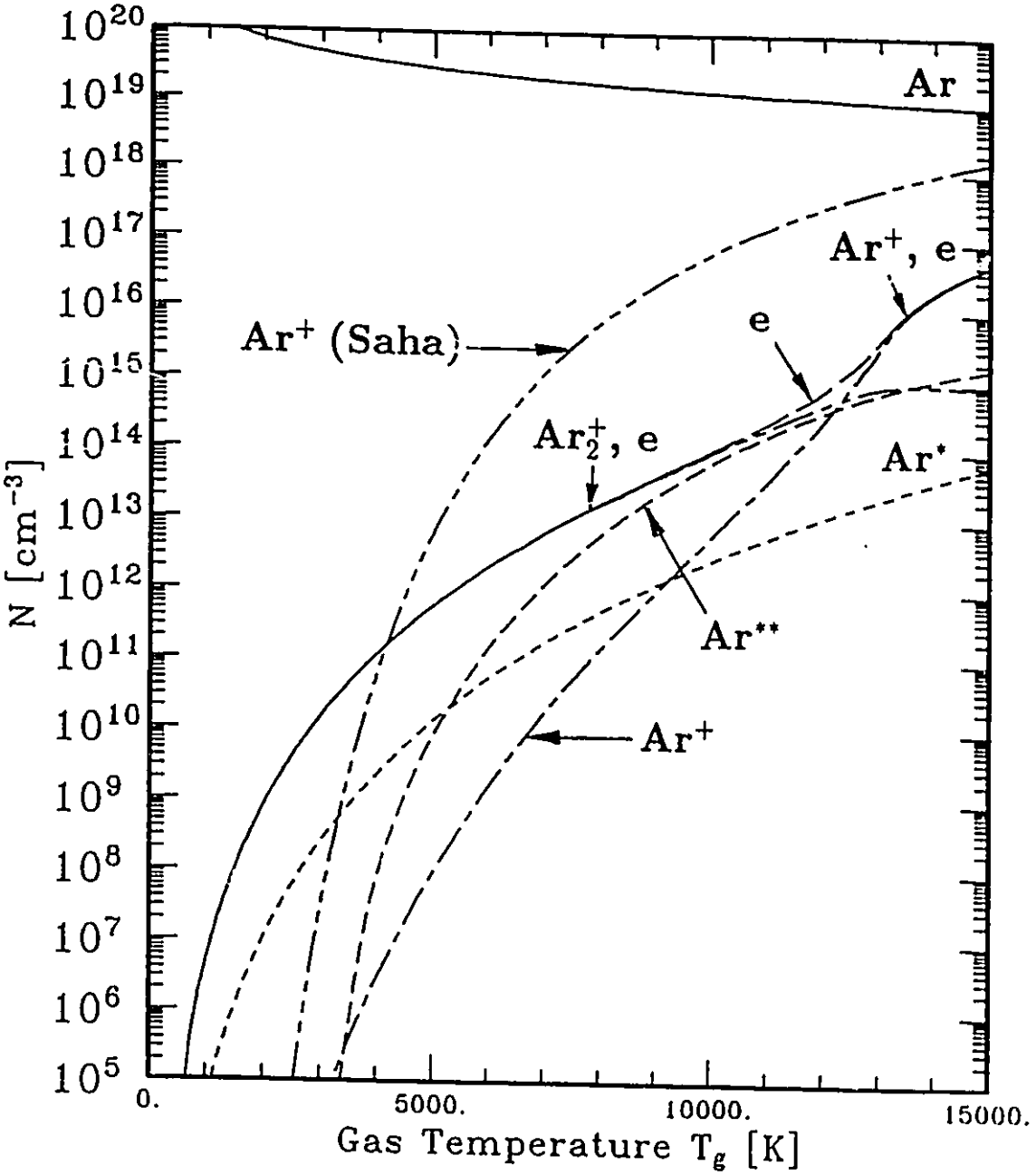

Figure 4.10: Ionized and neutral species concentrations as a function of gas temperature for argon with p = 15200 Torr, and $T_e = T_g$.

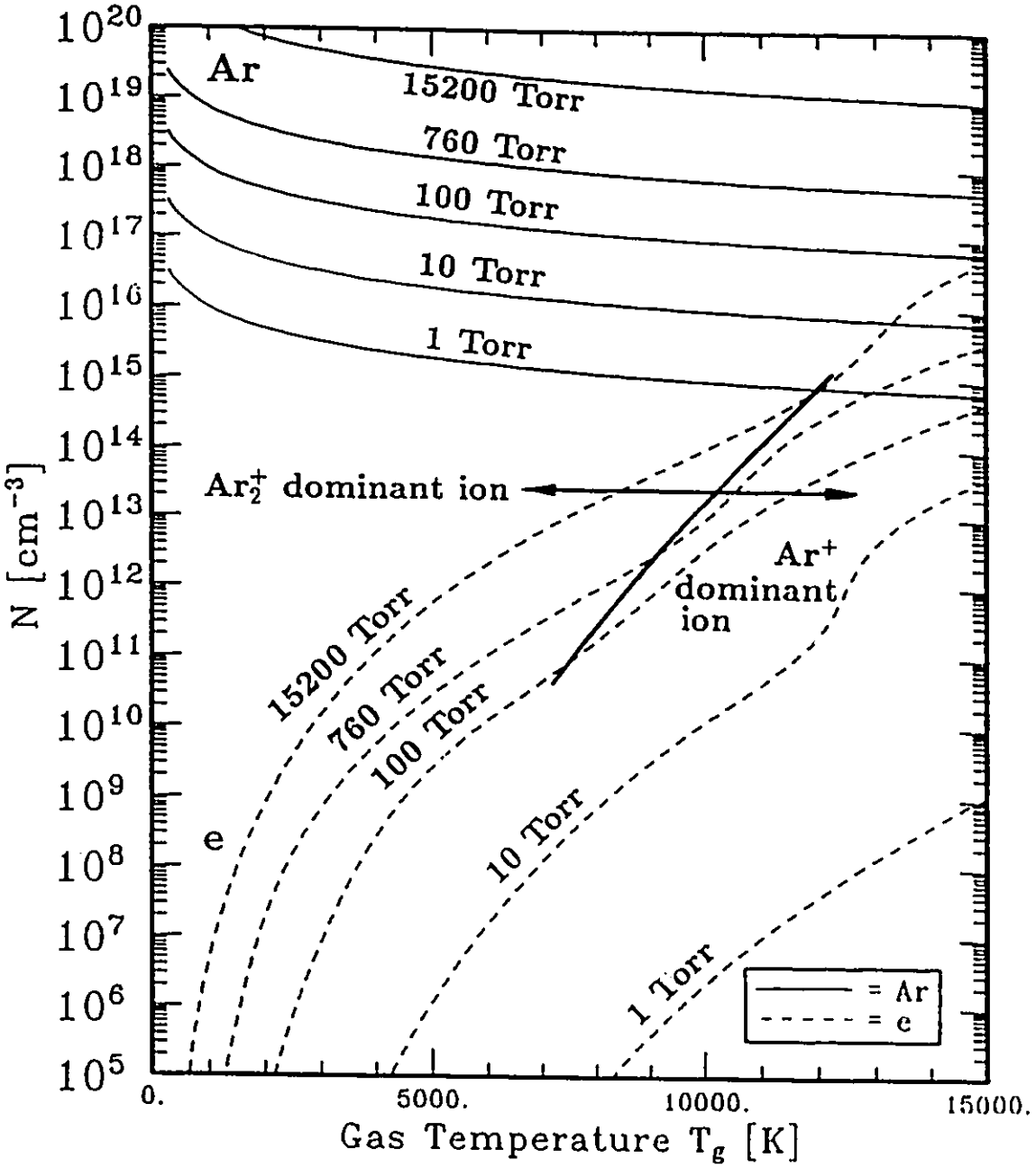

Figure 4.11: Summary of the effect of changing pressure on the temperature dependent concentrations of Ar and e for a pure argon plasma.

A summary of the effects of pressure on the degree of ionization has been compiled in Figure 4.12 for pressures between 1 Torr and 15200 Torr, where the degree of ionization is defined as

$$\alpha = \frac{[e]}{[Ar] + [Ar^*] + [Ar^{**}] + [Ar^+] + 2[Ar_2^+]} \tag{4.7}$$

As indicated in Figure 4.12, the degree of ionization tends to increase with increasing pressure at temperatures less than T_g = 6500 K under thermodynamic equilibrium conditions. At these temperatures, the electron concentration is primarily due to Ar_2^+ ions. At temperatures greater than T_g = 6500 K however, the degree of ionization tends to have a non-monotonic dependence on pressure, increasing with pressure from p = 1 Torr to p = 100 Torr, and subsequently decreasing with pressure at pressures greater than p = 100 Torr. This effect is most likely due to the increase in Ar_2^+ concentration and the higher Ar_2^+ to Ar^+ dominance transition temperatures at higher pressures. Higher pressures tend to favour the formation of Ar_2^+ and as a result cause a decrease in α.

4.4 Comparison with Previous Models

As mentioned in Section 4.1, numerous researchers have assembled models of argon plasmas ranging from simple modifications of the Saha equation to complex multi-levelled collisional-radiative models. A comparison with the Saha equation has been made throughout this chapter. These results tend to indicate that the use of the Saha equation alone for the description of argon thermal plasmas is somewhat over-simplified, providing at best a rough approximation of the behaviour of argon under thermal plasma conditions. A more detailed application of the fundamental principles underlying the Saha equation have been undertaken by Kröpelin et al.[68], however, the end results are still essentially the same as those predicted by the simple Saha equation in the range of temperatures presently under consideration.

Complex collisional-radiative models such as those of Vlček[82] represent a formidable computational task. As their main objective is to compute the radiative emissions of argon plasmas, the results of such models are never presented in a

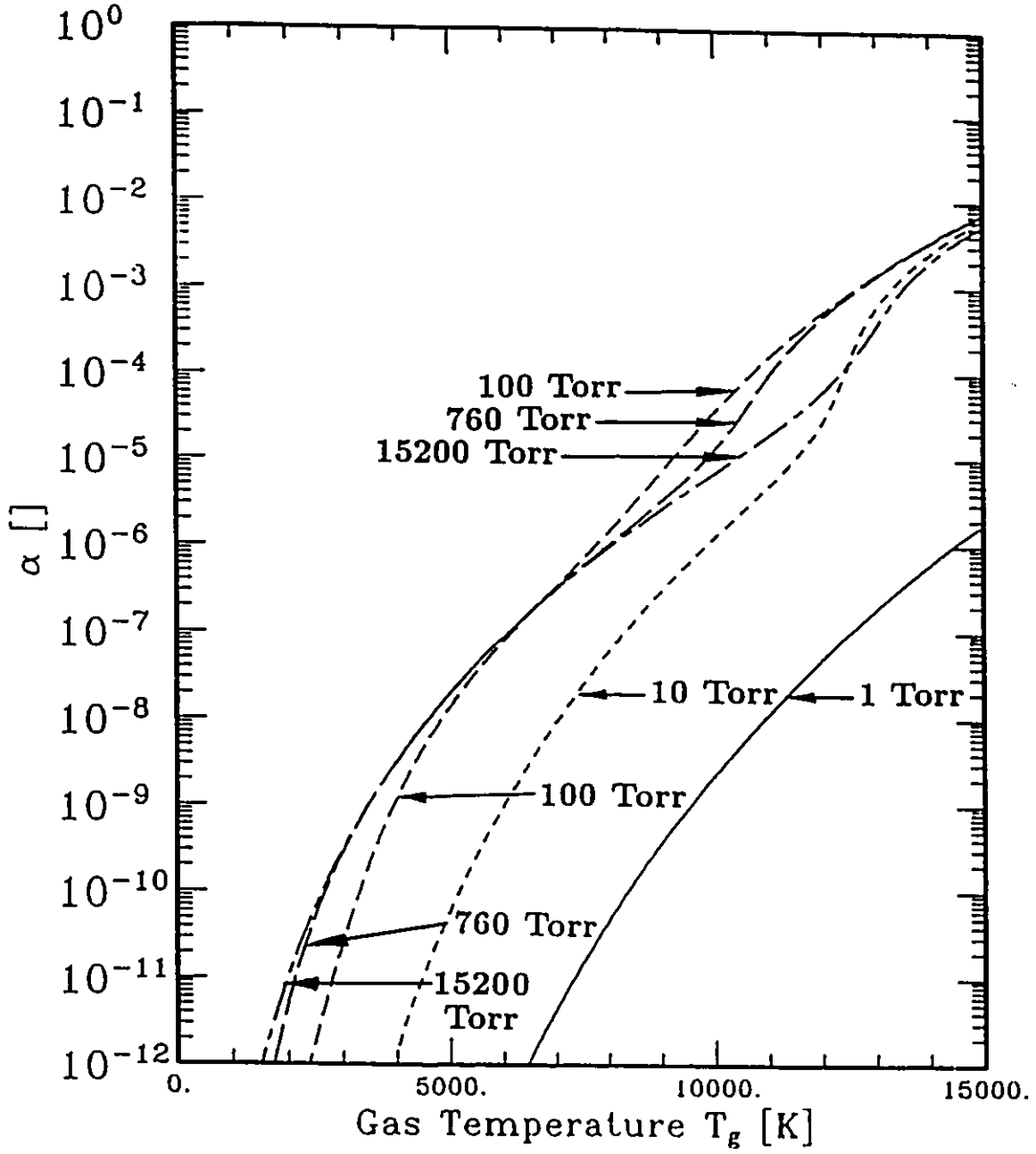

Figure 4.12: Summary of the effect of changing pressure on the degree of ionization for a pure argon plasma.

manner amenable to comparison with the present model. Suffice to say that with few exceptions, collisional-radiative models closely follow the same general theoretical considerations underlying the Saha equation, and as such should produce similar results.

Of the reduced-level models, perhaps the most interesting and advanced is the three-level model of Braun and Kunc[89][90][91]. This model considers three different temperature ranges:

1. A "hot" or high temperature range (T_g, $T_e \geq 9000$ K) in which electron impact collisions dominate the model,

2. A "cold" or low temperature range ($4000 \leq T_g$, $T_e \leq 6000$ K) in which electron impact as well as atom impact reactions are important, and

3. A region which extends the low temperature range below 4000 K.

As shown in Figure 4.13, in the high temperature range the plasma density calculated by Braun and Kunc's model is lower than that predicted by the Saha equation, but larger than that calculated by the present model. The discrepancy with the present model may be due to the fact that Braun and Kunc did not consider the presence of Ar_2^+ ions in their model and thus have lower Ar^+ losses.

In the $T_g = 6000$–9000 K temperature range, Braun and Kunc do not feel their model is applicable. In this temperature range, the present chemical kinetic model tends to indicate that Ar_2^+ exerts a strong influence on the plasma density, causing the greatest discrepancies with the Saha model as discussed earlier.

At temperatures less than 6000 K, the Ar^+ density predicted by Braun and Kunc's results agrees well with the results predicted by the present model. The prediction of slightly larger Ar^+ densities by Braun and Kunc may be due to the fact that their model does not include the losses incurred by the three body conversion reaction Ar7

$$Ar^+ + Ar + Ar \xrightarrow{k_{Ar7}} Ar_2^+ + Ar$$

which represents the main source of Ar_2^+.

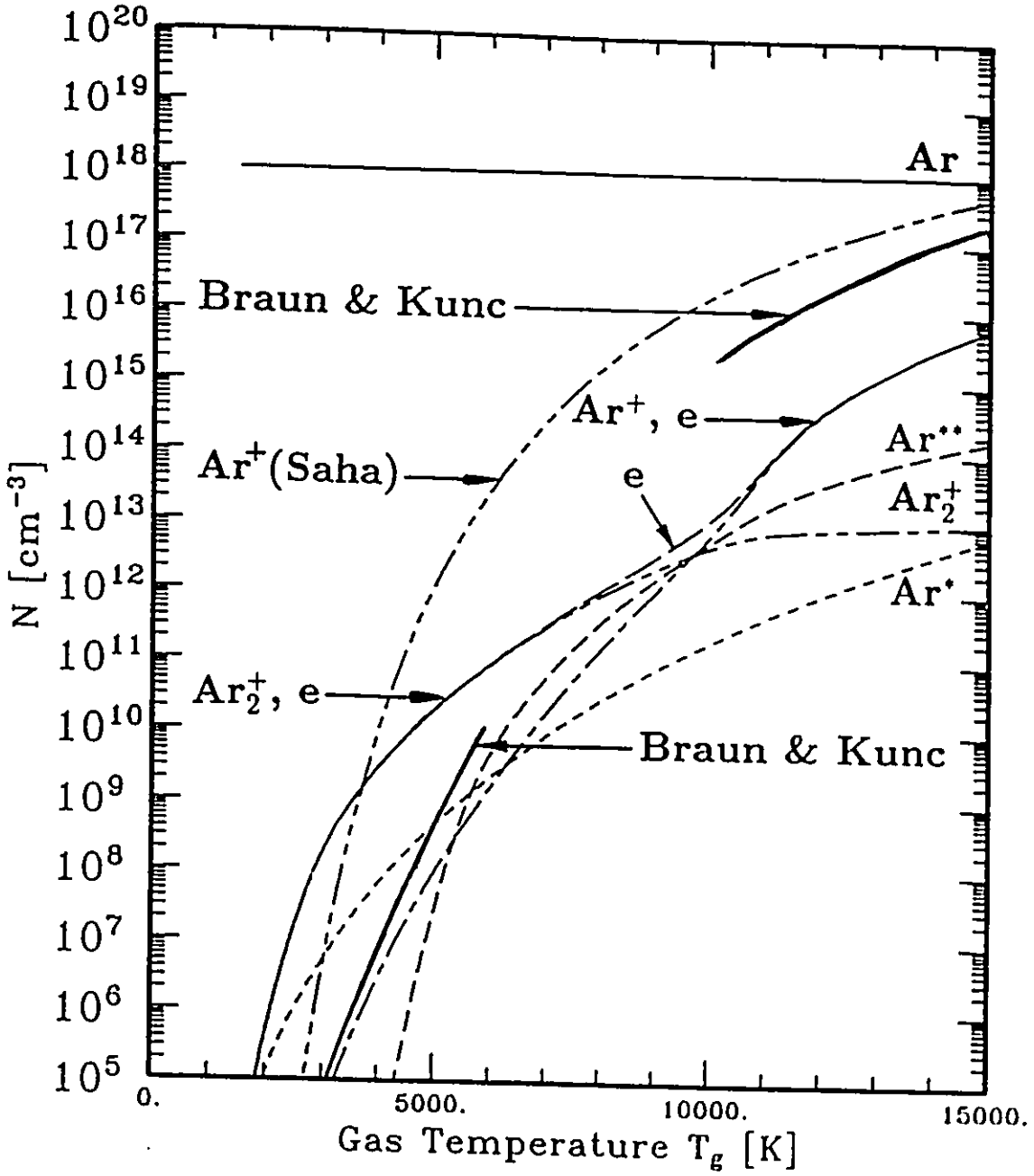

Figure 4.13: Ionized and neutral species concentrations as a function of electron temperature. Comparison of the present results with those of Braun and Kunc [90][91].

4.5 Comparison with Previous Experimental Results

There is some controversy concerning the conditions which are necessary to achieve local thermodynamic equilibrium in an arc discharge[43][110]. Experimental results show that argon arcs operated at atmospheric pressure are relatively close to being in local thermodynamic equilibrium. It should be noted however that the observed electron densities consistently fall below the concentrations predicted by the Saha equation, a result which tends to agree with the present model[44][45][111].

As mentioned in Section 4.2, the presence of Ar_2^+ in argon plasmas has been noted by a number of authors investigating low gas temperature, medium pressure glow discharges or high gas temperature and high pressure plasma afterglows[83]–[87]. These discharge conditions, in which the Ar_2^+ three-body generation reaction

$$Ar^+ + Ar + Ar \xrightarrow{k_{Ar7}} Ar_2^+ + Ar$$

is of importance, tend to lead to the production of significant quantities of Ar_2^+ molecular ions. A comparison of the experimental evidence of Chang et al.[112] with the present results indicates that the present model agrees qualitatively well with the Ar_2^+/Ar^+ ratio measured using mass spectroscopy under medium pressure glow discharge conditions as shown in Figure 4.14.

4.6 Summary of Ar Thermal Plasmas

In carrying out this investigation, a chemical kinetic model of argon has been assembled based on the best experimental and theoretical data for the reaction rate constants available at this time, with particular emphasis given to experimentally derived values. The model can be used to simulate a wide variety of different conditions including those experienced in electric arcs or plasma jets (high T_g and T_e, high pressure, atmospheric or reduced pressure) or glow discharges (high T_e, low T_g and low to medium pressure).

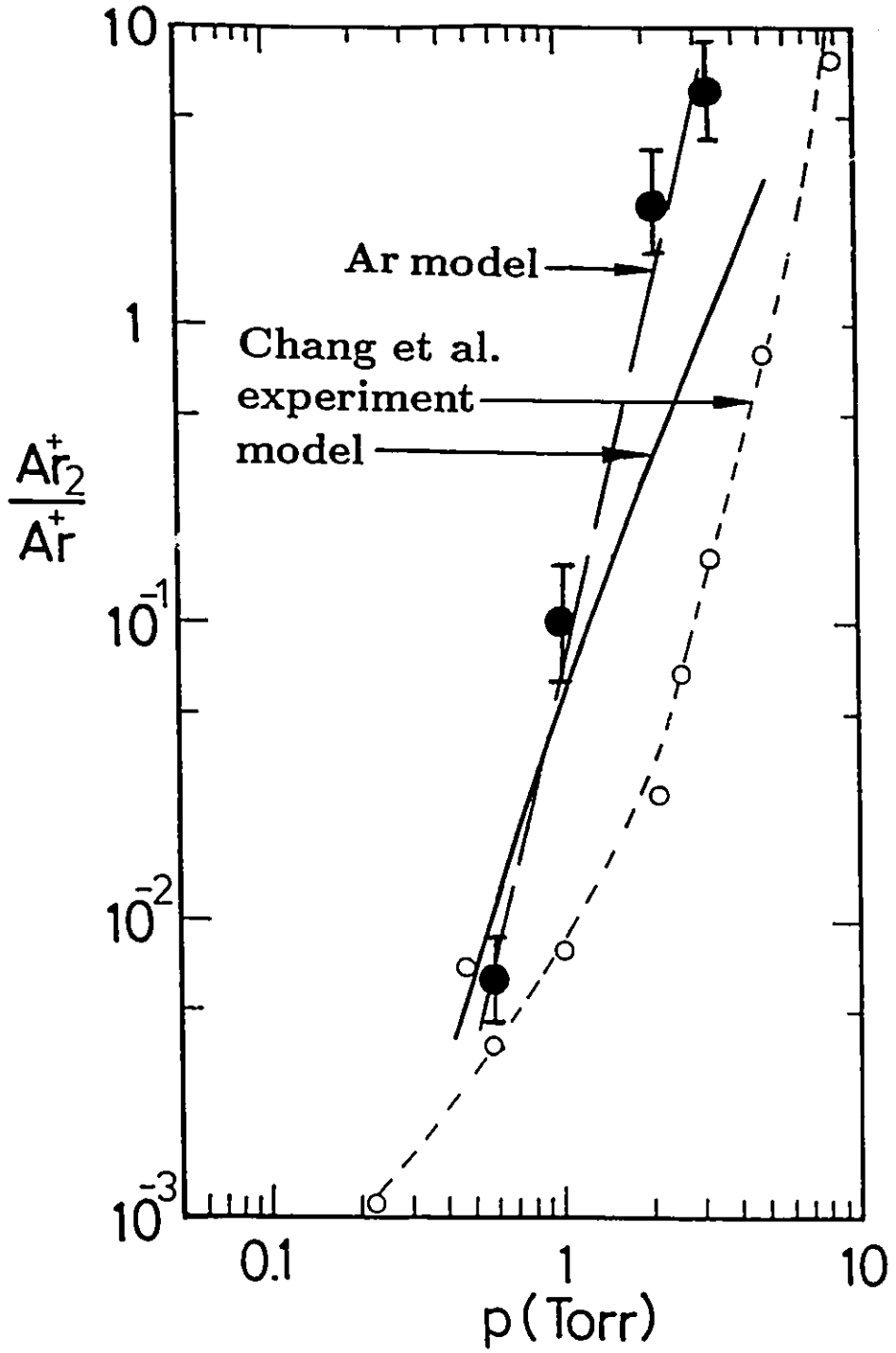

Figure 4.14: Comparison of the experimental and numerical results of Chang et al.[112] and the present chemical kinetic model.

Results show that significant concentrations of Ar^*, Ar^{**}, Ar^+, and Ar_2^+ occur under thermal plasma conditions. The concentrations of these species tend to increase with increasing gas and electron temperature. At lower temperatures, Ar_2^+ tends to be the dominant ion, and at higher temperatures, Ar^+ tends to be the dominant ion. Under thermodynamic equilibrium conditions, the concentrations of Ar^+ and Ar_2^+ exceed those of Ar^*, and Ar^{**}, however, under thermodynamic non-equilibrium conditions, the concentration of Ar^{**} may exceed those of Ar^+ and Ar_2^+. The concentrations of all species are seen to increase with increasing pressure, however detailed analysis indicates that Ar_2^+ is preferentially formed at higher pressures. The degree of ionization may exhibit a non-monotonic dependence on pressure as a result.

A number of calculations have been carried out under various imposed physical conditions to illustrate the behaviour of the chemical kinetic model and compare it with the Saha equation. The results indicate that the Saha equation almost always predicts electron and Ar^+ concentrations which significantly over-estimate or underestimate those calculated by the present chemical kinetic model at higher and lower temperatures respectively. In addition, the chemical kinetic model predicts the presence of Ar_2^+ at gas temperatures below 6000 K. The results of the present model compare favourably with the Ar^+ density predicted by Braun and Kunc's model for $T_g \leq 6600$ and the experimental results of Chang et al. at medium gas pressure ($10^{-1} \leq P \leq 10$ Torr).

Chapter 5

Numerical Model of Ar-C Thermal Plasma

5.1 Ar-Atom Thermal Plasmas

Argon-atom mixture plasmas occur relatively frequently in experiments as well as under process conditions. Argon is often used in thermal plasma torches as it creates a relatively high arc temperature with low electrode wear at a reasonable cost. In order to achieve higher plasma temperatures and increase the enthalpy of the plasma, small amounts of an atomic gas such as helium are often added to the argon[113]. Argon-atom mixtures are also commonly used in glow or rf discharges to study the fundamental behaviour of these mixtures under low pressure high electron temperature conditions[114]. Argon-atom mixtures also occur as a side effect of the discharge itself. For example, recent studies have examined arc contamination by copper vapour resulting from ablation of the electrodes[115][116][117]. Similarly, such contaminant vapours can also occur in the jet portion of the plasma due to the evaporation of particles injected during plasma spraying operations[118][119].

Argon-carbon plasmas commonly occur either as a result of electrode ablation when carbon electrodes are used[120], or as a result of plasma processing, for example when coal is injected into the jet portion of a DC plasma torch[121][122]. Little attention has been focused on numerical investigations to identify ion and neutral

species in Ar-C mixtures under thermal plasma conditions. The present model thus serves as an initial examination of the Ar-C system under thermal plasma conditions as well as representing a step in the development of the Ar-CO_2 model of Chapter 6.

5.2 Chemistry of Ar-C Mixture Plasmas

The fundamental form of the model established in Chapter 3 and applied in Chapter 4 was also applied in this case. For the Saha equation, the ratio of the partition functions for carbon is $U_{i,C}/U_{a,C} = 6/9 = 2/3$ over the temperature range considered in this model[35]. The first ionization energy of carbon is $E_{i,C} = 11.256$ eV.

The reactions involving both carbon and argon are shown in Table 5.1. Adding these reactions to the reactions shown in Table 4.1 completes the Ar-C model. The major source of C^+ ions stems from thermal

$$C + C \xrightarrow{k_{C1}} C^+ + C + e$$

and electron impact

$$C + e \xrightarrow{k_{C2}} C^+ + e + e$$

ionization reactions, whereby the thermal impact ionization reactions account for the majority of the C^+ generation under thermodynamic equilibrium conditions. Although the electron impact ionization cross-section for carbon is relatively well known[123][95] no experimental results for the thermal ionization of carbon exist. For this reason, the theoretical expression suggested by von Engel[124] has been used in this case. Reactions between neutral or ionized argon and carbon species such as charge exchange or clustering reactions have not been observed. Thus, the electrons in the Ar-C plasma represent the only direct coupling between the two species.

Loss of C^+ ions occurs through radiative recombination

$$C^+ + e \xrightarrow{k_{C3}} C + h\nu$$

and diffusion. Three body recombination has not been included in the present model due to the absence of both theoretical and experimental data at this time. Similarly,

the investigation of two-step reactions in the thermal and electron impact ionization processes have not been reported. Other authors have discussed the possibility of such species as C_2, C_3, and C^- occurring in thermal plasmas[14][24][125], but the reactions leading to these species and their rate constants are as yet unclear. A summary of the chemical kinetics of the Ar-C system has been outlined in Figure 5.2, where Ar1–Ar10 and C1–C3 refer to the reactions outlined in Tables 4.1 and 5.1. In order to illustrate the relative importance of these reactions at various temperatures, Figure 5.1 shows the gas and electron temperature dependencies of reaction rate constants k_{Ar1}–k_{Ar10}, and k_{C1}–k_{C3}, as well as the equivalent "k" values of the diffusion reactions included in the model.

The coupled rate equations for the different species at the centre of a cylindrical discharge tube can be written as follows:

$$\frac{d[Ar^*]}{dt} = k_{Ar1}[Ar]^2 - k_{Ar2}[Ar^*][Ar] - \frac{q^2 D_{Ar^*-Ar}[Ar^*]}{R^2} \quad (5.1)$$

$$\frac{d[Ar^{**}]}{dt} = k_{Ar4}[Ar][e] - k_{Ar5}[Ar^{**}][e] - 2k_{Ar6}[Ar^{**}]^2 - \frac{q^2 D_{Ar^{**}-Ar}[Ar^{**}]}{R^2} \quad (5.2)$$

$$\frac{d[Ar^+]}{dt} = k_{Ar2}[Ar^*][Ar] + k_{Ar3}[Ar][e] + k_{Ar5}[Ar^{**}][e] + f_{Ar6}k_{Ar6}[Ar^{**}]^2 \quad (5.3)$$
$$-k_{Ar7}[Ar^+][Ar]^2 - k_{Ar8}[Ar^+][e] - k_{Ar9}[Ar^+][e]^2 - \frac{q^2 D_{Ar^+-Ar}[Ar^+]}{R^2}$$

$$\frac{d[Ar_2^+]}{dt} = (1 - f_{Ar6})k_{Ar6}[Ar^{**}]^2 + k_{Ar7}[Ar^+][Ar]^2 \quad (5.4)$$
$$-k_{Ar10}[Ar_2^+][e] - \frac{q^2 D_{Ar_2^+-Ar}[Ar_2^+]}{R^2}$$

$$\frac{d[C^+]}{dt} = k_{C1}[C][C] + k_{C2}[C][e] \quad (5.5)$$
$$-k_{C3}[C^+][e] - \frac{q^2 D_{C^+-C}[C^+]}{R^2}$$

where the form of the nomenclature and the choice of radii follow that used in equations 4.1–4.4. The diffusion coefficients used in the model are listed in Tables 4.2 and 5.2.

The ideal gas law is used as in Chapter 4 to calculate the overall concentration of both Ar and C in the system. Significant depletions of Ar can be compensated for as in equation 4.5. For carbon, such depletions can be corrected through the following

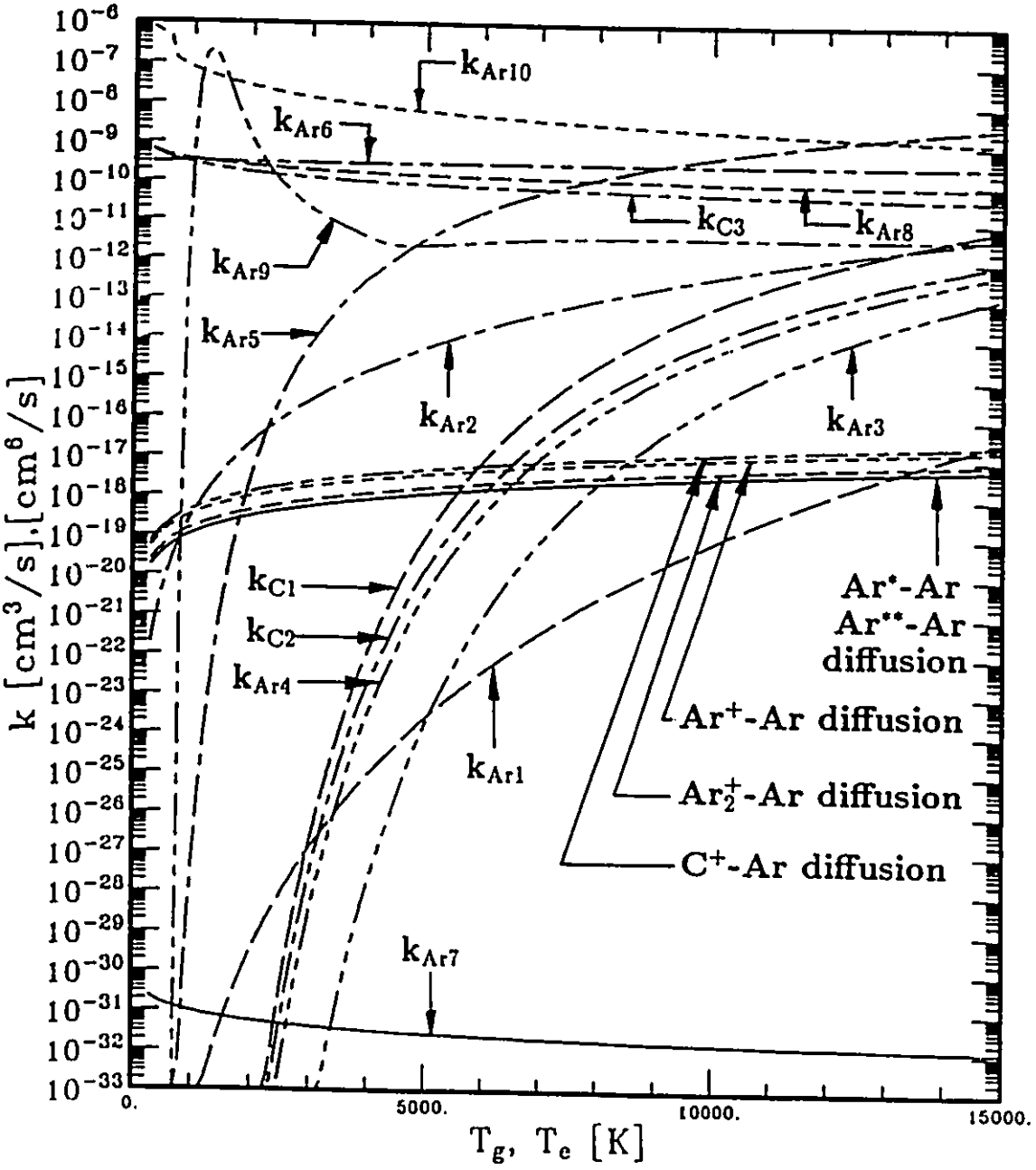

Figure 5.1: Temperature dependence of the values of the reaction rate constants for the chemical kinetic Ar-C thermal plasma model.

Table 5.1: Reactions for the argon-carbon system.

Reactions	Reaction Rate Constants†		T_g, T_e [K]	Ref.
$C + C \xrightarrow{k_{C1}} C^+ + C + e$	k_{C1}	$210.1pT_g^{1/2}N_c^{-1}*$ $e^{\frac{(1.3\times10^5}{T_g})}(1 + 1.3 \times 10^5/T_g)$	Theory	[124]
$C + e \xrightarrow{k_{C2}} C^+ + e + e$	k_{C2}	$4.1 \times 10^{-11}T_e^{1/2}*$ $(1 + 1.5 \times 10^{-5}T_e)e^{(\frac{-1.3\times10^5}{T_e})}$	Cross Section	[123][95]
$C^+ + e \xrightarrow{k_{C3}} C + h\nu$	k_{C3}	$1.0 \times 10^{-12}(300/T_e)^{0.7}$	Theory	[73][62]

†[cm^3/s] for two-body reactions and [cm^6/s] for three-body reactions.

Table 5.2: Diffusion constants for the argon-carbon system at 1 Torr, 300 K.

Diffusion Species	D_ip [cm^2Torr/s]	References
C^+-Ar	100	[62]

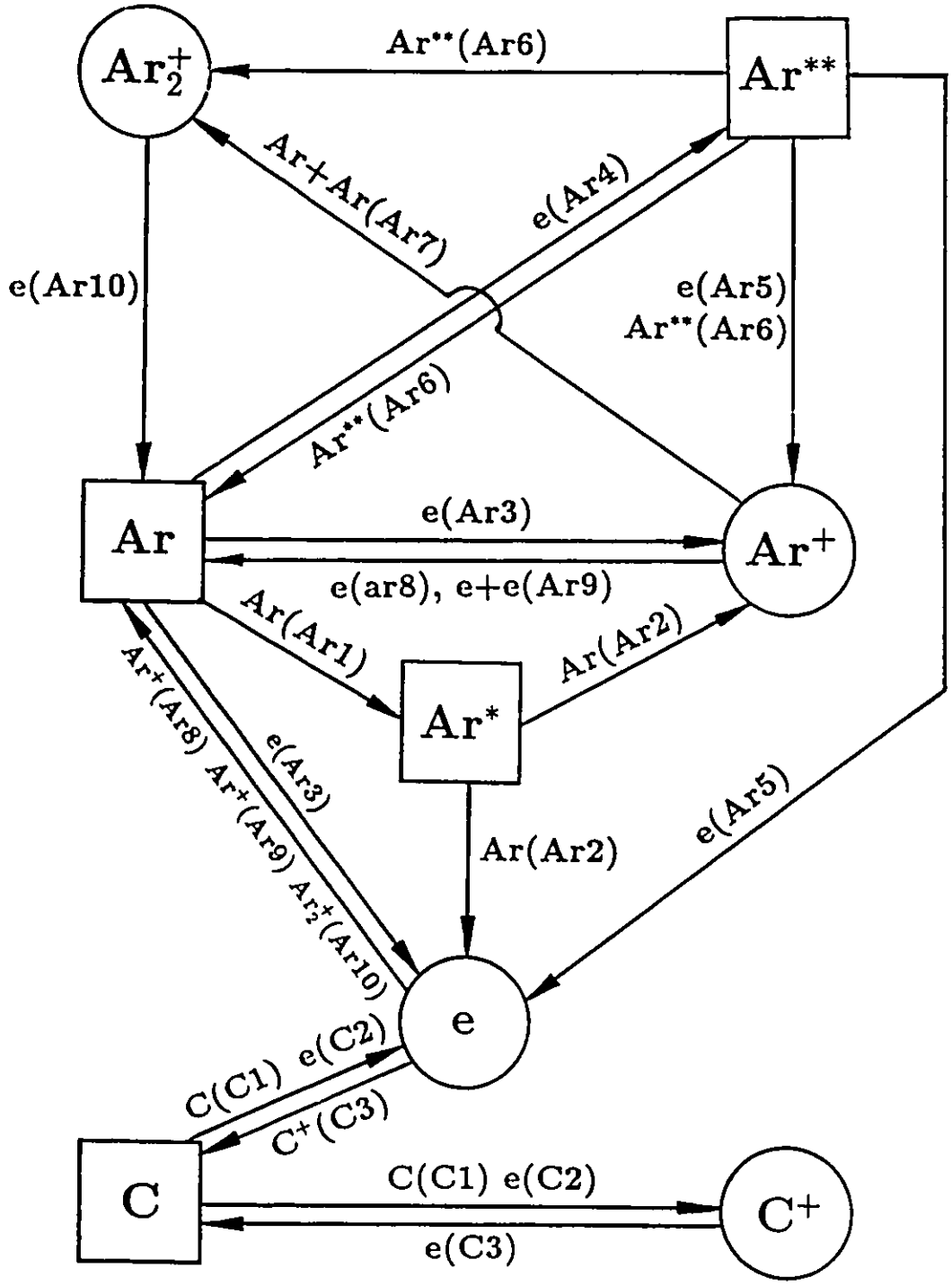

Figure 5.2: Plasma chemistry for an Ar-C discharge including molecular ions, and thermal and electron impact reactions.

mass balance:

$$[C] = [C]_{IG} - [C^+] \tag{5.6}$$

where $[C]_{IG}$ represents the concentration of carbon as calculated by the ideal gas law. Assuming the existence of a quasi-neutral plasma, the electron concentration can be calculated using a charged particle balance:

$$[e] = [Ar^+] + [Ar_2^+] + [C^+] \tag{5.7}$$

5.3 Numerical Results

5.3.1 Gas Temperature Effects

Figure 5.3 shows the ionic and neutral species in an Ar-1%C plasma as a function of gas temperature for p = 760 Torr. The Ar-C plasma shows a significantly different ion composition when compared with the pure argon plasma. As shown in Figure 5.3, at temperatures less than $T_g = 3800$ K, Ar_2^+ is the dominant ion, between $3800 \leq T_g \leq 12800$ K C^+ is the dominant ion, and at temperatures greater than $T_g = 12800$ K, Ar^+ is the dominant ion.

Over the gas temperature range considered, a comparison between Figures 5.3 and 4.3 shows that the gas temperature dependence of the calculated Ar_2^+ concentration is significantly affected by the 1% mixture of carbon in the system. Using equation 5.4, the equilibrium concentration of Ar_2^+ can be expressed as:

$$[Ar_2^+] = \frac{(1 - f_{Ar6})k_{Ar6}[Ar^{**}]^2 + k_{Ar7}[Ar^+][Ar]^2}{k_{Ar10}[e] + \frac{q^2 D_{Ar_2^+ - Ar}}{R^2}} \tag{5.8}$$

Since the terms representing diffusion and reaction Ar6 are relatively small in comparison to the other two terms under these conditions, equation 5.8 can be simplified to:

$$[Ar_2^+] = \frac{k_{Ar7}[Ar^+][Ar]^2}{k_{Ar10}[e]} \tag{5.9}$$

Since both the Ar^+ and Ar concentrations are relatively unchanged, they do not significantly affect the equilibrium concentration of Ar_2^+. The ionization of the C atoms into C^+ ions has significantly increased the concentration of electrons however, and thus the equilibrium concentration of Ar_2^+ shown in Figure 5.3 is lower than that shown in Figure 4.3.

The concentration of Ar^+ shown in Figure 5.3 is slightly higher in the temperature range $7000 \leq T_g \leq 10000$ K than that shown in Figure 4.3 for a pure argon plasma. This increase in Ar^+ concentration may be caused by an increase in the production of Ar^+ via the electron impact ionization reactions

$$Ar + e \xrightarrow{k_{Ar4}} Ar^{**} + e$$

$$Ar^{**} + e \xrightarrow{k_{Ar5}} Ar^+ + e + e$$

due to the increase in electron density over this temperature range. The Ar^+ density predicted for temperatures greater than $T_g = 10000$ K is approximately 30% less in the argon-carbon plasma than in the pure argon plasma. This difference may be due to the fact that the three-body recombination reaction

$$Ar^+ + e + e \xrightarrow{k_{Ar8}} Ar + e$$

is causing a reduction in the Ar^+ density due to the increase in electron concentration over this temperature range caused by the ionization of carbon.

The Ar^* concentration is relatively unaffected by the presence of 1% carbon in the system since it depends only on the concentration of argon for its generation and loss mechanisms. The concentration of Ar^{**} differs from that found in the pure argon plasma however. At temperatures less than $T_g = 10000$ K, the Ar^{**} concentration is approximately 30% higher in the Ar-1%C system than in the pure Ar plasma. The increase in electron density caused by the ionization of the carbon is most likely responsible for the increased Ar^{**} concentration due to the Ar^{**} generation reaction

$$Ar + e \xrightarrow{k_{Ar4}} Ar^{**} + e$$

At temperatures greater than $T_g = 10000$ K, the Ar^{**} concentration is almost the same in the Ar-1%C plasma as it is in the pure argon plasma, most likely due to the

fact that the change in the electron concentration may not be large enough over this temperature range to have a significant influence on the Ar^{**} concentration.

The discrepancy between the gas temperature dependence of the Ar^+ concentration predicted by the chemical kinetic model and the Saha equation has already been discussed in detail in Chapter 4. The C^+ concentration also shows the same tendency. The C^+ concentration predicted by the chemical kinetic model is at least 1 order of magnitude smaller than that predicted by the Saha equation for C^+. Since thermal impact ionization constitutes the single dominant ionization channel in the thermodynamic equilibrium case and presently available results do not indicate the presence of significant concentration of molecular carbon ions which could disturb the electron concentration gas temperature dependencies, as in the pure argon model, the two concentrations come close to being proportional to each other over the gas temperature range in question.

5.3.2 Electron Temperature Effects

Figure 5.4 shows the ion and neutral species as a function of electron temperature for $T_g = 300$ K, p = 760 Torr. As in the pure argon model under these conditions, the concentrations of Ar^+, Ar_2^+, and Ar^{**} increase with increasing electron temperature. The C^+ concentration also increases with increasing electron temperature. The metastable atom density Ar^{**} can be larger than the plasma density, but the difference between them is no longer as large as it can be in the pure argon model. A minimum electron temperature of $T_e = 6000$ K must be attained for the plasma to be sustained. In the $T_e = 6000$–19000 K temperature range, the Ar^+, Ar_2^+ and Ar^{**} compositions are larger than those shown in Figure 4.6 for the pure argon plasma. Here, C^+ forms the dominant positive ion, and the higher electron concentration generated by the electron impact ionization reaction

$$C + e \xrightarrow{k_{C2}} C^+ + e + e$$

may tend to increase the concentration of Ar^+, Ar_2^+ and Ar^{**} through electron impact reactions.

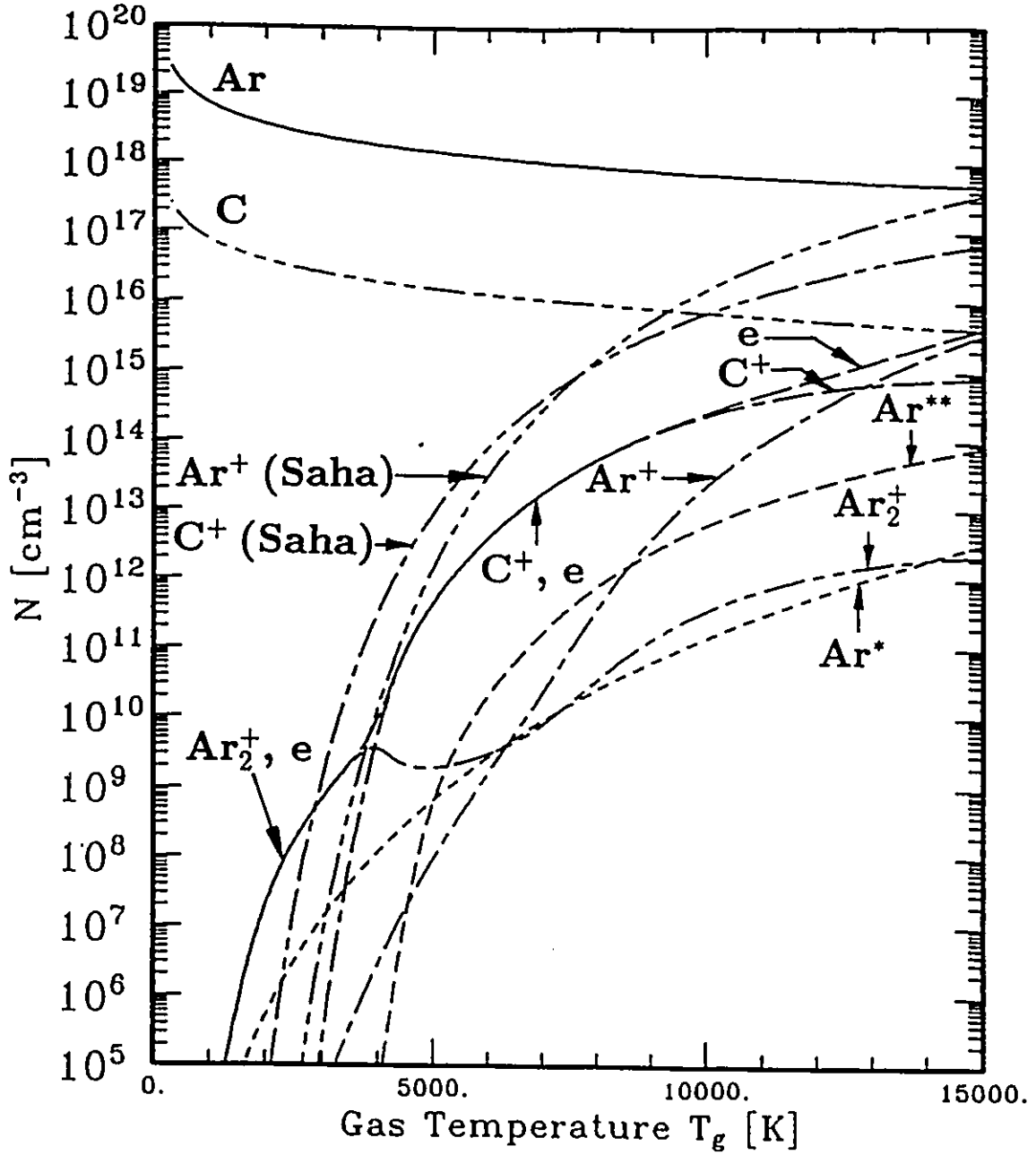

Figure 5.3: Ionized and neutral species concentrations as a function of gas temperature for an argon-1% carbon mixture with p = 760 Torr, and $T_e = T_g$.

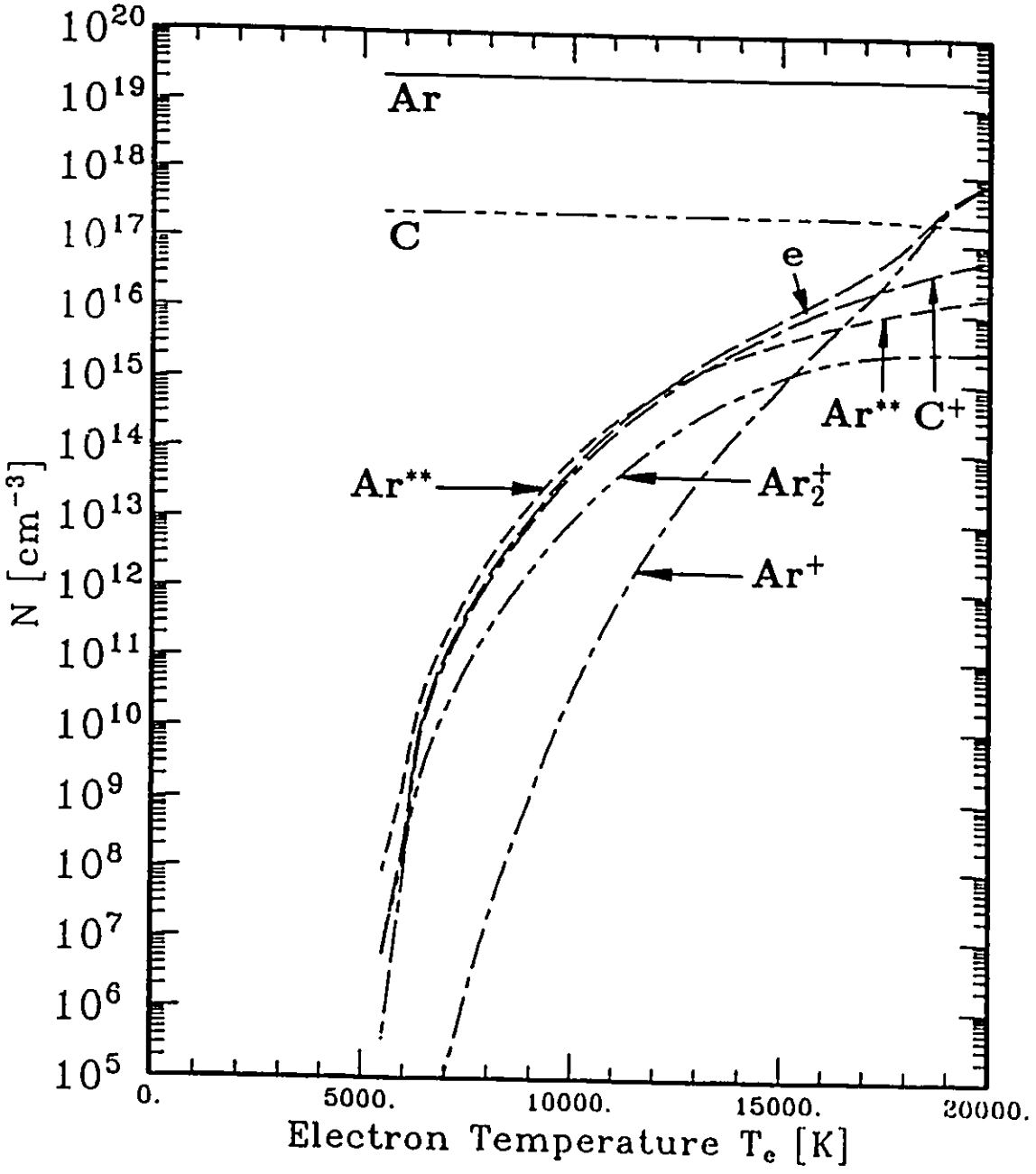

Figure 5.4: Ionized and neutral species concentrations as a function of electron temperature for an argon-1% carbon mixture with T_g = 300 K, and p = 760 Torr.

At temperatures greater than $T_e = 17200$ K, Ar^+ is the dominant ion, and the presence of C^+ has a diminishing influence on the electron concentration. Here the Ar^+, Ar_2^+ and Ar^{**} temperature dependent concentrations approach those of the pure argon model shown in Figure 4.6 for the same electron temperature range. The concentration of carbon ions is more than 1 order of magnitude smaller than that of the Ar^+ at $T_g = 20000$ K. Although argon has a higher ionization energy than carbon (15.769 versus 11.256 eV respectively), the Ar^+ concentration is higher than the C^+ concentration at this temperature, most likely due to the increased generation of Ar^+ via the two-step electron impact ionization reactions

$$Ar + e \xrightarrow{k_{Ar4}} Ar^{**} + e$$

and

$$Ar^{**} + e \xrightarrow{k_{Ar5}} Ar^+ + e + e$$

as opposed to the single-step electron impact ionization reaction for carbon

$$C + e \xrightarrow{k_{C2}} C^+ + e + e$$

Figure 5.5 illustrates the predicted temperature dependent species concentrations for an Ar-1%C mixture plasma under the same conditions as those found in Figure 5.4 when the gas temperature is raised to $T_g = 5000$ K. At temperatures greater than $T_e = 15000$ K, the species concentrations of Ar^{**}, Ar^+, and Ar_2^+ are essentially unchanged from those shown in Figure 4.4 for the pure argon plasma, most likely due to the fact that Ar^+ is the dominant ionized species in this temperature range. As a result, the electron concentration is the same in both cases. At temperatures lower than $T_e = 14000$ K however, the model predicts the dominance of C^+ and Ar_2^+ ions, but Ar^+ ions also occur in significant concentrations. These ion concentrations are most likely the result of the thermal and electron impact reactions for C^+ and Ar^+

$$C + C \xrightarrow{k_{C1}} C^+ + C + e$$

$$Ar + Ar \xrightarrow{k_{Ar1}} Ar^* + Ar \xrightarrow{k_{Ar3}} Ar^+ + e + Ar$$

$$C + e \xrightarrow{k_{C2}} C^+ + e + e$$

$$Ar + e \xrightarrow{k_{Ar4}} Ar^{**} + e \xrightarrow{k_{Ar5}} Ar^+ + e + e$$

and the three-body reaction Ar7 in the case of Ar_2^+

$$Ar^+ + Ar + Ar \xrightarrow{k_{Ar7}} Ar_2^+ + Ar$$

The Ar^+, and Ar_2^+ concentrations are slightly larger than those found in the pure argon model in Figure 4.5 in this temperature range most likely due to the increased electron concentration due to the presence of the dominant C^+ ion. The Ar^* concentration, which depends only on the concentration of Ar and the gas temperature, is constant. Its concentration is essentially the same as that found in the pure argon model shown in Figure 4.5. At electron temperatures less than T_e = 7000 K, the density of Ar^+, Ar_2^+, and C^+ tend to reach a constant value with decreasing temperature, most likely due to the increased importance of thermal impact ionization reactions due to the high gas temperature.

The Ar^+ and C^+ concentrations predicted by the Saha equation which appear in Figure 5.5 are again not realistic in this case as the Saha equation cannot account for either the presence of molecular ions or a temperature disequilibrium.

5.3.3 Gas Pressure Effects

Figure 5.6 shows the ion and neutral species concentrations as a function of T_e for p = 10 Torr and T_g = 300 K. Ar^+ now forms the dominant ion at temperatures greater than T_e = 11700 K, C^+ is the dominant ion over the temperature range T_e = 10000–11700 K, and at temperatures less than T_e = 10000 K, Ar_2^+ forms the dominant ion. At temperatures less than T_e = 11700 K, the Ar^{**} concentration is larger than the plasma density, as defined by the electron density. When compared to Figure 5.4 (p = 760 Torr), the plasma "onset" temperature has now increased to T_e = 8000 K, and the concentration of all species, both neutral and ionic have decreased due to the decrease in pressure.

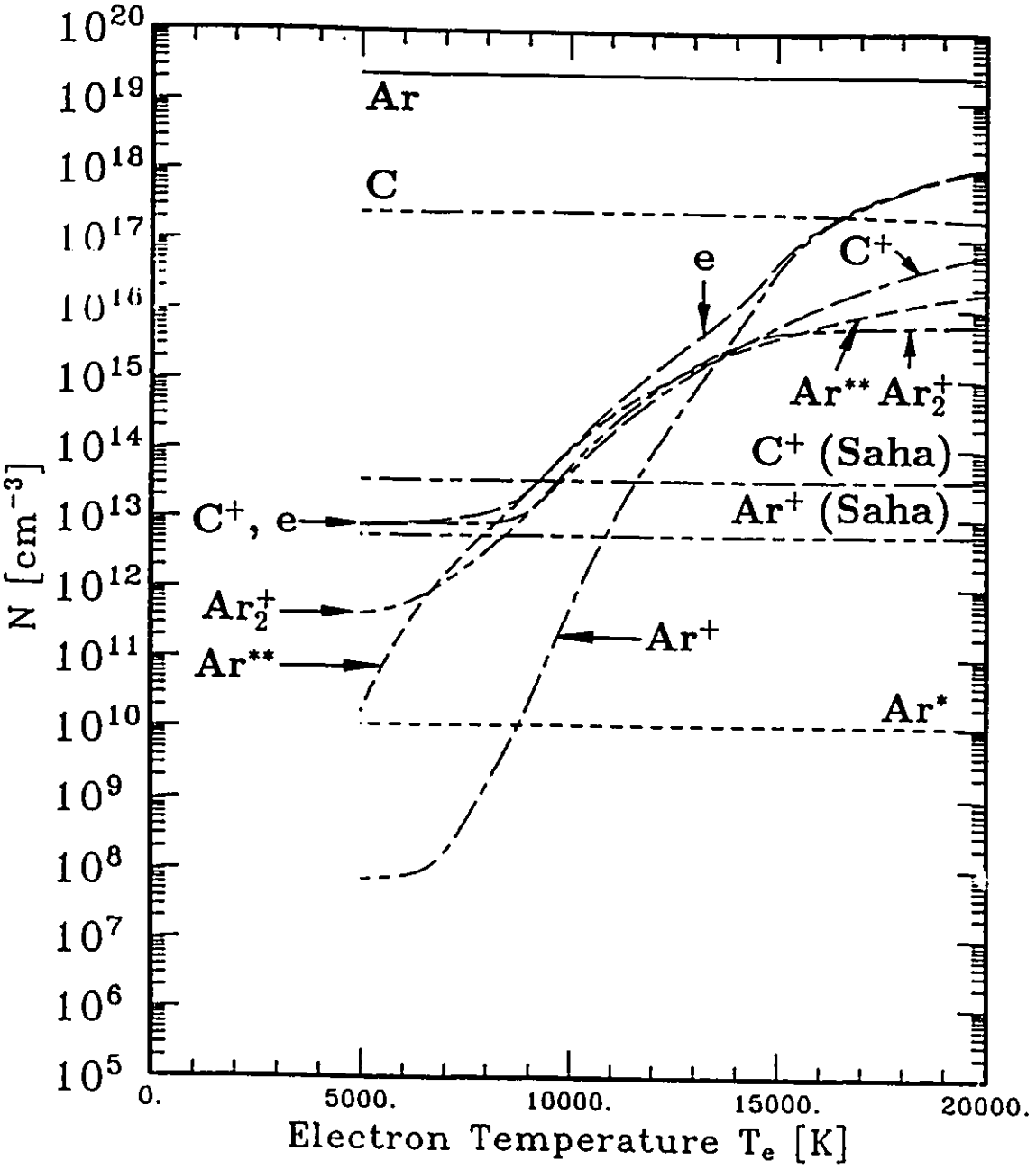

Figure 5.5: Ionized and neutral species concentrations as a function of electron temperature for an argon-1% carbon mixture with T_g = 5000 K, and p = 760 Torr.

As shown in Figure 5.7, increasing the gas temperature to $T_g = 5000$ K at p = 10 Torr tends to increase the concentration of Ar_2^+ at temperatures greater than $T_e = 12000$ K, but leaves the concentration of Ar^+, C^+, and Ar^{**} relatively unaffected. At temperatures less than $T_e = 12000$ K, the increased generation of ionic species, most likely through thermal impact ionization reactions, tends to increase the ionic species concentrations and causes these species to reach constant values with decreasing electron temperature.

Figures 5.8 and 5.9 illustrate the neutral and ionic species concentrations as a function of gas temperature for the Ar-1%C model for constant system pressures of 100 and 10 Torr respectively. The assumption of thermodynamic equilibrium ($T_g = T_e$) has been made in both cases.

When compared to the results shown in Figure 4.8 for the pure argon plasma (p = 100 Torr), the predicted temperature dependencies of the Ar^+, Ar_2^+, Ar^* and Ar^{**} concentrations at p = 100 Torr illustrated in Figure 5.8 show essentially the same differences as between Figures 5.3 and 4.3 for the pure argon and Ar-1%C plasmas respectively at p = 760 Torr. As with the Ar^+ concentration, the relative difference between the C^+ ion concentration predicted by the chemical kinetic model and the Saha equation has increased, most likely due to the relatively stronger loss of these ionized species by diffusion caused by the reduction in the system pressure.

If the pressure in the system is reduced further to 10 Torr as shown in Figure 5.9, this trend continues. The difference in the C^+ concentration predicted by the Saha equation and that calculated by the chemical kinetic model is now more than three orders of magnitude. Comparing Figure 5.9 to the equivalent Figure 4.9 for the pure argon plasma in Chapter 4, it is evident that the increased concentration of electrons caused by the presence of C^+ has increased the Ar^{**} equilibrium concentration in the $6000 \leq T_g \leq 12000$ K temperature range. Sensitivity analysis shows that this increase in Ar^{**} density has the effect of causing the rapid increase in Ar_2^+ density at $T_g = 8500$ K through the reaction

$$Ar^{**} + Ar^{**} \xrightarrow{(1-f_{Ar6})k_{Ar6}} Ar_2^+ + e$$

If the system pressure is increased to p = 15200 Torr as shown in Figure 5.10, a comparison with the results predicted by the pure argon model (Figure 4.10) shows

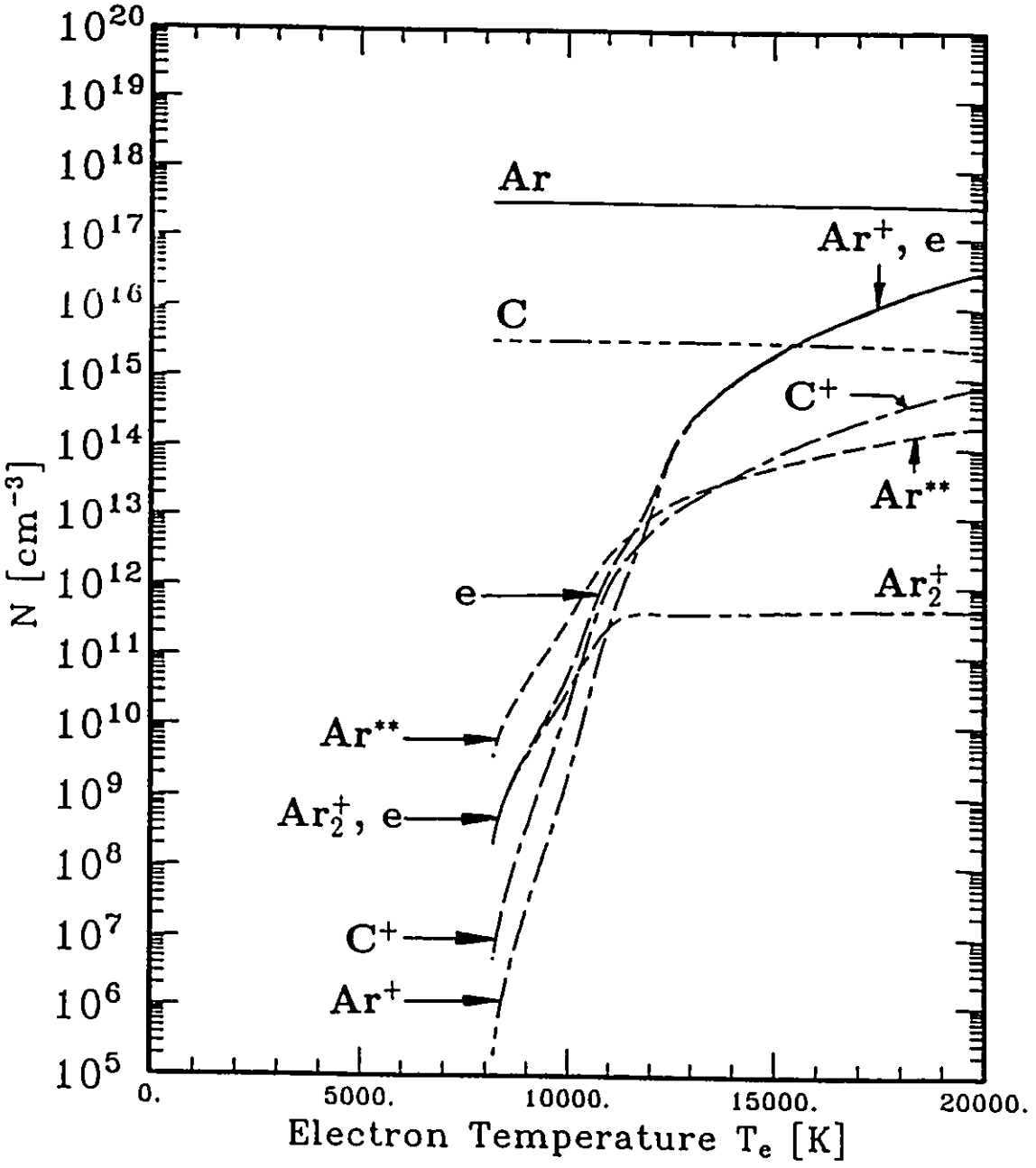

Figure 5.6: Ionized and neutral species concentrations as a function of electron temperature for an argon-1% carbon mixture with T_g = 300 K, and p = 10 Torr.

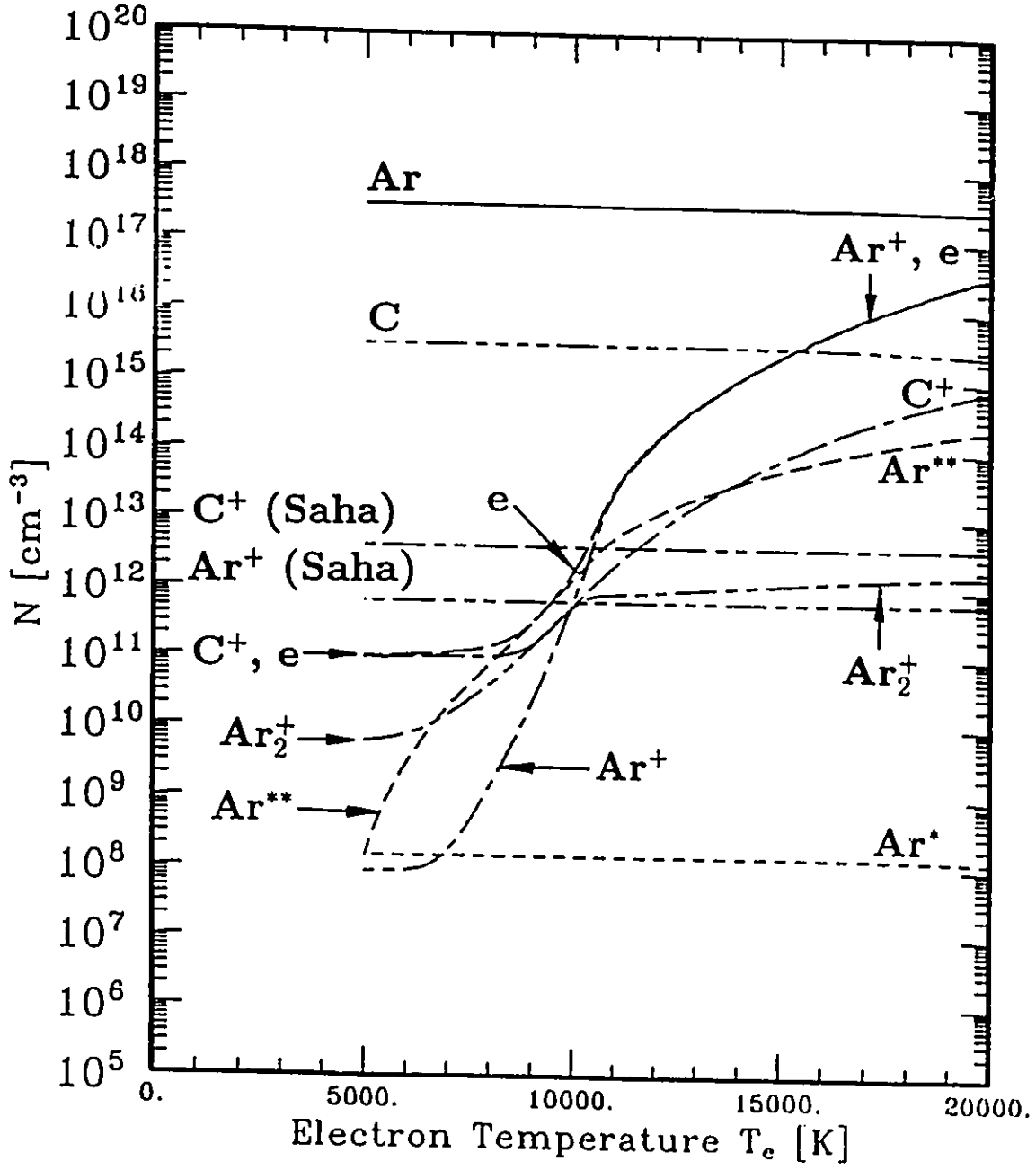

Figure 5.7: Ionized and neutral species concentrations as a function of electron temperature for an argon-1% carbon mixture with T_g = 5000 K, and p = 10 Torr.

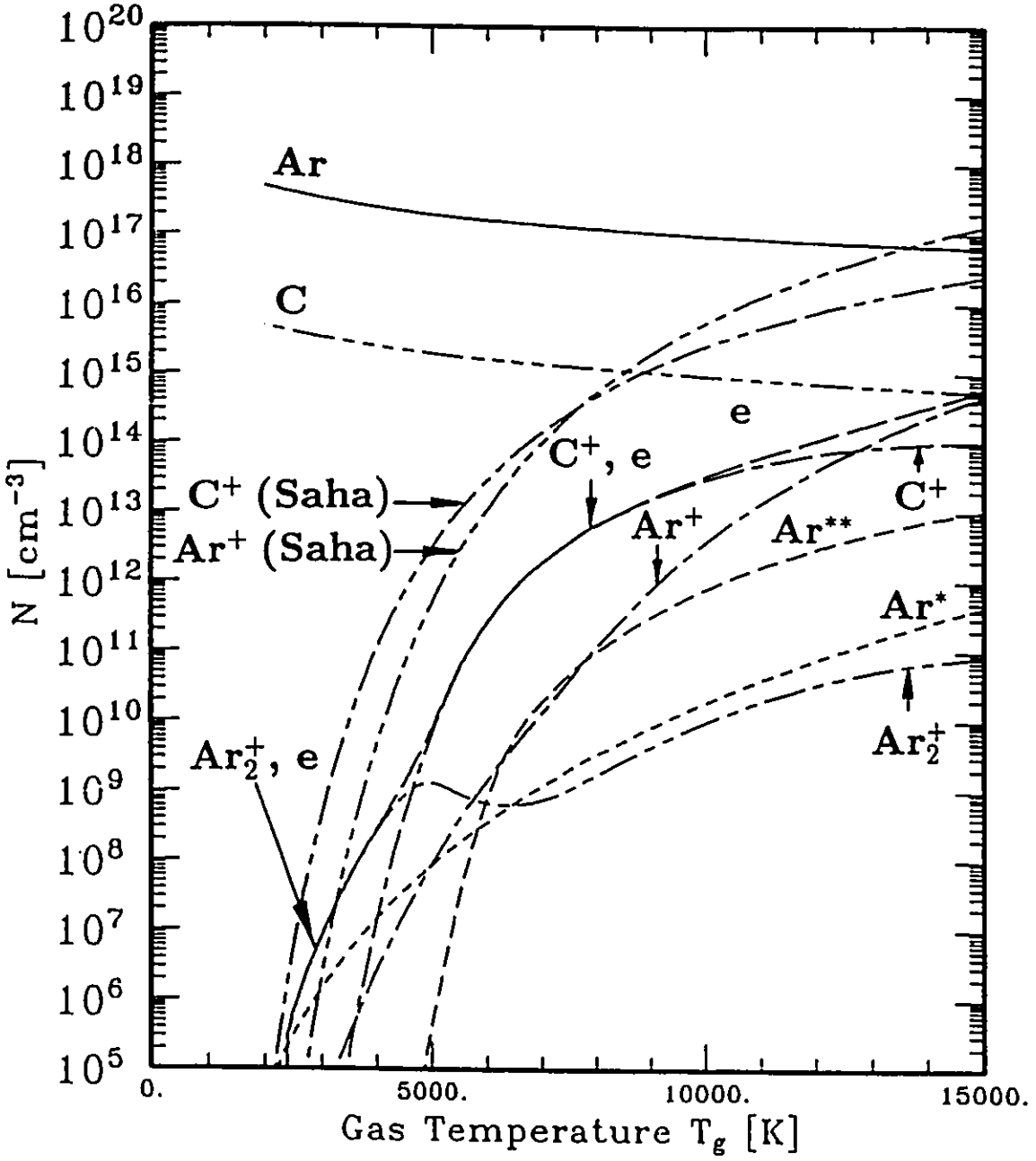

Figure 5.8: Ionized and neutral species concentrations as a function of gas temperature for an argon-1% carbon mixture with p = 100 Torr and $T_e = T_g$.

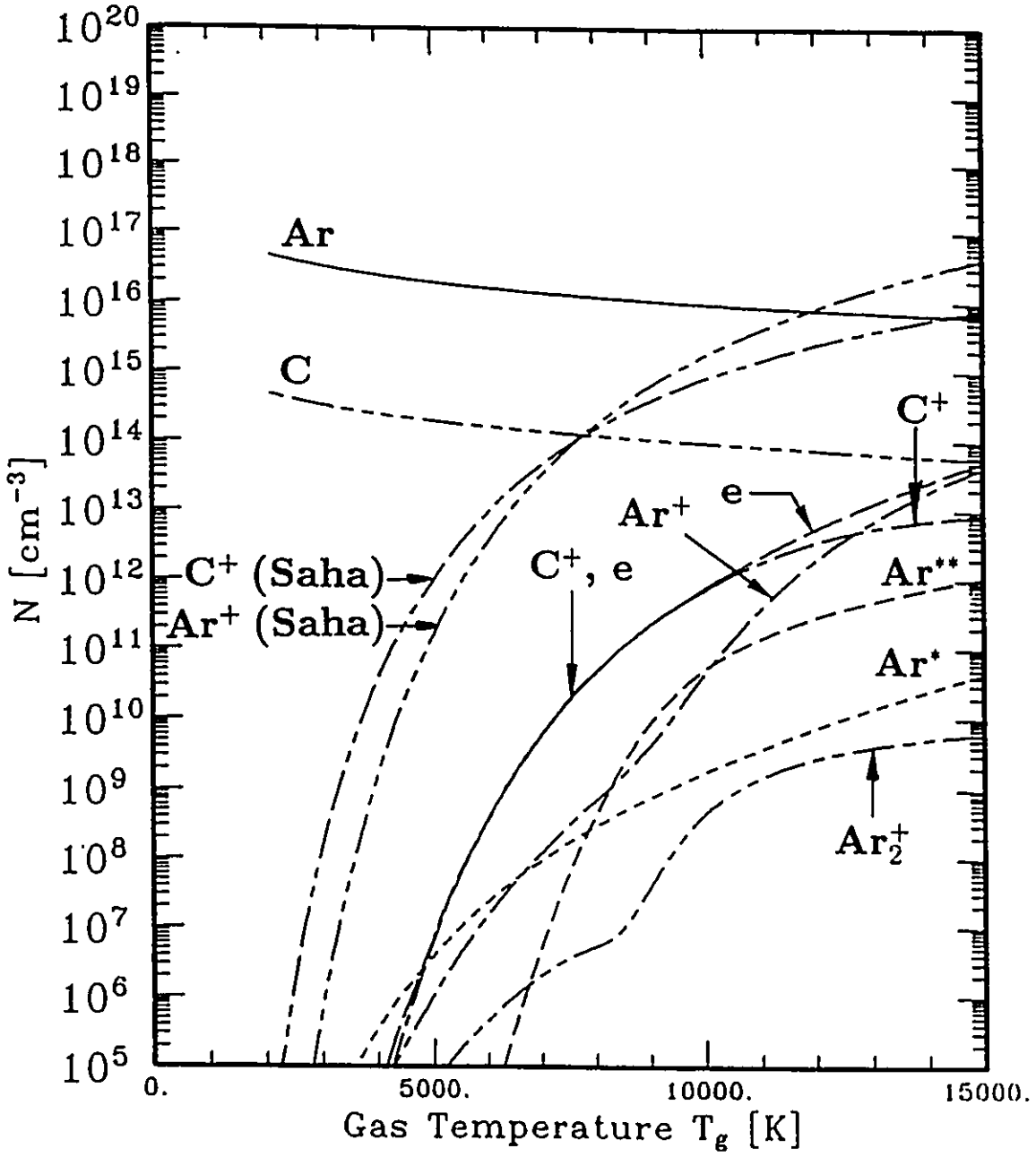

Figure 5.9: Ionized and neutral species concentrations as a function of gas temperature for an argon-1% carbon mixture with p = 10 Torr, and $T_e = T_g$.

that aside from the presence of the C and C^+ species in the system and a slight increase in the Ar^{**} concentration for the same reason as just outlined, the two models predict essentially the same results. The C^+ concentration gas temperature dependence is now also closer to that predicted by the Saha equation as the system comes closer to equilibrium with the increase in system pressure and the losses by diffusion decrease.

Summary of Pressure Effects

The gas temperature dependent concentrations of Ar, C, and the plasma density (as represented by the electron concentration) for pressures between 1 Torr and 15200 Torr have been summarized in Figure 5.11. The concentration of Ar^*, Ar^{**}, Ar^+, Ar_2^+, and C^+ have been omitted for the sake of clarity. Figure 5.11 illustrates the increases in absolute density which occur with increasing pressure.

The temperature ranges over which Ar_2^+, C^+, and Ar^+ form the dominant ionized species have also been indicated on this figure. As shown, the Ar_2^+ to C^+ ion dominance transition temperature tends to decrease with increasing pressure. The C^+ to Ar^+ ion dominance transition temperature tends to increase with increasing pressure. Thus, the temperature range over which C^+ is predicted to form the dominant ionized species increases with increasing pressure.

A summary of the effects of pressure on the degree of ionization has been compiled in Figure 5.12 for pressures between 1 Torr and 15200 Torr, where the degree of ionization is defined as

$$\alpha = \frac{[e]}{[Ar] + [Ar^*] + [Ar^{**}] + [Ar^+] + 2[Ar_2^+] + [C] + [C^+]} \tag{5.10}$$

As indicated in Figure 5.12, the degree of ionization tends to increase with increasing pressure over the entire temperature range. However, as the pressure increases, the increase in the degree of ionization becomes smaller, until there is almost no difference between the temperature dependent value of α at 760 Torr and the temperature dependent value of α at 15200 Torr.

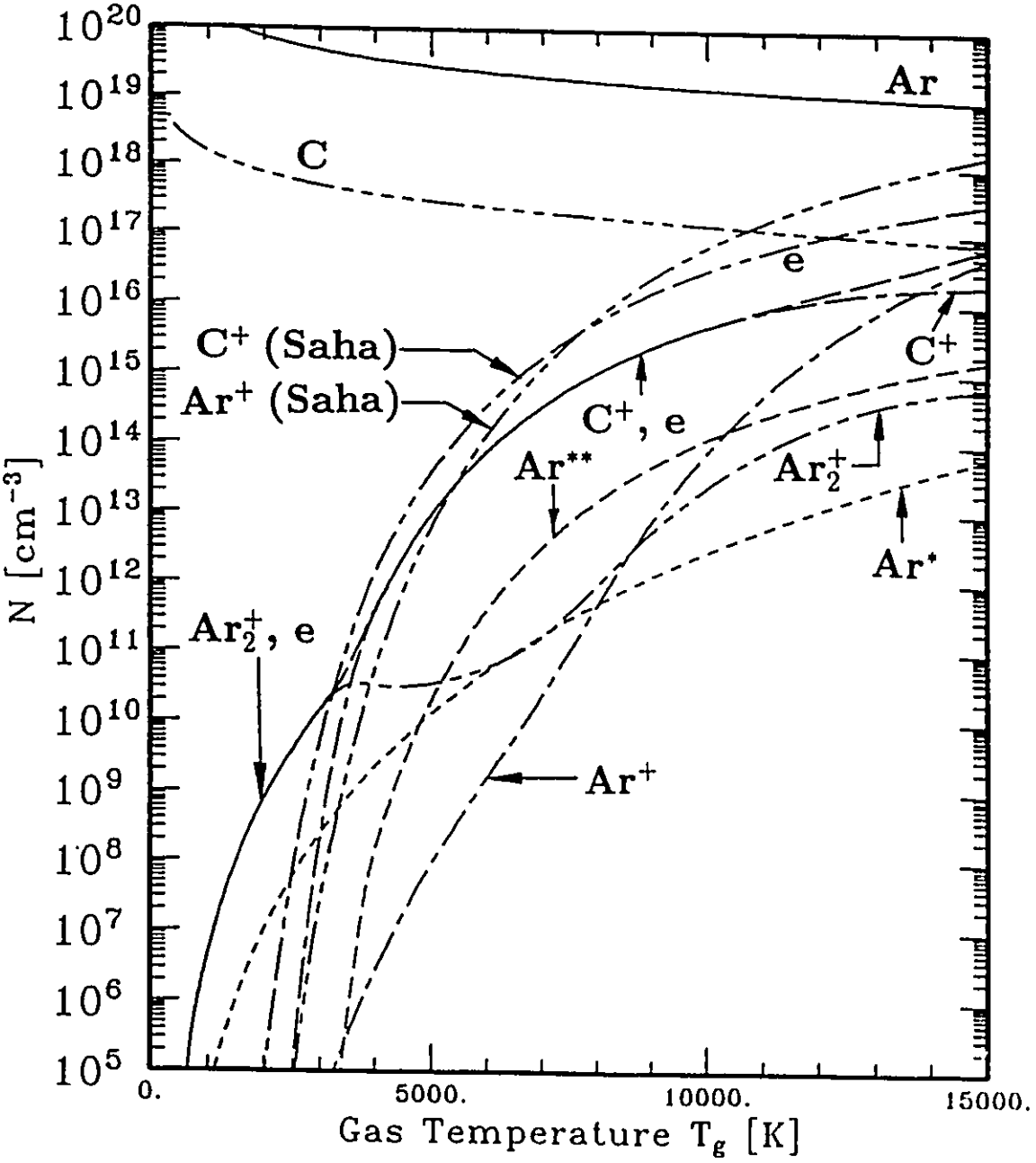

Figure 5.10: Ionized and neutral species concentrations as a function of gas temperature for an argon-1% carbon mixture with p = 15200 Torr, and $T_e = T_g$.

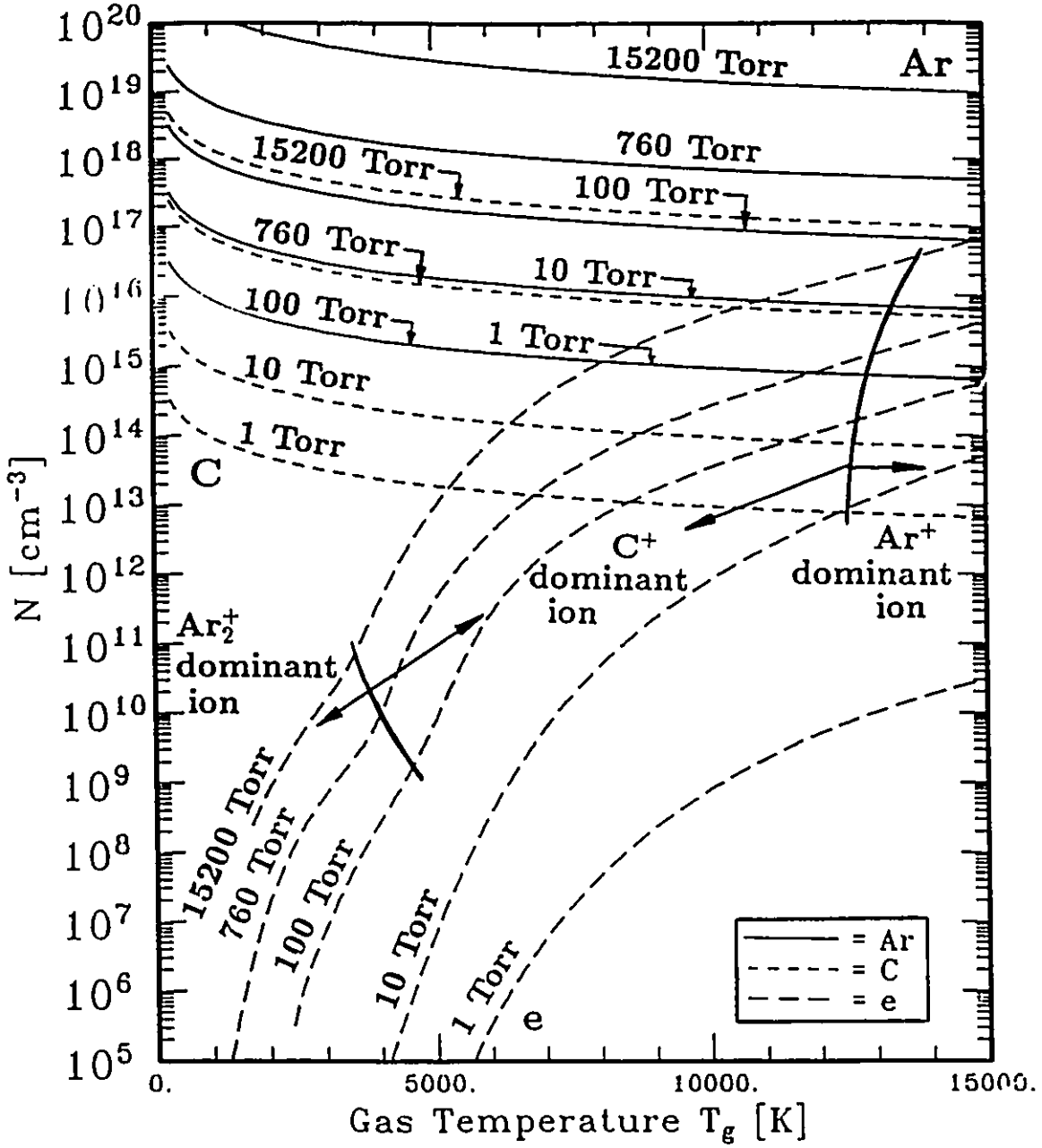

Figure 5.11: Summary of the effect of changing pressure on the temperature dependent concentrations of Ar, C, and e for an Ar-1%C mixture plasma.

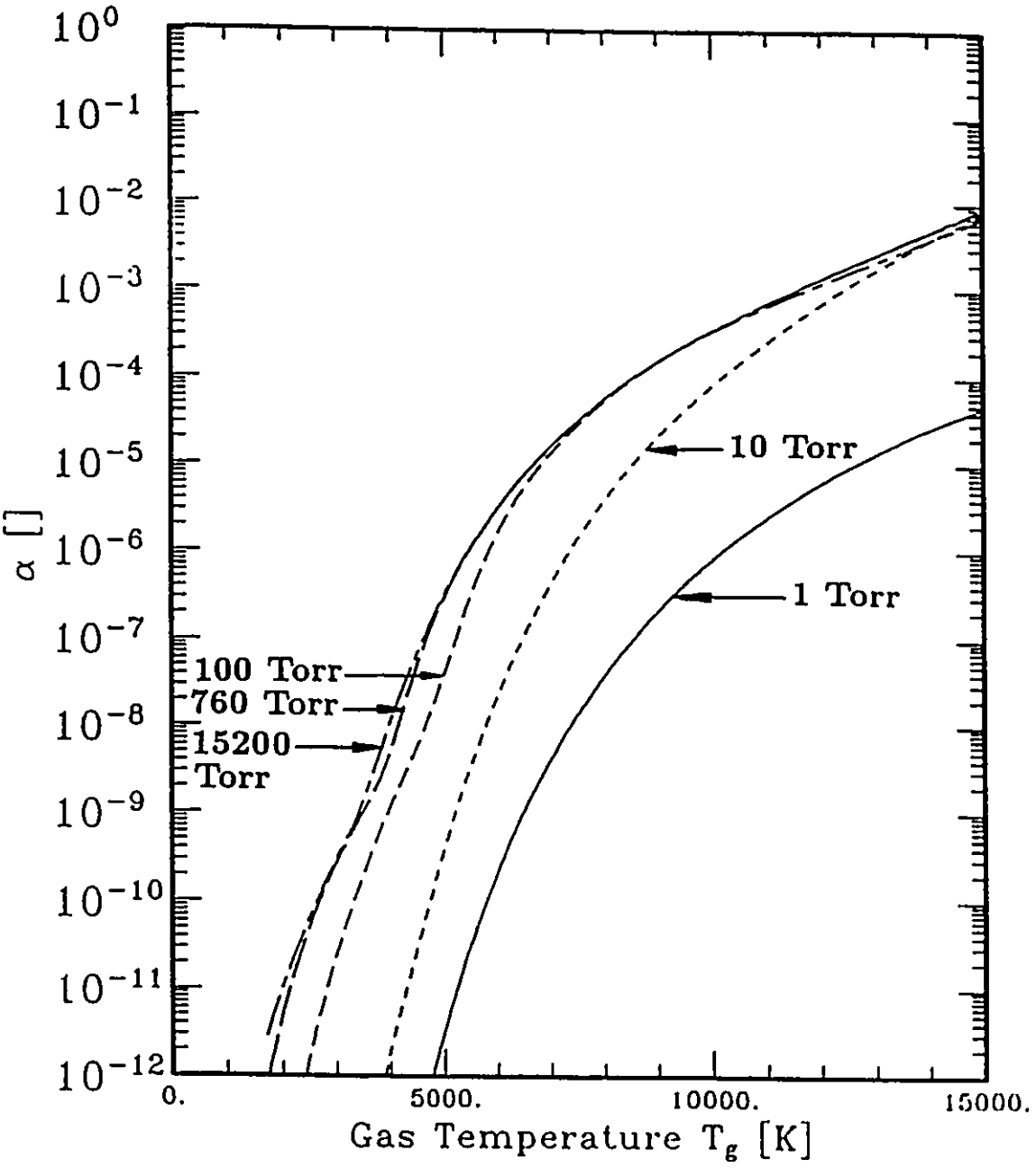

Figure 5.12: Summary of the effect of changing pressure on the degree of ionization for an Ar-1%C mixture plasma.

5.3.4 Carbon Percentage Mixture Effects

Since the argon and carbon reactions are coupled together via electrons, an increase or decrease in the relative percentage of carbon in the system can have a significant effect on the Ar-C plasma. Reducing the carbon percentage to values less than 1% causes the Ar-C plasma temperature dependent species concentrations to approach those of the pure argon plasma shown in Chapter 4.

Figure 5.13 shows the gas temperature dependent neutral and ionic species concentrations when the carbon percentage is increased to 10% for p = 760 Torr with $T_e = T_g$. As shown in this figure, the increase of carbon concentration in the plasma has caused a concomitant increase in the C^+ concentration, most likely through the thermal impact ionization reaction

$$C + C \xrightarrow{k_{C1}} C^+ + C + e$$

as well as the electron impact ionization reaction

$$C + e \xrightarrow{k_{C2}} C^+ + e + e$$

Here, C^+ forms the dominant ionized species over the temperature range T_g = 3500–12500 K. When compared to Figure 5.3, the results of Figure 5.13 show that the increase in electron concentration caused by the increase in C^+ density over this temperature range has the tendency to increase the Ar^+, Ar_2^+, and Ar^{**} density. Likely causes for the increases in the densities of these species have been discussed in detail in Section 5.3.1.

Summary of Percentage Carbon Effects

The effect of changing the percentage of carbon on the temperature dependent concentrations of Ar, C, and the plasma density (as represented by the concentration of electrons) for carbon percentages between 0.1% and 40% has been summarized in Figure 5.14. The concentrations of Ar^*, Ar^{**}, Ar^+, Ar_2^+, and C^+ have been omitted for the sake of clarity. As indicated in this figure, the plasma density tends to increase with increasing percentage of carbon. As shown, this effect occurs primarily over the

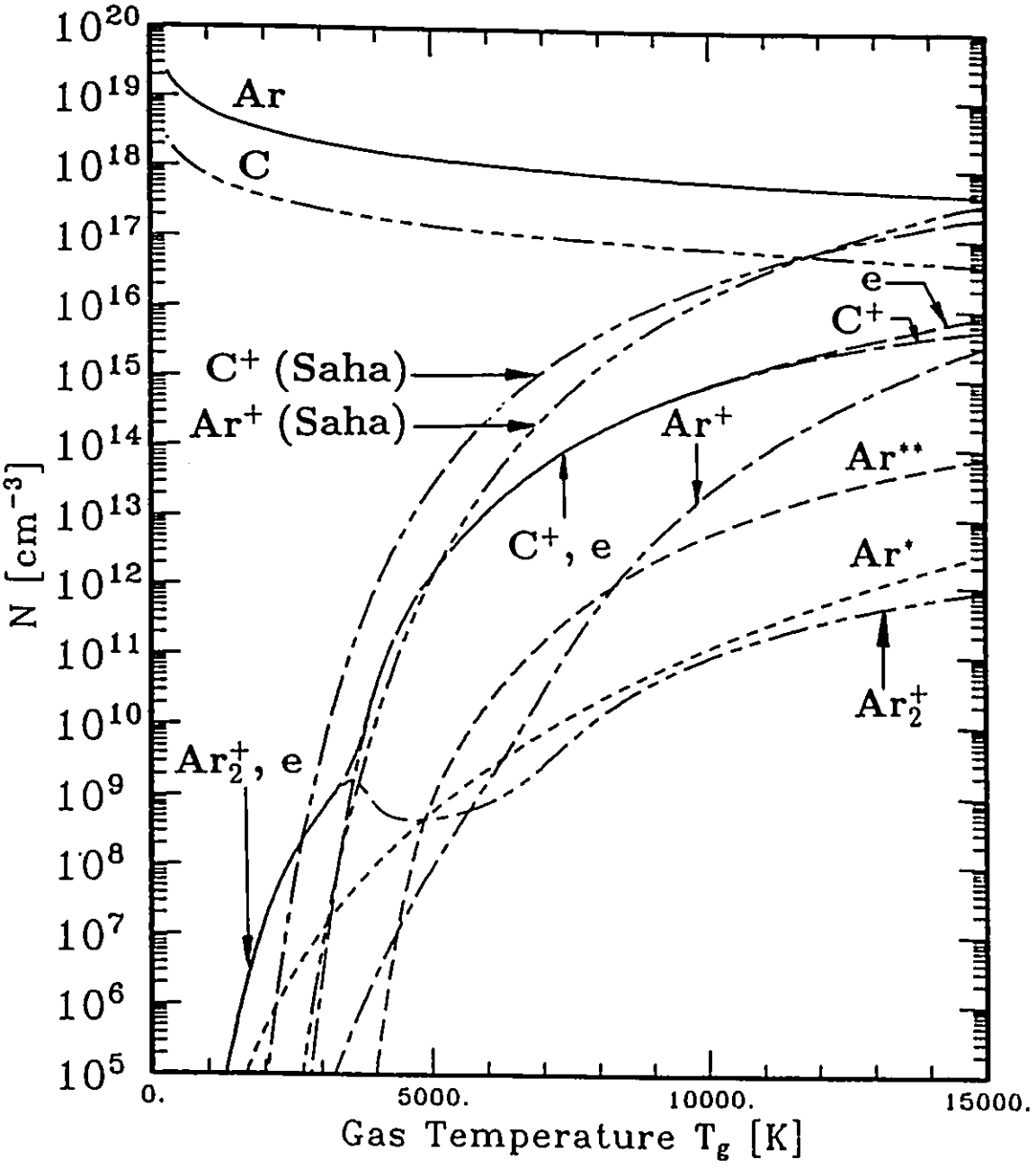

Figure 5.13: Ionized and neutral species concentrations as a function of gas temperature for an argon-10% carbon mixture with p = 760 Torr, and $T_e = T_g$.

T_g = 4000–15000 K temperature range. In this temperature range, the concentration of C^+ either forms the dominant ion, or its presence has a significant effect on the electron concentration through the charge balance relationship defined in equation 5.7.

At temperatures less than T_g = 3500 K, the plasma density remains relatively unaffected by changes in percentage carbon. Here, the C^+ ion neither forms the dominant ion, nor does it significantly affect the concentration of electrons. Instead, the Ar_2^+ ion, which is not significantly affected by the change in percentage carbon in this temperature range, forms the dominant ion.

The degree of ionization α, is also sensitive to changes in the percentage of carbon as shown in Figure 5.15 for percentages of carbon between 0.1 and 40%. In this case, the degree of ionization tends to follow the same trends as shown by the electron density in Figure 5.15 due to the fact that the total species concentration does not change with changes in percentage carbon.

5.4 Comparison with Experimental Results

Although numerous investigations have examined plasmas produced by electrical discharges using carbon electrodes[126][127][128] and some authors have considered the rate of erosion of the electrodes used in such experiments[129], very little interest has been focused on the concentration of carbon-bearing species produced under such circumstances. Similarly, when carbon or coal are fed into an arc or reside there by virtue of the process being undertaken, interest is normally focused only on the overall thermodynamic behaviour of the plasma itself[130]. Spectroscopic studies, including those of Beuthe et al. seem to indicate that C^+ is the primary ion expected under thermal plasma conditions[120][122][131]. This result tends to agree with the present predictions.

5.5 Summary of Ar-C Thermal Plasmas

The pure argon thermal plasma model developed in Chapter 4 has been extended to include atomic carbon. The results indicate that aside from electrons,

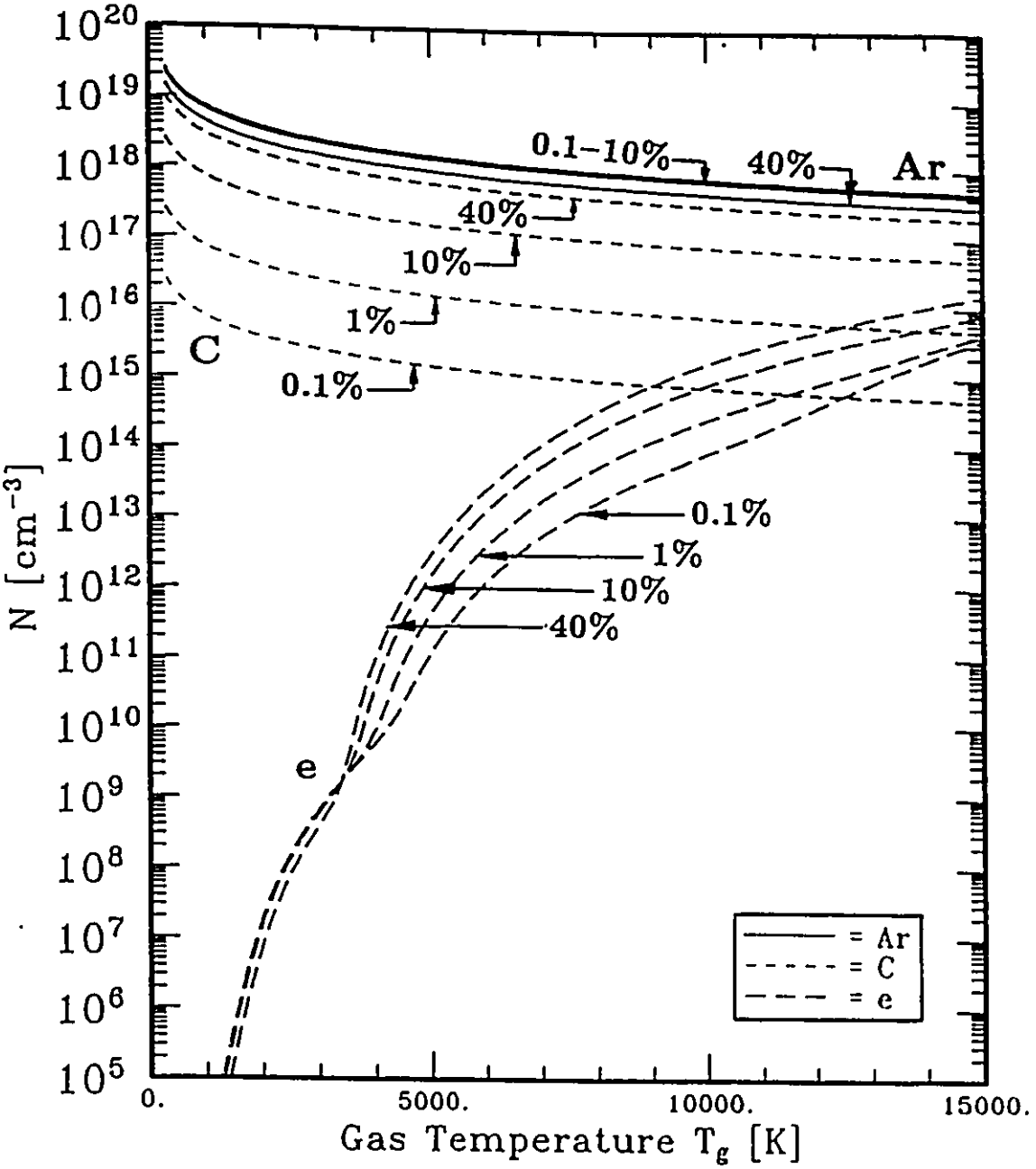

Figure 5.14: Summary of the effect of changing percentage carbon on the temperature dependent concentrations of Ar, C, and e for an Ar-C mixture plasma.

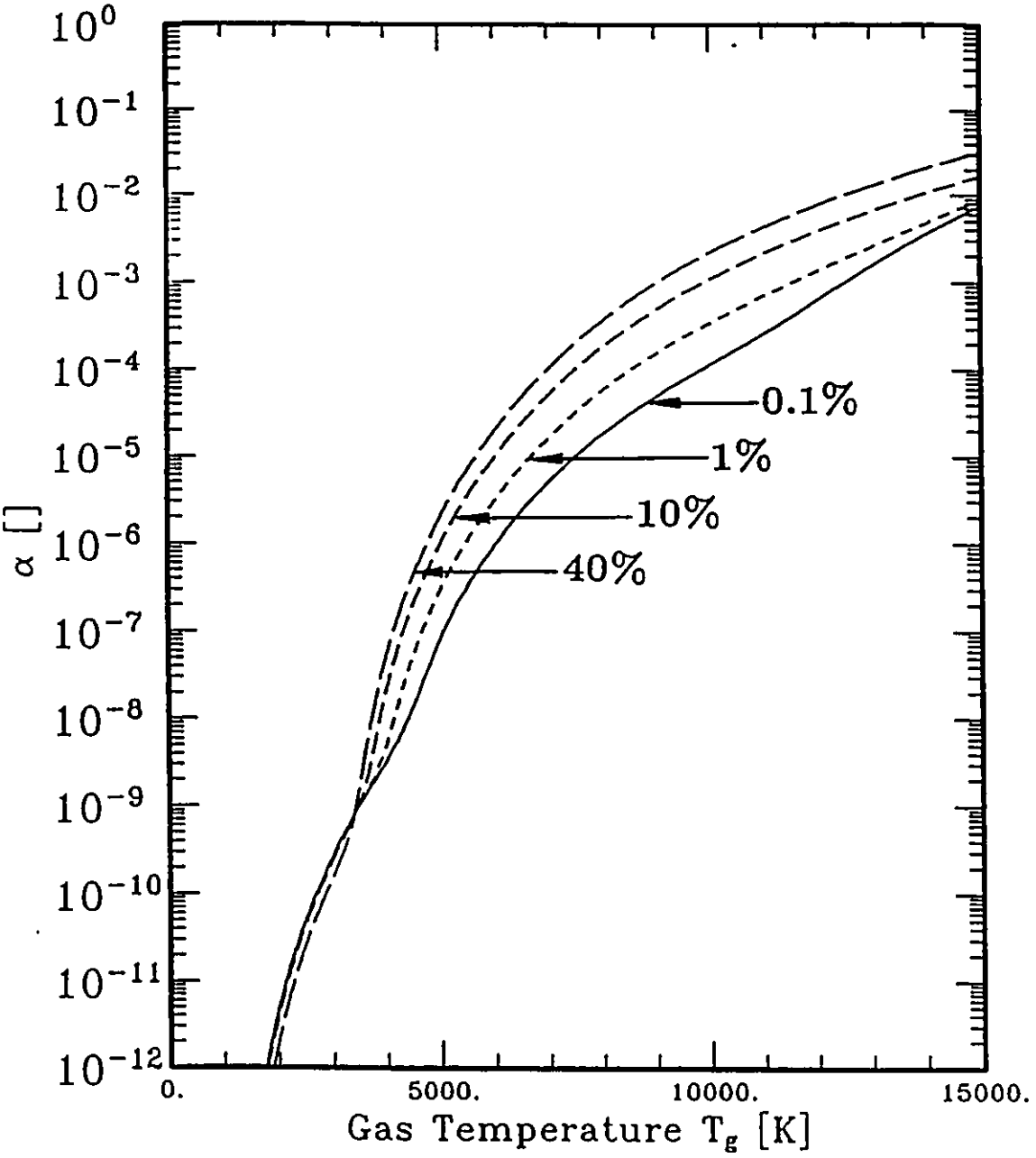

Figure 5.15: Summary of the effect of changing percentage carbon on the degree of ionization for an Ar-C mixture plasma.

there is no other direct coupling between the argon and the carbon in the plasma. A number of calculations have been done under various imposed physical conditions to examine the effect of the carbon on the argon plasma.

Results show that, other than the species Ar^*, Ar^{**}, Ar^+, and Ar_2^+ which were also encountered in the pure argon model of Chapter 4, an Ar-C mixture plasma also contains significant concentrations of C^+ ions. The concentrations of all excited and ionized species tend to increase with increasing gas and electron temperature. Under thermodynamic equilibrium conditions, at lower temperatures, Ar_2^+ tends to form the dominant ionized species, but is replaced by C^+ as temperature increases. At the higher temperatures, Ar^+ constitutes the dominant ionized species.

As in the pure argon model, under thermodynamic equilibrium conditions, the concentrations of Ar_2^+, C^+, and Ar^+ exceed that of the excited species Ar^* and Ar^{**}. Under thermodynamic non-equilibrium conditions, the concentration of Ar^{**} can exceed those of the positive ions, however the difference between the two tends to be significantly smaller than in the case of the pure argon model. Increases in pressure tend to increase the concentration of ionized species as well as increasing the temperature range over which C^+ forms the dominant ion. Increases in pressure are also seen to increase the degree of ionization, however the size of these increases also tend to diminish with increasing pressure. Changes in the percentage of carbon also significantly affect the ion concentrations, tending to increase the absolute ion concentration, as well as the degree of ionization with increasing percentage carbon. Increases in the C^+ concentration are the most likely cause of this effect.

The results indicate that the predicted concentration of ionic and excited species in the Ar-C plasma are comparable with the results of the pure argon plasma of Chapter 4 except over those temperatures at which C^+ is the dominant ion and the concomitant increase in electron density causes a significant change in the excited and ionized argon species. Comparison with the temperature dependent concentrations predicted by the Saha equations for Ar^+ and C^+ indicate that the results of the Ar-C chemical kinetic model tend to be significantly closer to the results predicted by the Saha equation than the pure argon model, but the Saha equation still consistently predicts a significantly higher plasma density than the present model.

Chapter 6

Numerical Model of Ar-CO_2 Thermal Plasma

6.1 Ar-Molecule Mixture Plasmas

Mixtures of argon with molecules represent a much more complex chemical kinetic system than the pure argon or argon-atom cases discussed in Chapters 4 and 5 respectively. Argon-molecule mixtures are commonly used under plasma conditions where it is desirable to alter the properties or composition of the gases or deposit a component of the molecular gas on a substrate. Such mixtures represent a formidable experimental and modelling challenge to investigators. The original molecules can break up and re-form into neutral or ionic atomic, di-atomic, or polyatomic species. The concentration of each of these species underlies a coupled set of generation and loss processes as described in Chapter 3.

As mentioned in Chapter 1, the Ar-CO_2 system has been a subject of some interest in the past. This combination of gases represents a mixture of relatively inert gases at room temperature, but the chemical composition of this mixture becomes a complex problem when the mixture is raised to the temperatures typically found in thermal plasmas. The Ar-C model developed in Chapter 5 must now be combined with a model to describe the behaviour of CO_2 and all its potential reaction products such as CO, O_2, O_3 as well as all potential ionic species.

The comprehensive models which have been used to describe the high temperature behaviour of Ar-CO_2 mixtures[10]–[28] are not yet well established. Under thermal plasma conditions, these models range from the very simplest which consider as few as 6 reactions[18], to slightly more complex formulations which may include a few dozen reactions[12]. In general, these studies normally consider only the presence of neutral species, using thermodynamic equilibrium models. Only passing consideration is given, if any, to ionic species. An initial examination of the possible ionic species to be found in an Ar-CO_2 plasma has been made by Maezono and Chang[30] based on a modified combustion gas model of Chang[31], but no comprehensive chemical kinetic models have been constructed to investigate the behaviour of Ar-CO_2 mixtures under thermal plasma conditions.

The objective of the present study is to assemble a chemical kinetic model which:

- Considers all neutral and ionic species for which sufficient chemical kinetic data exists to construct a model
- Uses the best experimental and theoretical data available but relies primarily on experimentally derived data wherever possible
- Takes into account both thermal and electron impact reactions
- Includes all relevant ionization, recombination, attachment, dissociation, ion-molecule and neutral reactions as well as accounting for diffusion
- Can be used to consider electron and gas temperature non-equilibrium conditions and pressure effects.

Special emphasis will be given to the types and concentrations of ionic, excited and neutral species which can be found in Ar-CO_2 mixtures under different electrical discharge plasma conditions.

6.2 Chemistry of Ar-CO_2 Mixture Plasmas

The fundamental form of the model established in Chapter 3 and already used in Chapters 4 and 5 will again be applied in this case. Since the model includes argon, carbon, and oxygen, the degree of ionization predicted by the Saha equation will be calculated for all three elements. The information needed to calculate the Saha equation for Ar and C can be found in Chapters 4 and 5 respectively. For oxygen, the ratio of the partition functions is $U_{i,O}/U_{a,O} = 4/9$ over the temperature range considered in this model[35]. The first ionization energy of oxygen is $E_{i,O} = 13.613$ eV. Ionic species considered in this model are Ar^+, Ar_2^+, C^+, $CArO^+$, CO^+, CO_2^+, CO_4^+, $C_2O_2^+$, O^+, O_2^+, O_4^+, O_5^+, CO_3^-, CO_4^-, O^-, O_2^-, O_3^- and electrons. Neutral species which have been considered are Ar, Ar^*, Ar^{**}, C, CO, CO_2, O, O_2 and O_3.

Reactions involving Ar or Ar+C have been listed previously in Tables 4.1 and 5.1. The reactions which complete the Ar-CO_2 model have been listed in Tables 6.1–6.7. Table 6.1 outlines electron impact (I1, I2, I4–I6) and thermal impact (I3, I8) ionization reactions, Table 6.2 includes electron impact attachment reactions, Table 6.3 contains electron impact dissociation reactions, Table 6.4 lists recombination reactions, Tables 6.5 and 6.6 outline ion-molecule reactions involving positive and negative species respectively, and Table 6.7 covers neutral reactions. The subscript letters I, A, D, R, M and N which are used to identify the reaction rate constants k denote **I**onization, **A**ttachment, **D**issociation, **R**ecombination, ion-**M**olecule and **N**eutral reactions respectively. Reactions will be referred to using these letters and the numbers associated with them as shown in Tables 6.1–6.7.

Important sources and sinks of neutral, positively charges species, and negatively charged species have been listed in Tables 6.8, 6.9, and 6.10 respectively. The major and minor sources of species were ascertained by systematic removal and replacement of each reaction in the model. In order for a reaction to qualify as a major source or sink of a particular species, its removal must have caused a change in the temperature dependent concentration profile of the species of at least 1 order of magnitude over the indicated temperature range. Where no temperature range was indicated, the entire temperature dependent concentration profile was affected. In

Table 6.1: Ionization reactions for the Ar-CO_2 system.

CO_2 System

Ionization Reactions	Reaction Rate Constants [cm^3/s],[cm^6/s]*	T_g, T_e [K]	Ref.
$CO + e \xrightarrow{f_{11,1}k_{11}} CO^+ + e + e$	$0.70 \times 1.4 \times 10^{-11} T_e^{1/2}(1 + 1.3 \times 10^{-5} T_e)$* $\exp(-1.5 \times 10^5/T_e)$	Cross Section	[132][133][134]
$\xrightarrow{f_{11,2}k_{11}} C^+ + O + e + e$	$0.20 \times k_{11}$		
$\xrightarrow{f_{11,3}k_{11}} C^+ + O^+ + e + e$	$0.10 \times k_{11}$		
$CO_2 + e \xrightarrow{f_{12,1}k_{12}} CO_2^+ + e + e$	$0.65 \times 1.4 \times 10^{-11} T_e^{1/2}(1 + 1.3 \times 10^{-5} T_e)$* $\exp(-1.5 \times 10^5/T_e)$	Cross Section	[132][135]
$\xrightarrow{f_{12,2}k_{12}} CO^+ + O + e + e$	$0.10 \times k_{12}$		
$\xrightarrow{f_{12,3}k_{12}} C^+ + O_2 + e + e$	$0.10 \times k_{12}$		
$\xrightarrow{f_{12,4}k_{12}} O^+ + CO + e + e$	$0.10 \times k_{12}$		
$\xrightarrow{f_{12,5}k_{12}} O_2^+ + C + e + e$	$0.05 \times k_{12}$		
$O + O \longrightarrow O^* + O \xrightarrow{k_{13}} O^+ + O + e$	$181.8 \times pT_g^{1/2}N_o^{-1}(1 + 1.6 \times 10^5/T_g)$* $\exp(-1.6 \times 10^5/T_g)$	Theory	[124]
$O + e \xrightarrow{k_{14}} O^+ + e + e$	$4.1 \times 10^{-11} T_e^{1/2}(1 + 1.3 \times 10^{-5} T_e)$* $\exp(-1.5 \times 10^5/T_e)$	Cross Section	[132][136]
$O_2 + e \xrightarrow{f_{15}k_{15}} O_2^+ + e + e$	$1.1 \times 10^{-12} T_e^{1/2}(1 + 1.4 \times 10^{-5} T_e)$* $\exp(-1.4 \times 10^5/T_e)$	Cross Section	[132][133][136]
$\xrightarrow{(1-f_{15})k_{15}} O + O^+ + e + e$	0.75		
$O_3 + e \xrightarrow{k_{16,1}} O_2^+ + O + e + e$	$3.2 \times 10^{-11} T_e^{1/2}(1 + 1.3 \times 10^{-5} T_e)$* $\exp(-1.5 \times 10^5/T_e)$	Cross Section	[136]
$\xrightarrow{k_{16,2}} O^+ + O^- + O + e + e$	$8.4 \times 10^{-12} T_e^{1/2}(1 + 9.4 \times 10^{-6} T_e)$* $\exp(-2.1 \times 10^5/T_e)$	Cross Section	[136]

*[cm^3/s] for two-body reactions and [cm^6/s] for three-body reactions.

Table 6.2: Attachment reactions for the Ar-CO_2 system.

Attachment Reactions	Reaction Rate Constants [cm^3/s],[cm^6/s]		T_g, T_e [K]	Ref.
$CO + e \xrightarrow{k_{A1}} C + O^-$	k_{A1}	$0.08 \times 10^{-13}(T_g/300)$	Theory	[134][137]
$CO_2 + e \xrightarrow{k_{A2}} CO + O^-$	k_{A2}	$5 \times 10^{-13}(T_g/300)^{3/2}(T_e/300)^{-1.5}$	Theory	[137]
$O + e \xrightarrow{k_{A3}} O^- + h\nu$	k_{A3}	$1.3 \times 10^{-15}(T_g/300)$	150-500	[136][138]
$O + e + M \xrightarrow{k_{A4}} O^- + M$	k_{A4}	$1.0 \times 10^{-31} \exp(300/T_g)$, M=$O_2$	Theory	[136][138]
$O_2 + e \xrightarrow{k_{A5}} O + O^-$	k_{A5}	$3 \times 10^{-12}(T_g/300)^{3/2}(T_e/300)^{-1.5}$	Theory	[136][139]
$O_2 + e + M \xrightarrow{k_{A6}} O_2^- + M$	k_{A6}	$2.2 \times 10^{-29}(300/T_g)^{1.5} \cdot \exp(-600/T_g)$, M=$O_2$	195-600	[136][138]
$O_3 + e \xrightarrow{k_{A7}} O^- + O_2$	k_{A7}	$8.9 \times 10^{-12}(T_g/300)^{1.5}$	300-6000	[138]
$O_3 + e + M \xrightarrow{k_{A8}} O_3^- + M$	k_{A8}	4.6×10^{-28}, M=O_2	300	[136]

Table 6.3: Dissociation reactions for the Ar-CO_2 system.

Dissociation Reactions	Reaction Rate Constants [cm^3/s],[cm^6/s]		T_g, T_e [K]	Ref.
$CO + e \xrightarrow{k_{D1}} C + O + e$	k_{D1}	1.0×10^{-12}	300	[137]
$CO_2 + e \xrightarrow{k_{D2}} CO + O + e$	k_{D2}	1.6×10^{-11}	300	[139]
$O_2 + e \xrightarrow{k_{D3}} O + O + e$	k_{D3}	$4.5 \times 10^{-11} T_e^{1/2}(1 + 2.9 \times 10^{-5} T_e) \cdot \exp(-7.0 \times 10^4/T_e)$	Cross Section	[136]
$O_3 + e \xrightarrow{k_{D4}} O_2 + O + e$	k_{D4}	9.0×10^{-10}	300	[136]

Table 6.4: Recombination reactions for the Ar-CO_2 system.

Recombination Reactions	Reaction Rate Constants [cm^3/s],[cm^6/s]		T_g, T_e [K]	Ref.
$CArO^+ + e \xrightarrow{k_{R1}} Ar + CO$	k_{R1}	$1 \times 10^{-6}(T_e/300)^{-0.5}$	Theory	[62]
$CO^+ + e \xrightarrow{k_{R2}} C + O$	k_{R2}	$6.8 \times 10^{-7}(T_e/300)^{-0.4}$	Theory	[62]
$CO_2^+ + e \xrightarrow{f_{R3}k_{R3}} CO + O$	k_{R3}	$3.4 \times 10^{-6}(T_e/300)^{-0.4}$	Theory	[62]
$\xrightarrow{(1-f_{R3})k_{R3}} C + O_2$	f_{R3}	0.50	Theory	[62]
$CO_4^+ + e \xrightarrow{k_{R4}} CO_2 + O_2$	k_{R4}	$1 \times 10^{-6}(T_e/300)^{-0.5}$	Theory	[62]
$C_2O_2^+ + e \xrightarrow{k_{R5}} CO + CO$	k_{R5}	$5 \times 10^{-6}(T_e/300)^{-0.5}$	Theory	[62]
$O^+ + e \xrightarrow{k_{R6}} O + h\nu$	k_{R6}	$3.5 \times 10^{-12}(T_e/300)^{-0.7}$	Theory	[136]
$O_2^+ + e \xrightarrow{k_{R7}} O + O$	k_{R7}	$2.3 \times 10^{-7}(T_e/300)^{-0.6}$	600-2500	[140]
$O_4^+ + e \xrightarrow{k_{R8}} O_2 + O_2$	k_{R8}	$2.3 \times 10^{-6}(T_e/300)^{-0.6}$	Theory	[62]
$O_5^+ + e \xrightarrow{k_{R9}} O_2 + O_3$	k_{R9}	$5 \times 10^{-6}(T_e/300)^{-0.6}$	Theory	[62]
$O_y^+ + e + e \xrightarrow{k_{R10}} O_m + O_n + e$	k_{R10}	$1 \times 10^{-29}(T_e/300)^{-4.5}$	Theory	[136][138]
$O_y^+ + e + M \xrightarrow{k_{R11}} O_m + O_n + M$	k_{R11}	$1 \times 10^{-26}(T_e/300)^{-0.5}$, $M=O_2$	Theory	[136][138]
$X^- + Y^+ \xrightarrow{k_{R12}}$ neutral species	k_{R12}	$1 \times 10^{-7}(T_e/300)^{-0.5}$	Theory	[136][138]
$X^- + Y^+ + M \xrightarrow{k_{R13}}$ neutral species + M	k_{R13}	$1 \times 10^{-25}(T_e/300)^{-2.5}$	Theory	[136][138]

Table 6.5: Ion-molecule reactions for the Ar-CO_2 system (positive ions).

Ion-Molecule Reactions	Reaction Rate Constants [cm^3/s],[cm^6/s]		T_g, T_e [K]	Ref.
$Ar^+ + CO \xrightarrow{k_{M1}} CO^+ + Ar$	k_{M1}	9.0×10^{-11}	300	[141]
$Ar^+ + CO_2 \xrightarrow{k_{M2}} CO_2^+ + Ar$	k_{M2}	7.6×10^{-10}	300	[141]
$Ar^+ + O \xrightarrow{k_{M3}} O^+ + Ar$	k_{M3}	0.64×10^{-11}	300	[142]
$Ar^+ + O_2 \xrightarrow{k_{M4}} O_2^+ + Ar$	k_{M4}	4.6×10^{-11}	300	[141]
$Ar_2^+ + CO \xrightarrow{f_{M5}k_{M5}} CO^+ + Ar + Ar$	k_{M5}	8.5×10^{-10}	300	[141]
$\xrightarrow{(1-f_{M5})k_{M5}} CArO^+ + Ar$	f_{M5}	0.50	300	
$Ar_2^+ + CO_2 \xrightarrow{k_{M6}} CO_2^+ + Ar + Ar$	k_{M6}	1.1×10^{-9}	300	[141]
$Ar_2^+ + O_2 \xrightarrow{k_{M7}} O_2^+ + Ar + Ar$	k_{M7}	1.2×10^{-10}	300	[141]
$C^+ + CO \xrightarrow{k_{M8}} CO^+ + C$	k_{M8}	5×10^{-13}	300	[141]
$C^+ + CO_2 \xrightarrow{k_{M9}} CO^+ + CO$	k_{M9}	1.1×10^{-9}	300	[141]
$C^+ + O_2 \xrightarrow{f_{M10}k_{M10}} O^+ + CO$	k_{M10}	9.9×10^{-10}	300	[141]
$\xrightarrow{(1-f_{M10})k_{M10}} CO^+ + O$	f_{M10}	0.62	300	
$CArO^+ + CO \xrightarrow{k_{M11}} C_2O_2^+ + Ar$	k_{M11}	4.6×10^{-10}	300	[141]
$CO^+ + CO_2 \xrightarrow{k_{M12}} CO_2^+ + CO$	k_{M12}	1.0×10^{-9}	300	[141]
$CO^+ + O \xrightarrow{k_{M13}} O^+ + CO$	k_{M13}	1.4×10^{-10}	300	[141]
$CO^+ + O_2 \xrightarrow{k_{M14}} O_2^+ + CO$	k_{M14}	1.2×10^{-10}	300	[141]
$CO_2^+ + O \xrightarrow{f_{M15}k_{M15}} O_2^+ + CO$	k_{M15}	2.6×10^{-10}	300	[141]
$\xrightarrow{(1-f_{M15})k_{M15}} O^+ + CO_2$	f_{M15}	0.63	300	
$CO_2^+ + O_2 \xrightarrow{k_{M16}} O_2^+ + CO_2$	k_{M16}	6.4×10^{-11}	300	[141]
$CO_4^+ + O_3 \xrightarrow{k_{M17}} O_5^+ + CO_2$	k_{M17}	1×10^{-10}	300	[141]
$O^+ + CO_2 \xrightarrow{f_{M18}k_{M18}} O_2^+ + CO$	k_{M18}	9×10^{-10}	300	[141]
$\xrightarrow{(1-f_{M18})k_{M18}} CO_2^+ + O$	f_{M18}	0.50	300	
$O^+ + O + M \xrightarrow{k_{M19}} O_2^+ + M$	k_{M19}	1.0×10^{-29}, M=O_2	300	[136]
$O^+ + O_2 \xrightarrow{k_{M20}} O_2^+ + O$	k_{M20}	$1.9 \times 10^{-11}(T_g/300)^{-0.5}$	Theory	[136][138][141]
$O_2^+ + CO_2 + M \xrightarrow{k_{M21}} CO_4^+ + M$	k_{M21}	2.3×10^{-29}, M=Ar	300	[141]
$O_2^+ + O_2 + M \xrightarrow{k_{M22}} O_4^+ + M$	k_{M22}	$4.0 \times 10^{-30}(T_g/300)^{-2.93}$, M=$O_2$	Theory	[136][138][141]
$O_4^+ + O \xrightarrow{k_{M23}} O_2^+ + O_3$	k_{M23}	3×10^{-10}	300	[141]
$O_4^+ + M \xrightarrow{k_{M24}} O_2^+ + O_2 + M$	k_{M24}	1.8×10^{-13}, M=O_2	300	[141]
$O_5^+ + CO_2 \xrightarrow{k_{M25}} CO_4^+ + O_3$	k_{M25}	1.0×10^{-11}	300	[141]

Table 6.6: Ion-molecule reactions for the Ar-CO_2 system continued (negative ions).

Ion-Molecule Reactions	Reaction Rate Constants [cm^3/s],[cm^6/s]		T_g, T_e [K]	Ref.
$CO_3^- + CO \xrightarrow{k_{M26}} CO_2 + CO_2 + e$	k_{M26}	5×10^{-13}	300	[139]
$CO_3^- + O \xrightarrow{k_{M27}} O_2^- + CO_2$	k_{M27}	1.1×10^{-10}	300	[141]
$CO_4^- + O \xrightarrow{f_{M28,1}k_{M28}} CO_3^- + O_2$	$f_{M28,1}k_{M28}$	$0.80 \times 1.4 \times 10^{-10}$	300	[141]
$\xrightarrow{f_{M28,2}k_{M28}} O^- + CO_2 + O_2$	$f_{M28,2}$	0.10	300	
$\xrightarrow{f_{M28,3}k_{M28}} O_3^- + CO_2$	$f_{M28,3}$	0.10	300	
$CO_4^- + O_3 \xrightarrow{k_{M29}} O_3^- + CO_2 + O_2$	k_{M29}	1.3×10^{-10}	300	[141]
$O^- + CO \xrightarrow{k_{M30}} e + CO_2$	k_{M30}	5.5×10^{-10}	300	[141]
$O^- + CO_2 + M \xrightarrow{k_{M31}} CO_3^- + M$	k_{M31}	3.1×10^{-28}, M=O_2	300	[141]
$O^- + O \xrightarrow{k_{M32}} e + O_2$	k_{M32}	1.9×10^{-10}	300	[136][141]
$O^- + O_2 \xrightarrow{k_{M33}} e + O_3$	k_{M33}	1×10^{-12}	300	[136][141]
$O^- + M \xrightarrow{k_{M34}} O + e + M$	k_{M34}	6.9×10^{-10}, M=O_2	300	[136]
$O^- + O_2 + M \xrightarrow{k_{M35}} O_3^- + M$	k_{M35}	$1.1 \times 10^{-30}(T_g/300)^{-1}$, M=$O_2$	Theory	[136][138]
$O^- + O_3 \xrightarrow{k_{M36}} O_3^- + O$	k_{M36}	8×10^{-10}	300	[136][141]
$O_2^- + CO_2 + M \xrightarrow{k_{M37}} CO_4^- + M$	k_{M37}	4.7×10^{-29}, M=O_2	300	[141]
$O_2^- + O \xrightarrow{f_{M38}k_{M38}} e + O_3$	k_{M38}	3.0×10^{-10}	300	[136][141]
$\xrightarrow{(1-f_{M38})k_{M38}} O^- + O_2$	f_{M38}	0.50	300	
$O_2^- + M \xrightarrow{k_{M39}} O_2 + e + M$	k_{M39}	$2.7 \times 10^{-10}(T_g/300)^{0.5} \cdot \exp(-5590/T_g)$, M=$O_2$	Theory	[136][138]
$O_2^- + O_3 \xrightarrow{k_{M40}} O_3^- + O_2$	k_{M40}	6×10^{-10}	300	[141]
$O_3^- + CO_2 \xrightarrow{k_{M41}} CO_3^- + O_2$	k_{M41}	5.5×10^{-10}	300	[141]
$O_3^- + O \xrightarrow{k_{M42}} O_2^- + O_2$	k_{M42}	2.5×10^{-10}	300	[141]
$O_3^- + M \xrightarrow{k_{M43}} O_3 + e + M$	k_{M43}	2.3×10^{-11}, M=O_2	300	[136]

Table 6.7: Neutral reactions for the Ar-CO_2 system.

Neutral Reactions	Reaction Rate Constants [cm^3/s],[cm^6/s]		T_g, T_e [K]	Ref.
$CO + O \xrightarrow{k_{N1}} CO_2 + h\nu$	k_{N1}	$4.15 \times 10^{-18} \exp(-1600/T_g)$	200-2000	[143]
$CO + O + M \xrightarrow{k_{N2}} CO_2 + M$	k_{N2}	$6.5 \times 10^{-33} \exp(-2183/T_g)$, M=Ar	250-500	[143]
$CO + O_2 \xrightarrow{k_{N3}} CO_2 + O$	k_{N3}	$4.2 \times 10^{-12} \exp(-24000/T_g)$	1500-3000	[143]
$CO + O_3 \xrightarrow{k_{N4}} CO_2 + O_2$	k_{N4}	4×10^{-25}	300	[144]
$CO + M \xrightarrow{k_{N5}} C + O + M$	k_{N5}	$1.46 \times 10^{6} T_g^{-3.52} \exp(-128700/T_g)$, M=Ar	7000-15000	[143]
$CO_2 + C \xrightarrow{k_{N6}} CO + CO$	k_{N6}	1.0×10^{-15}	300	[137]
$CO_2 + O \xrightarrow{k_{N7}} CO + O_2$	k_{N7}	$2.8 \times 10^{-11} \exp(-26500/T_g)$	1500-3000	[143]
$CO_2 + M \xrightarrow{k_{N8}} CO + O + M$	k_{N8}	$6.06 \times 10^{-10} \exp(-25252/T_g)$, M=Ar	2400-4400	[145]
$O + C + M \xrightarrow{k_{N9}} CO + M$	k_{N9}	$9.1 \times 10^{-22} T_g^{-3.08} \exp(2114/T_g)$, M=Ar	7000-14000	[143]
$O + O + M \xrightarrow{k_{N10}} O_2 + M$	k_{N10}	$5.24 \times 10^{-35} \exp(900/T_g)$, M=Ar	190-4000	[136]
		$6.2 \times 10^{-32} \exp(-750/T_g)$, M=O	1000-8000	
		$1.3 \times 10^{-32} (T_g/300)^{-1} \exp(-170/T_g)$, M=$O_2$	1000-8000	
$O + O_2 + M \xrightarrow{k_{N11}} O_3 + M$	k_{N11}	$3.6 \times 10^{-34} (T_g/300)^{-1.93}$, M=Ar	200-1100	[136][143]
$O_2 + M \xrightarrow{k_{N12}} O + O + M$	k_{N12}	$3.0 \times 10^{-6} T_g^{-1} \exp(-59380/T_g)$, M=Ar	3000-18000	[143]
$O_3 + O \xrightarrow{k_{N13}} O_2 + O_2$	k_{N13}	$2.0 \times 10^{-11} \exp(-2280/T_g)$	220-1000	[136][143]
$O_3 + M \xrightarrow{k_{N14}} O_2 + O + M$	k_{N14}	$4.1175 \times 10^{-10} \exp(-11430/T_g)$, M=Ar	200-1000	[136][143]

cases where no major sources or sinks are listed, this is meant to indicate that there were no dominant sources or sinks. The results shown in Tables 6.8, 6.9, and 6.10 were compiled from the results of the chemical kinetic model assuming thermodynamic equilibrium conditions ($T_e = T_g$), p = 760 Torr, and an Ar-10%CO_2 mixture. Sources and sinks of Ar^*, Ar^{**}, Ar^+, Ar_2^+, and C^+ have not been included in the present analysis as they are essentially the same as discussed in Chapter 4 and Chapter 5. It should be noted however that the ion-molecule reactions M1–M10 also represent significant sinks of Ar^+, Ar_2^+, and C^+.

A summary of the chemical kinetics of the Ar-CO_2 system has been outlined in Figures 6.1, 6.2 and 6.3 for neutral species, positive ions and negative ions respectively. In order to maintain the clarity of Figure 6.1, only neutral-neutral and ion-neutral collision reactions which act as sources or sinks of neutral species were included. The reactions have been indicated according to the letters (I, A, D, R, M, and N) and numbers used to define them in Tables 6.1–6.7. As indicated in Table 6.8, according to the results of the present chemical kinetic model, there are no ion-ion collision reactions which act as significant sources or sinks of neutral species. Thus, Figure 6.1 represents a concise summary of the important neutral species chemistry in an Ar-CO_2 thermal plasma.

Figures 6.2 and 6.3 include all neutral-ion and ion-ion collision reactions which act as sources or sinks of positive and negative ions respectively. To avoid making these figures unnecessarily complex, neutral-neutral reactions and reactions which generate neutral species have only been included in cases where these reactions act as significant sources or sinks of ionic species. A full summary of the sources and sinks of all species considered in the present Ar-CO_2 chemical kinetic thermal plasma model has been included in Appendix A.

The coupled rate equations for the different species in an Ar-CO_2 mixture plasma at the centre of a cylindrical discharge tube can be written as shown in Appendix B. The form of the nomenclature the choice of radii follow that used in equations 4.1–4.4. The diffusion coefficients used in the model are listed in Tables 4.2, 5.2 and 6.11.

In order to illustrate the relative importance of the major and minor source

Table 6.8: Important sources and sinks of all neutral species included in the chemical kinetic Ar-CO_2 thermal plasma model.

Species	Sources		Sinks		Comments
	Major	Minor	Major	Minor	
C	D1				$T \leq 3000$ K
	N5				$T \geq 3000$ K
			N9		
CO	N8				$T \leq 5000$ K
	N9				$5000 \leq T \leq 9000$ K
	M10				$T \geq 9000$ K
		N7			
			N2		$1000 \leq T \leq 5000$ K
			N5		$5000 \leq T \leq 9000$ K
CO_2	N2				$T \geq 4000$ K
		N3			$T \geq 4000$ K
		N4			$T \geq 4000$ K
			N7		$T \geq 4000$ K
			N8		$T \geq 4000$ K
O	N8				
		N3			$1500 \leq T \leq 3000$ K
			N2		
				N7	
				N10	
O_2	N10				$4000 \leq T \leq 8000$ K
	N7				$T \leq 5000$ K
O_3	N11				$T \leq 7000$ K
	M33				$T \geq 8000$ K
			N14		

Table 6.9: Important sources and sinks of all positive ions included in the chemical kinetic Ar-CO_2 thermal plasma model.

Species	Sources		Sinks		Comments
	Major	Minor	Major	Minor	
$CArO^+$	M5				
			R1		
			M11		$T \leq 7000$ K
CO^+	M1				
	M10				
		M9			$T \leq 11000$ K
		I1			$T \leq 10000$ K
			R2		$9000 \leq T \leq 15000$
			M13		$T \leq 9000$ K
CO_2^+	M18				$5000 \leq T \leq 10000$ K
	M12				$T \geq 10000$ K
			R3		
CO_4^+	M21				
			R4		
$C_2O_2^+$	M11				
			R5		
O^+	M3				
	I3				$T \geq 9000$ K
	I4				$T \geq 9000$ K
		M10			$T \geq 9000$ K
		M13			$T \geq 9000$ K
			R10		
O_2^+	M14				$5000 \leq T \leq 6000$ K
	M15				$5000 \leq T \leq 6000$ K
	M16				$5000 \leq T \leq 6000$ K
	M20				$T \geq 8000$ K
		M4			$T \geq 10000$ K
		M18			$6000 \leq T \leq 8000$ K
			M21		$T \leq 7000$ K
			R7		$T \geq 6000$ K
O_4^+	M22				
			M23		
				M24	
O_5^+	M17				
			M25		

Table 6.10: Important sources and sinks of all negative ions included in the chemical kinetic Ar-CO_2 thermal plasma model.

Species	Sources		Sinks		Comments
	Major	Minor	Major	Minor	
CO_3^-	M31				
			M27		
CO_4^-	M37				
			M28		
O^-	A5				$T \leq 5000$ K
	A3				$T \geq 5000$ K
			M30		$T \leq 5000$ K
O_2^-	A6				
			M38		
O_3^-	M35				
			M41		
			M42		

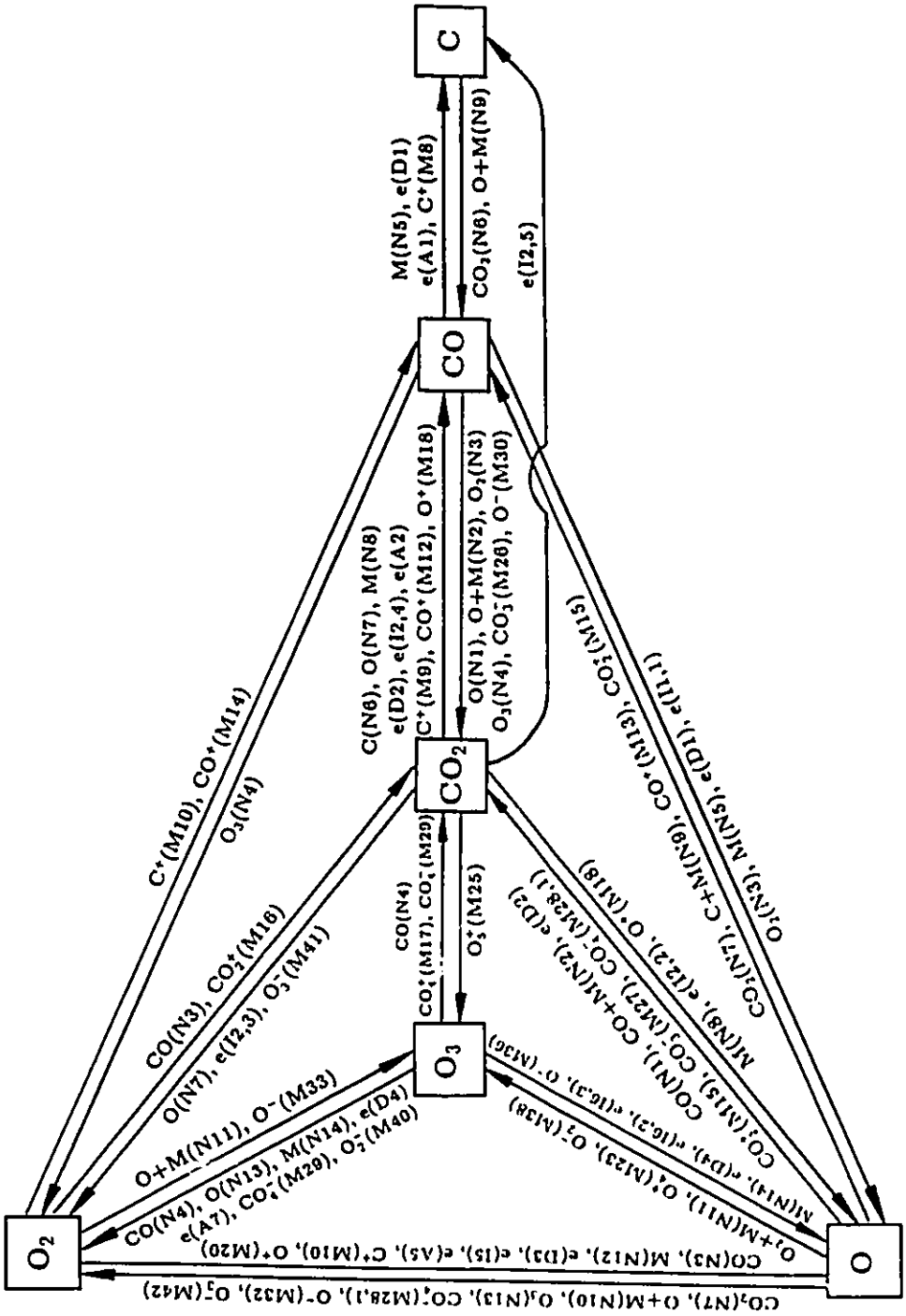

Figure 6.1: Neutral species chemistry for an Ar-CO_2 mixture gas.

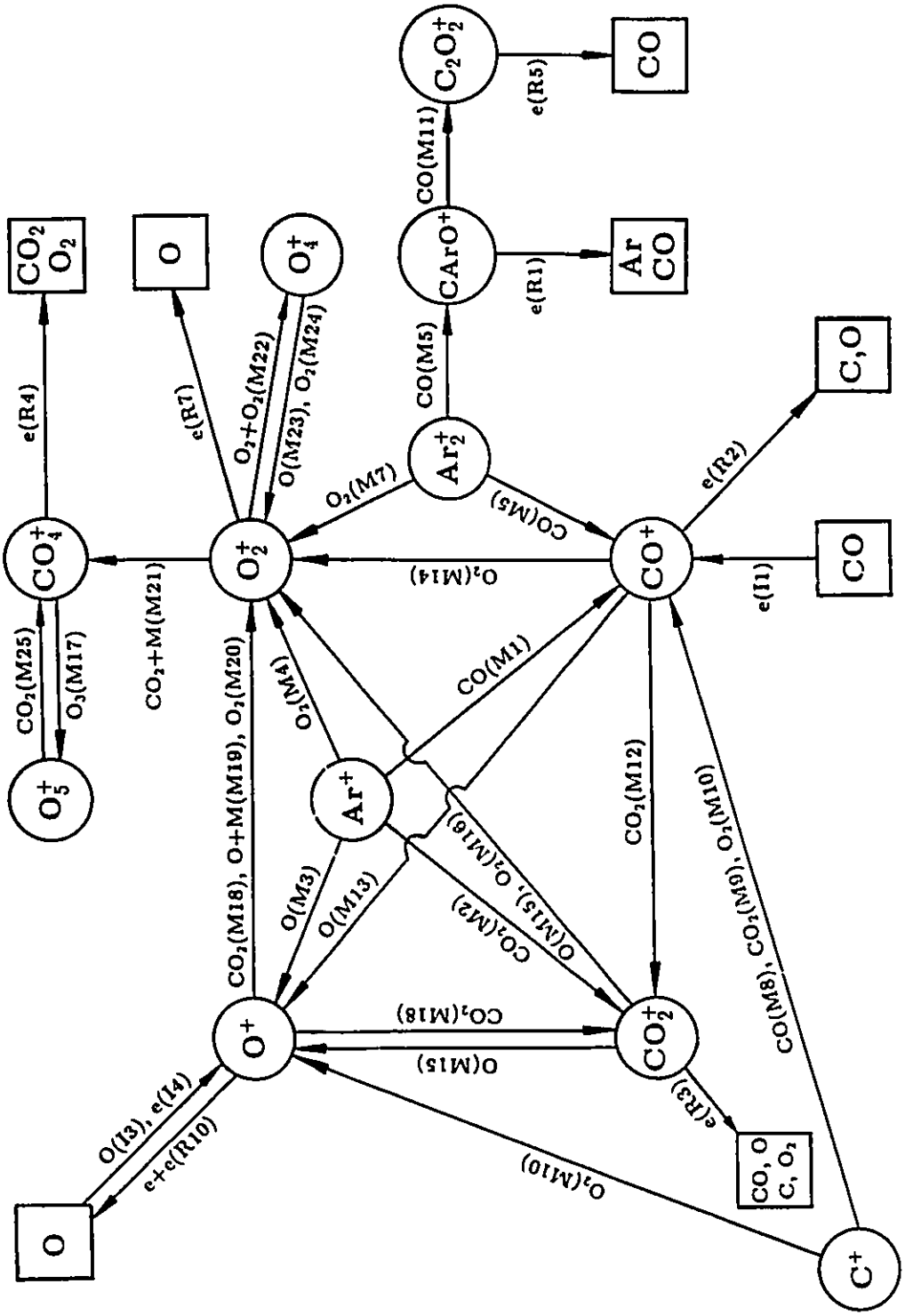

Figure 6.2: Positive ion chemistry for an Ar-CO_2 mixture gas.

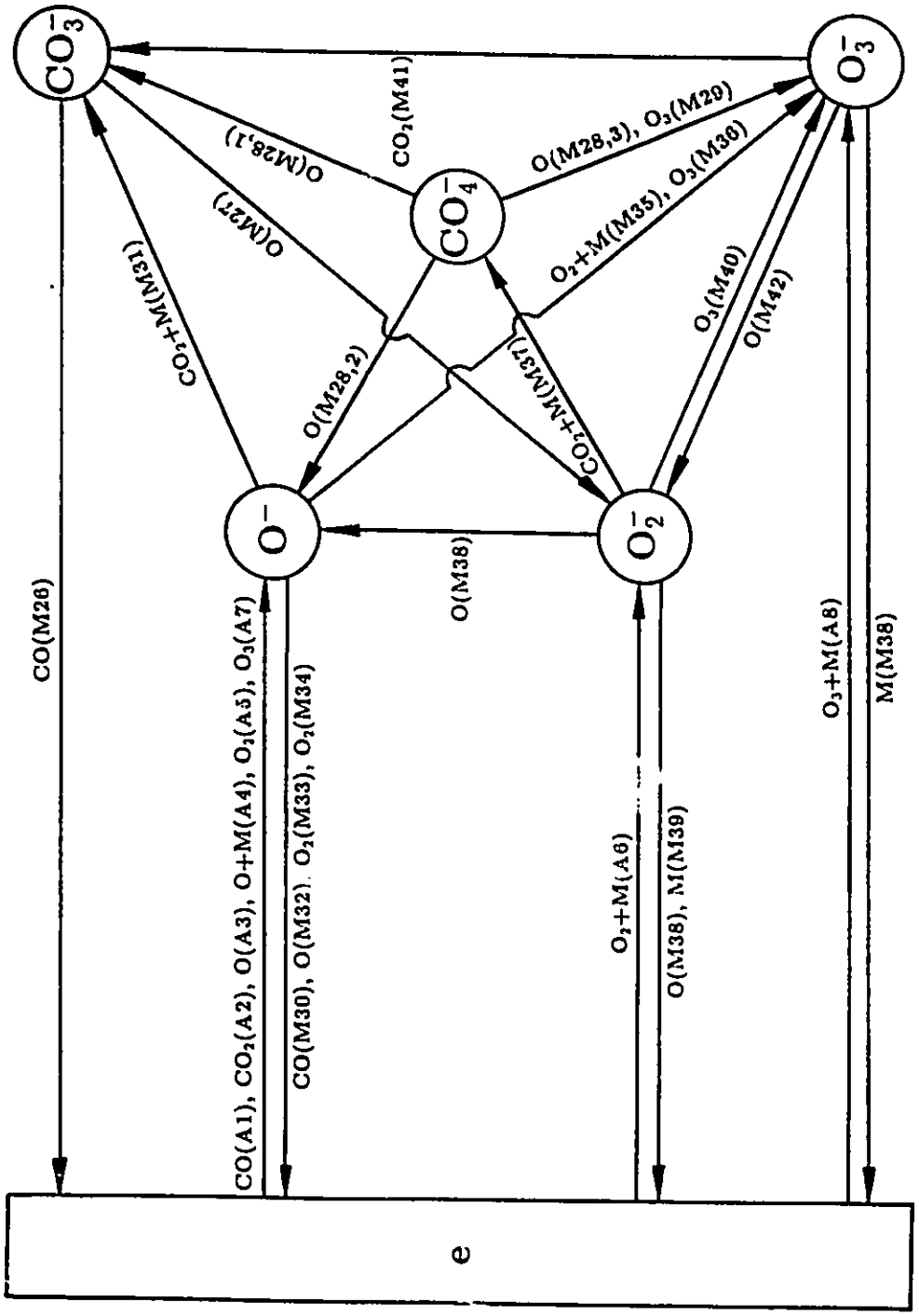

Figure 6.3: Negative ion chemistry for an Ar-CO_2 mixture gas.

Table 6.11: Diffusion constants for the Ar-CO_2 system at 1 Torr, 300 K.

Diffusion Species	D_i [cm^2 Torr/s][b]	References
O^+-Ar	50	[62]
O_2^+-Ar	25	
O_4^+-Ar	12.5	
O_5^+-Ar	10	
C^+-Ar	50	
$CArO^+$-Ar	10	
CO^+-Ar	10	
CO_2^+-Ar	10	
CO_4^+-Ar	10	
C_2O^+-Ar	10	
O^--Ar	50	
O_2^--Ar	25	
O_3^--Ar	16.5	
O_4^--Ar	12.5	
CO_2^--Ar	10	
CO_3^--Ar	10	
CO_4^--Ar	10	

[a] The values of ambipolar diffusion coefficients used in the rate equations in appendix B were calculated as follows:

$$D = \left(\frac{D_i}{p}\right)\left(\frac{T_g}{300}\right)\left(1 + \frac{T_e}{T_g}\right)$$

where P is the system pressure in Torr.

and sink reactions outlined in Tables 6.8, 6.9, and 6.10 and illustrated in Figures 6.1, 6.2, and 6.3, the values of the reaction rate constants of these sources and sinks have been summarized in Tables 6.12, 6.13, and 6.14 for neutral species, positive ions and negative ions respectively. The values of all temperature dependent reaction rate constants outlined in Tables 6.12, 6.13, and 6.14 are also shown as a function of gas and electron temperature in Figures 6.4, 6.5, and 6.6.

Over the range of temperatures considered in this model, the overall concentration of species can be calculated via the ideal gas law as described in Chapter 3. Significant depletions of the dominant species can be calculated via a mass balance. In this case, the derivation of the mass balance differs somewhat from the previous two models since the dominant species change with temperature. The Ar-CO_2 chemical kinetic model exhibits 4 temperature ranges over which different species are the dominant species:

1. Temperature range over which Ar, CO_2, and CO are the dominant species.
2. Temperature range over which Ar, CO, and O are the dominant species.
3. Temperature range over which Ar, C, and O are the dominant species.
4. Temperature range over which Ar, C, and O^+ are the dominant species.

The use of the word range in this chapter refers to the above defined ranges. Each range has its own specific mass balance.

To derive these mass balances, it is useful to first define several relationships. Let R_{ALL} be the sum of the densities of all species in the system with the exception of the possible dominant species Ar, CO_2, CO, O, C, O^+, and C^+. Thus

$$\begin{aligned} R_{ALL} = {} & [Ar^*] + [Ar^{**}] + [Ar^+] + [Ar_2^+] \\ & + [O_2] + [O_3] \\ & + [O_2^+] + [O_4^+] + [O_5^+] \\ & + [CArO^+] + [CO^+] + [CO_2^+] + [CO_4^+] + [C_2O_2^+] \\ & + [O^-] + [O_2^-] + [O_3^-] + [CO_3^-] + [CO_4^-] \end{aligned} \tag{6.1}$$

Table 6.12: Summary of the values of the reaction rate constants for important sources and sinks of all neutral species included in the chemical kinetic Ar-CO_2 thermal plasma model.

Reaction Rate Constant [cm^3/s],[cm^6/s]	
k_{D1}	1.0×10^{-12}
k_{M10}	9.9×10^{-10}
k_{M33}	1×10^{-12}
k_{N2}	$6.5 \times 10^{-33} \exp(-2183/T_g)$
k_{N3}	$4.2 \times 10^{-12} \exp(-24000/T_g)$
k_{N4}	4×10^{-25}
k_{N5}	$1.46 \times 10^{6} T_g^{-3.52} \exp(-128700/T_g)$
k_{N7}	$2.8 \times 10^{-11} \exp(-26500/T_g)$
k_{N8}	$6.06 \times 10^{-10} \exp(-25252/T_g)$
k_{N9}	$9.1 \times 10^{-22} T_g^{-3.08} \exp(2114/T_g)$
k_{N10}	$5.24 \times 10^{-35} \exp(900/T_g)$
k_{N11}	$3.6 \times 10^{-34} (T_g/300)^{-1.93}$
k_{N14}	$4.1175 \times 10^{-10} \exp(-11430/T_g)$

Table 6.13: Summary of the values of the reaction rate constants for important sources and sinks of all positive ions included in the chemical kinetic Ar-CO_2 thermal plasma model.

Reaction Rate Constant $[cm^3/s],[cm^6/s]$	
k_{I1}	$1.4 \times 10^{-11} T_e^{1/2}(1 + 1.3 \times 10^{-5} T_e) \exp(-1.5 \times 10^5/T_e)$
k_{I3}	$181.8 \times p T_g^{1/2} N_o^{-1}(1 + 1.6 \times 10^5/T_g) \exp(-1.6 \times 10^5/T_g)$
k_{I4}	$4.1 \times 10^{-11} T_e^{1/2}(1 + 1.3 \times 10^{-5} T_e) \exp(-1.5 \times 10^5/T_e)$
k_{R1}	$1 \times 10^{-6}(T_e/300)^{-0.5}$
k_{R2}	$6.8 \times 10^{-7}(T_e/300)^{-0.4}$
k_{R3}	$3.4 \times 10^{-6}(T_e/300)^{-0.4}$
k_{R4}	$1 \times 10^{-6}(T_e/300)^{-0.5}$
k_{R5}	$5 \times 10^{-6}(T_e/300)^{-0.5}$
k_{R7}	$2.3 \times 10^{-7}(T_e/300)^{-0.6}$
k_{R10}	$1 \times 10^{-29}(T_e/300)^{-4.5}$
k_{M1}	9.0×10^{-11}
k_{M3}	0.64×10^{-11}
k_{M4}	4.6×10^{-11}
k_{M5}	8.5×10^{-10}
k_{M9}	1.1×10^{-9}
k_{M10}	9.9×10^{-10}
k_{M11}	4.6×10^{-10}
k_{M12}	1.0×10^{-9}
k_{M13}	1.4×10^{-10}
k_{M14}	1.2×10^{-10}
k_{M15}	2.6×10^{-10}
k_{M16}	6.4×10^{-11}
k_{M17}	1×10^{-10}
k_{M18}	9×10^{-10}
k_{M20}	$1.9 \times 10^{-11}(T_g/300)^{-0.5}$
k_{M21}	2.3×10^{-29}
k_{M22}	$4.0 \times 10^{-30}(T_g/300)^{-2.93}$
k_{M23}	3×10^{-10}
k_{M24}	1.8×10^{-13}
k_{M25}	1.0×10^{-11}

Table 6.14: Summary of the values of the reaction rate constants for important sources and sinks of all negative ions included in the chemical kinetic Ar-CO_2 thermal plasma model.

Reaction Rate Constant $[cm^3/s],[cm^6/s]$	
k_{A3}	$1.3 \times 10^{-15}(T_g/300)$
k_{A5}	$3 \times 10^{-12}(T_g/300)^{3/2}(T_e/300)^{-1.5}$
k_{A6}	$2.2 \times 10^{-29}(300/T_g)^{1.5} * \exp(-600/T_g)$
k_{M27}	1.1×10^{-10}
k_{M28}	1.4×10^{-10}
k_{M30}	5.5×10^{-10}
k_{M31}	3.1×10^{-28}
k_{M35}	$1.1 \times 10^{-30}(T_g/300)^{-1}$
k_{M37}	4.7×10^{-29}
k_{M38}	3.0×10^{-10}
k_{M41}	5.5×10^{-10}
k_{M42}	2.5×10^{-10}

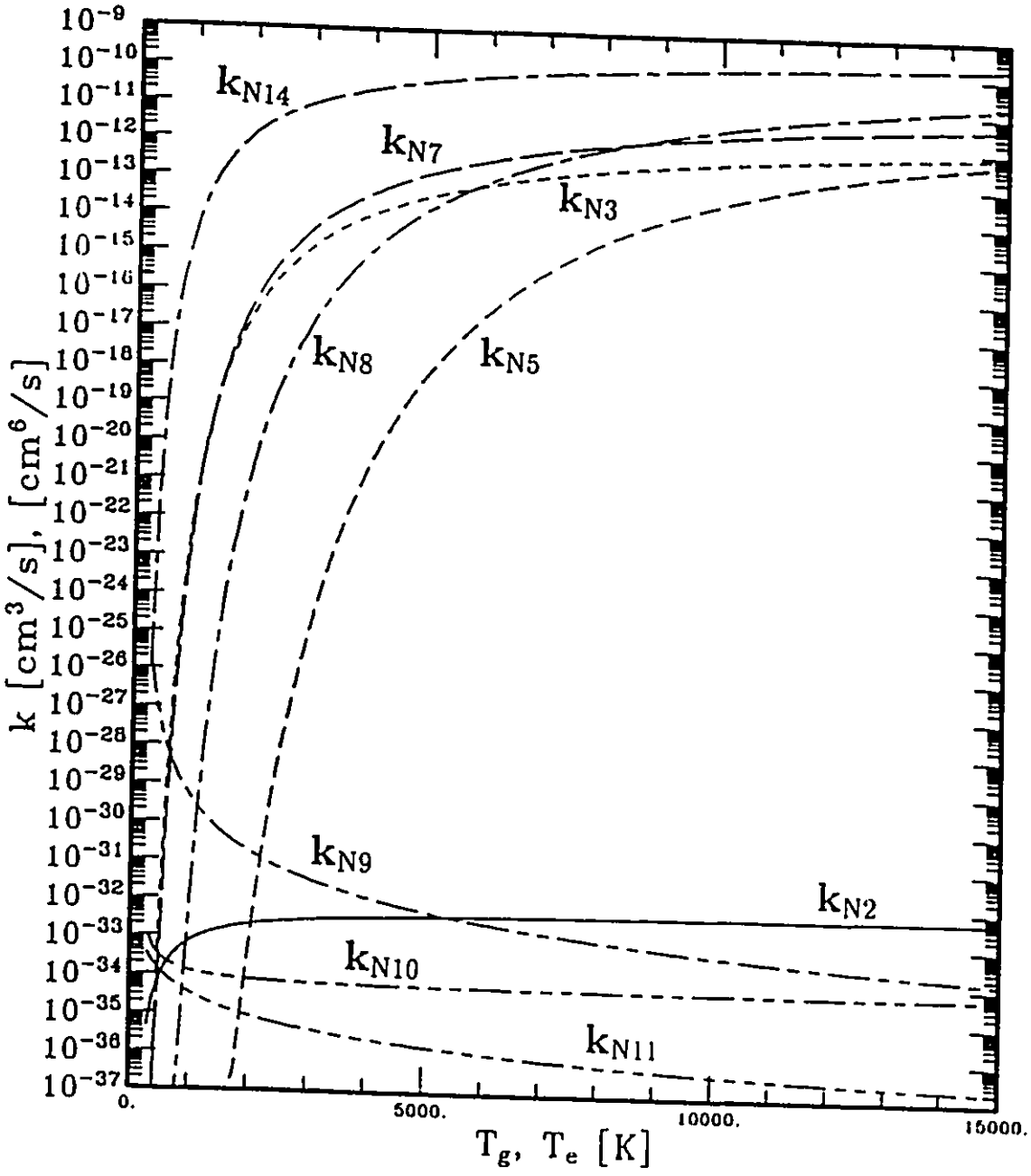

Figure 6.4: Temperature dependence of the values of the reaction rate constants for important sources and sinks of all neutral species included in the chemical kinetic Ar-CO_2 thermal plasma model.

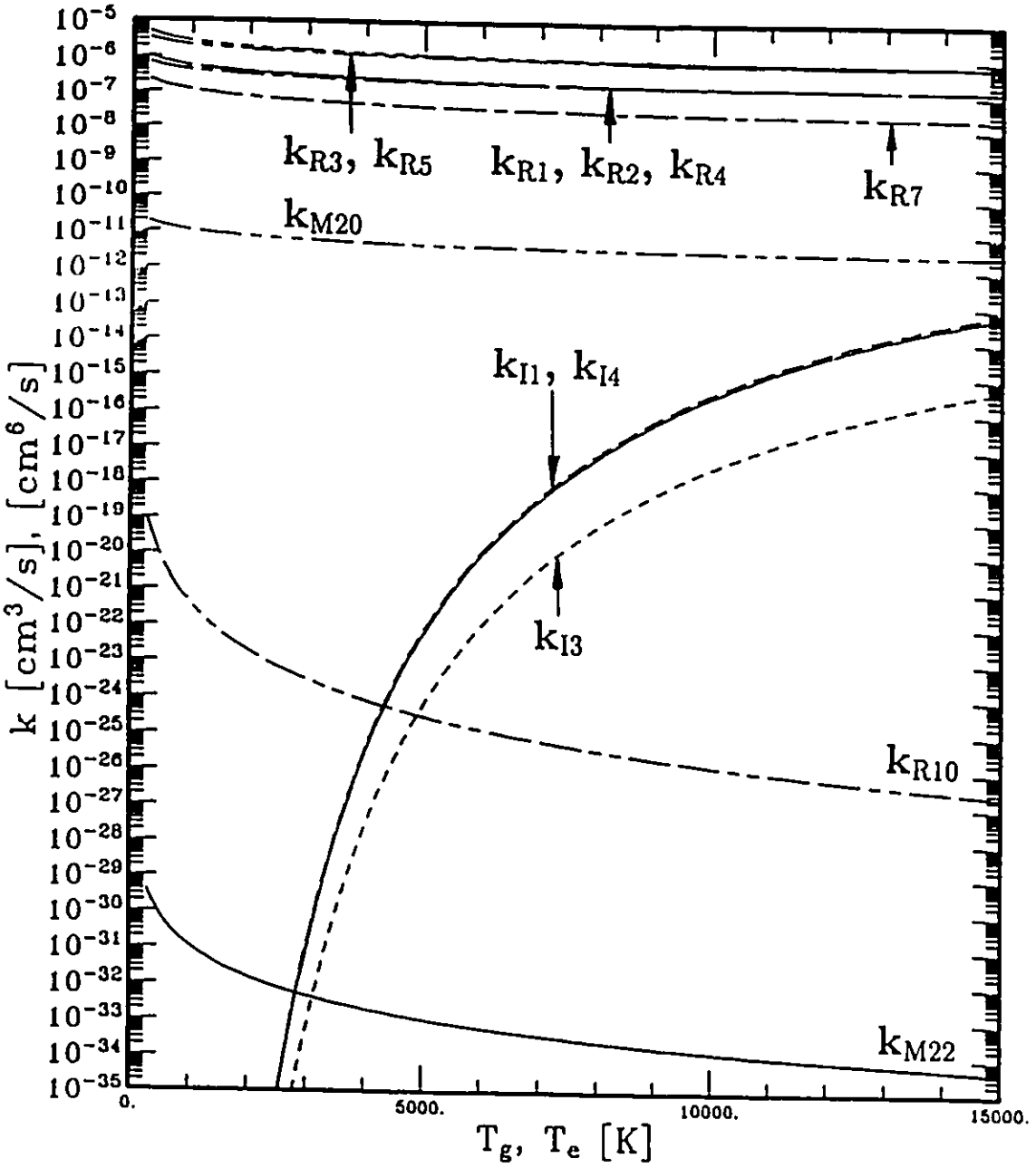

Figure 6.5: Temperature dependence of the values of the reaction rate constants for important sources and sinks of all positive ions included in the chemical kinetic Ar-CO_2 thermal plasma model.

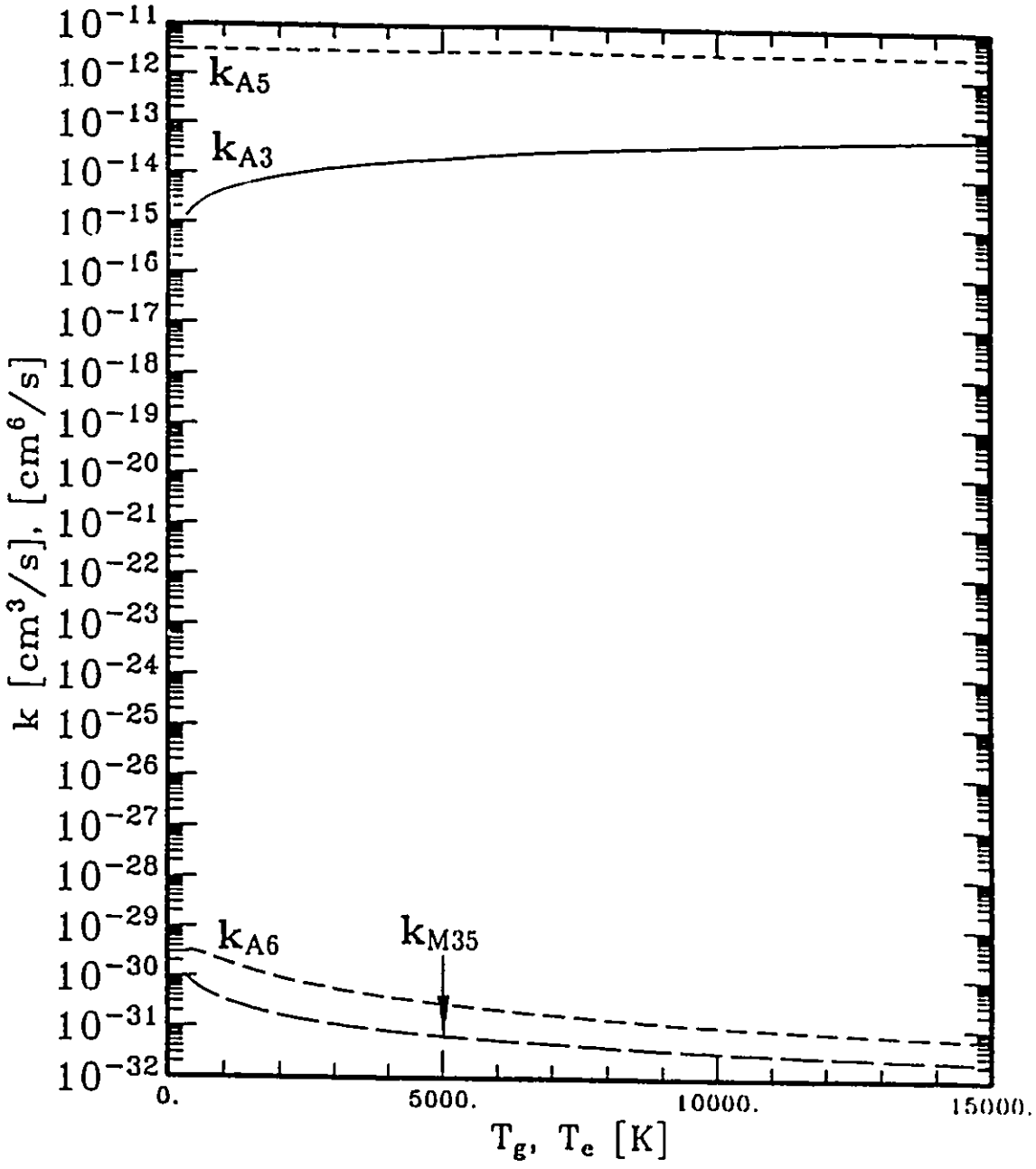

Figure 6.6: Temperature dependence of the values of the reaction rate constants for important sources and sinks of all negative ions included in the chemical kinetic Ar-CO_2 thermal plasma model.

Let R_C, R_O, and R_{Ar} be defined as the total density of carbon, oxygen and argon atoms in the system respectively, excluding the carbon, oxygen and argon atoms found in the possible dominant species Ar, CO_2, CO, O, C, O^+, and C^+. Thus,

$$\begin{aligned} R_C &= [CArO^+] + [CO^+] + [CO_2^+] + [CO_4^+] + 2[C_2O_2^+] \\ &\quad + [CO_2^-] + [CO_3^-] + [CO_4^-] \end{aligned} \tag{6.2}$$

$$\begin{aligned} R_O &= 2[O_2^+] + 4[O_4^+] + 5[O_5^+] \\ &\quad + [CArO^+] + [CO^+] + 2[CO_2^+] + 4[CO_4^+] + 2[C_2O_2^+] \\ &\quad + [O^-] + 2[O_2^-] + 3[O_3^-] + 3[CO_3^-] + 4[CO_4^-] \\ &\quad + 2[O_2] + 3[O_3] \end{aligned} \tag{6.3}$$

$$R_{Ar} = [Ar^*] + [Ar^{**}] + [Ar^+] + 2[Ar_2^+] + [CArO^+] \tag{6.4}$$

If N_{TOT} is the total concentration of species in the system as predicted by the ideal gas law, then

$$N_{TOT} = [Ar] + [CO_2] + [CO] + [O] + [C] + [O^+] + [C^+] + R_{ALL} \tag{6.5}$$

If f_{CO_2} denotes the fraction of CO_2 in the system, then

$$[Ar]_{IG} = (1 - f_{CO_2}) N_{TOT} \tag{6.6}$$

and

$$[CO_2]_{IG} = f_{CO_2} N_{TOT} \tag{6.7}$$

where the subscript IG is used in this case to denote that the density $[X]_{IG}$ of species X is as originally specified by the ideal gas law before any reactions take place in the system.

The atomic fractions of carbon and oxygen in the system can be expressed as follows:

$$\frac{[CO] + [CO_2] + [C] + [C^+] + R_C}{[Ar] + R_{Ar}} = \frac{f_{CO_2}}{1 - f_{CO_2}} \tag{6.8}$$

$$\frac{[CO] + 2[CO_2] + [O] + [O^+] + R_O}{[Ar] + R_{Ar}} = \frac{2 f_{CO_2}}{1 - f_{CO_2}} \tag{6.9}$$

Using these relationships, a mass balance can be derived for each of the dominant species in the 4 ranges defined above. In range 1, Ar, CO_2, and CO are the

dominant species. Combining equations 6.8 and 6.9 results in the following relationship for the concentration of CO:

$$[CO] = ([O] + [O^+] + R_O) - 2([C] + [C^+] + R_C) \tag{6.10}$$

Combining equations 6.8 and 6.5 results in a mass balance expression for the concentration of the CO_2 in the system

$$[CO_2] = f_{CO_2}(N_{TOT} + R_{Ar} - R_{ALL} - ([O] + [O^+])) - (1 - f_{CO_2})R_C - ([CO] + [C] + [C^+]) \tag{6.11}$$

and re-arranging equation 6.5, the density of argon can be calculated as follows:

$$[Ar] = N_{TOT} - ([CO_2] + [CO] + [O] + [C] + [O^+] + [C^+] + R_{ALL}) \tag{6.12}$$

Further combinations of equations 6.5, 6.8, and 6.9 lead to similar expressions which can be used to calculate the concentration of the dominant species O, C, O^+, and C^+ in ranges 2–4. These relationships are needed not only to satisfy the ideal gas law but also to ensure that the transition from one range to another takes place without de-stabilizing the highly coupled rate equations outlined in Appendix B.

In range 2, the concentration of CO can be calculated via the relationship:

$$[CO] = f_{CO_2}(N_{TOT} + R_{Ar} - R_{ALL} - ([O] + [O^+])) - (1 - f_{CO_2})R_C - ([CO_2] + [C] + [C^+]) \tag{6.13}$$

and the concentration of O can be calculated via

$$\begin{aligned} [O] \;=\; & \frac{1}{1 + f_{CO_2}}(2f_{CO_2}(N_{TOT} + R_{Ar} - R_{ALL} - ([C] + [C^+])) \\ & -(1 - f_{CO_2})R_O - 2[CO_2]) - ([CO] + [O^+]) \end{aligned} \tag{6.14}$$

In range 3, the concentration of O can be derived as above in equation 6.14, and the concentration of C can be calculated via:

$$[C] = f_{CO_2}(N_{TOT} + R_{Ar} - R_{ALL} - ([O] + [O^+])) - (1 - f_{CO_2})R_C - ([CO] + [CO_2] + [C^+]) \tag{6.15}$$

which effectively represents a re-arrangement of equation 6.13. This relationship can also be used to calculate the concentration of C in range 4. The concentration of O^+

in range 4 can be calculated by rearranging equation 6.14 above:

$$\begin{aligned}[O^+] &= \frac{1}{1+f_{CO_2}}(2f_{CO_2}(N_{TOT}+R_{Ar}-R_{ALL}-([C]+[C^+])) \\ &\quad -(1-f_{CO_2})R_O-2[CO_2])-([CO]+[O]) \end{aligned} \tag{6.16}$$

Assuming the existence of a quasi-neutral plasma, the electron concentration can be calculated using a charged particle balance:

$$\begin{aligned}[e] &= [Ar^+]+[Ar_2^+]+[O^+]+[O_2^+]+[O_4^+]+[O_5^+] \\ &\quad +[C^+]+[CArO^+]+[CO^+]+[CO_2^+]+[CO_4^+]+[C_2O_2^+] \\ &\quad -[O^-]-[O_2^-]-[CO_3^-]-[CO_4^-] \end{aligned} \tag{6.17}$$

In this model, the assumption has been made that the vibrational and rotational temperature and the temperature of species with excited states are the same as the translational gas temperature.

$$T_g = T_{translation} = T_{excitation} = T_{vibration} = T_{rotation} \tag{6.18}$$

Metastable or excited states were not included unless they were of critical importance to the model, for example in the formation of Ar^+ through electron impact. Species which were not included in the model but have been mentioned in the literature as possible constituents of an Ar-CO_2 thermal plasma include: C_2, C_2O, C^-, C_2^-, O_4^-, and CO_2^- [13][14][24][125]. The reaction rate constants of the reactions leading to these species are either very small, form an incomplete set (no sources or no sinks), or are not well defined both experimentally and theoretically.

6.3 Numerical Results

6.3.1 Gas Temperature Effects

Figures 6.7, 6.8, and 6.9, show the temperature dependent neutral species, positive ion, and negative ion concentrations respectively as predicted by the Ar-CO_2 chemical kinetic model, with p = 760 Torr, $T_e = T_g$ and a 10% CO_2 mixture. Over

the gas temperatures shown in Figure 6.7, the first three ranges defined in Section 6.2 occur over the following temperatures:

Table 6.15: Temperature ranges in the Ar-10%CO_2 model, p = 760 Torr, $T_e = T_g$.

Range	T_g [K]
1 (Ar, CO_2, CO dominant)	$\leq$ 3800
2 (Ar, CO, O dominant)	3800-6800
3 (Ar, C, O dominant)	$\geq$ 6800

Neutral Species

As shown in Figure 6.7, Ar, CO_2, CO, O_2, O, and C are the dominant species in the system. At the lowest temperatures ($T_g \leq 3200$ K), CO_2 forms the dominant C-O bearing species. The predicted temperature dependent equilibrium concentration of all other species is significantly less than 10% of total concentration of species in the system at these temperatures, and thus CO_2 remains the dominant species through the mass balance equation 6.11. At temperatures higher than $T_g = 3200$ K, CO becomes the dominant carbon bearing species. The generation of CO may occur mainly via the thermal dissociation reaction N8

$$CO_2 + M \xrightarrow{k_{N8}} CO + O + M,\ M = Ar$$

in which collisions of Ar and CO_2 remove an oxygen atom from the CO_2 to form CO. The oxygen atom remains in atomic form, or recombines with other oxygen atoms to form diatomic oxygen molecules. At temperatures lower than $T_g = 3800$ K, the free oxygen occurs primarily as O_2, and is most likely formed via reaction N10

$$O + O + M \xrightarrow{k_{N10}} O_2 + M,\ M = Ar$$

or via reaction N7

$$CO_2 + O \xrightarrow{k_{N7}} CO + O_2$$

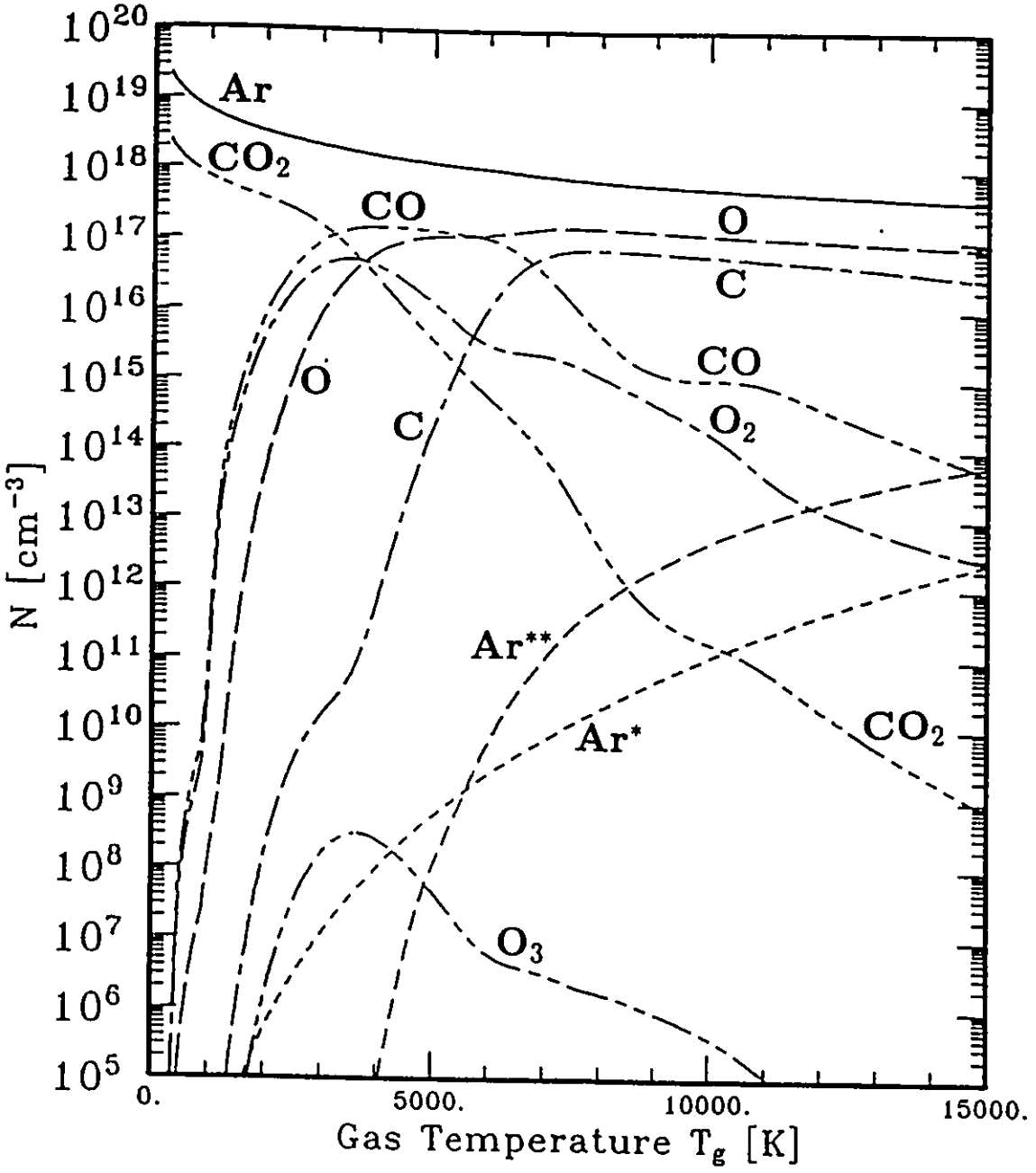

Figure 6.7: Neutral species concentrations as a function of gas temperature for an Ar-10%CO_2 mixture, with p = 760 Torr, and $T_e = T_g$.

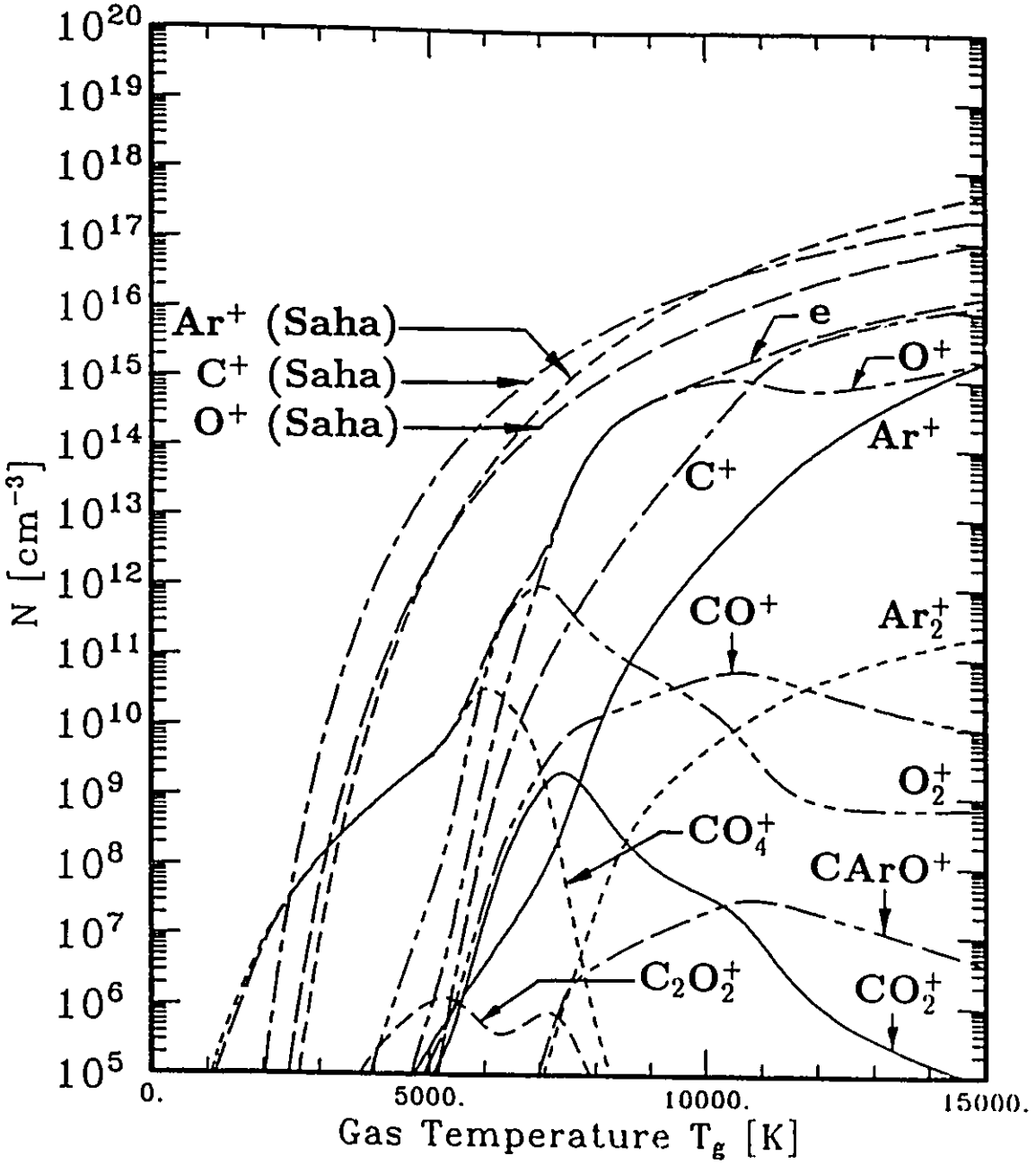

Figure 6.8: Positive ion concentrations as a function of gas temperature for an Ar-10%CO_2 mixture, with p = 760 Torr, and $T_e = T_g$.

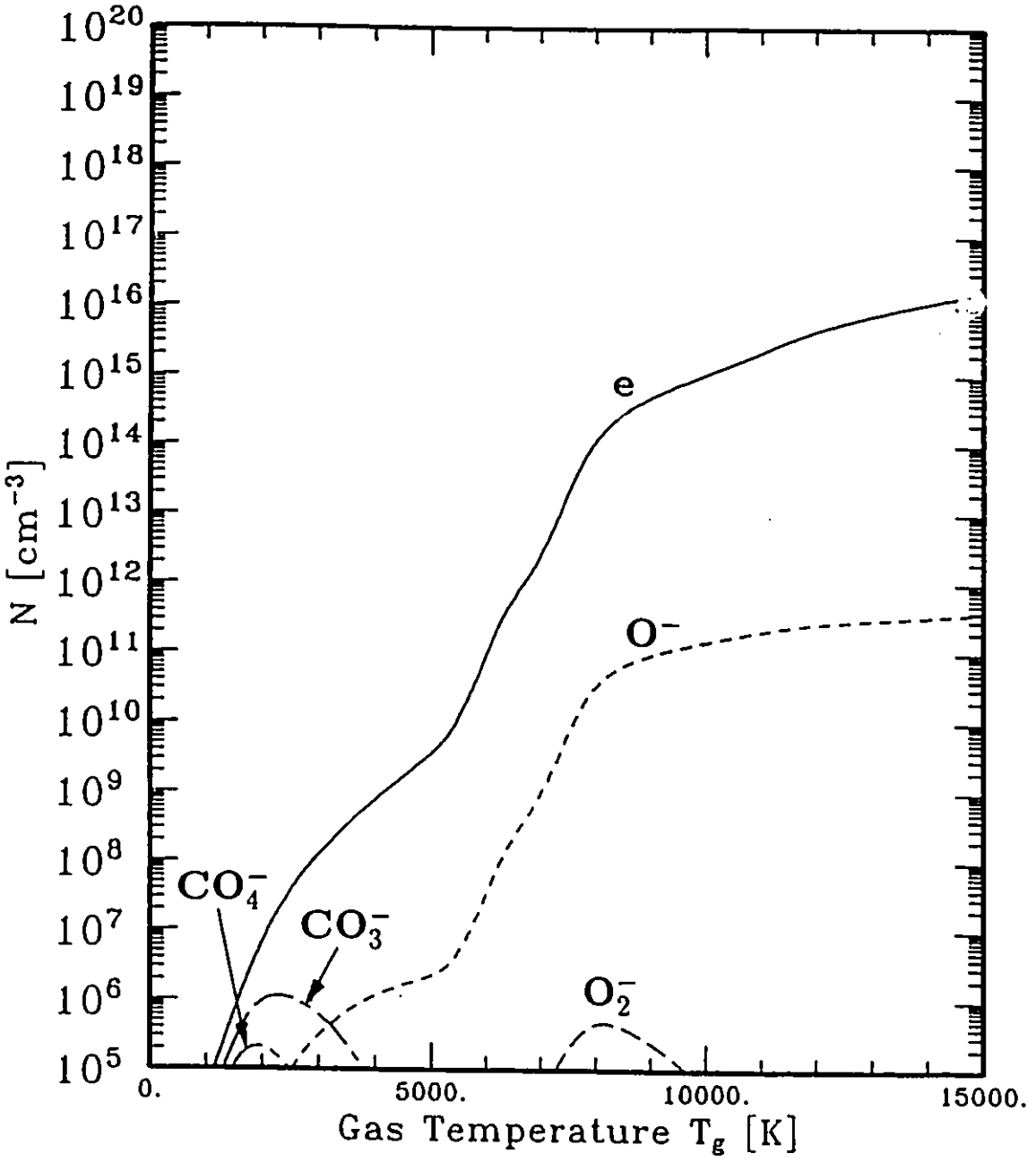

Figure 6.9: Negative ion concentrations as a function of gas temperature for an Ar-10%CO_2 mixture, with p = 760 Torr, and $T_e = T_g$.

which also leads to the further generation of CO molecules.

If the gas temperature is increased above T_g = 3800 K, the chemical kinetic model predicts an oxygen atom density [O] which is higher than the oxygen molecule density [O_2]. This may be due to a decreasing importance of the three-body oxygen free radical recombination reaction

$$O + O + M \xrightarrow{k_{N10}} O_2 + M,\ M{=}Ar$$

as a source of O_2 with increasing temperature as illustrated in Figure 6.4.

At temperatures greater than T_g = 6000 K, the combination of the large concentration of CO and the increasing value of the k_{N5} reaction rate constant (see Figure 6.4) may cause the N5 reaction

$$CO + M \xrightarrow{k_{N5}} C + O + M,\ M = Ar$$

to exert a strong influence on the concentration of the CO, tending to dissociate it into its atomic components. As a result, atomic carbon C and atomic oxygen O become the two dominant species in the system. The ratio of their concentrations is C:O = 1:2, reflecting their origins in the CO_2 molecule.

The sources and sinks of Ar^* and Ar^{**} are unchanged from Chapter 4. Since the concentration of Ar^* depends only on the concentration of Ar, the temperature dependent concentration of Ar^* has been reduced only slightly in response to the 10% reduction in the concentration of Ar due to the presence of CO_2. The temperature dependent concentration of Ar^{**} has also remained relatively unchanged when compared to the pure argon case shown in Figure 4.3. The comparative insensitivity of the source and sink reactions of Ar^{**} to the concentration of electrons and the relatively unchanged concentration of Ar may be the primary reasons for the minor changes in the Ar^{**} temperature dependent concentration.

Positive Ions

All positive ion species concentrations fall well below the concentrations predicted by the Saha equation for Ar^+, O^+, and C^+, with the exception of CO_2^+ which

exceeds the Saha equation plasma density predictions at temperatures less than T_g = 2000–3000 K as shown in Figure 6.8. Dominant positive ions and the temperatures over which they form the dominant ionized species are as shown in Table 6.16.

Table 6.16: Dominant positive ions in the Ar-10%CO_2 model, $T_e = T_g$, p = 760 Torr.

Ion	T_g [K]
CO_4^+	$\leq$ 6000
O_2^+	6000–7000
O^+	7000–11000
C^+	$\geq$ 11000

Other ionized species which occur in significant concentrations ($\geq 10^8$ cm^{-3}) at temperatures exceeding T_g = 3000 K are Ar_2^+, and CO^+. The species $C_2O_2^+$, CO_2^+ and $CArO^+$ also occur in smaller concentrations (10^5–10^8 cm^{-3}), but no significant O_4^+ or O_5^+ concentrations are predicted by the model. An examination of the major sources and sinks of O_4^+ or O_5^+ as illustrated in Figure 6.2 reveals that reaction M22 is most likely the major source of O_4^+

$$O_2^+ + O_2 + O_2 \xrightarrow{k_{M22}} O_4^+ + O_2$$

and reaction M17 may be the major source of O_5^+

$$CO_4^+ + O_3 \xrightarrow{k_{M17}} O_5^+ + CO_2$$

The relatively small concentrations of O_2^+ and CO_4^+ as shown in Figure 6.8 are thus most likely the cause of the small ($\leq 10^5$ cm^{-3}) equilibrium concentrations of O_4^+ and O_5^+.

As outlined in Table 6.9, the major source of CO_4^+ is most likely through reaction M21

$$O_2^+ + CO_2 + M \xrightarrow{k_{M21}} CO_4^+ + M$$

via the collision of O_2^+ with CO_2. For this reason, the CO_4^+ concentration increases sharply between $1000 \leq T_g \leq 6000$ K as the M21 reaction converts a significant fraction of the O_2^+ generated over these temperatures into CO_4^+. At temperatures greater than $T_g = 6000$ K, the density of CO_2 decreases rapidly, thus reducing the generation of CO_4^+. In addition, the increasing concentration of electrons may strengthen the major sink reaction of CO_4^+, through recombination reaction R4

$$CO_4^+ + e \xrightarrow{k_{R4}} CO_2 + O_2$$

causing a rapid decline in the concentration of CO_4^+ with increasing temperature.

The major source of $CArO^+$ occurs through reaction M5

$$Ar_2^+ + CO \xrightarrow{(1-f_{M5})k_{M5}} CArO^+ + Ar$$

which involves a collision between Ar_2^+ and CO. At temperatures less than $T_g = 8000$ K, the concentration of $CArO^+$ increases sharply with increasing gas temperature, reflecting the increase in Ar_2^+ concentration over these temperatures. At temperatures between $8000 \leq T_g \leq 11000$ K the $CArO^+$ concentration does not change with gas temperature, and at temperatures greater than $T_g = 11000$ K, the concentration of $CArO^+$ decreases with increasing temperature, reflecting the decrease in CO concentration, and the less rapidly increasing Ar_2^+ concentration.

The concentration of $C_2O_2^+$, whose major source term is dependent on the $CArO^+$ concentration through reaction M11

$$CArO^+ + CO \xrightarrow{k_{M11}} C_2O_2^+ + Ar$$

exhibits two maxima in its temperature dependent concentration profile at $T_g = 5200$ and 7100 K. The first maximum most likely reflects the maximum in the concentration of CO at $T_g = 5200$. The initial rise from $T_g = 6200$ to 7100 K which leads to the second maximum in the $C_2O_2^+$ concentration may reflect the rapid increase in the $CArO^+$ concentration over these temperatures. At temperatures higher than $T_g = 7100$ K the rapidly increasing electron concentration may increase the loss of $C_2O_2^+$ through the R5 recombination reaction

$$C_2O_2^+ + e \xrightarrow{k_{R3}} CO + CO$$

and consequently lead to the second maximum in the $C_2O_2^+$ concentration.

Between $5000 \leq T_g \leq 7000$ K the concentration of CO_2^+ increases sharply with gas temperature, and decreases again at temperatures greater than $T_g = 7000$ K. The major source of CO_2^+ may be through the M18 reaction

$$O^+ + CO_2 \xrightarrow{(1-f_{M18})k_{M18}} CO_2^+ + O$$

The rapid increase in CO_2^+ between $5000 \leq T_g \leq 7000$ K may reflect the rapid increase in O^+ concentration over these temperatures. A likely cause of the decrease in CO_2^+ at temperatures higher than $T_g = 7000$ K may be the losses caused by reaction R3

$$CO_2^+ + e \xrightarrow{f_{R3}k_{R3}} CO + O$$

$$\xrightarrow{(1-f_{R3})k_{R3}} C + O_2$$

due to the rapid increase in electron concentration with temperature. Additionally, the decrease of CO_2 concentration may decrease the generation rate of CO_2^+ through reaction M18.

The origin of CO^+ stems mainly from the charge exchange reaction M1

$$Ar^+ + CO \xrightarrow{k_{M1}} CO^+ + Ar$$

between Ar^+ and CO and the conversion of C^+ into CO^+ through the collision of C^+ ions with oxygen molecules

$$C^+ + O_2 \xrightarrow{(1-f_{M10})k_{M10}} CO^+ + O$$

The concentration of CO^+ increases with gas temperature above $T_g = 5000$ K, reflecting the increase in Ar^+ in the system, however, at temperatures greater than $T_g = 8000$ K, the dissociative recombination reaction R2

$$CO^+ + e \xrightarrow{k_{R2}} C + O$$

may become significant as the density of electrons in the system increases, and may tend to dissociate the CO^+ into C and O.

At temperatures between $6000 \leq T_g \leq 7000$ K, O_2^+ constitutes the dominant ionized species. The major reactions contributing to the formation of O_2^+ are the ion-molecule reactions between CO_x^+ ions and O_y M14, M15 and M16

$$CO^+ + O_2 \xrightarrow{k_{M14}} O_2^+ + CO$$

$$CO_2^+ + O \xrightarrow{f_{M15}k_{M15}} O_2^+ + CO$$

$$CO_2^+ + O_2 \xrightarrow{k_{M16}} O_2^+ + CO_2$$

With increases in temperature above $T_g = 7000$ K, the concentration of CO_x^+ species decrease as discussed previously. This may lead to the decrease in the O_2^+ concentration through the above reactions. At temperatures greater than $T_g = 8000$ K, sensitivity analysis indicates that the charge exchange reaction M20

$$O^+ + O_2 \xrightarrow{k_{M20}} O_2^+ + O$$

may account for the major source of O_2^+, and also accounts for the recovery of the O_2^+ concentration in this temperature region.

Ar^+, Ar_2^+, C^+, and O^+ form the dominant ionized species at temperatures greater than $T_g = 7000$ K. The major sources and sinks Ar^+, Ar_2^+, and C^+ are essentially the same as those discussed in Chapters 4 and 5 with the exception of the ion-molecule reactions M1–M10 as mentioned previously. Comparing the temperature dependent concentrations of Ar^+, Ar_2^+ and C^+ shown in Figure 6.8 for an Ar-10%CO_2 mixture with those shown in Figures 4.3 and 5.3 for pure argon and an Ar-1%C mixture respectively, it can be seen that concentrations of these species are smaller in the Ar-10%CO_2 mixture case. It is suggested that the additional loss of these species may be accounted for through charge transfer reactions M1–M10.

O^+ is generated primarily through thermal and electron impact ionization reactions I3 and I4

$$O + O \longrightarrow O^* + O \xrightarrow{k_{I3}} O^+ + O + e$$

$$O + e \xrightarrow{k_{I4}} O^+ + e + e$$

as well as through the charge transfer reaction M3 with Ar^+.

$$Ar^+ + O \xrightarrow{k_{M3}} O^+ + Ar$$

Negative Ion

As shown in Figure 6.9 O^- is the only negatively charged species, other than the electron, which appears in significant concentrations. The main source of O^- at temperatures less than $T_g = 5000$ K, is most likely through dissociative attachment reaction A5

$$O_2 + e \xrightarrow{k_{A5}} O + O^-$$

At temperatures greater than $T_g = 5000$ K, the O_2 concentration decreases with increasing temperature, thus reducing the contribution of this reaction to the production of O^-. Here the radiative attachment reaction A3

$$O + e \xrightarrow{k_{A3}} O^- + h\nu$$

may become the major source for O^- ions. The O^- concentration tends to have a similar temperature dependence as the electron concentration profile, most likely due to the fact that both of the above dominant O^- generation reactions depend on the density of electrons.

Summary of Gas Temperature Effects

A comparison of Figures 6.7, 6.8, and 6.9 with their counterparts Figures 4.3 and 5.3 for the pure argon model and the Ar-C model in Chapters 4 and 5 respectively shows that CO_2 now almost completely dominates the behaviour of the model. In the pure argon model, the thermal energy primarily went into the formation of Ar^+ and Ar_2^+ at temperatures less than $T_g = 5000$ K. In the Ar-CO_2 model however, the reactions which cause the conversion of CO_2 into CO and subsequently into C and O now dominate the model at these temperatures. The relative temperature

dependence of the Ar-CO_2 plasma density, as defined by the electron concentration, is similar to that found in the pure argon or Ar-C mixture plasma. However, the concentration of electrons is somewhat smaller in the Ar-CO_2 mixture plasma at gas temperatures below T_g = 6000 K, and significantly larger above T_g = 6000 K. At temperatures below T_g = 5000 K, the temperature dependent concentration of the CO_4^+ molecular ion crosses over the Ar^+, C^+, and O^+ concentrations predicted by the Saha equation in a manner reminiscent of the Ar_2^+ density predicted by the pure argon model. Similar to the Ar_2^+ in the pure argon model, the generation of CO_4^+ underlies different physical mechanisms than those governing the Saha equation, and as such the predicted results cannot be directly compared.

Another significant similarity in the behaviour of the pure argon and the Ar-CO_2 models is the large difference in the plasma density predicted by the Saha equation and that predicted by the chemical kinetic model for the Ar-10%CO_2 mixture between 3000 $\leq T_g \leq$ 5000 K. As in the pure argon model, molecular ions form the dominant ionized species at these temperatures. At temperatures greater than T_g = 5000 K, the generation mechanisms of C^+ and O^+ become significant, and C^+ and O^+ become the dominant ionized species. Above T_g = 7000 K, the plasma density is less than one order of magnitude less than the densities predicted by the Saha equations for O^+.

6.3.2 Electron Temperature Effects

Figures 6.10, 6.11, and 6.12 illustrate the electron temperature dependent species concentrations for neutral, positive and negative species for an Ar-10%CO_2 mixture when the gas temperature is T_g = 6000 K, and the pressure p = 760 Torr.

Neutral Species

As shown in Figure 6.10, the dominant species are argon, carbon monoxide, and atomic oxygen. As a result of the high gas temperature (T_g = 6000 K), the thermal dissociation reactions, which have a dominant effect on the neutral species composition, determine the density of the neutral species at electron temperatures

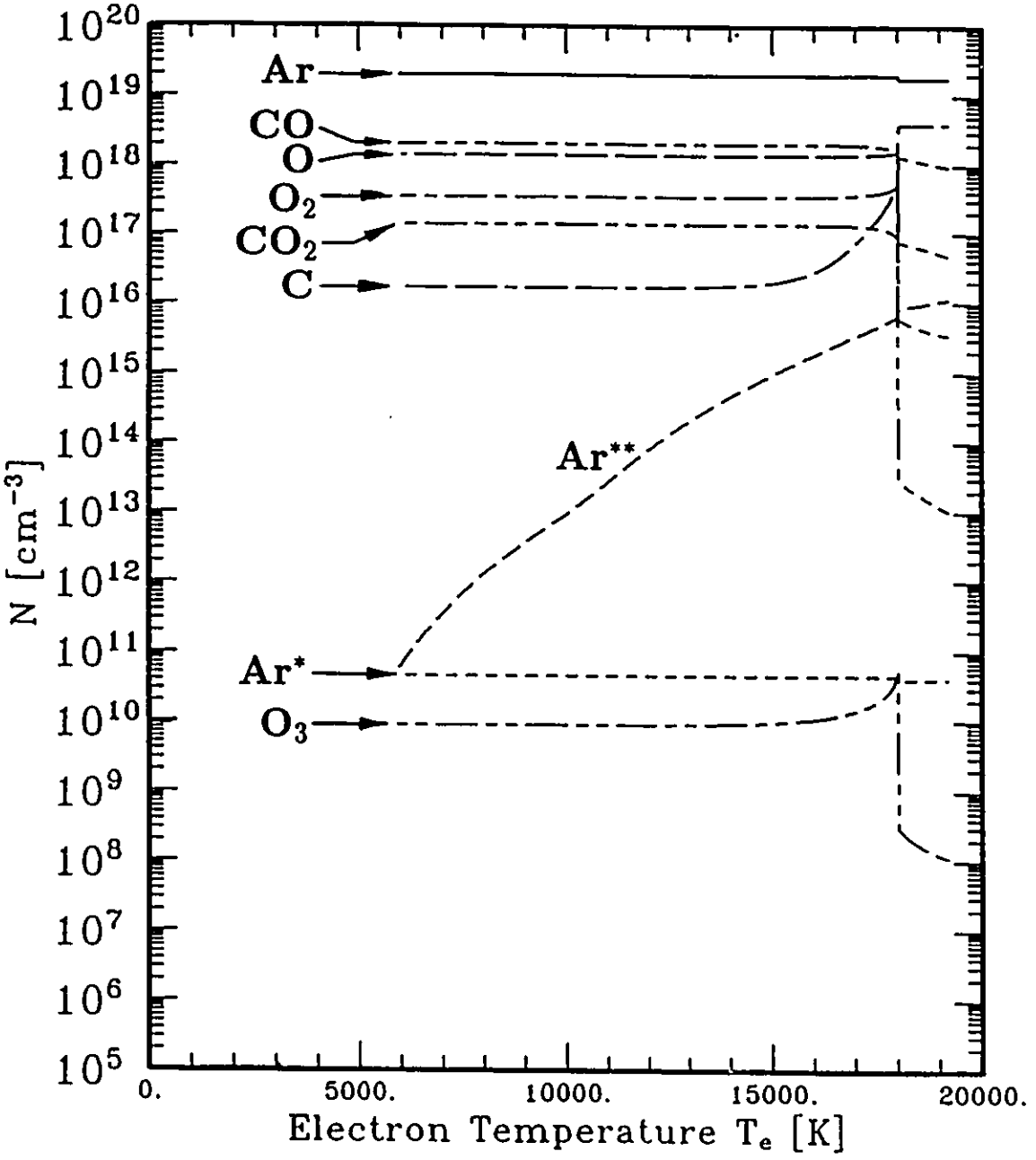

Figure 6.10: Neutral species concentrations as a function of electron temperature for an Ar-10%CO_2 mixture with p = 760 Torr and T_g = 6000 K.

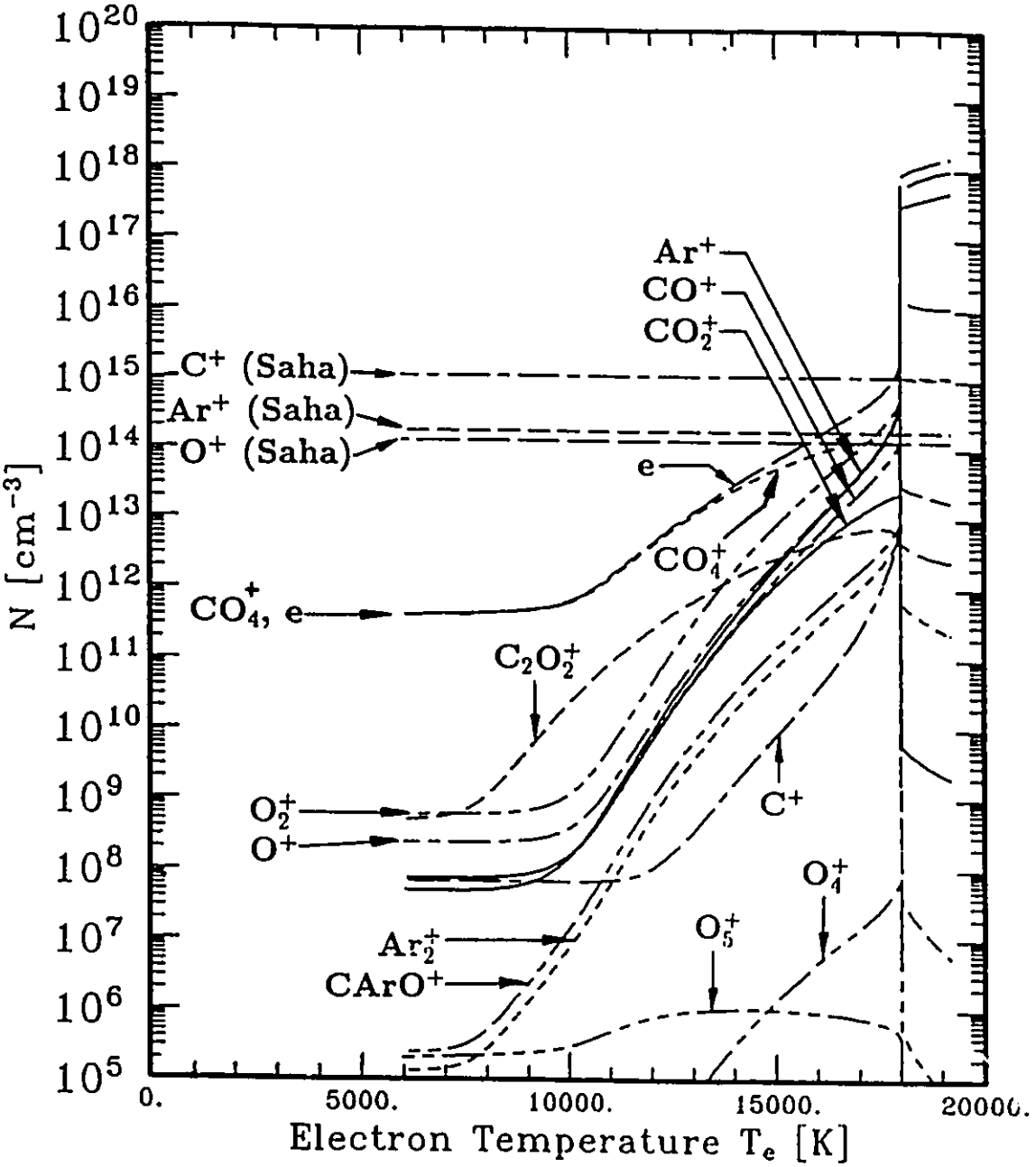

Figure 6.11: Positive species concentrations as a function of electron temperature for an Ar-10%CO_2 mixture with p = 760 Torr, and T_g = 6000 K.

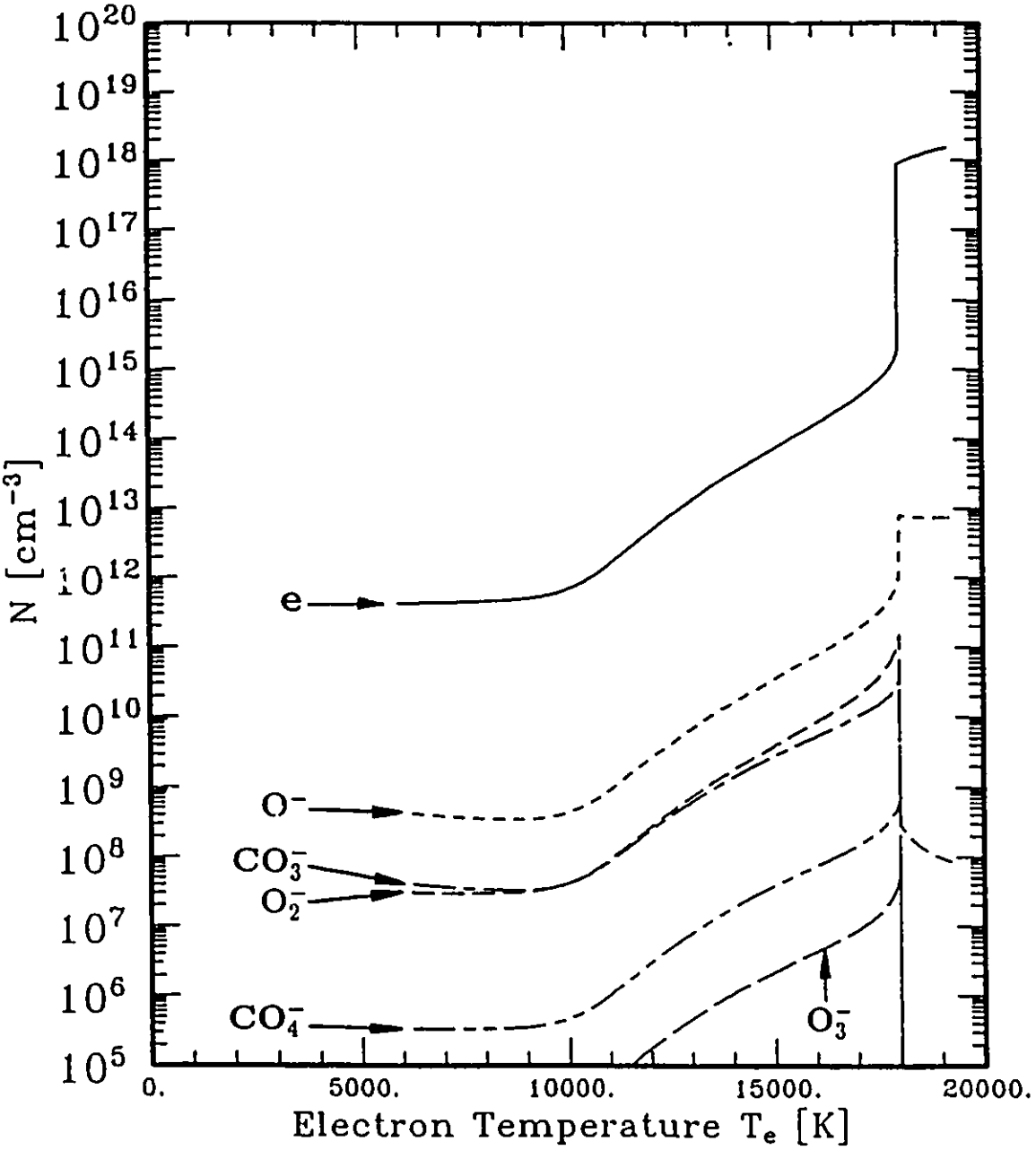

Figure 6.12: Negative species concentrations as a function of electron temperature for an Ar-10%CO_2 mixture with p = 760 Torr, and T_g = 6000 K.

less than T_e = 15000 K as shown in Figure 6.10. Since the gas temperature does not vary with electron temperature in this case, the concentrations of the neutral species are also constant at these electron temperatures. At temperatures greater than T_e = 15000 K, electron impact reactions become increasingly important and begin to influence these densities, increasing the concentration of C and decreasing the concentrations of CO_2 and CO.

Positive Ions

The positively charged species in the system are predominantly generated by thermal impact reactions at temperatures less than T_e = 9000 K. The concentrations of positively charged species found at these temperatures are essentially the same as those found at T_g = 6000 K in Figure 6.8. For this reason, CO_4^+ constitutes the dominant positive ion at electron temperatures less than T_e = 9000 K.

At temperatures greater than T_e = 9000 K, electron impact reactions, especially those leading to the ionization of Ar, C, CO, CO_2, O and O_2, may become increasingly important, increasing the density of Ar^+, C^+, CO^+, CO_2^+, O^+ and O_2^+ in response. The increased density of these species may also cause the generation of greater concentrations of $CArO^+$, O_4^+, and O_5^+ at these electron temperatures through the reactions examined in the previous section. The dominant positive ion remains CO_4^+ at electron temperatures of T_e = 9000–17000 K, most likely as a result of the O_2^+–CO_2–M three-body reaction

$$O_2^+ + CO_2 + M \xrightarrow{k_{M2}} CO_4^+ + M, \text{ M=Ar}$$

as discussed in section 6.3.1.

The rapid increase of plasma density at T_e = 18000 K corresponds to the "onset" of plasma conditions discussed in Sections 4.3.2 and 5.3.2. If the gas temperature were reduced from 6000 K to 300 K, the plasma density would all but disappear at electron temperatures lower than T_e = 18000 K since the electron temperature would no longer be large enough to sustain plasma conditions within the Ar-CO_2 gas mixture.

Negative Ions

As shown in Figure 6.12, the condition of thermodynamic non-equilibrium causes the concentration of all negative species to increase when compared to the results shown in the equilibrium case in Figure 6.9. Significant concentrations ($\geq 10^5$ cm^{-3}) of CO_3^-, O_2^-, and CO_4^- can be found at electron temperatures between T_e = 6000–18000 K. At electron temperatures greater then T_e = 12000 K, the concentration of O_3^- also becomes greater than 10^5 cm^{-3}. This increase in the concentration of negative ions is most likely a result of increased importance of electron impact generation reactions as outlined in Figure 6.3. This supposition is further supported by the fact that the densities of these species tend to have the same relative temperature dependence as that of the electrons.

6.3.3 Gas Pressure Effects

In order to investigate the effect of changing the system gas pressure on the temperature dependent species concentrations, this section will examine an Ar-10%CO_2 mixture with $T_e = T_g$ under p = 10 Torr, 100 Torr, and 15200 Torr conditions.

(i) 100 Torr Pressure

Figures 6.13, 6.14, and 6.15 outline the gas temperature dependence of the neutral, positive, and negative species concentrations at p = 100 Torr under thermodynamic equilibrium conditions. Aside from the overall reduction of all species concentrations due to the reduction of the system pressure, a comparison of the species concentrations shown in these figures with those at atmospheric pressure shown in Figures 6.7, 6.8, and 6.9 indicates that the temperatures at which the transitions between ranges occurs has also been decreased. As shown in Table 6.17, the transition temperature from range 1 to range 2 has decreased to 3200 K, and the transition temperature from range 2 to range 3 has decreased to 6100 K when compared with Table 6.15.

As shown in Figures 6.14 and 6.15, a decrease in pressure also causes the

Table 6.17: Temperature ranges in the Ar-10%CO_2 model, p = 100 Torr, $T_e = T_g$.

Range	T_g [K]
1 (Ar, CO_2, CO dominant)	$\leq$ 3200
2 (Ar, CO, O dominant)	3200–6100
3 (Ar, C, O dominant)	$\geq$ 6100

temperature dependent concentrations of positively and negatively charged species to decrease. The temperatures which separate the regions over which the dominant positive ions occur have also decreased as shown in Table 6.18. The largest concentrations of electrons and O^- ions (at T_g = 15000 K) have now decreased to less than 3×10^{15} cm^{-3} and 5×10^{10} cm^{-3} respectively.

Table 6.18: Dominant positive ions in the Ar-10%CO_2 model, $T_e = T_g$, p = 100 Torr.

Ion	T_g [K]
CO_4^+	$\leq$ 5100
O_2^+	5100–6300
O^+	6300–10200
C^+	$\geq$ 10200

(ii) 10 Torr Pressure

When the pressure is reduced further to p = 10 Torr, the transition temperatures between ranges are reduced to the values shown in Table 6.19. The transitions between range 1 and 2 and range 2 and 3 now occur at 2900 and 5600 K respectively.

The pressure reduction to p = 10 Torr also causes a decrease in the temperature dependent concentrations of positively and negatively charged species as shown in Figures 6.14 and 6.15. The temperatures which separate the regions over which the dominant positive ions occur have decreased to the values shown in Table 6.20. Unlike the p = 760 Torr and 100 Torr cases where C^+ became the dominant ionized species at temperatures greater than 11000 and 10200 K respectively, C^+ never becomes a

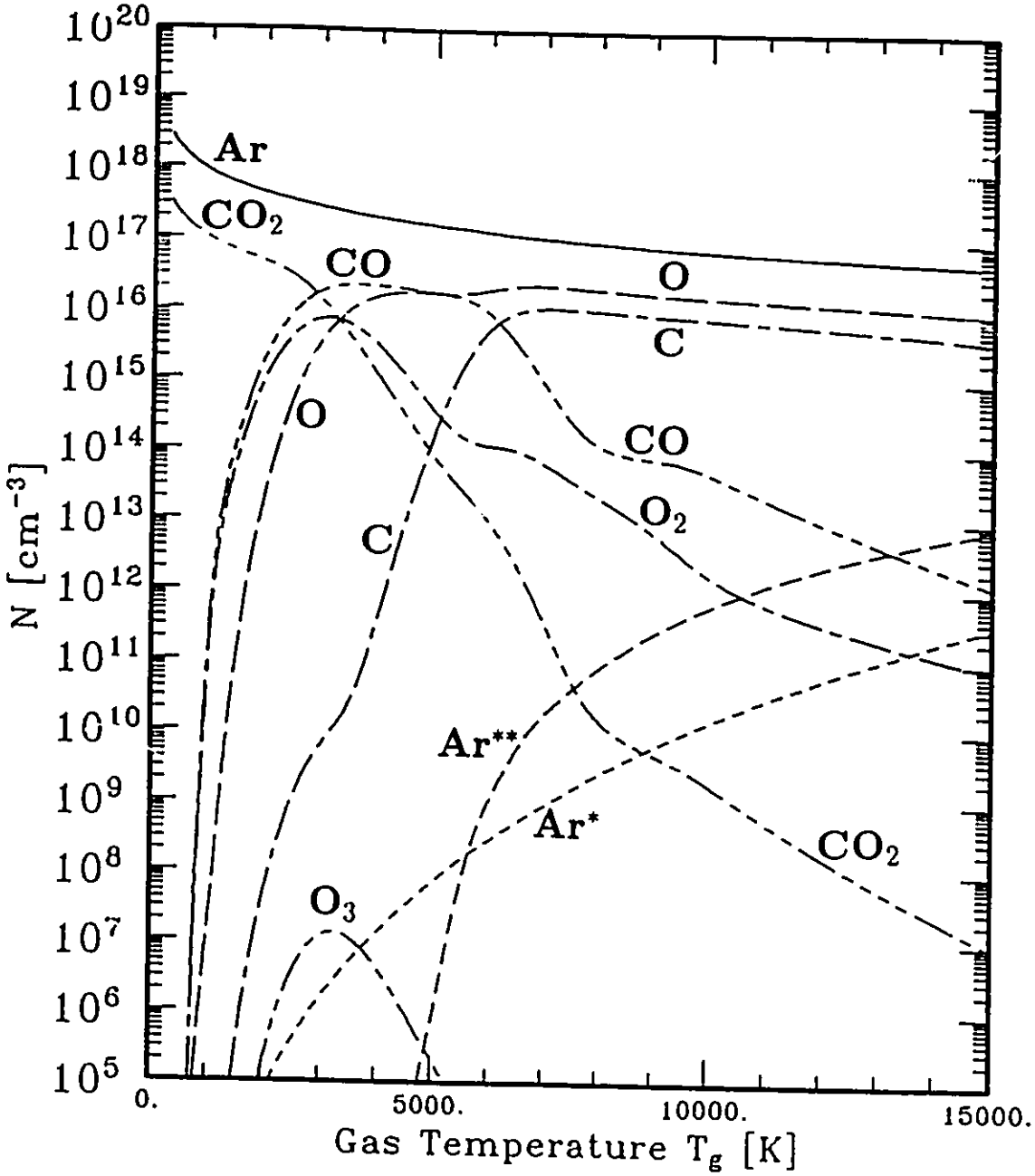

Figure 6.13: Neutral species concentrations as a function of gas temperature for an Ar-10%CO_2 mixture with p = 100 Torr and $T_e = T_g$.

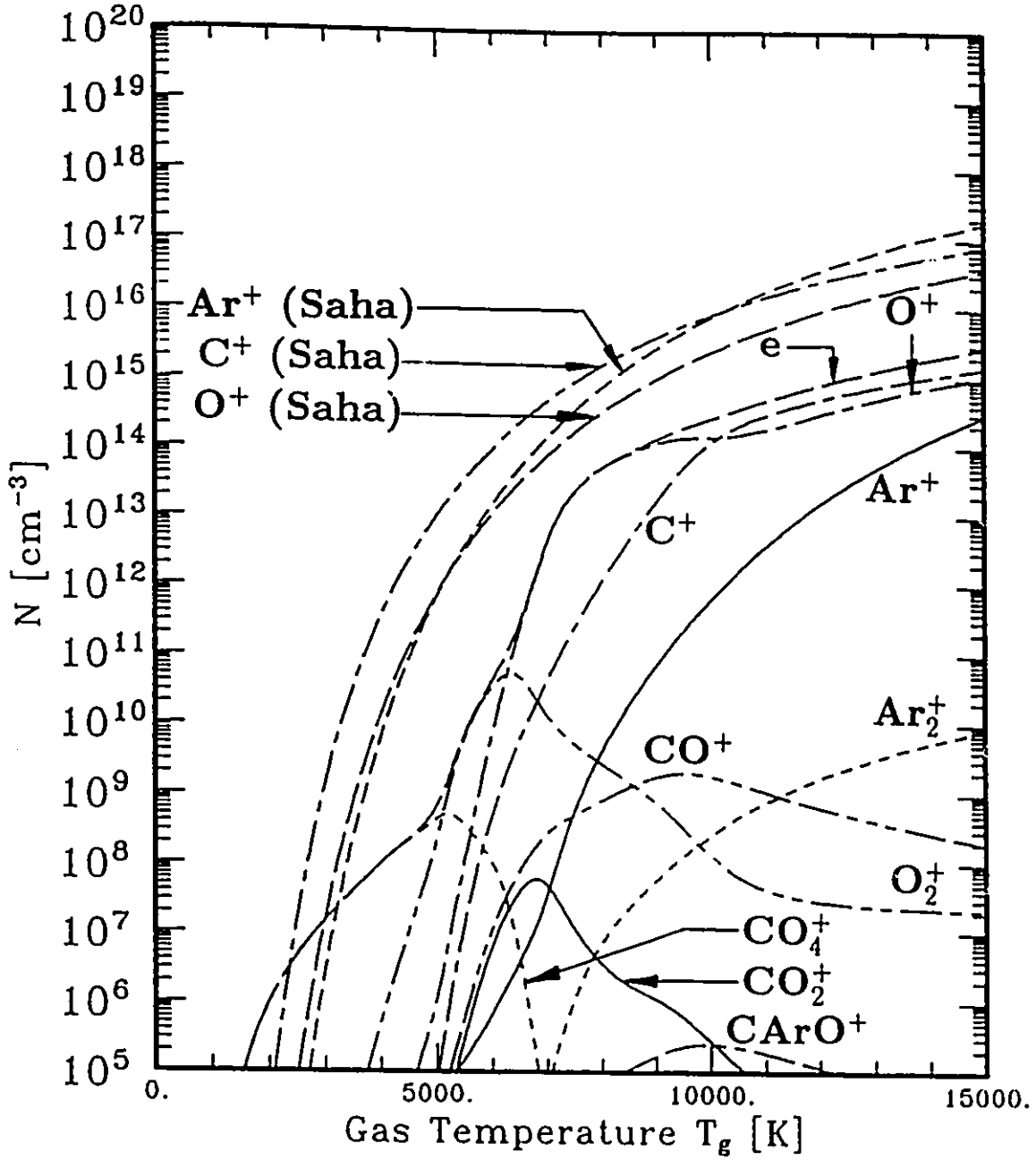

Figure 6.14: Positive ›n concentrations as a function of gas temperature for an Ar-10%CO_2 mixture with p = 100 Torr and $T_e = T_g$.

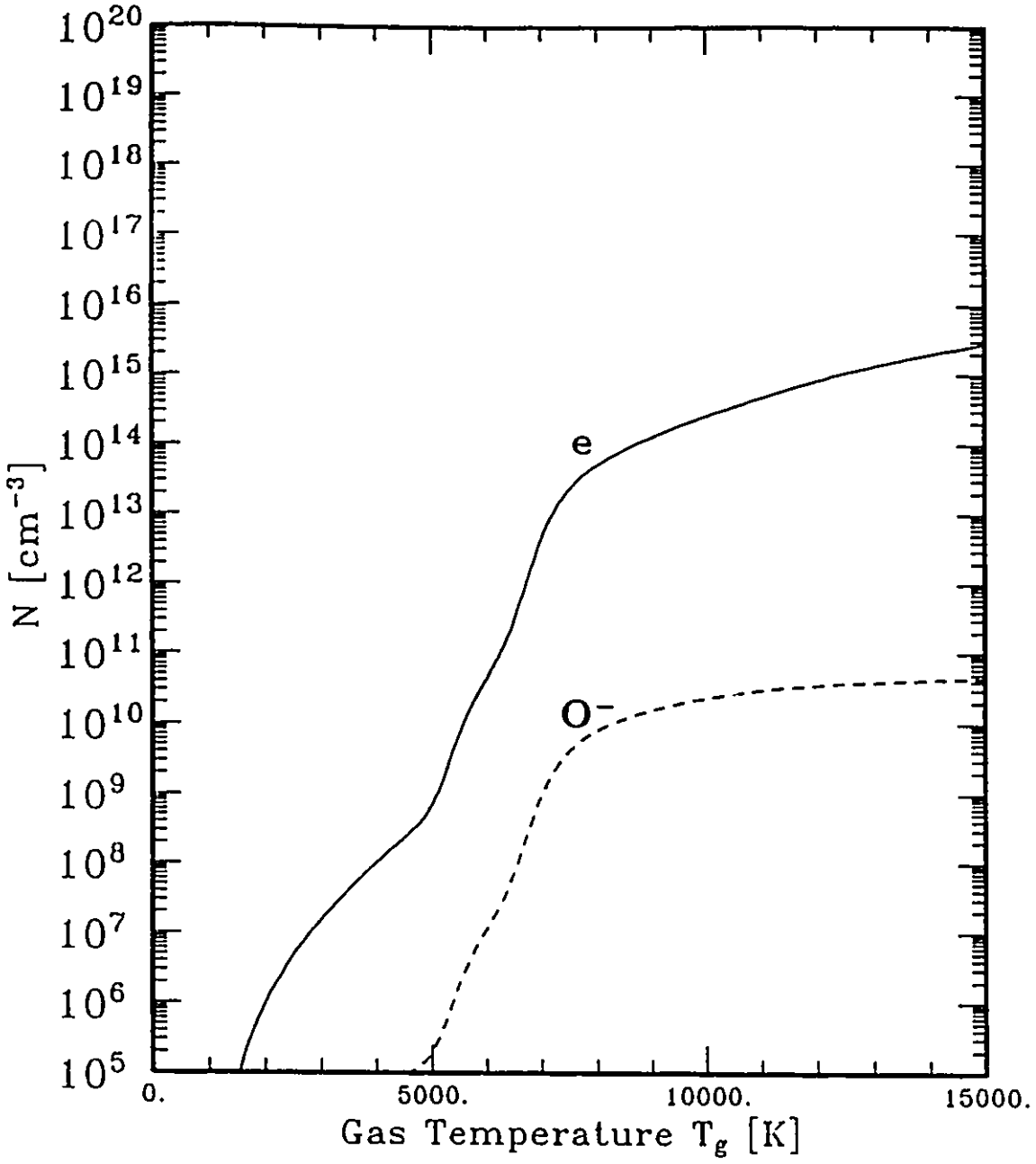

Figure 6.15: Negative ion concentrations as a function of gas temperature for an Ar-10%CO_2 mixture with p = 100 Torr and $T_e = T_g$.

Table 6.19: Temperature ranges in the Ar-10%CO_2 model, p = 10 Torr, $T_e = T_g$.

Range	T_g [K]
1 (Ar, CO_2, CO dominant)	$\leq$ 2900
2 (Ar, CO, O dominant)	2900-5600
3 (Ar, C, O dominant)	$\geq$ 5600

dominant ionized species at p = 10 Torr at temperatures less than T_g = 15000 K.

The largest concentrations of electrons and O^- ions (at T_g = 15000 K) have decreased to less than 5×10^{14} cm^{-3} and 4×10^9 cm^{-3} respectively. The concentration of O^-, which increased monotonically at p = 760 and 100 Torr now decreases with temperature above T_g = 13000 K as shown in Figure 6.15.

Table 6.20: Dominant positive ions in the Ar-10%CO_2 model, $T_e = T_g$, p = 10 Torr.

Ion	T_g [K]
CO_4^+	$\leq$ 4200
O_2^+	4200-5600
O^+	$\geq$ 5600

(iii) 15200 Torr Pressure

Figures 6.19, 6.20, and 6.21 illustrate the temperature dependent concentrations of neutral species, positive ions and negative ions respectively when the pressure is increased to 15200 Torr. As shown in these figures, there has been an increase in the concentration of all species due to the increase in pressure when compared to the p = 760 Torr results shown in Figures 6.7, 6.8, and 6.9. A further contributing factor to this increase in species concentrations, may also be the reduction of the loss of species due to diffusion and the increased importance of three-body reactions at this elevated pressure.

When compared to the results for p = 760 Torr shown in Figure 6.7, the transition temperatures between ranges 1 and 2 and ranges 2 and 3 have increased to

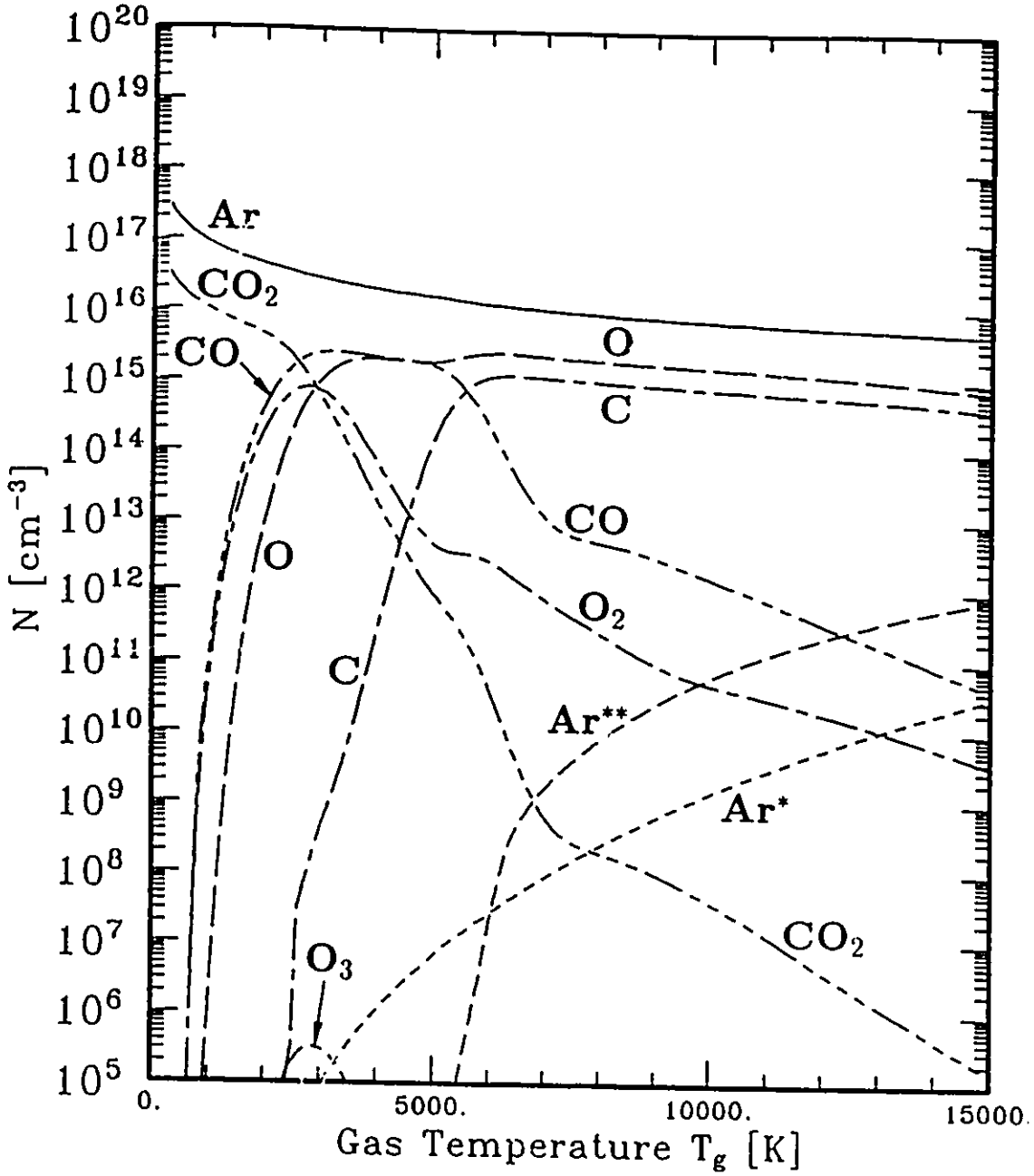

Figure 6.16: Neutral species concentrations as a function of gas temperature for an Ar-10%CO_2 mixture with p = 10 Torr, and $T_e = T_g$.

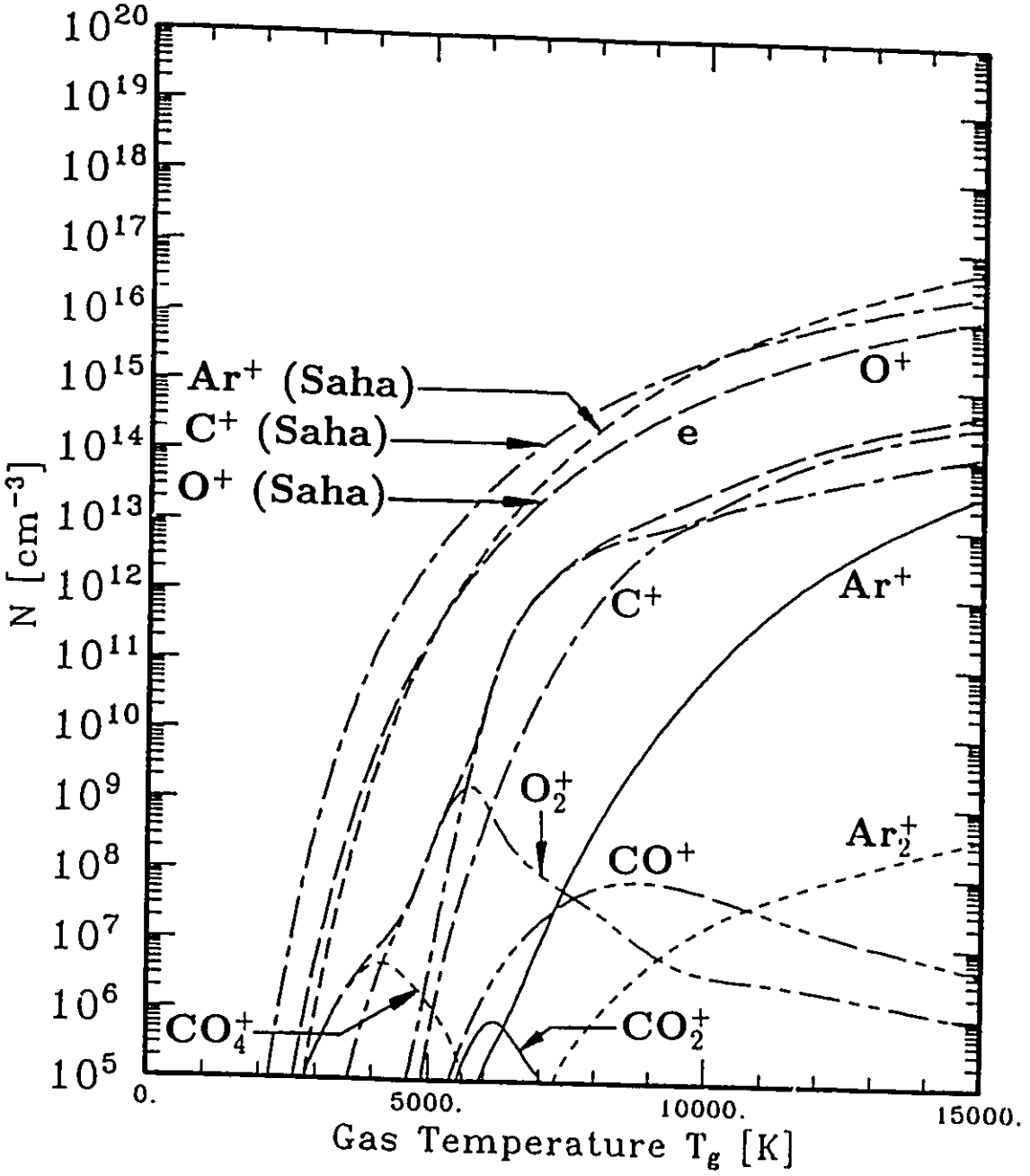

Figure 6.17: Positive ion concentrations as a function of gas temperature for an Ar-10%CO_2 mixture with p = 10 Torr, and $T_e = T_g$.

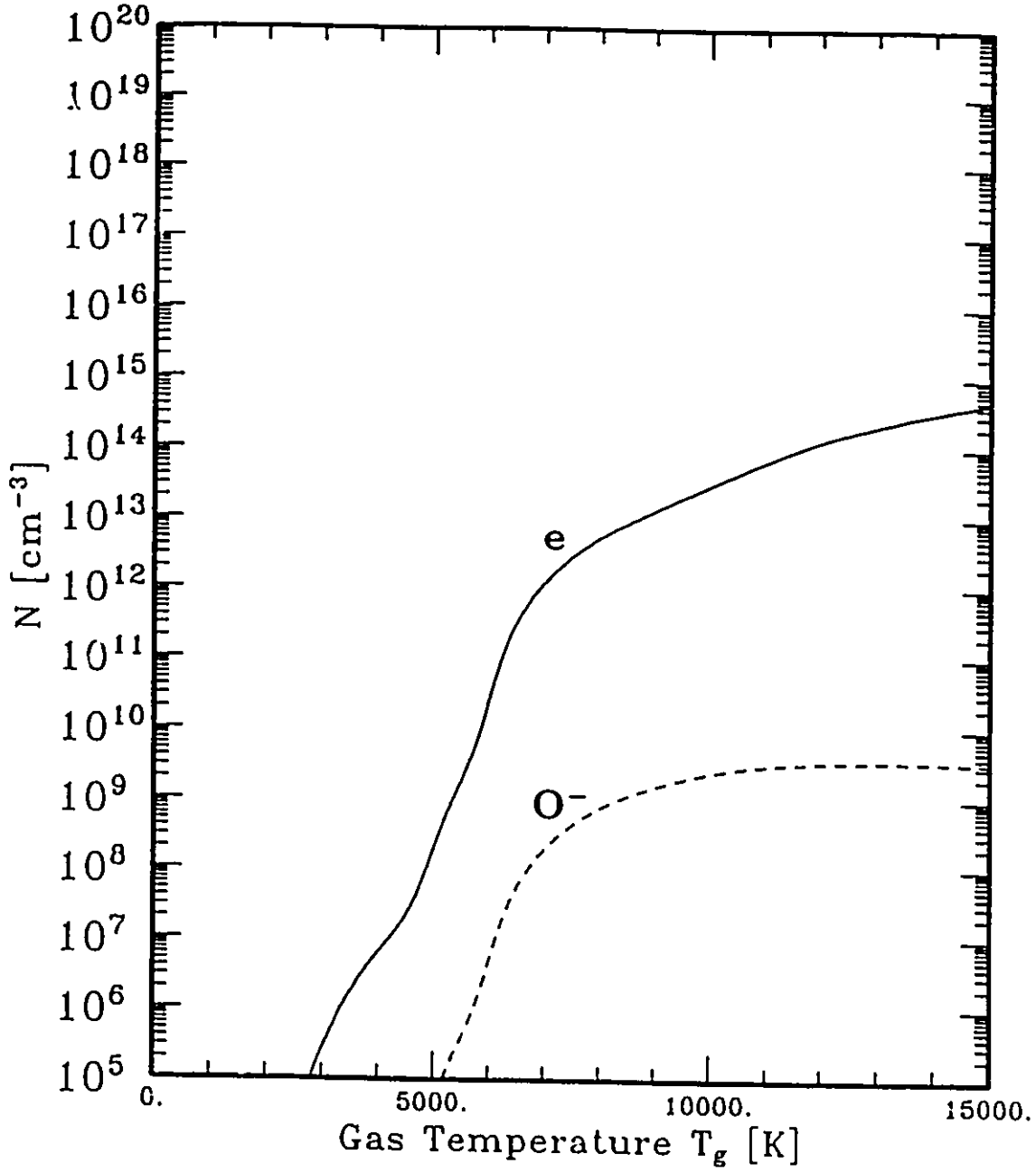

Figure 6.18: Negative ion concentrations as a function of gas temperature for an Ar-10%CO_2 mixture, with p = 10 Torr, and $T_e = T_g$.

4700 and 7900 K respectively as shown in Table 6.21. This trend is consistent with that shown at reduced pressures.

Table 6.21: Temperature ranges in the Ar-10%CO_2 model, p = 15200 Torr, $T_e = T_g$.

Range	T_g [K]
1 (Ar, CO_2, CO dominant)	$\leq$ 4700
2 (Ar, CO, O dominant)	4700–7900
3 (Ar, C, O dominant)	$\geq$ 7900

In keeping with this trend, the temperature dependent concentrations of positively and negatively charged ions have also significantly increased with increasing pressure as shown in Figures 6.20 and 6.21. The temperatures which separate the regions over which the dominant positive ions occur has also increased to the values shown in Table 6.22. It should be noted however that the temperatures over which O_2^+ dominates the positive ion concentrations is relatively small when compared to the results for p = 760, 100 and 10 Torr.

Table 6.22: Dominant positive ions in the Ar-10%CO_2 model, $T_e = T_g$, p = 15200 Torr.

Ion	T_g [K]
CO_4^+	$\leq$ 7600
O_2^+	7600–8100
O^+	8100–13000
C^+	$\geq$ 13000

The increase in the pressure has caused the maximum concentration of CO_2^+, $CArO^+$, and $C_2O_2^+$ to increase to 10^{14}, 5×10^{11}, and 10^{11} cm^{-3} respectively, most likely due to an increase of the concentrations of colliding species in the reactions which constitute the major source reactions of these species. The constituents in the reactions which act as major sources of O_4^+, and O_5^+ (as explained in Section 6.3.1) have most likely also become large enough to generate significant concentrations

($\geq 10^5$ cm^{-3}) of O_4^+, and O_5^+ at temperatures between 6000 and 9000 K, as shown in Figure 6.20.

The increase in species concentrations due to the increase in pressure is also reflected in the increase of negative ion species concentrations shown in Figure 6.21. All negative ion species now occur at concentrations greater than 10^5 cm^{-3} over most of the temperature range considered in the present investigation.

(iv) Summary of Pressure Effects

The neutral species concentrations and the plasma density (as represented by the electron concentration) for pressures between 10 Torr and 15200 Torr have been summarized in Figure 6.22. In order to maintain the clarity of the figure, only CO_2, CO, C, and O neutral species have been included. The temperatures at which the transitions between ranges 1 and 2 and ranges 2 and 3 occur have also been included to give an impression of the manner in which these temperatures change in response to changes in pressure.

As shown in Figure 6.22, an overall assessment of the changes brought on by the changes of the system pressure indicates that the gross features of the temperature dependencies of the ionized and neutral species have been conserved, but the relative concentration of species such as CO_2 and CO increase with increasing pressure as shown. The combined effects of the decreased importance of diffusion losses with increasing pressure, and the increase of the importance of three-body reactions in favour of two-body reactions due to the increased species densities brought on by the increase in the system pressure may be important contributing factors to this trend. The plasma density also increases with increasing pressure, but the change in the relative concentration of electrons with pressure can only be examined properly via the degree of ionization. A summary of the effects of pressure on the degree of ionization has been assembled in Figure 6.23 for pressures between 10 Torr and 15200 Torr, where the degree of ionization is defined as

$$\alpha = \frac{[e]}{N_{TOT}} \tag{6.19}$$

As indicated in Figure 6.23, the degree of ionization tends to decrease with increasing

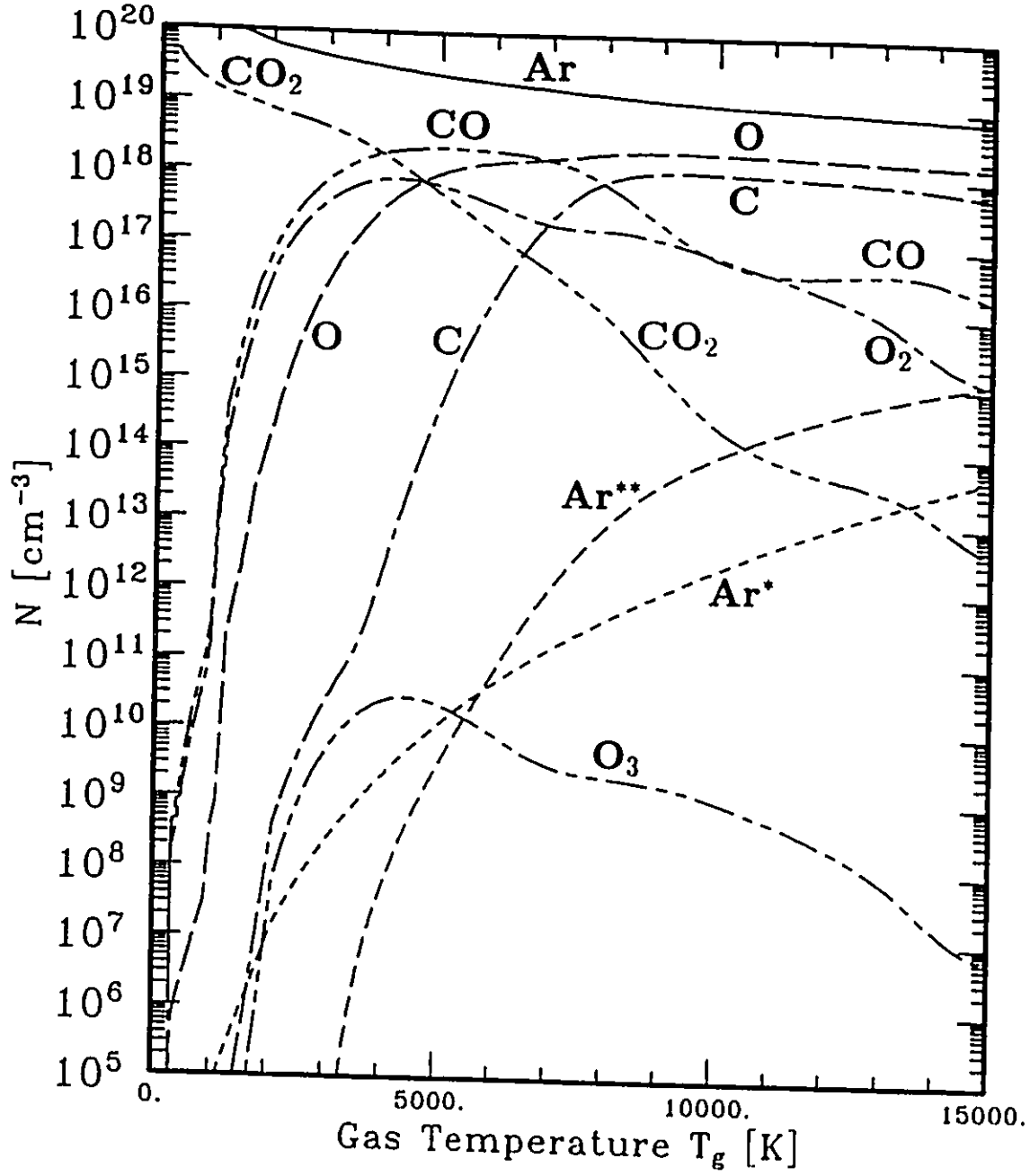

Figure 6.19: Neutral species concentrations as a function of gas temperature for an Ar-10%CO_2 mixture with p = 15200 Torr, and $T_e = T_g$.

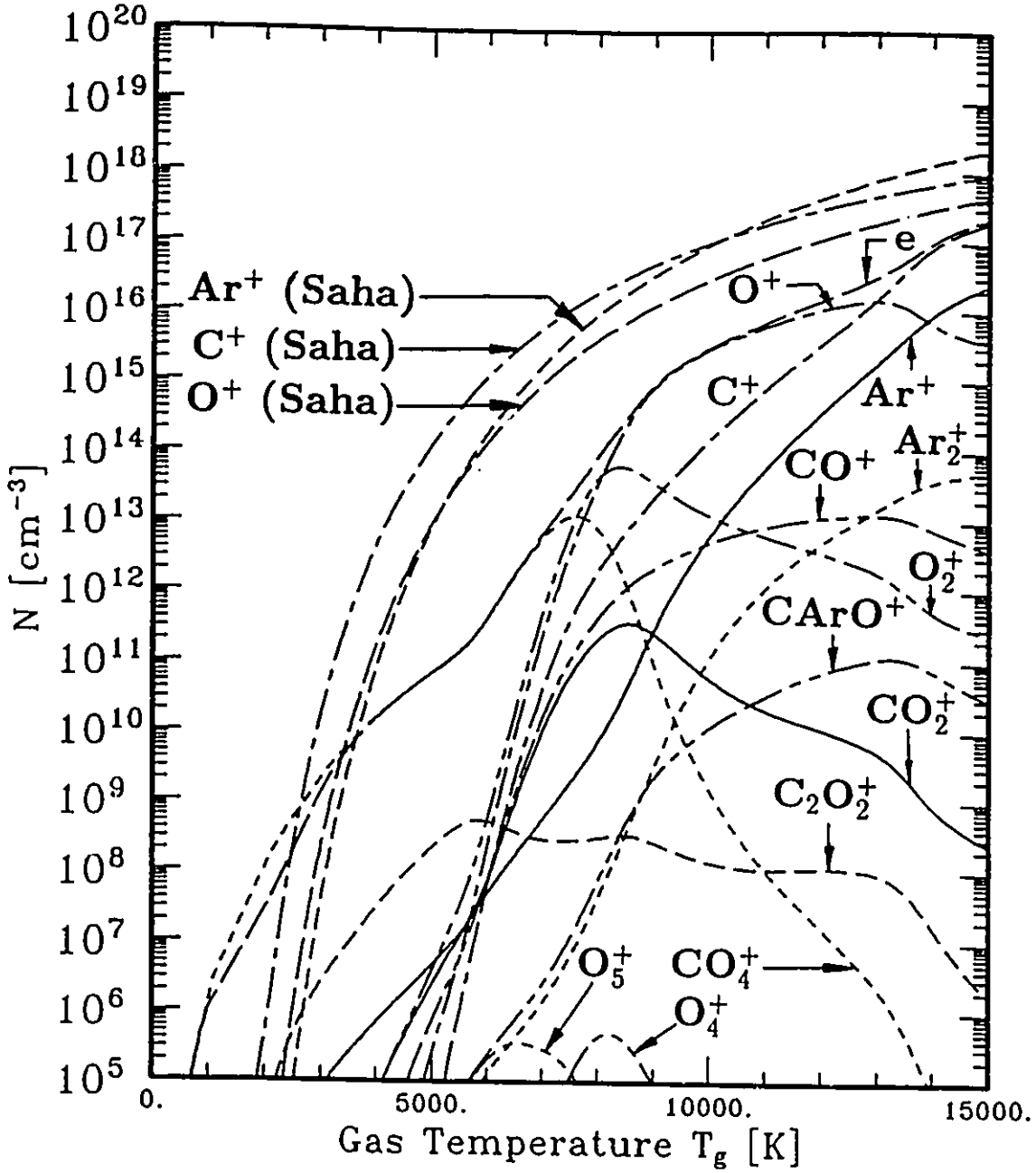

Figure 6.20: Positive ion concentrations as a function of gas temperature for an Ar-10%CO_2 mixture with p = 15200 Torr, and $T_e = T_g$.

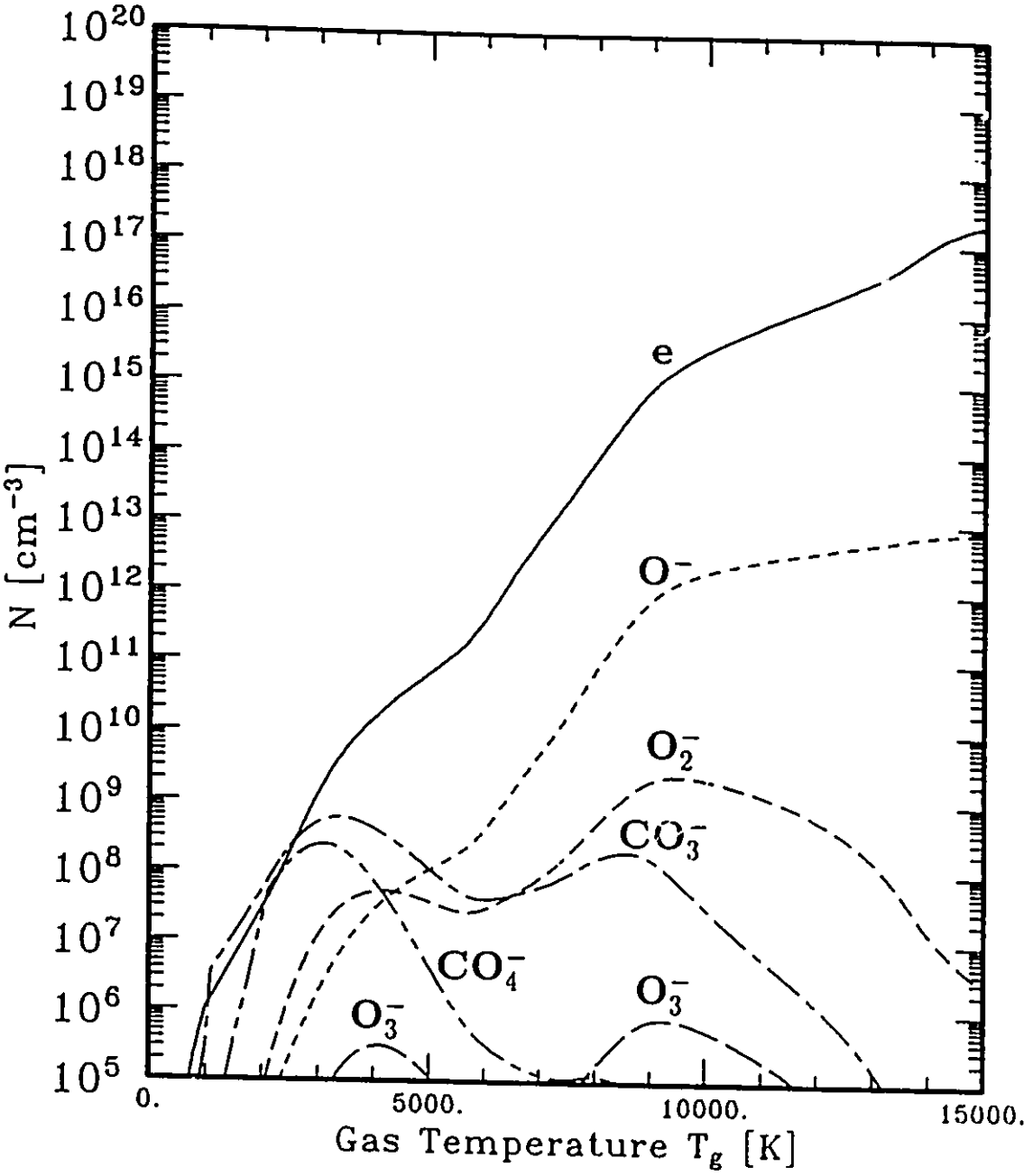

Figure 6.21: Negative ion concentrations as a function of gas temperature for an Ar-10%CO_2 mixture with p = 15200 Torr, and $T_e = T_g$.

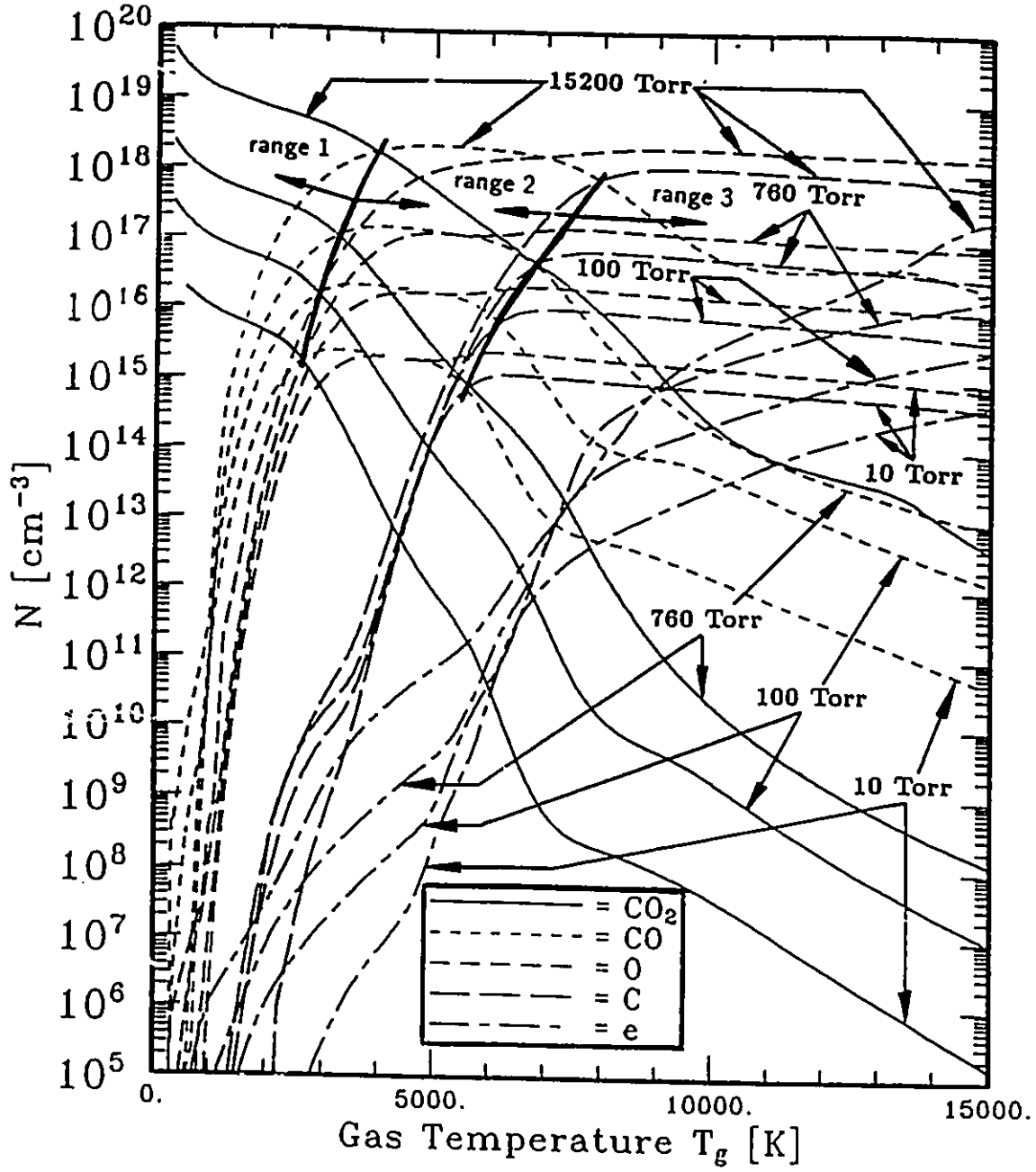

Figure 6.22: Summary of the effect of changing pressure on the temperature dependent concentrations of CO_2, CO, C, O, and electrons for an Ar-10%CO_2 mixture plasma.

pressure at temperatures greater than $T_g = 4500$ K. The largest degree of ionization $\alpha \approx 7 \times 10^{-2}$ occurs at $T_g = 15000$ K when p = 10 Torr. At temperatures greater than $T_g = 4500$ K, the electron concentration is determined primarily by the concentrations of O_2^+, O^+, and C^+ ions through the charge balance relationship shown in equation 6.17. Thus, although the absolute concentration of these species increases with increasing pressure as shown in Figure 6.22, the concentration relative to the total concentration actually decreases. This effect may be due to a relative reduction in the concentration of the species in the reactions which act as major sources of O_2^+, O^+, and C^+ due to an increase in the relative concentration of such species as CO_2 and CO.

At temperatures less than $T_g = 4500$ K however, the degree of ionization tends to have a non-monotonic dependence on pressure, increasing with increases in pressure from p = 10 Torr to p = 100 Torr, remaining relatively constant between p = 100 Torr and p = 760 Torr, and decreasing at pressures greater than p = 760 Torr. The behaviour of the degree of ionization at these low temperatures is determined primarily by the concentration of the CO_4^+ ion through the charge balance relationship shown in equation 6.17. The sources and sinks of CO_4^+ have been discussed in Section 6.3.1.

6.3.4 CO_2 Percentage Mixture Effects

Unlike the Ar-C model in which the Ar and C species are only coupled through the electrons, the Ar, C and O bearing species are closely coupled via ion-molecule, attachment, recombination and neutral reactions in the Ar-CO_2 model. Thus, a change in the percentage of CO_2 in the Ar-CO_2 mixture can have a significant effect on the temperature dependent concentration of all neutral and ionic species. Figures 6.24, 6.25, and 6.26 show the Ar-CO_2 plasma composition at 1% CO_2, $T_e = T_g$, and p = 760 Torr for neutral, positive and negative species respectively.

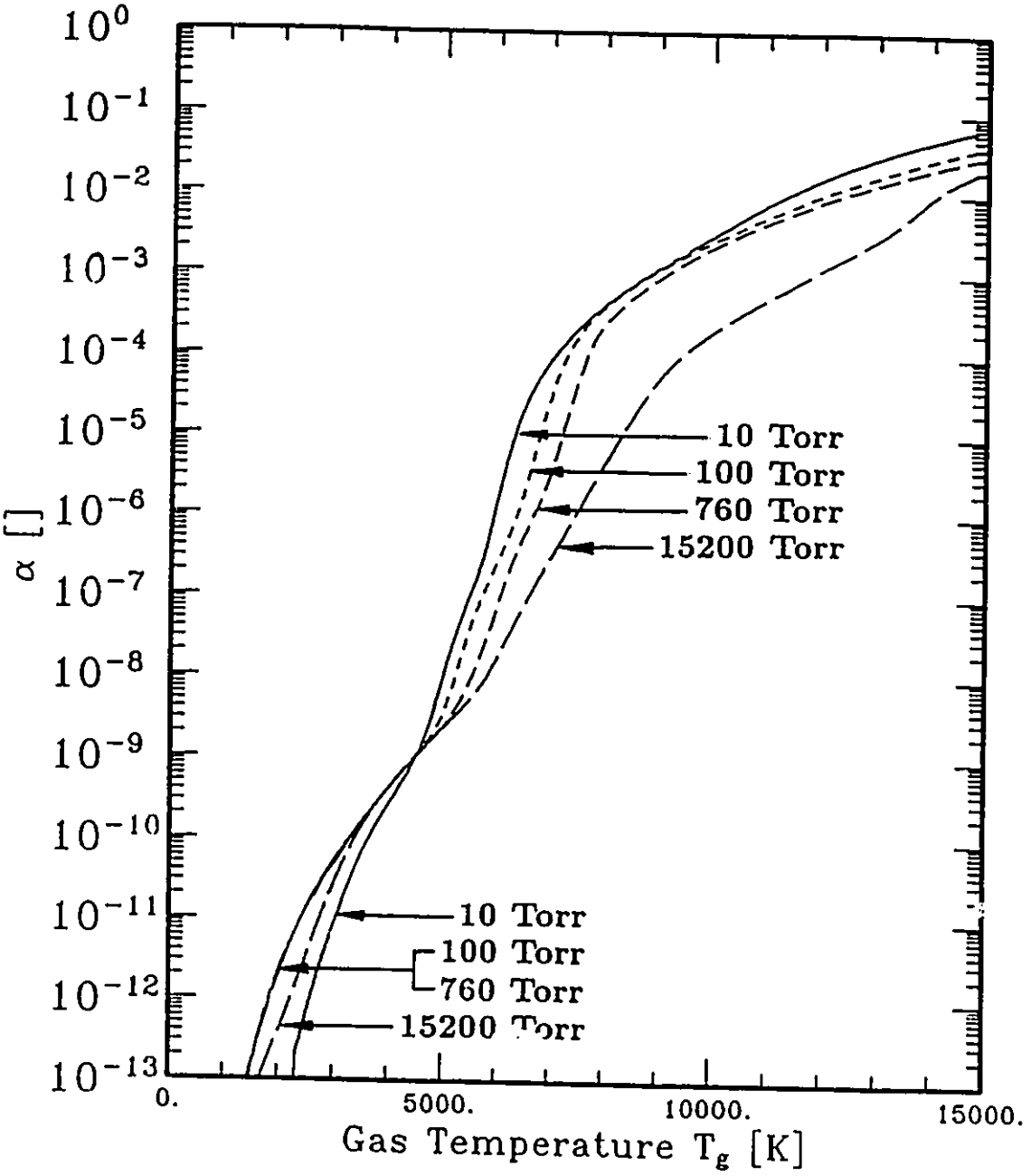

Figure 6.23: Summary of the effect of changing pressure on the degree of ionization for an Ar-10%CO_2 mixture plasma.

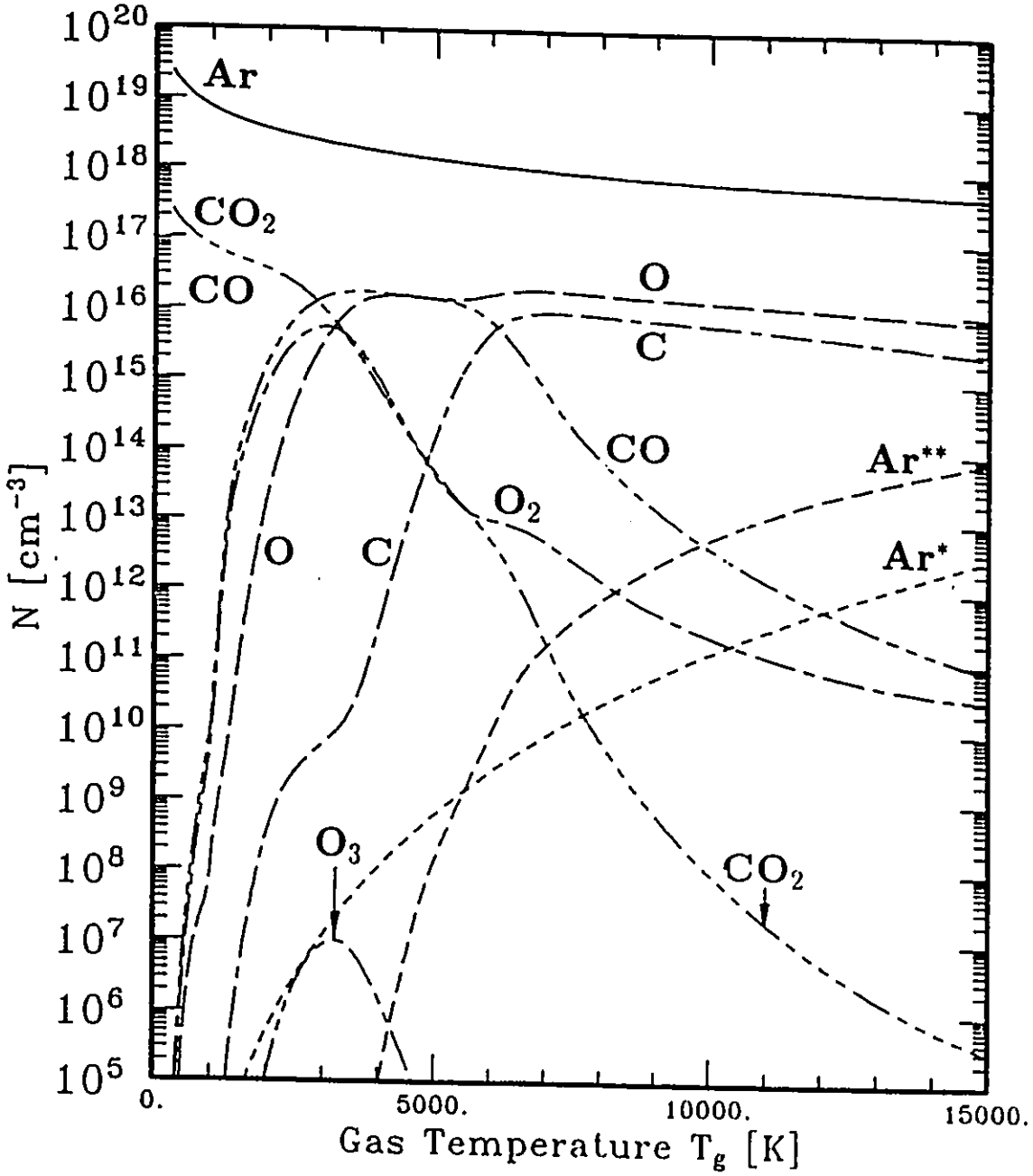

Figure 6.24: Neutral species concentrations as a function of gas temperature for an Ar-1%CO_2 mixture with p = 760 Torr, and $T_e = T_g$.

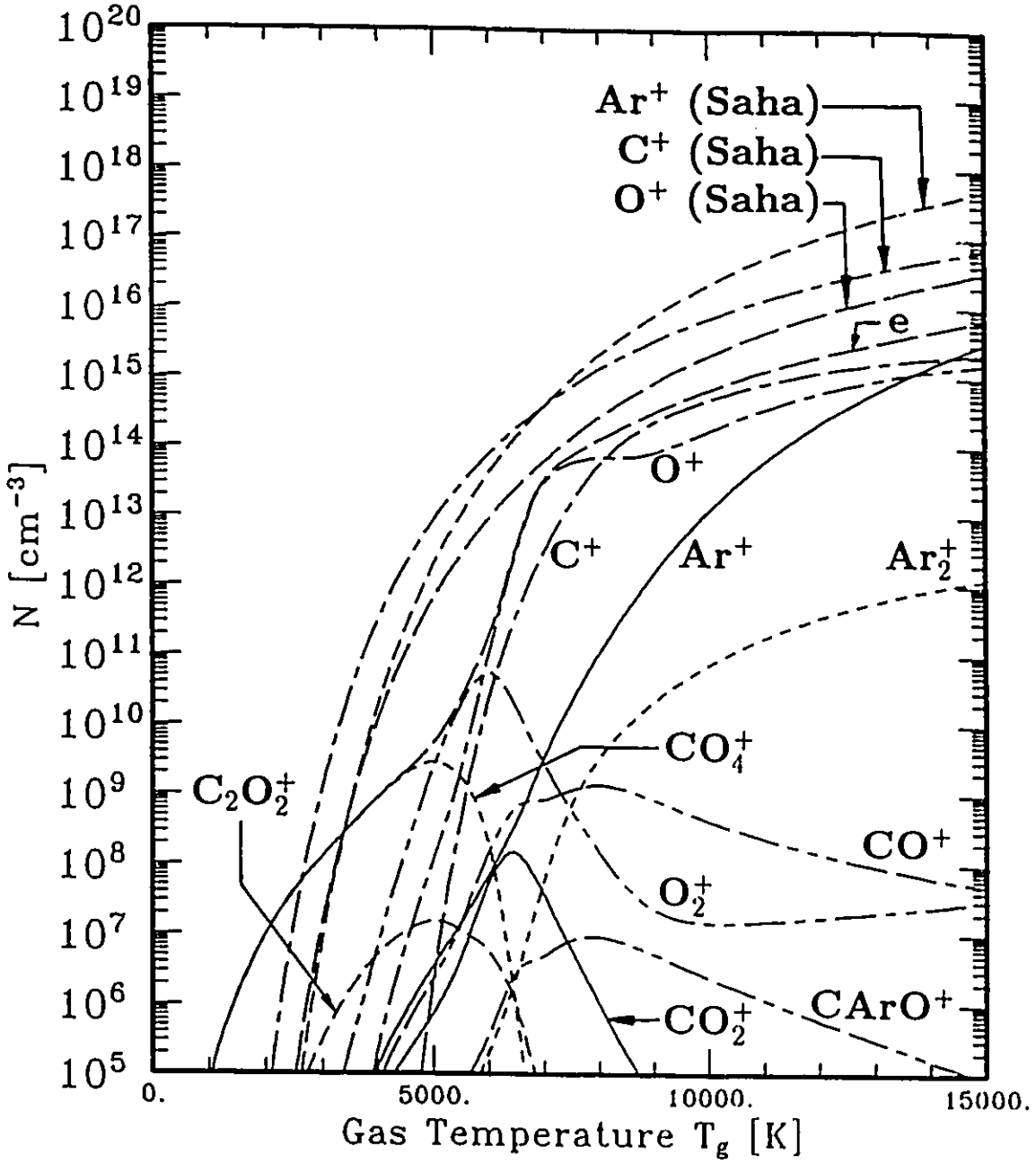

Figure 6.25: Positive ion concentrations as a function of gas temperature for an Ar-1%CO_2 mixture with p = 760 Torr, and $T_e = T_g$.

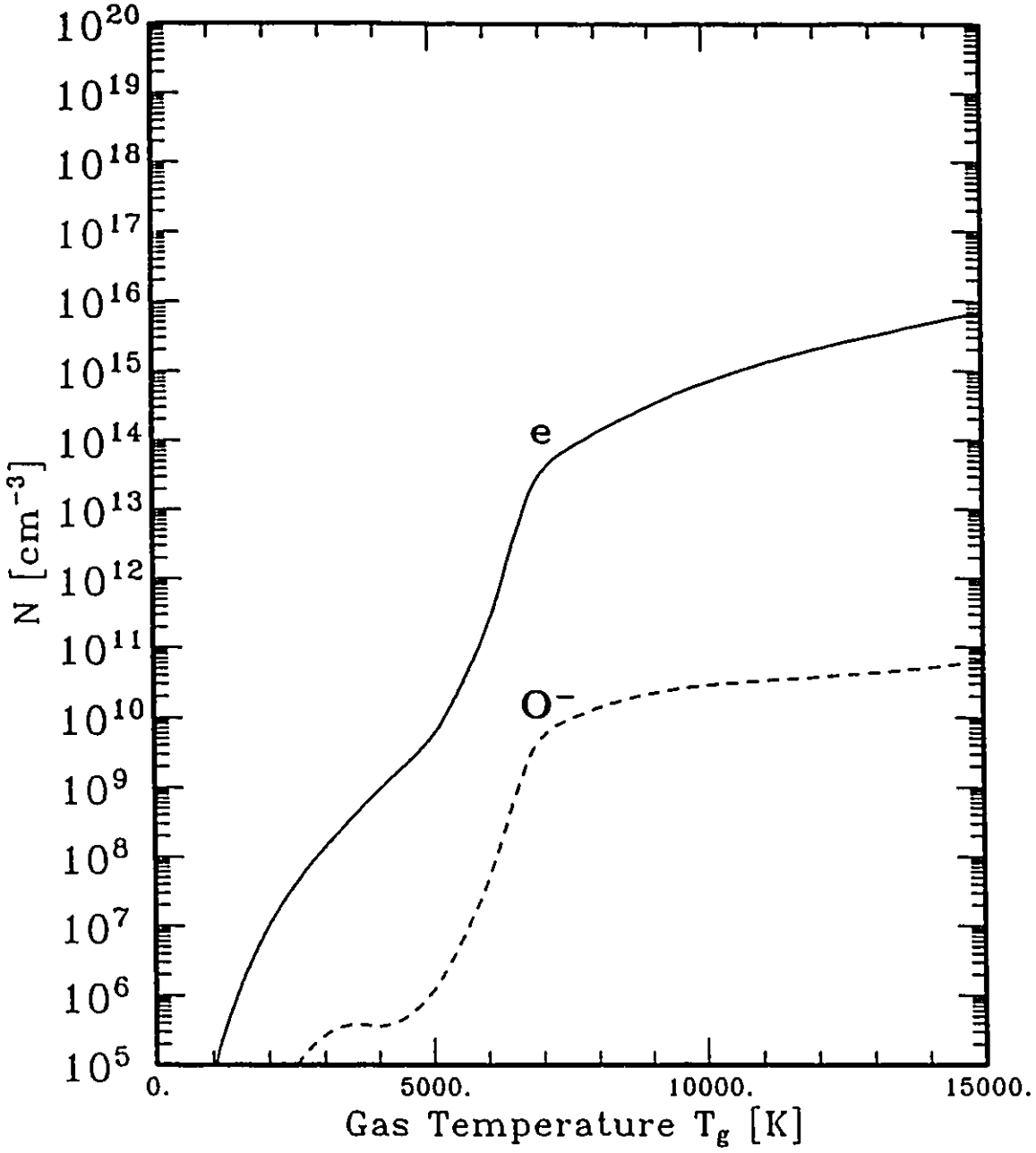

Figure 6.26: Negative ion concentrations as a function of gas temperature for an Ar-1%CO_2 mixture with p = 760 Torr, and $T_e = T_g$.

Neutral Species

A comparison of Figure 6.7 (Ar-10%CO_2 mixture) with Figure 6.24 (Ar-1%CO_2 mixture) illustrates the decrease of neutral species concentrations over most temperatures with decreasing percentage CO_2. At temperatures lower than T_g = 2000 K, in the region where the CO_2 is just beginning to dissociate into CO, O and O_2, these differences are relatively minor. At temperatures greater than T_g = 5000 K however, there is a general decrease in the temperature dependent neutral species concentrations by at least one order of magnitude. These decreases may be as large as 4–5 orders of magnitude, especially at the lower concentrations, and may have been caused by the decreased importance of the three-body reactions leading to these species due to the reduction in the percentage of CO_2. Notably, the temperature dependent CO_2, CO and O_2 concentrations are much smaller. The O_3 concentration has also decreased significantly. It now has a concentration greater than 10^5 cm^{-3} only at temperatures between T_g = 2000–4500 K. Similarly, the transition temperatures between ranges 1 and 2 and ranges 2 and 3 shown in Table 6.23 have also decreased to 3200 and 6100 K respectively when compared the results for an Ar-10%CO_2 mixture shown in Table 6.15.

Table 6.23: Temperature ranges in the Ar-1%CO_2 model, p = 760 Torr, $T_e = T_g$.

Range	T_g [K]
1 (Ar, CO_2, CO dominant)	$\leq$ 3200
2 (Ar, CO, O dominant)	3200–6100
3 (Ar, C, O dominant)	$\geq$ 6100

Ar^*, and Ar^{**} concentrations have increased slightly in response to the increased Ar concentration in the system. These changes are minimal when compared to the Ar-10%CO_2 mixture results however, since there has only been a 9% change in the Ar concentration, and relatively little change in the electron concentration.

Positive Ions

Turning to the temperature dependent concentration of the ionic species, a comparison of Figure 6.25 (Ar-1%CO_2 mixture) with Figure 6.8 (Ar-10%CO_2 mixture), shows that although the concentrations of the individual positive ions may be significantly different in some cases, the overall plasma density as defined by the electron concentration is not as strongly affected by the change in percentage CO_2. The differences are less than a factor of 2 in most cases.

As shown in Table 6.24, the temperatures which separate the regions over which the dominant positive ions occur have decreased with decreasing percentage CO_2. In this case, the reduction of percentage CO_2 has also caused Ar^+ to become the dominant positive ion at temperatures greater than T_g = 14400 K.

Table 6.24: Dominant positive ions in the Ar-1%CO_2 model, $T_e = T_g$, p = 760 Torr.

Ion	T_g [K]
CO_4^+	$\leq$ 5000
O_2^+	5000–6000
O^+	6000–8100
C^+	8100–14400
Ar^+	$\geq$ 14400

The CO_4^+ temperature dependent concentration profile has remained relatively unaffected by the change in percentage CO_2 at temperatures below T_g = 5000 K. In this case, the change in the concentration of colliding species in the dominant CO_4^+ generation reaction M21

$$O_2^+ + CO_2 + M \xrightarrow{k_{M21}} CO_4^+ + M,\ M = Ar$$

may balance each other out in such a way (increased $[O_2^+]$, decreased $[CO_2]$, increased [Ar], as shown in Figure 6.25) that the net effect leaves the resultant CO_4^+ concentration relatively unchanged. At temperatures higher than T_g = 5000 K however, the concentration of CO_4^+ is more than 2 orders of magnitude smaller in an Ar-1%CO_2

mixture than in an Ar-10%CO_2 mixture. This may be a result of the fact that both the O_2^+ and the CO_2 concentrations are lower at these temperatures.

The CO_2^+, CO^+, and O_2^+ concentrations have decreased significantly, most likely due to the decreases in the concentration of the reacting species such as CO_2, CO, and O_2 which are important in the charge transfer reactions acting as major sources of these molecular ions as outlined in Section 6.3.1. The $C_2O_2^+$ concentration has increased with decreasing percentage CO_2 at temperatures between T_g = 3000–7000 K, perhaps as a result of an increase in $CArO^+$ concentration over this temperature region which may tend to cause the additional generation of $C_2O_2^+$ through reaction M11

$$CArO^+ + CO \xrightarrow{k_{M11}} C_2O_2^+ + Ar$$

as outlined in Section 6.3.1. The $CArO^+$ concentration tends to be larger below T_g = 8000 K, but smaller above this temperature. Considering the generation and loss processes of $CArO^+$

$$Ar_2^+ + CO \xrightarrow{(1-f_{M5})k_{M5}} CArO^+ + Ar$$

$$CArO^+ + CO \xrightarrow{k_{M11}} C_2O_2^+ + Ar$$

$$CArO^+ + e \xrightarrow{k_{R1}} Ar + CO$$

the equilibrium concentration of $CArO^+$ can be written as

$$[CArO^+] = \frac{[Ar_2^+]k_{M5}}{k_{M11} + \frac{[e]k_{R1}}{[CO]}} \tag{6.20}$$

At temperatures less then T_g = 8000 K, the $[e]k_{R1}/[CO]$ term in the denominator is relatively small in comparison to the k_{M11} term due to the comparatively small electron concentration at these temperatures. The Ar_2^+ concentration, which has increased with decreasing percentage CO_2 may therefore tend to increase the concentration of $CArO^+$. At temperatures higher than T_g = 8000 K, the increased concentration of electrons and decreased concentration of CO may tend to cause the $[e]k_{R1}/[CO]$ term to become the dominant term in equation 6.20. Coupled with the

fact that the concentration of CO tends to decrease with decreasing percentage CO_2 this may have the effect of decreasing the concentration of $CArO^+$ at temperatures greater than $T_g = 8000$ K.

Both the Ar_2^+ and the Ar^+ temperature dependent concentrations have increased with decreasing percentage CO_2. These increases are most likely due to the fact that the ion-molecule reactions M1–M7:

$$\begin{aligned}
Ar^+ + CO &\xrightarrow{k_{M1}} CO^+ + Ar \\
Ar^+ + CO_2 &\xrightarrow{k_{M2}} CO_2^+ + Ar \\
Ar^+ + O &\xrightarrow{k_{M3}} O^+ + Ar \\
Ar^+ + O_2 &\xrightarrow{k_{M4}} O_2^+ + Ar \\
Ar_2^+ + CO &\xrightarrow{f_{M5}k_{M5}} CO^+ + Ar + Ar \\
&\xrightarrow{(1-f_{M5})k_{M5}} CArO^+ + Ar \\
Ar_2^+ + CO_2 &\xrightarrow{k_{M6}} CO_2 + Ar + Ar \\
Ar_2^+ + O_2 &\xrightarrow{k_{M7}} O_2^+ + Ar + Ar
\end{aligned}$$

may exert a much smaller influence on the system as sinks of Ar^+ and Ar_2^+ due to the decreased concentration of CO_2, CO, O_2, and O caused by the decrease of the percentage CO_2.

The C^+ and O^+ concentrations have also increased below temperatures of $T_g = 11000$ K and $T_g = 8000$ K respectively with decreasing percentage CO_2, for potentially the same reason. At temperatures higher than these, the C^+ and O^+ concentrations have decreased with decreasing percentage CO_2. In this case, the primary generation reactions, thermal impact and electron impact ionization depend only on the concentrations of C, O, and electrons. Since the temperature dependent electron concentration has not changed appreciably with the increase in percentage CO_2, the calculated decrease in C^+ and O^+ concentrations is most likely a consequence of decreased C and O concentrations.

Negative Ions

Concentrations of O^-, O_2^-, O_3^-, CO_3^-, and CO_4^- have decreased in comparison with those found in the Ar-10%CO_2 mixture. Since the electron concentration has

remained relatively unaffected by the decrease in the percentage CO_2, these decreases in negative ion concentration may have been caused by a decrease in the concentration of the reacting neutral species which drive the dominant source reactions for negative ions listed in Table 6.10.

Summary of CO_2 Percentage Mixture Effects

The neutral species concentrations and the plasma density (as represented by the electron concentration) for percentage CO_2 mixtures of 0.1, 1, 10, and 40% have been summarized in Figure 6.27. As in Figure 6.22, only the concentrations of the neutral species CO_2, CO, C, and O have been included to maintain the clarity of the figure. The transition temperatures between ranges have been indicated to give an overall impression of the change in these values with changing percentage CO_2.

As indicated in Figure 6.27, the temperature dependent concentrations of neutral species tend to increase with increasing percentage CO_2. The transition temperatures between ranges also experience a significant shift to higher temperatures with increasing percentage CO_2. Figure 6.27 also clearly shows the manner in which the plasma density tends to decrease with increasing percentage CO_2 at temperatures below T_g = 6000–7000 K, and increase with increasing percentage CO_2 at temperatures higher than this.

The degree of ionization α, as defined in equation 6.19, is also sensitive to changes in percentage CO_2 as shown in Figure 6.28 for percentages of CO_2 between 0.1% to 40%. In this case, the degree of ionization follows the same trends as shown by the electron density in Figure 6.27 since the total concentration of species N_{TOT} in equation 6.19 does not change with changes in percentage CO_2.

6.4 Comparison with Previous Results

6.4.1 Previous Numerical Results

Various numerical equilibrium models have been created to examine the behaviour of CO_2 under thermal plasma conditions, notably those of Nishimura and

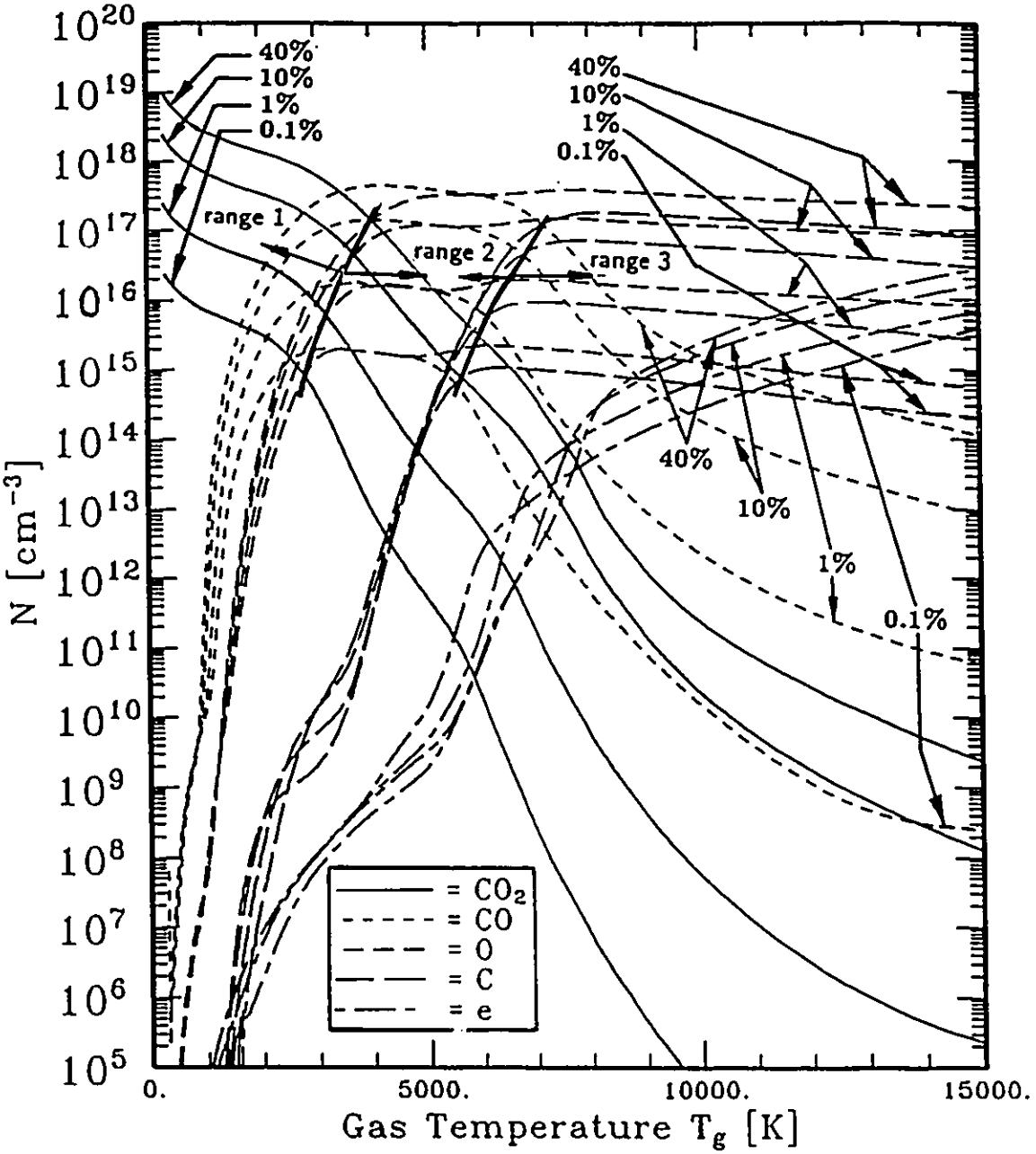

Figure 6.27: Summary of the effect of changing percentage CO_2 on the temperature dependent concentrations of CO_2, CO, C, O, and electrons for an Ar-10%CO_2 mixture plasma.

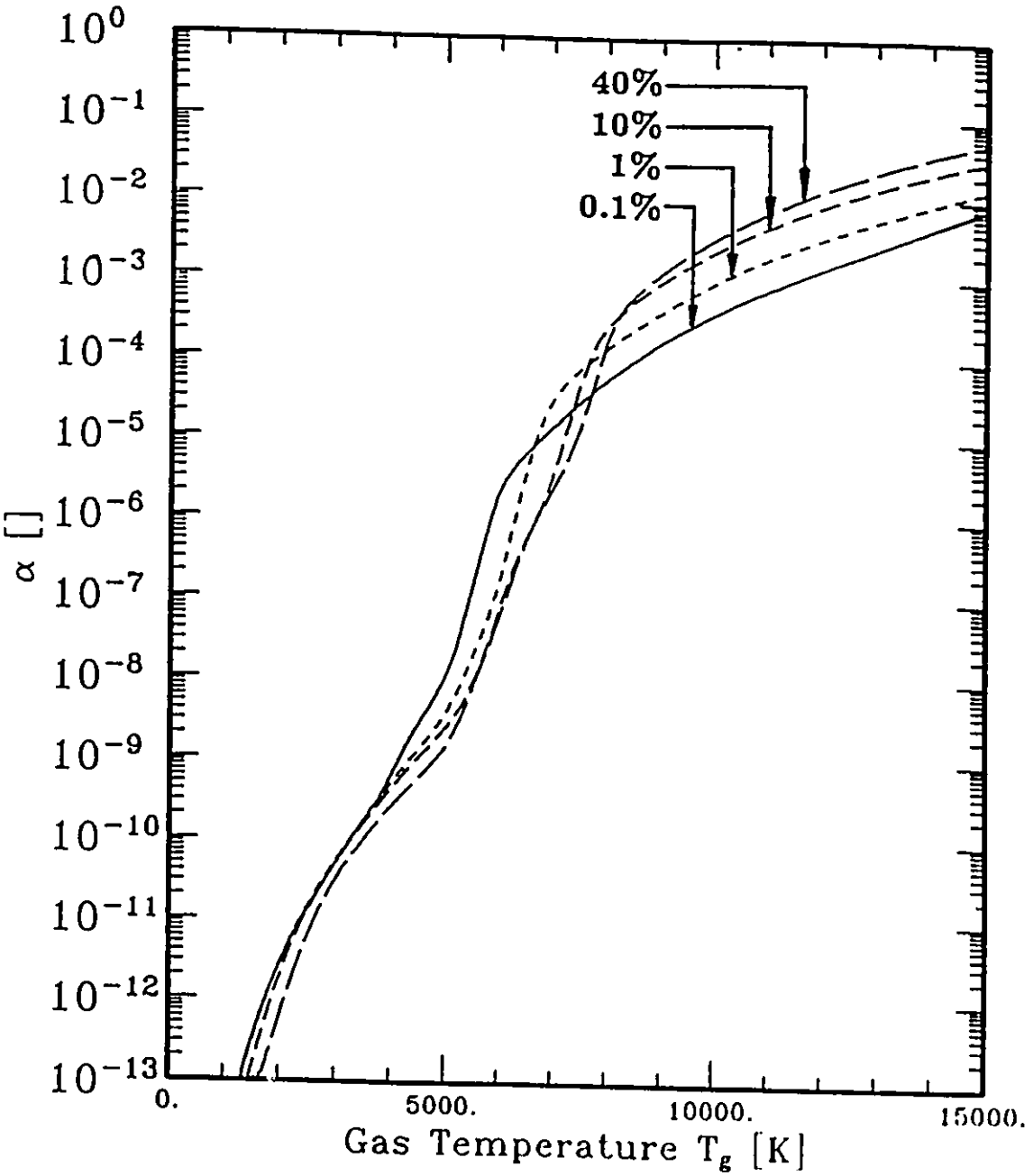

Figure 6.28: Summary of the effect of changing percentage CO_2 on the degree of ionization for an Ar-10%CO_2 mixture plasma.

Takenouchi[13], Lapicque et al.[21], Huczko[20] and Kapoun et al.[24]. A comparison of their results with the present chemical kinetic model has been made in Figures 6.29, 6.30, 6.31, and 6.32 respectively. In all cases, the relative concentration of all C-O bearing species has been plotted as a molar fraction to facilitate comparison with the previous models.

As shown in Section 6.3.4 the percentage of CO_2 in an Ar-CO_2 mixture plasma can have a significant effect on the resultant temperature dependent species concentrations. In spite of the fact that all of the previous models mentioned above were intended to describe the behaviour experimental thermal plasmas consisting of a mixture of Ar and CO_2, none of the models considered the effect of argon on their results. For this reason, these previous results were compared with the present chemical kinetic model using both Ar-0.1%CO_2 and Ar-10%CO_2 mixtures.

Nishimura and Takenouchi use an energy minimization technique to predict the equilibrium composition of species in a C-O system where the C:O ratio is 1:2. As shown in Figure 6.29, Nishimura and Takenouchi's model is in good qualitative agreement with the present model at temperatures less than T_g = 5000 K. However, quantitatively, the results fall between the 0.1% and 10% mixture results of the present model, leading to mis-predictions of the neutral species relative densities. At temperatures greater than T_g = 5000 K, Nishimura and Takenouchi's model tends to predict temperature dependent concentrations of CO which are significantly greater than those predicted by the present model, and concentrations of C which are significantly less than those predicted by the present model. Also, Nishimura and Takenouchi's model does not predict the presence of C^+ and O^+, which figure prominently in the present chemical kinetic model at temperatures greater than T_g = 6000 K for an Ar-0.1%CO_2 mixture and at temperatures greater than T_g = 7000 K for an Ar-10%CO_2 mixture.

Lapicque et al. use an LTE approach to calculate the equilibrium composition of CO_2 under thermal plasma conditions. The model of Lapicque et al. is in good qualitative agreement with the present model, but again does not predict a CO_2 mixture effect as shown in Figure 6.30.

The results of Huczko are very close to those of Lapicque et al.. Both authors

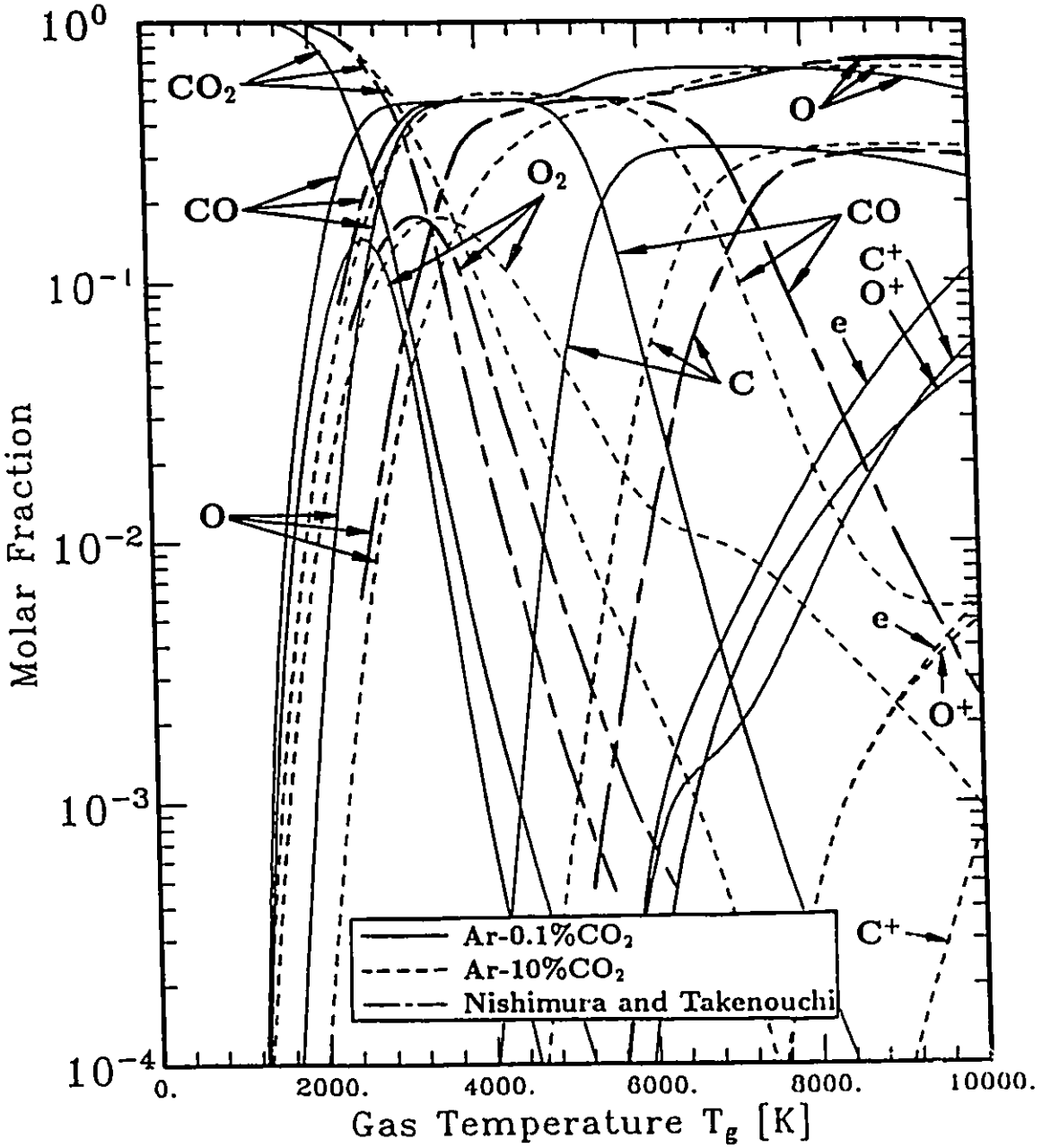

Figure 6.29: Comparison of the energy minimization model by Nishimura and Takenouchi[13] with the Ar-CO_2 chemical kinetic model.

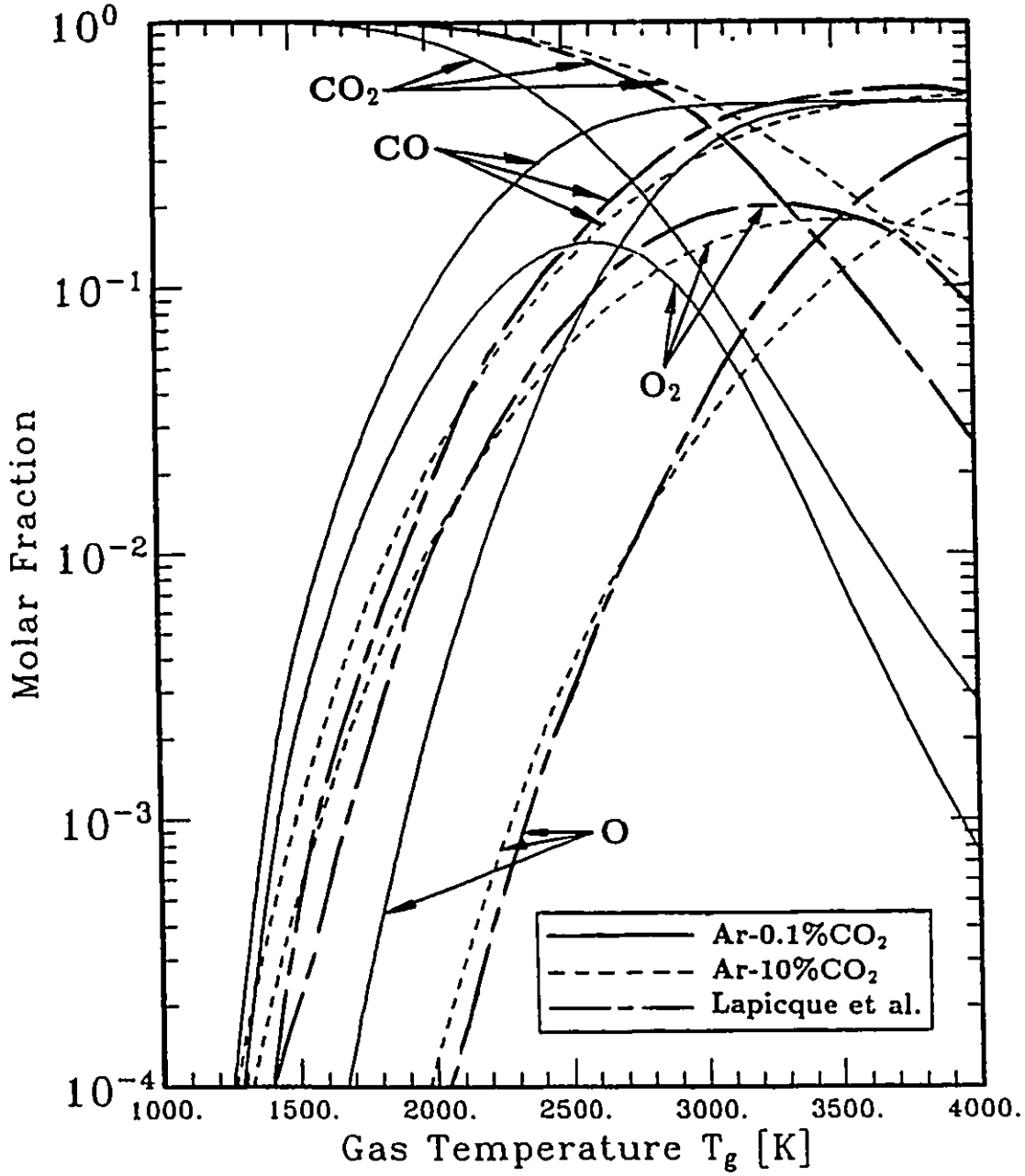

Figure 6.30: Comparison of the local thermodynamic equilibrium model by Lapicque et al.[21] with the Ar-CO_2 chemical kinetic model.

seem to have used the same approach in calculating their models. Huczko considers a smaller molar fraction range than Lapicque et al., but a larger temperature range as shown in Figure 6.31. Again, there is good qualitative, but not quantitative agreement between Huczko's results and the present model. As with results of Lapicque et al. and Nishimura and Takenouchi, the greatest discrepancies between Huczko's model and the present model occur at higher temperatures. At temperatures greater than T_g = 5000 K, Huczko's model predicts CO_2 and O_2 concentrations which are more than one order of magnitude less than those calculated by the present model.

Finally, the equilibrium model of Kapoun et al.[24], represents a significant extension of the type of models used by Lapicque et al.[21] and Huczko[20]. The same LTE type theoretical approach has been used, but, as illustrated in Figure 6.32, Kapoun includes a greater number of potential species, and considers a larger temperature range. As shown in Figure 6.32, the results of Kapoun et al. tend to fall between the Ar-0.1%CO_2 and Ar-10%CO_2 mixture results predicted by the present chemical kinetic model for CO, O_2, C, and O, however the temperature dependent concentrations of CO_2 seem to be significantly smaller than those predicted by the present chemical kinetic model for both 0.1%CO_2 and 10%CO_2 mixtures. Of the four previous models examined here, the model of Kapoun et al. represents the only study which considers the presence of ionized species. The temperature dependent concentrations of electrons and C^+ and O^+ ions predicted by Kapoun et al. qualitatively agree well with the results predicted for the present model. However, quantitatively, the large discrepancies between Kapoun et al. and the present model may be a result of the fact that ionization occurs via two major channels simultaneously under thermodynamic equilibrium conditions (thermal and electron impact ionization), whereas an LTE model like that of Kapoun may only consider a thermal ionization.

In summary, although the computational techniques applied to the prediction of the behaviour of the temperature dependent species concentration of CO_2 under thermal plasma conditions by Nishimura and Takenouchi, Huczko, Lapicque et al., and Kapoun et al. differ from the present model, the results seem to agree well qualitatively, but not quantitatively with the present model. Some significant differences do exist, especially at temperatures greater than T_g = 4000 K however it should also

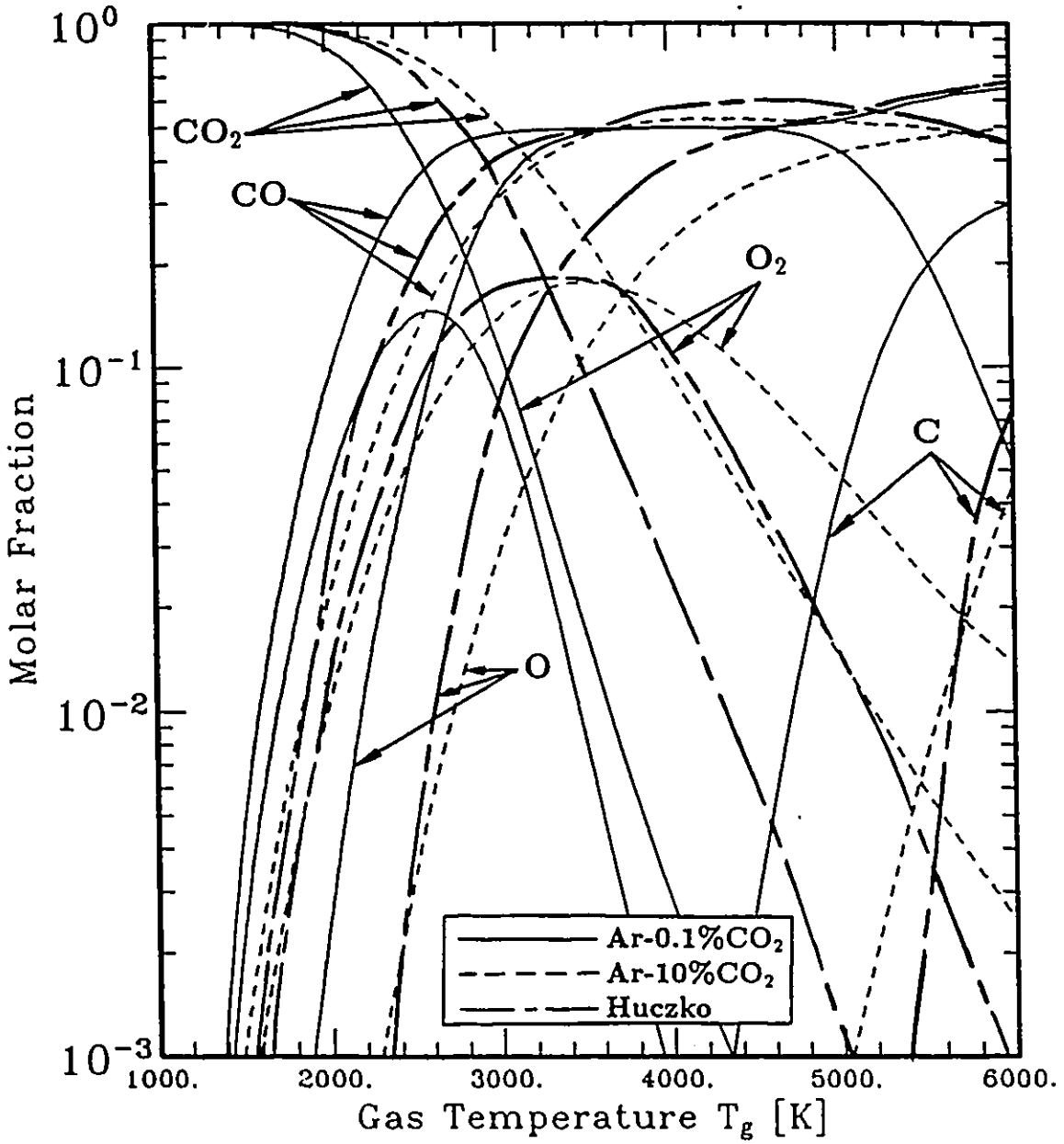

Figure 6.31: Comparison of the local thermodynamic equilibrium model by Huczko[20] with the Ar-CO_2 chemical kinetic model.

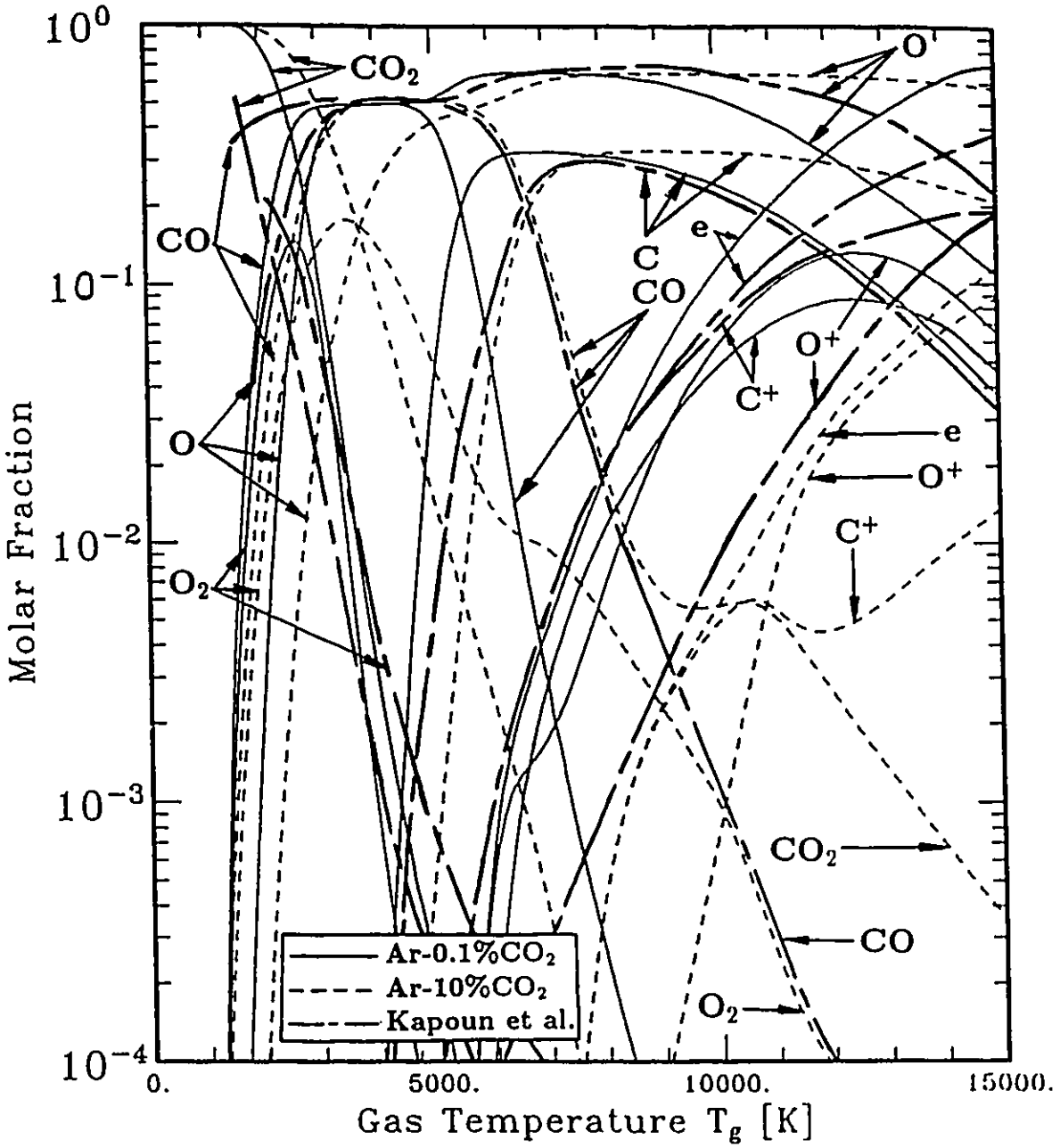

Figure 6.32: Comparison of the local thermodynamic equilibrium model by Kapoun et al.[24] with the Ar-CO_2 chemical kinetic model.

be kept in mind that the models applied by these previous authors do not take into account the presence of ionic species (with the exception of Kapoun et al.) or the presence of argon, and in the case of the local thermodynamic equilibrium models of Lapicque et al., Huczko, and Kapoun et al. consider only a small fraction of the chemical reactions considered in the present model.

6.4.2 Previous Experimental Results

Although numerous experiments have been performed to examine the behaviour of CO_2 under thermal plasma conditions, these investigations have concentrated primarily on the degree to which CO_2 is dissociated into CO, O_2 and O, notably those of Nishimura and Takenouchi[13], Honda et al.[18], and Huczko[20]. In all cases, the authors did not attempt to measure the electron temperature. A comparison of their results with the present chemical kinetic model has been made in Figures 6.33 and 6.34 by assuming $T_e = T_g$ and p = 760 Torr. In all cases, the relative degree of CO_2 dissociation α_{CO_2} has been plotted as a function of gas temperature to facilitate comparison with previous models, where α_{CO_2} is defined as

$$\alpha_{CO_2} = \frac{[CO_2]_{IG} - [CO_2]}{[CO_2]_{IG}} \tag{6.21}$$

As shown in Figure 6.33, the DC plasma torch experimental results of Honda et al.[18] and Huczko[20] agree well qualitatively with the present model both in terms of CO_2 percentage mixture and gas temperature dependencies. Quantitatively however, their results fall somewhat closer to the Ar-0.1%CO_2 and Ar-1%CO_2 results of the present chemical kinetic model, in spite of the fact that Honda et al. used an Ar-6.7%CO_2 mixture, and Huczko used a mixture containing more than 18% CO_2. However, the quantitative discrepancy between the present model and existing experimental results may be due to non-equilibrium effects ($T_e \geq T_g$). As indicated in Chapter 2, the experiments of previous authors may not have been in thermal equilibrium. Since the CO_2 dissociation rate can be expected to increase when $T_e \geq T_g$, the quantitative comparison between the present model and previous experimental results may improve.

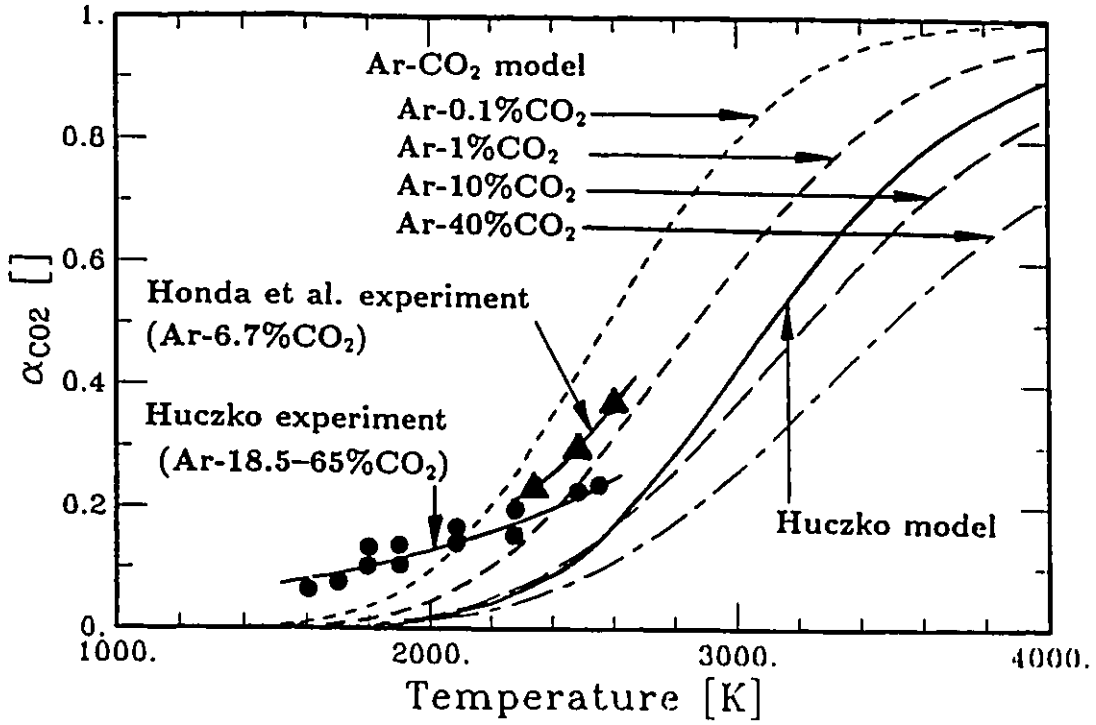

Figure 6.33: Comparison of the experimental results of Honda et al.[18] and Huczko[20] with the Ar-CO_2 chemical kinetic model.

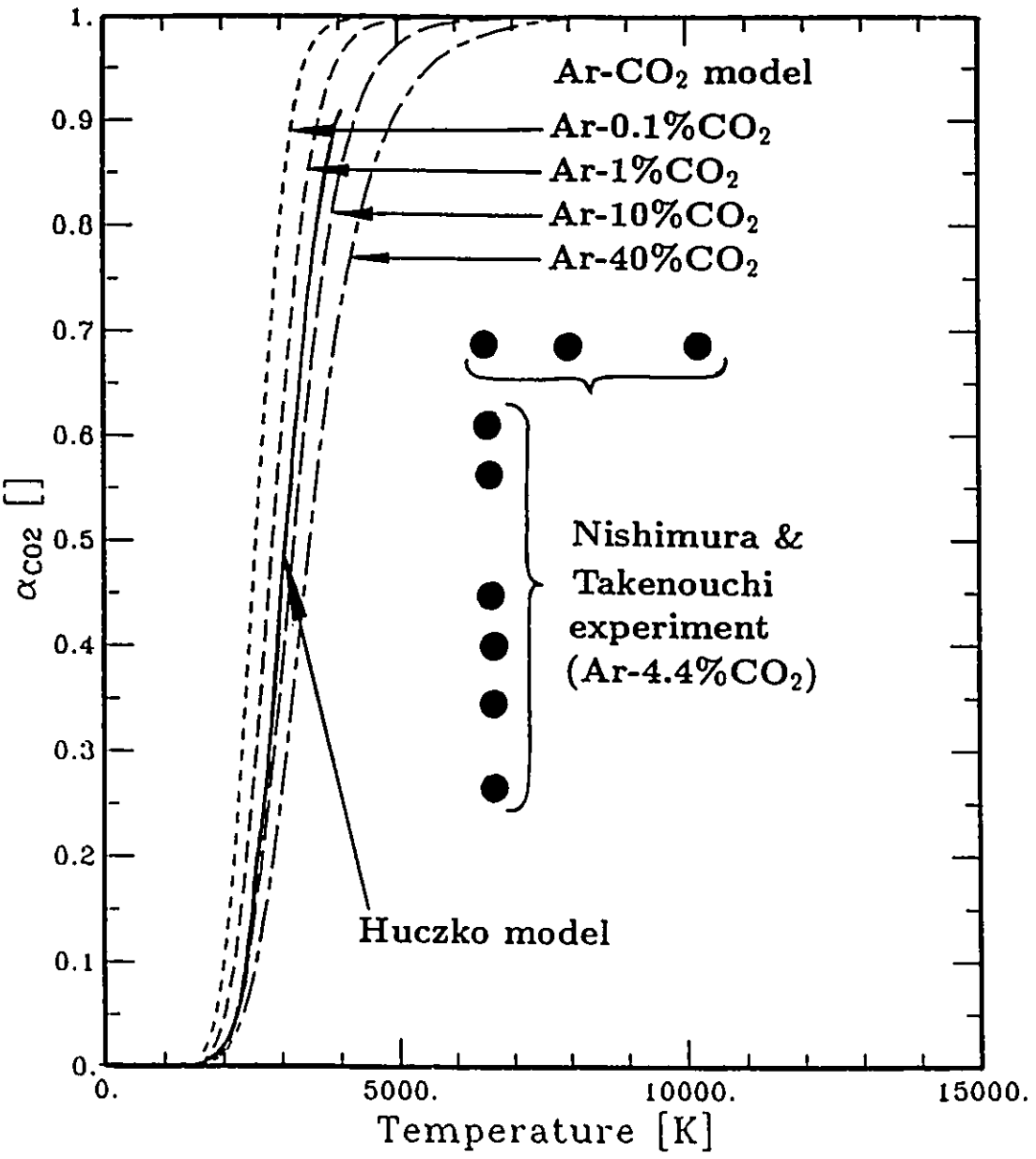

Figure 6.34: Comparison of the experimental results of Nishimura and Takenouchi[13] with the Ar-CO_2 chemical kinetic model.

As shown in Figure 6.34, the RF plasma torch experimental results of Nishimura and Takenouchi agree qualitatively, but not quantitatively with the present model. In this case, Nishimura and Takenouchi may have experienced some difficulties in acquiring reliable experimental results from the gas samples which were used to obtain their results due to a bias introduced by their probe.

6.5 Summary of Ar-CO_2 Thermal Plasmas

A detailed chemical kinetic model has been developed to predict the behaviour of Ar-CO_2 gas mixtures under thermal plasma conditions. Increasing the gas temperature of the mixture above room temperature tends to dissociate the CO_2 into CO, O_2 and O. Further increases in temperature cause the neutral molecular species to dissociate into C and O, and finally into their ionized states C^+ and O^+. More complex molecular ions are also predicted to occur, but normally at lower concentrations.

Pressure, percentage CO_2 mixture and electron temperature, also have a significant effect on the concentrations of both the neutral and ionic species. The results indicate that increases in pressure and percentage CO_2 mixture tend to increase the transition temperatures at which the system changes from a neutral species composition consisting primarily of Ar, CO_2, and CO, to a mixture of Ar, CO, and O, and finally a mixture which consists primarily of Ar, C, and O. This shift of concentrations to higher temperatures with increasing percentage CO_2 and increasing pressure is also reflected in an increase of the temperatures which separate the regions over which the dominant positive ions occur, as well as an increase of both positive and negative ion concentrations.

The effect of pressure and percentage CO_2 on the degree of ionization is somewhat more complicated however. At higher temperatures, increases in pressure tend to decrease the degree of ionization, but increases in percentage CO_2 tend to increase the degree of ionization. At lower temperatures, the degree of ionization exhibits a non-monotonic effect with changes in pressure, but tends to decrease with increases in percentage CO_2.

Under non-equilibrium conditions in which $T_e \neq T_g$, and T_g remains constant,

increases in electron temperature T_e tend to increase primarily the concentration of positively and negatively charged species. Increases in neutral species concentrations are also seen with increases in T_e, however the effect is not as pronounced as in the case of ionic species.

The present chemical kinetic Ar-CO_2 model has been successfully utilized to investigate the composition of Ar-CO_2 mixtures from 0.1 to 40% under pressure conditions ranging from p = 10 Torr to 15200 Torr, and gas and electron temperatures from 300 to 15000 and 300 to 20000 K respectively. The results compare well qualitatively with the modelling and experimental results of previous authors, and significantly extend the scope of these previous efforts.

Chapter 7

Conclusion

Chemical kinetic models have been constructed to predict the concentration of neutral and ionic species in pure Ar, Ar-C and Ar-CO_2 mixtures under thermal plasma conditions. The numerical method employed allowed for the calculation of species concentrations under thermodynamic equilibrium as well as non-equilibrium conditions. Numerical results have been investigated for gas temperatures from 300 to 15000 K, electron temperatures from 300 to 20000 K, and pressures from 1 Torr to 15200 Torr. Percentage mixtures of C and CO_2 were varied from 0.1 to 40%. Electron impact, thermal impact, ion-molecule and recombination reactions as well as the effects of diffusion were included. A concerted effort was made to use primarily experimentally derived reaction rate constants. Where needed, these rate constants were derived directly from collision cross-section data. The model considers important metastable and excited species as well as the presence of molecular ions.

The results of the pure argon model indicate that significant concentrations ($\geq 10^5$ cm^{-3}) of Ar^*, Ar^{**}, Ar^+, Ar_2^+ and electrons occur in thermal plasmas under thermodynamic equilibrium conditions. The concentrations of all of these species tend to increase with increasing gas temperature. At lower temperatures, Ar_2^+ forms the dominant ionic species, whereas at higher temperatures, Ar^+ becomes the dominant ionic species. Under thermodynamic equilibrium conditions, the concentrations of Ar^+ and Ar_2^+ exceed those of Ar^*, and Ar^{**}. The concentrations of all ionic and excited species are seen to increase with increasing pressure, however, further

analysis indicates that the degree of ionization can exhibit a non-monotonic effect with increasing pressure, most likely due to fact that Ar_2^+ is preferentially produced at higher pressures. Under thermodynamic non-equilibrium conditions, increases in electron temperature were found to increase the concentration of Ar^{**}, Ar^+, Ar_2^+, and electrons. It was also found that the concentration of Ar^{**} can exceed that of the ionic species under thermodynamic non-equilibrium conditions. Comparison with the results of the Saha equation indicate that the Saha equation almost always predicts electron concentrations which are significantly different from those calculated via the chemical kinetic model. At lower temperatures, where Ar_2^+ forms the dominant ion, the chemical kinetic model can predict concentrations of electrons which are significantly larger than those predicted by the Saha equation. At higher temperatures where Ar^+ forms the dominant ion, the electron concentration predicted by the chemical kinetic model can be significantly smaller than those predicted by the Saha equation. Comparisons show that the present chemical kinetic model for argon are in good agreement with previous experimental and theoretical results.

Results of the Ar-C mixture model indicate that significant concentrations of Ar^*, Ar^{**}, Ar^+, Ar_2^+, C^+, and electrons occur under thermal plasma conditions. As in the pure argon model, the concentrations of all of these species tend to increase with increasing gas and electron temperatures under thermodynamic equilibrium conditions. At lower temperatures, Ar_2^+ is still the dominant ionized species, however C^+ replaces the Ar_2^+ as the temperature increases. At higher temperatures, Ar^+ subsequently replaces the C^+ as the dominant ionized species. In keeping with the pure argon model, the Ar_2^+, C^+, and Ar^+ concentrations exceed those of the excited species concentrations Ar^*, and Ar^{**}. Increases in pressure are shown to increase the concentration of ionized species, the temperature range over which C^+ forms the dominant ion, and the degree of ionization. Increases in percentage carbon tend to increase both the concentration of ionized species as well as the degree of ionization. Under thermodynamic non-equilibrium conditions, increases in electron temperature were found to increase the concentration of Ar^{**}, Ar^+, Ar_2^+, C^+, and electrons. It was found that the concentration of Ar^{**} could exceed that of the ionized species, albeit with smaller differences between the two concentrations than in the pure argon

model. Comparison with the results predicted by the Saha equation for Ar^+ and C^+ shows that the results of the Saha equation can lead to significant mis-predictions of the plasma density. At lower temperatures, the Saha equation tends to predict a significantly lower concentration of electrons since it cannot account for the presence of Ar_2^+. At higher temperatures, the electron concentrations are somewhat closer to those predicted by the Saha equation due to the presence of the C^+ ion, however the concentration of electrons predicted by the chemical kinetic model for an Ar-C mixture plasma are consistently lower than those predicted by the Saha equation.

The results of the Ar-CO_2 model indicate that significant concentrations of neutral and excited species, Ar, Ar^*, Ar^{**}, C, CO, CO_2, O, O_2, and O_3, positive ions, Ar^+, Ar_2^+, C^+, $CArO^+$, CO^+, CO_2^+, CO_4^+, $C_2O_2^+$, O^+ and O_2^+, and negative ions, CO_3^-, CO_4^-, O^-, O_2^-, and O_3^- as well as electrons can occur under the investigated temperature and pressure ranges. Under thermodynamic equilibrium conditions, the dominant neutral species were found to be Ar, CO_2, CO, O and C, dominant positive ions were found to be CO_4^+, O_2^+, O^+, C^+, and Ar^+, and the dominant negatively charged species were found to be O^- and e. Under thermodynamic equilibrium conditions, increases in gas temperature were found to initially dissociate the CO_2 into CO, O, and O_2, and subsequently into atomic C and O. Further increases in temperature primarily caused an increase in the concentrations of C^+ and O^+ ions, as well as a significant increase in Ar^+ concentrations. Pressure and percentage CO_2 mixture can have a significant effect on the relative temperature dependent concentrations of both neutral and ionic species. Increases in pressure and percentage CO_2 tend to increase the temperatures at which the system changes from a mixture of predominantly Ar, CO_2, and CO, to a mixture of Ar, CO, and O, and finally to a mixture of Ar, C, and O. Increases in pressure and percentage CO_2 mixture also tend to increase the concentration of all ionized and neutral species. The effect of these variables on the degree of ionization is somewhat more complicated however. Increases in pressure tend to decrease the degree of ionization at higher temperatures, but at lower temperatures, the degree of ionization exhibits a non-monotonic dependence on pressure. Increases in the percentage of CO_2 tend to increase the degree of ionization at higher temperatures, but decrease the degree of ionization at lower temperatures.

Under thermodynamic non-equilibrium conditions, increases in the electron temperature under constant gas temperature conditions tend to increase the concentration of positive and negative ions. Increases in the concentration of neutral species such as carbon also occur with increasing T_e, but the effect is not as pronounced as in the case of ionic species.

Comparison of the present Ar-CO_2 thermal plasma model results with those predicted by the Saha equation tend to indicate that the simplifying assumptions made by the Saha equation can lead to significant overpredictions of the plasma density of a thermal plasma by at least an order of magnitude. The temperature dependent concentrations of species were found to be in good agreement with the experimental and theoretical results of previous investigations.

Chapter 8

Recommendations for Future Work

A number of potential research directions exist which could lead to productive future work using the presently developed chemical kinetic models. The Ar-CO_2 model as it now stands contains the reactions necessary to model any mixture of Ar, C, CO, CO_2, and O_2 in which Ar constitutes the majority gas. Mixtures of two components such as Ar-CO or Ar-O_2 or even mixtures of three or more components such as Ar-CO-CO_2, Ar-C-CO_2 Ar-CO-O_2, Ar-CO_2 or Ar-CO-CO_2-O_2 could be modelled. As mentioned above, the present model assumes that Ar constitutes the majority gas in such mixtures, however only minor additional modifications would have to be made to allow the investigation of mixtures in which C, CO, CO_2 or O_2 represent the majority gases.

In their present form, the chemical kinetic models which have been constructed in this investigation use a simplified expression to account for the effects of diffusion. In the present range of investigated pressures, the diffusion mechanism represents a relatively minor loss or gain term of species. It may also be desirable to investigate the chemical kinetic behaviour of Ar-CO_2 and other mixtures as outlined above at low pressures ($p \ll 1$ Torr). Under these conditions, diffusion becomes an important gain or loss mechanism for the species in the model, necessitating a more accurate accounting of the diffusion mechanism.

The information provided by the present model could also be used to investigate the time dependent behaviour of Ar, Ar-C, and Ar-CO_2 thermal plasmas by including the time dependent component of the transport equation as shown in equation 3.5 in Chapter 3. Such a model could be also be coupled to a nozzle flow model for example to yield information on the spatially dependent species concentrations in a plasma jet.

A further application of the present model could involve the prediction of electron and gas temperatures within a thermal plasma based on the pressure and the species concentrations. A similar approach has already been applied with some success to the prediction of electron temperatures in medium pressure glow discharges by Ichikawa and Teii[146].

The investigation of the behaviour of air under thermal plasma conditions also represents a topic of some interest. Since the major gaseous components of air consist of N_2, O_2, CO_2, and Ar, the only species which remains unaccounted for in the present chemical kinetic model is nitrogen. The addition of nitrogen to the Ar-CO_2 model would allow investigations of the neutral and ionized species which occur in thermal plasmas generated in air.

Finally, it is suggested that further experimental results are needed to verify the presence of molecular ions in Ar, Ar-C and Ar-CO_2 thermal plasmas. The present results tend to indicate that significant quantities of such ions should be present in thermal plasmas. Measurements of both gas and electron temperatures and electron densities are also needed in future experiments. Such measurements are of importance not only as inputs to the Ar, Ar-C, and Ar-CO_2 chemical kinetic models developed in this work, but would also help to clarify the degree to which thermodynamic equilibrium is present in mixture thermal plasmas, as well as the degree of ionization present.

References

[1] Keim, W., "Industrial Uses of Carbon Dioxide", Ch. 2 in "Carbon Dioxide as a source of Carbon", Vol. 206 in Series C of the NATO ASI series, eds. M. Aresta and G. Forti, D. Reidel Publishing Company, Dordrecht, 1986.

[2] Novozhilov, N.M., "Fundamental Metallurgy of Gas-Shielded Arc Welding", Gordon and Breach Science Publishers, New York, 1988.

[3] Santén, S., Bentell, L., Johanssen, B., and Westerlund, P., "Applications of Plasma Technology in Ironmaking", Chapter 9 in "Plasma Technology in Metallurgical Processing", J. Feinman, ed., The Iron and Steel Society Inc., Warrendale, USA, 1987.

[4] Rosenqvist, T., "Principles of Extractive Metallurgy", McGraw-Hill, New York, 1983.

[5] Beuthe, T.G., Chang, J.S., Irons, G.A., Lu, W.K., Berezin, A.A., and Chu, F.Y., "A Study of the Solid and Gaseous Products Generated by a DC Plasma Torch under Coal and Steam Injection", Proceedings of the Fifth Annual International Pittsburg Coal Conference, Pittsburg USA, pp. 1191–1202, 1988.

[6] Beuthe, T.G., Masters Thesis, Dept. Eng. Phys., McMaster University, 1988.

[7] Probstein, R.F., and Hicks, R.E., "Synthetic Fuels", pH Press, Cambridge, 1990.

[8] Falbe, J., "New Synthesis with Carbon Monoxide", Springer Verlag, Berlin, 1980.

[9] Giacobbe, F.W., and Schmerling, D.W., "Production of Carbon Monoxide from Carbon and Carbon Dioxide in a Plasma Arc Reactor", Plasma Chemistry and Plasma Processing, Vol. 3, No. 4, pp. 383–392, 1983.

[10] Blanchet, J.L., Parent, J.R., and Lavallee, H.C., "Calibration of an Argon Plasma Jet and Preliminary Application to Production of Oxygen by Carbon Dioxide Reduction", The Canadian Journal of Chemical Engineering, Vol. 47, pp. 160–165, 1969.

[11] Brown, L.C., and Bell, A.T., "Kinetics of the Oxidation of Carbon Monoxide and the Decomposition of Carbon Dioxide in a Radiofrequency Electric Discharge. I. Experimental Results", Ind. Eng. Chem. Fundam., Vol. 13, No. 3, pp. 203–210, 1974.

[12] Brown, L.C., and Bell, A.T., "Kinetics of the Oxidation of Carbon Monoxide and the Decomposition of Carbon Dioxide in a Radiofrequency Electric Discharge. II. Theoretical Interpretation", Ind. Eng. Chem. Fundam., Vol. 13, No. 3, pp. 210–218, 1974.

[13] Nishimura, Y., and Takenouchi, T., "Decomposition of Carbon Dioxide in an Induction-Coupled Argon Plasma Jet", Ind. Eng. Chem., Fundam., Vol. 15, No. 4, pp. 266–269, 1976.

[14] Butylkin, Yu. P., Grinenko, A.A., Levitskii, A.A., Polak, L.S., Rytova, N.M., and Slovetskii, D.I., "Mathematical Modelling of the Kinetics of the Thermal Decomposition of Carbon Dioxide in an Electric Arc Discharge and Quenching of the Products", High Energy Chemistry, Vol. 13, Iss. 6, pp. 456–461, 1977.

[15] Hirotsu, T., "Plasma Reaction Behaviours of Carbon Disulphide and Carbon Dioxide in Glow Discharges", J. Macromol. Sci.–Chem., Vol. A16, No. 7, pp. 1217–1224, 1981.

[16] Lietzke, M.H., and Mullins, C., "The Thermal Decomposition of Carbon Dioxide", J. Inorg. Nucl. Chem., Vol. 43, pp. 1769–1771, 1981.

[17] Huczko, A., and Szymański, A., "Decomposition of Carbon Dioxide in an Arc Discharge Plasma", Z. Phys. Chemie, Leipzig, Vol. 263, No. 6, pp. 1210–1216, 1982.

[18] Honda, T., Takahira, S., and Kanzawa, A., "Thermal Decomposition and Quenching of CO_2 in Argon Thermal Plasma", Proceedings of the 8th International Symposium on Plasma Chemistry, pp. 264–269, Eds. K. Akashi and A. Kinbara, Tokyo, 1987.

[19] Huczko, A., and Szymański, A., "Thermal Decomposition of Carbon Dioxide in an Argon Plasma Jet", Plasma Chemistry and Plasma Processing, Vol. 4, No. 1, pp. 59–72, 1984.

[20] Huczko, A., and Szymański, A., "Plasma Decomposition of Carbon Dioxide", AIChE Journal, Vol. 30, No. 5, pp. 811–815, 1984.

[21] Lapicque, F., Lédé, J., Villermaux, J., "Cinétique Chimique. - Production de monoxyde de carbon par décomposition thermique directe de dioxyde de carbon", C.R. Acad. Sc. Paris, t. 298, Série II, n° 6, pp. 191–194, 1984.

[22] Szymański, A., and Huczko, A., "Studies on the Decomposition of Carbon Dioxide in a Low-Temperature Plasma", Beitr. Plasmaphys., Vol. 24, No. 6, pp. 621–627, 1984.

[23] Baiterekov, A.T., Givotov, V.K., Kerimkulov, M.A., Minducshev, E.V., Otorbaev, D.V., "The Gas Temperature in Microwave Discharge at Plasmochemical Dissociation of Carbon Dioxide", Proceedings of the 7th International Symposium on Plasma Chemistry, pp. 742–748, Eds. C.J. Timmermans, Eindhoven, 1985.

[24] Kapoun, K., Coufal, O., Kapička, "Composition of Ar, N_2, CO_2, and H_2O and Air at Normal Pressure and Temperatures between 3000 K and $20 \cdot 10^3$ K", Proceedings of the XVII International Conference on Phenomena in Ionized Gases (ICPIG) in Budapest, Hungary, 8–12 July 1985, pp. 838–837, eds. J.S. Bakos, and Z. Sörlei.

[25] Baiterekov, A.T., Zhivotov, V.K., Kerimkulov, M.A., Mindukshev, E.V., Otorbaev, D.K., Rusanov, V.D., and Fridman, A.A., "Gas Temperature in a Microwave Discharge during Plasma-Chemical Dissociation of Carbon Dioxide", High Energy Chemistry, Vol. 21, Iss. 1, pp. 55–59, 1987.

[26] Sekiguchi, H., Honda, T., and Kanzawa, A., "Effect of Gas Addition on the Thermal Decomposition of CO_2 using a Thermal Argon Plasma", Proceedings of the 8th International Symposium on Plasma Chemistry, pp. 713–718, Eds. K. Akashi and A. Kinbara, Tokyo, 1987.

[27] Pustogarov, A.V., Slovetskii, D.I., Karabut, A.B., Sharshakov, V.N., and Vishnevskii, V.Yu., "Nonequilibrium in an Arc in a Permeable Channel with Fast Gas Injection", Journal of Engineering Physics, Vol. 54, No. 4, pp. 394–398, 1988.

[28] Chan, K.K., and Venugopalan, M., "Microwave Plasma Decomposition of Carbon Dioxide", Proceedings of the 10th International Symposium on Plasma Chemistry, pp. 2.3-21-1–6, Eds. H.G. Lergon and K. Wiesemann, Bochum, 1991.

[29] Hayashi, H., Beuthe, T.G., Nagai, K., and Chang, J.S., "Mechanism of CO_2 Decomposition by a Thermal Plasma under Reduced Pressures". 1992 ICPIG in UK.

[30] Maezono, I., and Chang, J.S., "Control of Thermal Plasma Produced Reforming Gas CO to CO_2 Concentration Ratio by Corona Torches", Proc. Jpn. Symp. Plasma Chem., Vol. 1, pp. 207–212, 1988.

[31] Chang, J.S., "Corona Discharge Treatment of CO_2 Gas in Plasma-Electrofluidized Bed Filter" Proc. of the IEEJ Meeting on Electrical Discharges, Vol. ED-87-68,69,71–75, pp. 45–54, 1987.

[32] Saha, M.N., "Ionization in the Solar Chromosphere", Phil. Mag., S. 6, Vol. 40, No. 238, 1920.

[33] Smith, N.O., "Elementary Statistical Thermodynamics, A Problem Approach", Plenum Press, New York, 1982.

[34] Vincenti, W.G., and Kruger, C.H., "Introduction to Physical Gas Dynamics", John Wiley & Sons, New York, 1965.

[35] Mitchner M., and Kruger, C.H., "Partially Ionized Gases", John Wiley & Sons, New York, 1973.

[36] Gross, B., Grycz, B., and Miklóssy, K., "Plasma Technology", American Elsevier, New York, 1969.

[37] White, W.B., "Chemical Equilibrium in Complex Mixtures", J. Chem. Phys., Vol. 28, No. 5, pp. 751–755, 1958.

[38] White, W.B., "Numerical Determination of Chemical Equilibrium and the Partitioning of Free Energy", J. Chem. Phys., Vol. 46, No. 11, pp. 4171–4175, 1967.

[39] Crooks, W., "On the Illumination of Lines of Molecular Pressure, and the Trajectory of Molecules", Phil. Mag., Vol. 7, p. 57, 1879.

[40] Langmuir, I., "The Interaction of Electron and Positive Ion Space Charges in Cathode Sheaths" Phys. Rev., Vol. 33, p. 954, 1929.

[41] Davy, H., "An Account of some new analytical Researches on the Nature of certain Bodies, particularly the Alkalies, Phosphorous, Sulphur, Carbonaceous Matter, and the Acids hitherto uncompounded; with some Observations on Chemical Theory", Phil. Trans. Roy. Soc., Vol. 97, p. 71, 1809.

[42] Hoyaux, M.F., "Arc Physics", Springer Verlag, New York, 1968.

[43] Eddy, T.L., and Sedghinasab, A., "The Type and Extent of Non-LTE in Argon Arcs at 0.1–10 Bar" IEEE Transactions on Plasma Science, Vol. 16, No. 4, pp. 444–452, 1988.

[44] Uhlenbusch, J.F., and Fischer, E., "Influence of Diffusion and Nonequilibrium Populations on Noble-Gas Plasmas in Electric Arcs", Proceedings of the IEEE, Vol. 59, No. 4, pp. 578–587, 1971.

[45] Shindo, H., Inaba, T., and Imazu, S., "An Experimental Investigation of Nonequilibrium Effects in Wall-Confined Argon Plasma Arcs", J. Phys. D: Appl. Phys., Vol. 13, pp. 805–815, 1980.

[46] Gleizes, A., Kafrouni, H., Dang Duc, H., and Maury, C., "The difference between the Electron Temperature and the Gas Temperature in a Stationary Arc Plasma at Atmospheric Pressure", J. Phys. D: Appl. Phys., Vol. 15, pp. 1031–1045, 1982.

[47] Hsu, K.C., Etemadi, K., and Pfender, E., "Study of the Free-Burning High-Intensity Argon Arc", J. Appl. Phys., Vol. 54, pp. 1293–1301, 1983.

[48] Pfender, E., "Fundamental Studies Associated with the Plasma Spray Process", Surface and Coatings Technology, Vol. 34, pp. 1–14, 1988.

[49] Rutscher, A., Deutsch, H., "Plasmatechnik, Grundlagen und Anwendung", VEB Fachbuchverlag, Leipzig, 1984.

[50] Ishii, I., Beuthe, T.G., Chang, J.S., and Chu, F.Y., "The Effect of Ar-H_2 Gas Mixtures on the Downstream Temperature Profiles of a Vortex Stabilized DC Plasma Torch", to be submitted.

[51] Beuthe, T.G., Chang, P.B., Chang, J.S., "The Effect of Plasma Gas Flow Patterns on the Thermal Performance of a DC Plasma Torch", Proceedings of the 1991 ASME National Heat Transfer Conference, Minneapolis, Minnisota, July 28–31, 1991, pp. 115–120, K. Etemadi and J. Mostaghimi eds., ASME, 1991.

[52] Donskoi, A.V., Goldfarb, V.M., and Klubnikin, V.S., "Physics and Technology of Low-Temperature Plasmas", S.V. Dresvin, ed., 1972, English edition translated by T. Cheron and edited by H.U. Eckert, Iowa State University Press, 1977.

[53] Ono, S., Beuthe, T.G., Tsuruta, Y., Teii, S., and Chang, J.S., "Thermal Plasma Properties of DC Plasma Jet Under Reduced Pressure", Paper #EP-91-17, pp. 39–48, Proceedings of the 1991 IEE Japan Plasma Science Symposium, IEE Japan Press.

[54] Ono, S., Beuthe, T.G., Tsuruta, Y., Teii, S., and Chang, J.S., "Thermal Plasma Properties of DC Plasma Jet Under Reduced Pressure", Proceedings of the XX International Conference on Phenomena in Ionized Gases (ICPIG) in Pisa, Italy, 8–12 July 1991, pp. 1355–1356, Institute of Atomic and Molecular Physics - CNR, Pisa, Italy, V. Palleschi and M. Vaselli, eds..

[55] Calcote, H.F., "Mechanisms for the Formation of Ions in Flames", Combustion and Flame, Vol. 1, No. 4, pp. 385–403, 1957.

[56] Bradley, J.N., "Flame and Combustion Phenomena", Methuen & Co. Ltd., London, 1969.

[57] Venugopalan, M., Ch. 6 in "Reactions under Plasma Conditions" edited by M. Venugopalan, John Wiley & Sons, New York, 1971.

[58] Morde, M., Private Communication, 1991.

[59] Greene, E.F., and Toennies, J.P., "Chemical Reactions in Shock Waves", Chapter 2, Academic Press Inc., New York, 1964.

[60] Meek, J.M., and Craggs, J.D., "Electrical Breakdown of Gases", Oxford University Press, London, 1953.

[61] Belozerov, A., and Measures, R.M., "The Initial Ionization of Hydrogen in a Strong Shock Wave", J. Fluid Mech., Vol. 6, Part 4, pp. 695–720, 1969.

[62] Chang, J.S., Hobson, R.M., Ichikawa, Y., and Kaneda, T., "Atomic and Molecular Processes in an Ionized Gas", Tokyo Denki University Press, Tokyo, 1984.

[63] Beuthe, T.G., Chang, J.S., "Chemical Equilibrium Model for Ar-H_2 Non-Local Thermodynamic Equilibrium Plasma", Proceedings of the 10th International Symposium on Plasma Chemistry, Bochum, Vol. 1, paper 1.1-29, U. Ehlmann, H.G. Lergon, K. Wiesemann eds., Union of Pure and Applied Chemistry, 1991.

[64] Chang, J.S., Beuthe, T.G., "Theory of Charged Aerosol Particle Deposition on an Electrically Enhanced Cylindrical Wire", Proceedings of the 3rd International Aerosol Conference, Kyoto, Japan, Vol. 1, pp. 383–386, S. Masuda and K. Takahashi, Eds., 1990, Pergamon Press.

[65] Chang, J.S., "Theory of Dense Plasma Afterglow", Physics Letters, Vol. 63A, No. 3, pp. 304–306, 1977.

[66] Hilsenrath, H., "Tables of Thermodynamic and Transport Properties of Air, Argon, Carbon Dioxide, Carbon Monoxide, Hydrogen, Nitrogen, Oxygen and Steam", Pergamon Press, Oxford, 1960.

[67] Drawin, H.W., "Thermodynamic Properties of the Equilibrium and Nonequilibrium States of Plasmas", Ch. 3 in "Reactions under Plasma Conditions" edited by M. Venugopalan, John Wiley & Sons, New York, 1971.

[68] Kröpelin, H., "Thermodynamic Diagrams for High Temperature Plasmas of Air, Air-Carbon, Carbon-Hydrogen Mixtures and Argon", Pergamon Press, Oxford, 1971.

[69] Conte, S.D., and de Boor, C., "Elementary Numerical Analysis, An Algorithmic Approach", McGraw-Hill Book Company, New York, 1980.

[70] Abramowitz, M., and Stegun, I.A., "Handbook of Mathematical Functions, with Formulas, Graphs and Mathematical Tables", Dover Publications, New York, 1972.

[71] Stewart, R.B., and Jacobson R.T., "Thermodynamic Properties of Argon from the Triple Point to 1200K with Pressures to 1000 MPa", J. Phys. Chem. Ref. Data, Vol. 18, No. 2, p. 639, 1989.

[72] Shahin, M.M., Ch. 5 in "Reactions under Plasma Conditions" edited by M. Venugopalan, John Wiley & Sons, New York, 1971.

[73] Bates, D.R., Kingston, A.E., and McWhirter, R.W.P., "Recombination between electrons and atomic ions I. Optically thin plasmas", Proc. Roy. Soc. London, Series A, Mathematical and Physical Sciences, Vol. 267, pp. 297–312, 1962.

[74] Giannaris, R.J., and Incropera, F.P., "Radiative and Collisional Effects in a Cylindrically Confined Plasma– I. Optically Thin Considerations", J. Quant. Spectrosc. Radiat. Transfer, Vol. 13, pp. 167–181, 1973.

[75] Fujimoto, T., "Kinetics of Ionization-Recombination of a Plasma and Population Density of Excited Ions. I. Equilibrium Plasma", Journal of the Physical Society of Japan, Vol. 47, No. 1, pp. 265–281, 1979.

[76] Gomés, A.M., "Criteria for partial LTE in an argon thermal discharge at atmospheric pressure; validity of the spectroscopically measured electronic temperature", J. Phys. D: Appl. Phys., Vol. 16, pp. 357–378, 1983.

[77] van der Sijde, B., van der Mullen, J.J.A.M., and Schram, D.C., "Collisional Radiative Models in Plasmas", Beitr. Plasmaphys., Vol. 24, pp. 447–473, 1984.

[78] Shirai, H., Tabei, K., and Koaizawa, H., "Optically Thick Model for Radiative and Collisional Effects in Nonequilibrium Argon Plasma Flows in a Circular Tube", Bulletin of JSME, Vol. 27, No. 229, pp. 1414–1421, 1984.

[79] Hasegawa, T., and Haraguchi, H., "A collisional-radiative model including radiation trapping and transport phenomena for diagnostics of an inductively coupled argon plasma", Spectrochimica Acta, Vol. 40B, Nos. 10–12, pp. 1505–1515, 1985.

[80] Cram, L.E., Poladian, L., and Roumeliotis, G., "Departures from equilibrium in a free-burning argon arc", J. Phys. D: Appl. Phys., Vol. 21, pp. 418–425, 1988.

[81] Bacri, J., and Gomes, A.M., "Influence of atom-atom collisions on thermal equilibrium in argon arc discharges at atmospheric pressure", J. Phys. D: Appl. Phys., Vol. 11, pp. 2185–2197, 1978.

[82] Vlček, J., "A collisional-radiative model applicable to argon discharges over a wide range of conditions. I: Formulation and basic data", J. Phys. D: Appl. Phys., Vol. 22, pp. 623–631, 1989.

[83] D. Morris, "Molecular Ions in Discharges in the Inert Gases", Proc. Phys. Soc. London, Vol. 68, pp. 11–17, 1954.

[84] Pahl, W., "Zur Bildung von Molekülen in stationären Edelgasentladungen", Z. Naturforschung, Vol. A14, pp. 239–246, 1959.

[85] Knewstubb, P.F., and Tickner, A.W., "Mass Spectrometry of Ions in Glow Discharges. I. Apparatus and Its Application to the Positive Column in Rare Gases", J. Chem. Phys., Vol. 36, No. 3, pp. 674–683, 1962.

[86] O'Malley, T.F., Cunningham, A.J., and Hobson, R.M., "Dissociative recombination at elevated temperatures II. Comparison between theory and experiment in neon and argon afterglows", J. Phys. B: Atom. Molec. Phys., Vol. 5, pp. 2126–2133, 1972.

[87] Fitzwilson R.L., and Chanin, L.M., "Positive Ion Ratio Measurement in Ar, Kr, and Xe Glow Discharges", J. Appl. Phys., Vol. 44, No. 12, pp. 5337–5346, 1973.

[88] Bretagne, J., Godart, J., and Puech, V., "Kinetic Study of Electron Beam Excited Argon", Beitr. Plasmaphys., Vol. 23, No. 3, pp. 295–312, 1983.

[89] Braun, C.G., and Kunc, J.A., "Collisional-radiative coefficients from a three-level atomic model in nonequilibrium argon plasmas", Phys. Fluids., Vol. 30, No. 2, pp. 499–509, 1987.

[90] Braun, C.G., and Kunc, J.A., "An analytical solution of a collisional-radiative model for nonequilibrium argon plasmas", Phys. Fluids., Vol. 31, No. 3, pp. 671–681, 1988.

[91] Braun, C.G., and Kunc, J.A., "Atom-atom inelastic collisions and three-body atomic recombination in weakly ionized argon plasmas", Phys. Fluids., Vol. B1, No. 1, pp. 258–260, 1989.

[92] Brake, M.L., and Repetti, T.E., "A Theoretical and Experimental Investigation of Long-Pulse, Electron-Beam-Produced Rare Gas Plasmas", IEEE Transactions on Plasma Science, Vol. 16, No. 5, pp. 581–589, 1988.

[93] Repetti, T.E., Fincke, J.R., and Neumann, W.A., "Relaxation Kinetics of Argon Thermal Plasmas", proceedings of The 28th National Heat Transfer Conference, section on Heat Transfer in Thermal Plasma Processing, K. Etemadi and J. Mostaghimi, eds., The American Society of Mechanical Engineers, HTD-Vol. 161, pp. 167–175, 1991.

[94] McLaren, T.I., and Hobson, R.M., "Initial Ionization Rates and Collision Cross Sections in Shock-Heated Argon", Phys. of Fluids, Vol. 11, No. 10, pp. 2162–2172, 1968.

[95] H. Tawara and T. Kato, "Total and Partial Ionization Cross Sections of Atoms and Ions by Electron Impact", Atomic Data and Nuclear Data Tables, Vol. 36, No. 2, pp. 167–353, 1987.

[96] Vriens, L., "Calculation of Absolute Ionization Cross Sections of He, He^*, Ne, Ne^*, Ne^+, Ar, Ar^*, Hg and Hg^*", Phys. Lett., Vol. 8, No. 4, pp. 260–261, 1964.

[97] Borst, W.L., "Excitation of Metastable Argon and Helium Atoms by Electron Impact", Phys. Rev. A, Vol. 9, No. 3, pp. 1195–2200, 1974.

[98] Ton-That, D., and Flannery, M.R., "Cross sections for ionization of metastable rare-gas atoms (Ne^*, Ar^*, Kr^*, Xe^*) and of metastable N_2^*, CO^* molecules by electron impact", Physical Review A, Vol. 15, No. 2, pp. 517–526, 1977.

[99] Ichikawa, Y., Chang, J.S., and Hobson, R.M., "The Mechanism of α–Si Thin Film Formation by an Argon-Silane Glow Discharge", Technical Meeting on Plasma, The Institute of Electrical Engineers of Japan, EP-81-52, pp. 89–98, 1981.

[100] Ta!'Rose, V.L., and Karachevtsev, G.V., Ch. 12 in "Reactions under Plasma Conditions" edited by M. Venugopalan, John Wiley & Sons, New York, 1971.

[101] Peterson, W., and Beaty, E.C., "The Reaction of Ar^+ with Argon to make Ar_2^+", Bull. Am. Phys. Soc., Vol. 14, pg. 260, 1969

[102] Biondi, M.A., "Recombination" in "Principles of Laser Plasmas", ed. G. Bekefi, John Wiley and Sons, New York, 1986.

[103] Talbot, L., Chou, Y.S., and Robbin, F., "Expansion of a Partially-Ionized Gas through a Supersonic Nozzle", Aero-Science Division, University of California, Berkley, Report AS-65-14, 1965.

[104] Evans, B.T.N., "The Investigation of the Electron Impact Ionization Cross Section of Vibrationally Excited Oxygen by a Shock Heated Molecular Beam", PhD Thesis, York University, 1980.

[105] Cunningham, A.J., and Hobson, R.M., "Experimental Measurements of Dissociative Recombination in Vibrationally Excited Gases", Phys. Rev., Vol. 185, No. 1, pp. 98-100, 1969.

[106] O'Malley, T.F., Cunninham A.J., and Hobson, R.M., "Dissociative Recombination at Elevated Temperatures II. Comparison between theory and experiment in neon and argon afterglows" J. Phys. B: Atom. Molec. Phys., Vol. 5, pp. 2126-2133, 1972.

[107] Thompson, D.L., "Trimer formation, atom exchange, and dissociation in argon dimer collisions", J. Chem. Phys., Vol. 77, No. 3, pp. 1269-1273, 1982.

[108] Chang, J.S., Hobson, R.M., Laframbiose, J.G., and Ogram, G.L., "Theory of density decay in diffusion-controlled atomic-gas afterglow plasmas", J. Phys. Lett., Vol. 68A, No. 2, pp. 233-235, 1978.

[109] Bauder, V.H., and Maecker, H.H., The Determination of Transport Properties from Arc Experiments: Methods and Results", Proceedings of the IEEE, Vol. 59, No. 4, pp. 588-592, 1971.

[110] Farmer, A.J.D., and Haddad, G.N., "Local Thermodynamic Equilibrium in Free-Burning Arcs in Argon", Appl. Phys. Lett., Vol. 45, No. 1, pp. 24–25, 1984.

[111] Nick, K.-P., Richter, J., and Helbig, V., "Non-LTE Diagnostic of an Argon Arc Plasma", J. Quant. Spectros. Radiat. Transfer, Vol. 32, No. 1, pp. 1–8, 1984.

[112] Chang, J.S., Ichikawa, Y., Hobson, R.M., Matsumura, S., Teii, S., "The Effect of Molecular Ions on the Plasma Parameters in a Medium Pressure Rare Gas RF Discharge Positive Column", J. Appl. Phys., to be published.

[113] Herterick, G.M., "Gas Selection in Plasma Spraying", Welding Journal, Vol. 2, pp. 27–30, Feb. 1987.

[114] Pahl, M., "Massenspektrometrische Untersuchungen and der positiven Säule in Ar, Ar-He- und Ar-H_2-Gemischen" Zeitschrift für Naturforschung, Vol. A18, No. 12, pp. 1276–1288, 1963.

[115] Cheminat, B., and Andanson, P., "Conduction in an electric arc column contaminated by copper vapour", J. Phys. D: Appl. Phys., Vol. 18, pp. 2183–2192, 1985.

[116] Ouajji, H., Cheminat, B., and Andanson, P., "Model of an electric arc column in the presence of copper vapour", J. Phys. D: Appl. Phys., Vol. 20, pp. 635–638, 1987.

[117] Etemadi, K., Zhao, G.Y., and Mostaghimi, J., "Impact of cathode evaporation on a free-burning arc", J. Phys. D: Appl. Phys., Vol. 22, pp. 635–638, 1989.

[118] Apelian, D., Paliwal, M., Smith, R.W., and Schilling, W.F., "Melting and solidification in plasma spray deposition – phenomenological review", International Metals Review, Vol. 28, No. 5, pp. 271–294, 1983.

[119] Gal-Or, B., "Plasma Spray Coating Processes: Physico-Mathematical Characterization", Journal of Engineering for Power, Vol. 102, pp. 589–593, 1980.

[120] Ito, T., Ueda, Y., Komura, H., and Nitta, T., "Spectroscopic Study of High Current Discharges", Proc. of the IEEE, Vol. 59, No. 4, pp. 573–578, 1971.

[121] Honda, T., Kanzawa, A., and Anekawa, H., "Gasification of Coal in the Thermal Plasma", Journal of Chemical Engineering of Japan, Vol. 18, No. 5, pp. 414–419, 1985.

[122] Beuthe, T.G., Chang, J.S., Ishii, I., Hayashi, N., Lu, W.K., Irons, G.A., Berezin, A.A., and Chu, F.Y., "An Investigation of the Product Gases Formed by Injecting Coal Powder and Steam into the Flame of a DC Plasma Torch", Proceedings of the International Symposium on Plasma Chemistry ISPC-8, K. Akashi and A. Kinbara, eds., Tokyo, Vol. 3, Paper D11-06, pp. 1880–1885, 1987.

[123] K.L. Bell, H.B. Gilbody, J.G. Hughes, A.E. Kingston and F.J. Smith, "Recommended Data on Electronic Impact Ionization of Light Atoms and Ions", J. Phys. Chem. Ref. Data, Vol. 12, No. 4, pp. 891–916, 1983.

[124] von Engel, A., "Ionized Gases", Oxford University Press, London, 1955.

[125] Blashkov, V.I., Ivanov, Y.Z., Ionikh, Y.Z., Penkin, N.P., Chernysheva, N.V., "Formation of CO_2 and C_2 Molecules in CO-He, CO-He-O_2 Discharge Plasma", Proceedings of the XVII International Conference on Phenomena in Ionized Gases (ICPIG) in Budapest, Hungary, 8–12 July 1985, pp. 299–301, eds. J.S. Bakos, and Z. Sörlei.

[126] Sperling, J., "Das Temperaturfeld im freien Kohlebogen", Zeitischrift für Physik, Vol. 128, pp. 269–278, 1950.

[127] Hagenah, W., "Das Strömungsfeld im freien Kohlebogen", Zetischrift für Physik, Vol. 128, pp. 279–288, 1950.

[128] Todorović, M.S., Kristić, M.S., and Georgijević, V.J., "Electrical characteristics of the graphite arc in argon flow", J. Phys. D: Appl. Phys., Vol. 14, pp. 45–48, 1981.

[129] Davies, C., and Abrahamson, J., "Limit to Erosion Rate in High-Current Carbon Arc", In. Eng. Chem. Process Res. Dev., Vol. 22, pp. 226–230, 1983.

[130] McKelliget, J.W., and Szekely, J., "A mathematical model of the cathode region of a high intensity carbon arc", J. Phys. D: Appl. Phys., Vol. 16, pp. 1007–1022, 1983.

[131] El-Farra, M.A., and Hughes, T.P., "Stark Broadening of Lines from Multiply-Charged Carbon Ions in a High-Density Arc Plasma", J. Quant. Spectros. Radiat. Transfer, Vol. 30, No. 4, pp. 335–343, 1983.

[132] Kieffer, L.J., "Low Energy Electron-Collision Cross-Section Data, Part 1: Ionization, Dissociation, Vibrational Excitation", Atomic Data, Vol. 1, pp. 19–89, 1969.

[133] Kieffer, L.J., Dunn, G.H., "Electron Impact Ionization Cross-Section Data for Atoms, Atomic Ions, and Diatomic Molecules: I. Experimental Data", Reviews of Modern Physics, Vol. 38, No. 1, pp. 1–35, Jan. 1966.

[134] Tate, J.J., and Lozier, W.W., "The Dissociation of Nitrogen and Carbon Monoxide by Electron Impact", Physical Review, Vol. 30, pp. 254–269, Jan. 15, 1932.

[135] Jackson, W.M., Brackmenn, R.T., and Fite, W.L., "Temperature Dependence of the Dissociative Ionization of CO_2", International Journal of Mass Spectrometry and Ion Physics, Vol. 13, pp. 237–250, 1974.

[136] Elaisson, B., and Kogelschatz, V., "Basic Data for Modelling of Electrical Discharges in Gases: Oxygen", Brown Boveri Forschungsbericht, KLR 86-11 C, 1986.

[137] Maksimov, A.I., Polak, L.S., Sergienko, A.F., and Slovetskii, D.I., "Mechanism of the Formation and Decomposition of CO_2 Molecules in a Glow Discharge in Carbon Monoxide", High Energy Chemistry, Vol. 13, No. 4, pp. 311–316, 1979.

[138] Chang, J.S., and Masuda, S., "Mechanism of the Ozone Formations in a Near Liquid Nitrogen Temperature Medium Pressure Glow Discharge Positive Column", Pure and Applied Chemistry, Vol. 60, No. 5, pp. 645–650, 1988.

[139] Ono, S., Teii, S., "Negative Electrons and their Effects on Electron Temperature in CO_2-N_2-He Mixture Gas Discharges", J. Phys. D: J. Appl. Phys., Vol. 17, pp. 1999–2008, 1984.

[140] Cunningham, A.J., and Hobson, R.M., "Dissociative Recombination at Elevated Temperatures, III. O_2^+ dominated afterglows", J. Phys. B: Atom. Molec. Phys., Vol. 5, pp. 2320–2327, 1972.

[141] Albritton, D.L., "Ion-Neutral Reaction-Rate Constants Measured in Flow Reactors through 1977", Atomic Data and Nuclear Data Tables, Vol. 22, No. 1, pp. 1–101, July 1978.

[142] Gaucherel, P., and Rowe, B., "Measurement of Rates of Charge Exchange and Dissociative Recombination Reactions in Ar-N_2, Ar-H_2, and Ar-O_2 Mixtures", International Journal of Mass Spectrometry and Ion Physics, Vol. 25, pp. 211–227, 1977.

[143] Baulch, D.L., Drysdale, D.D., Duxbury, J., and Grant, S.J., "Evaluated Kinetic Data for High Temperature Reactions, Vol. 3: Homogeneous Gas Phase Reactions of the O_2-O_3 System, CO-O_2-H_2 System, and of Sulphur-Containing Species", Buttersworth, Toronto, 1976.

[144] Hampson, R.F., "Chemical Kinetic and Photochemical Data Sheets for Atmospheric Reactions", National Bureau of Standards, Washington, FAA-EE-80-17, 1980.

[145] Burmeister, M., and Roth, P., "ARAS Measurements on the Thermal Decomposition of CO_2 behind Shock Waves", AIAA Journal, Vol. 28, No. 3, pp. 402–504, March 1990.

[146] Ichikawa, Y., and Teii, S., "Molecular Ion and Metastable Atom Formation and their Effects on the Electron Temperature in Medium-Pressure Rare-Gas Positive-Column Plasmas", J. Phys. D: Appl. Phys., Vol. 13, pp. 2031–2043, 1980.

Appendix A

Ar-CO_2 Thermal Plasma Species Sources and Sinks

As discussed in Chapter 6, the Ar-CO_2 model considers the concentrations of neutral and excited species, Ar, Ar^*, Ar^{**}, C, CO, CO_2, O, O_2, and O_3, positive ions, Ar^+, Ar_2^+, C^+, $CArO^+$, CO^+, CO_2^+, CO_4^+, $C_2O_2^+$, O^+, O_2^+, O_4^+, and O_5^+, and negative ions, CO_3^-, CO_4^-, O^-, O_2^-, and O_3^- as well as electrons under thermal plasma conditions. A complete summary of all sources and sinks of these species has been provided below in Figures A.1–A.27. The reactions have been indicated according to the letters (Ar, C, I, A, D, R, M, and N) and numbers used to define them in Tables 4.1, 5.1, and 6.1–6.7. Concise summaries of the important source and sink reactions for these species and their reaction rate constants as determined by a sensitivity analysis of the model have been outlined in Tables 6.8–6.10, and 6.12–6.14 and Figures 6.1–6.6 in Chapter 6.

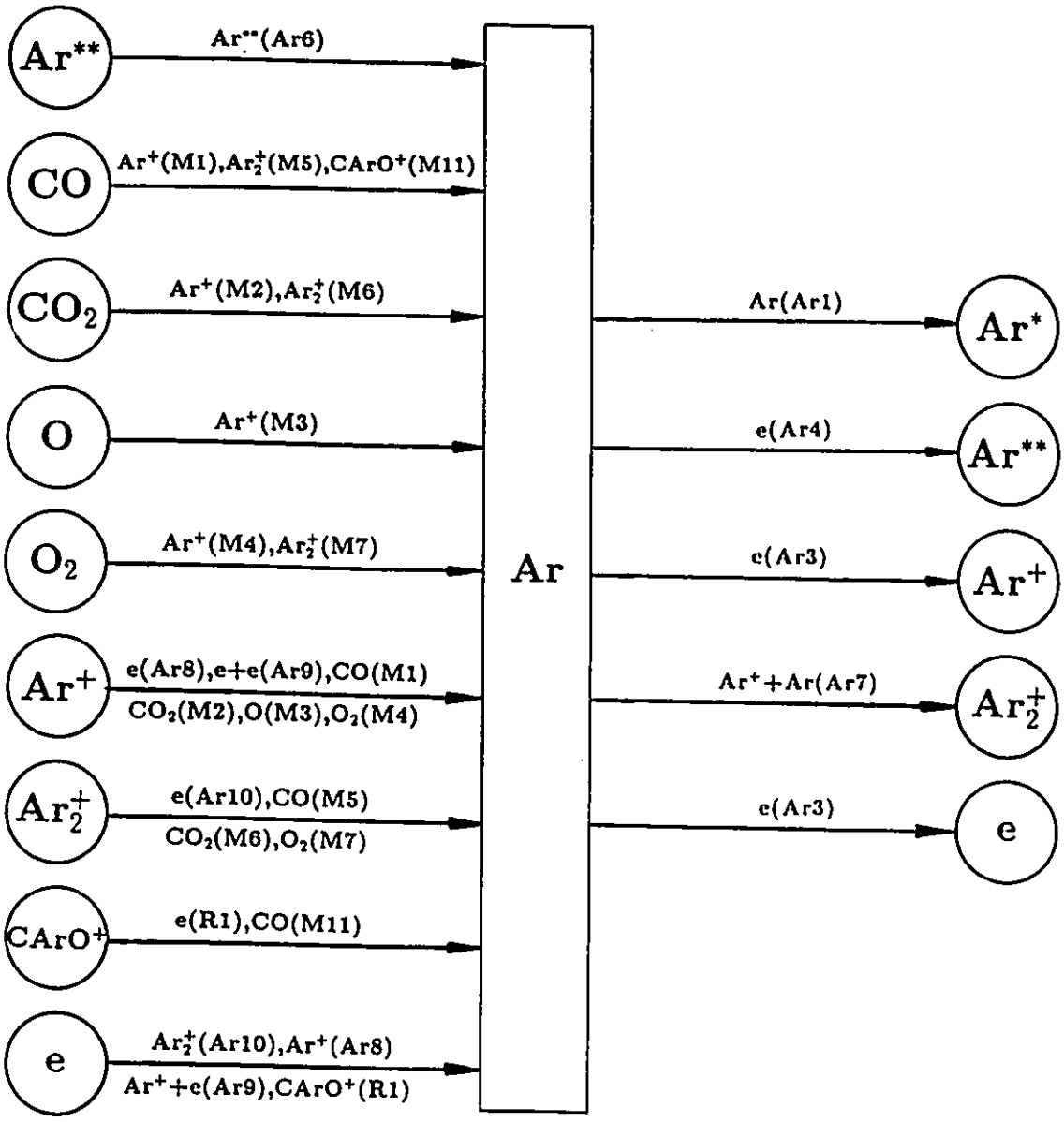

Figure A.1: Sources and sinks of Ar included in the chemical kinetic Ar-CO_2 thermal plasma model.

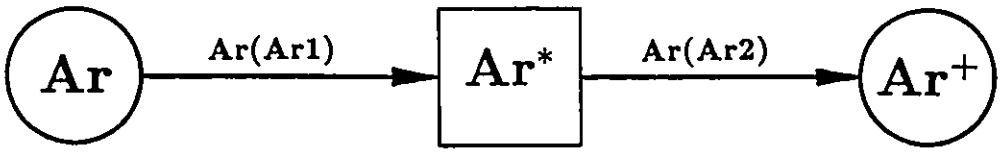

Figure A.2: Sources and sinks of Ar^* included in the chemical kinetic Ar-CO_2 thermal plasma model.

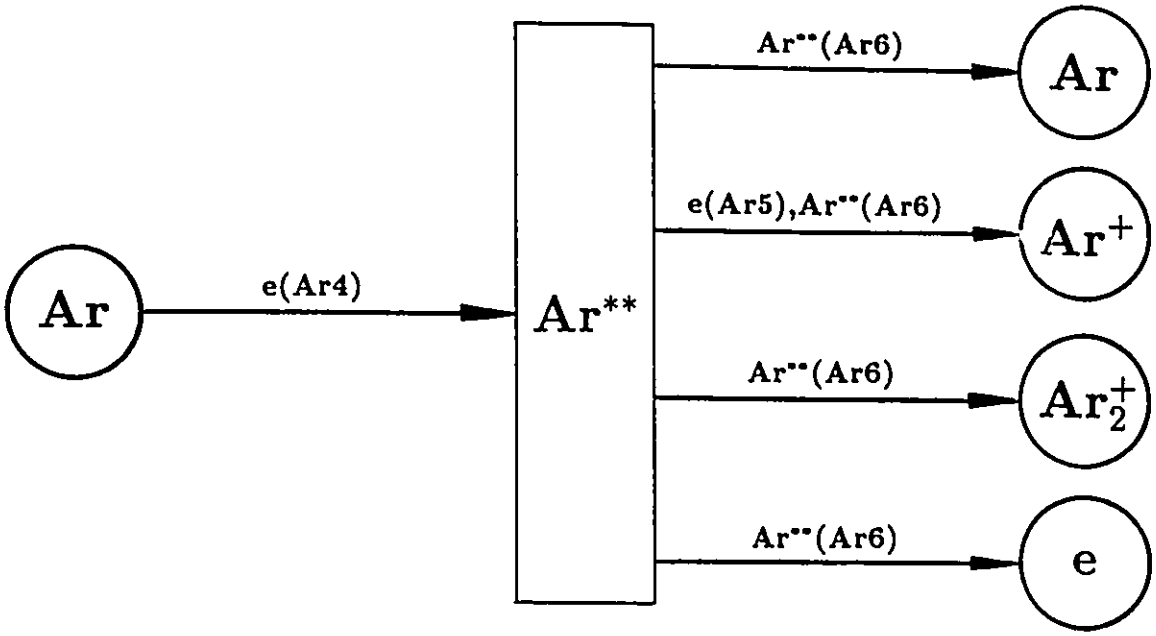

Figure A.3: Sources and sinks of Ar^{**} included in the chemical kinetic Ar-CO_2 thermal plasma model.

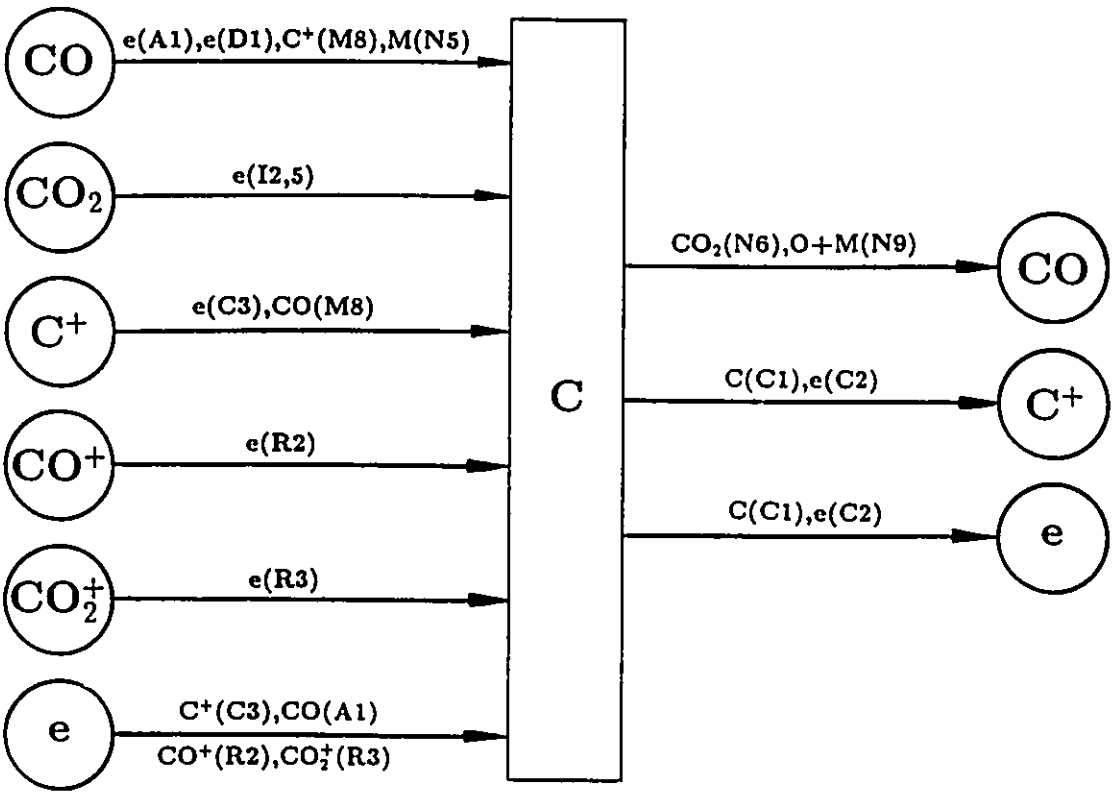

Figure A.4: Sources and sinks of C included in the chemical kinetic Ar-CO_2 thermal plasma model.

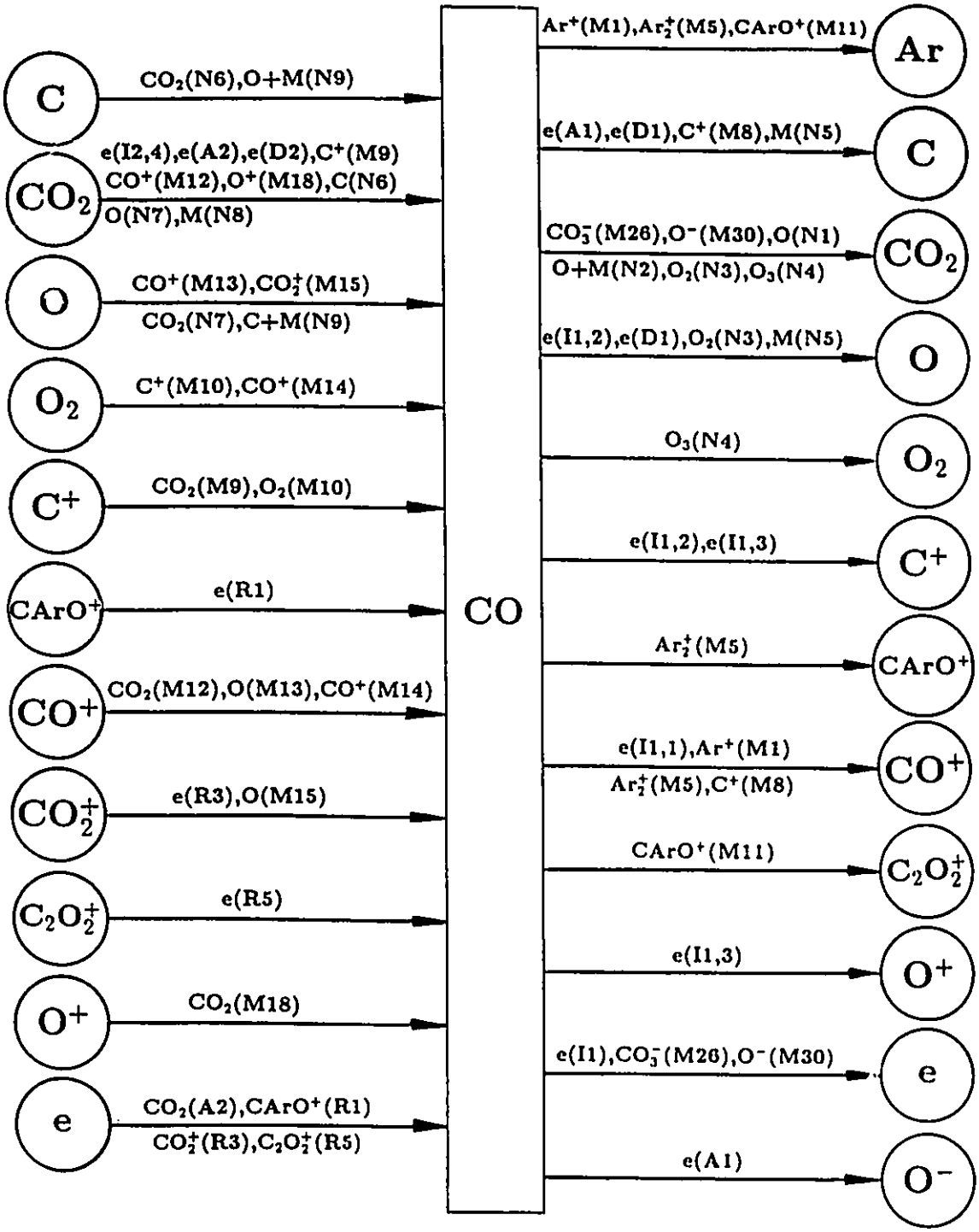

Figure A.5: Sources and sinks of CO included in the chemical kinetic Ar-CO_2 thermal plasma model.

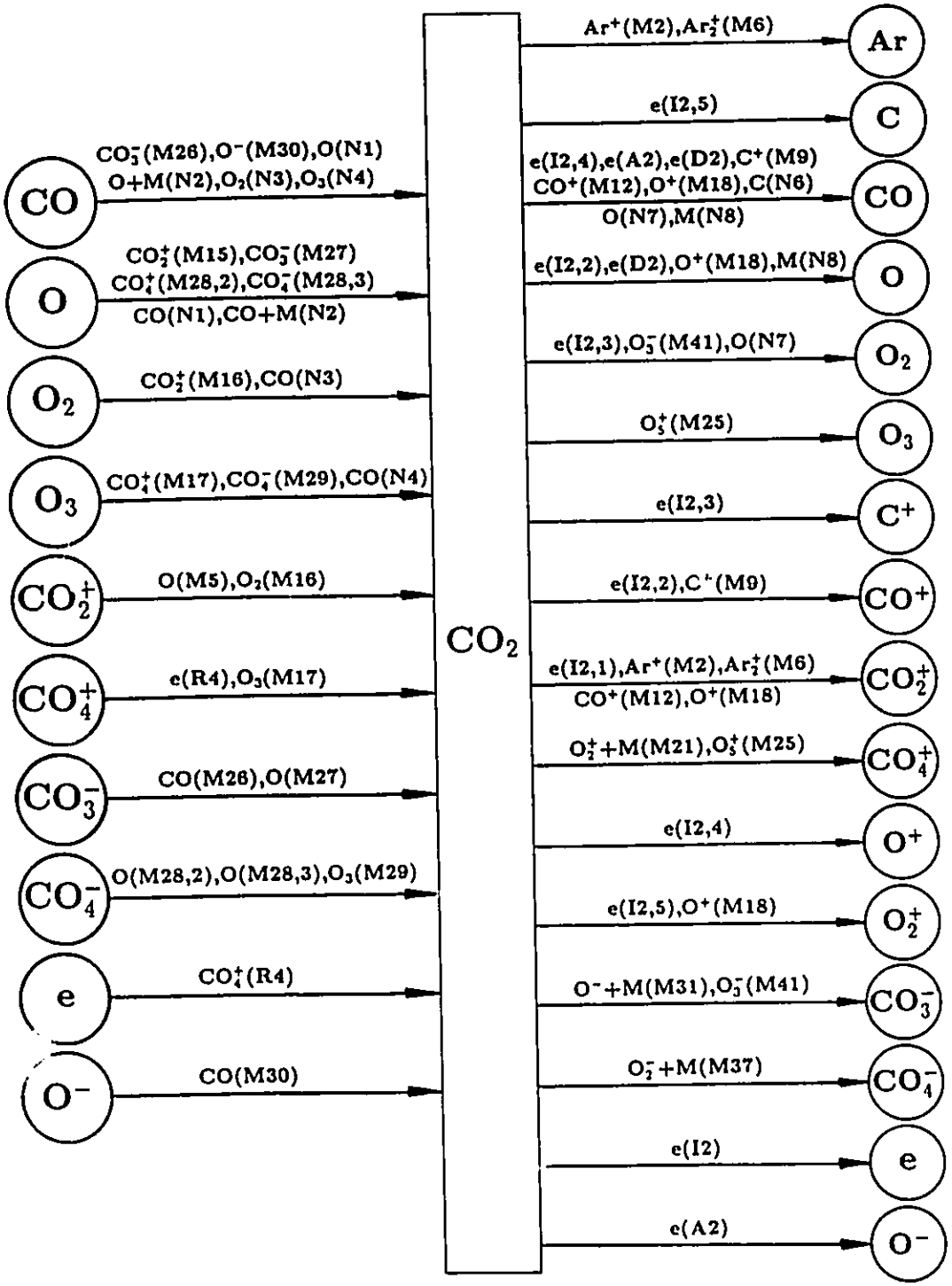

Figure A.6: Sources and sinks of CO_2 included in the chemical kinetic Ar-CO_2 thermal plasma model.

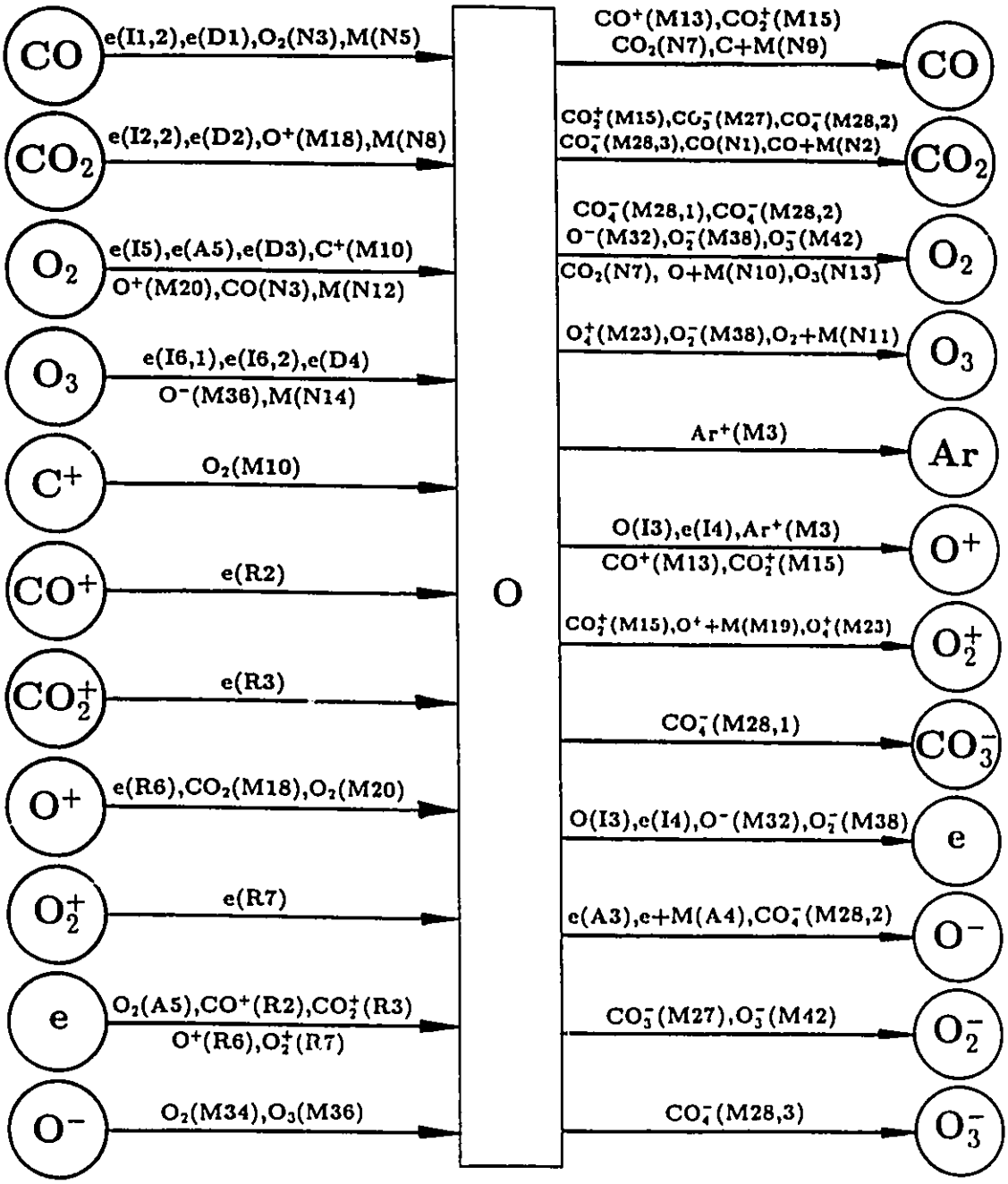

Figure A.7: Sources and sinks of O included in the chemical kinetic Ar-CO_2 thermal plasma model.

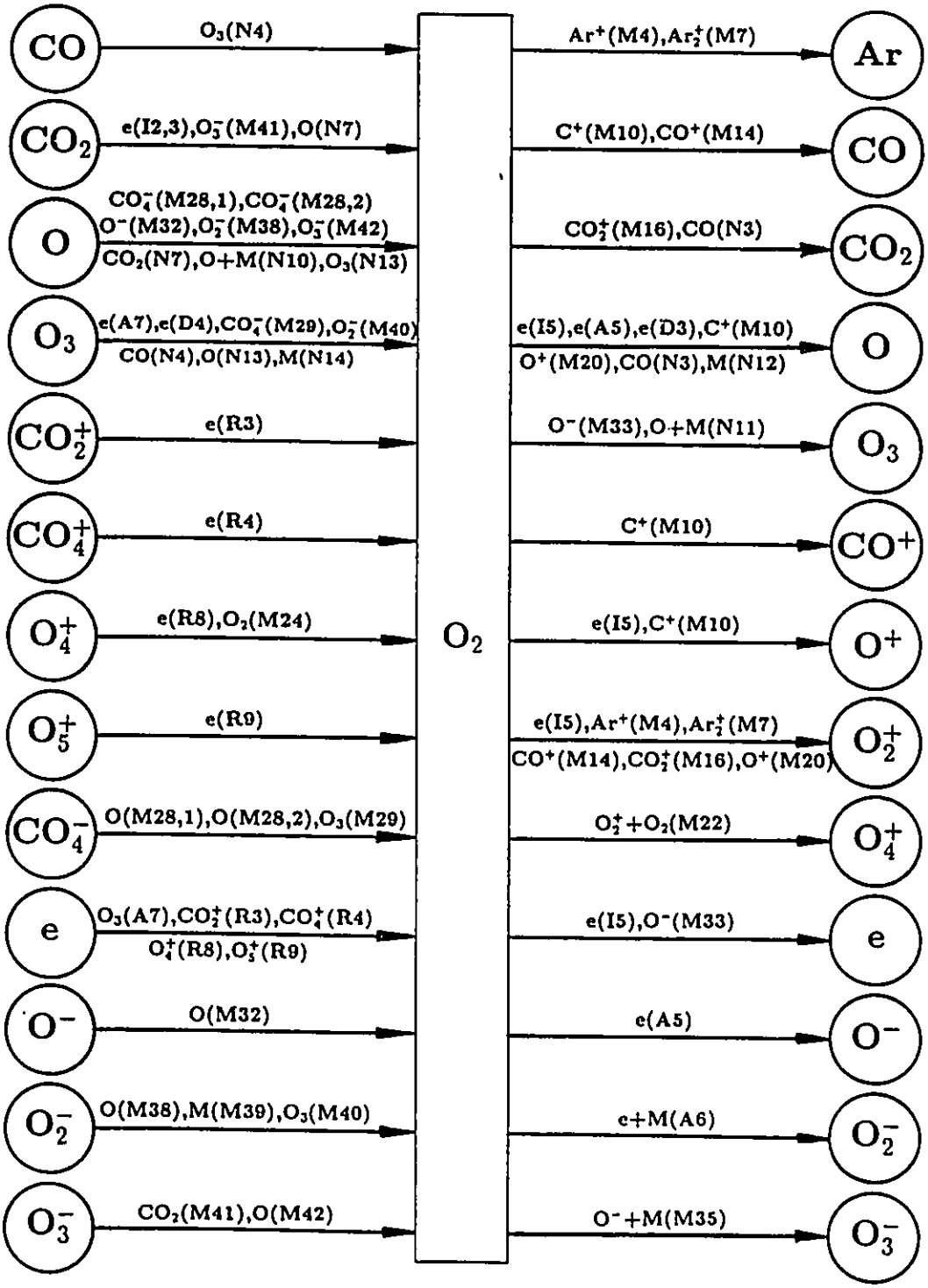

Figure A.8: Sources and sinks of O_2 included in the chemical kinetic Ar-CO_2 thermal plasma model.

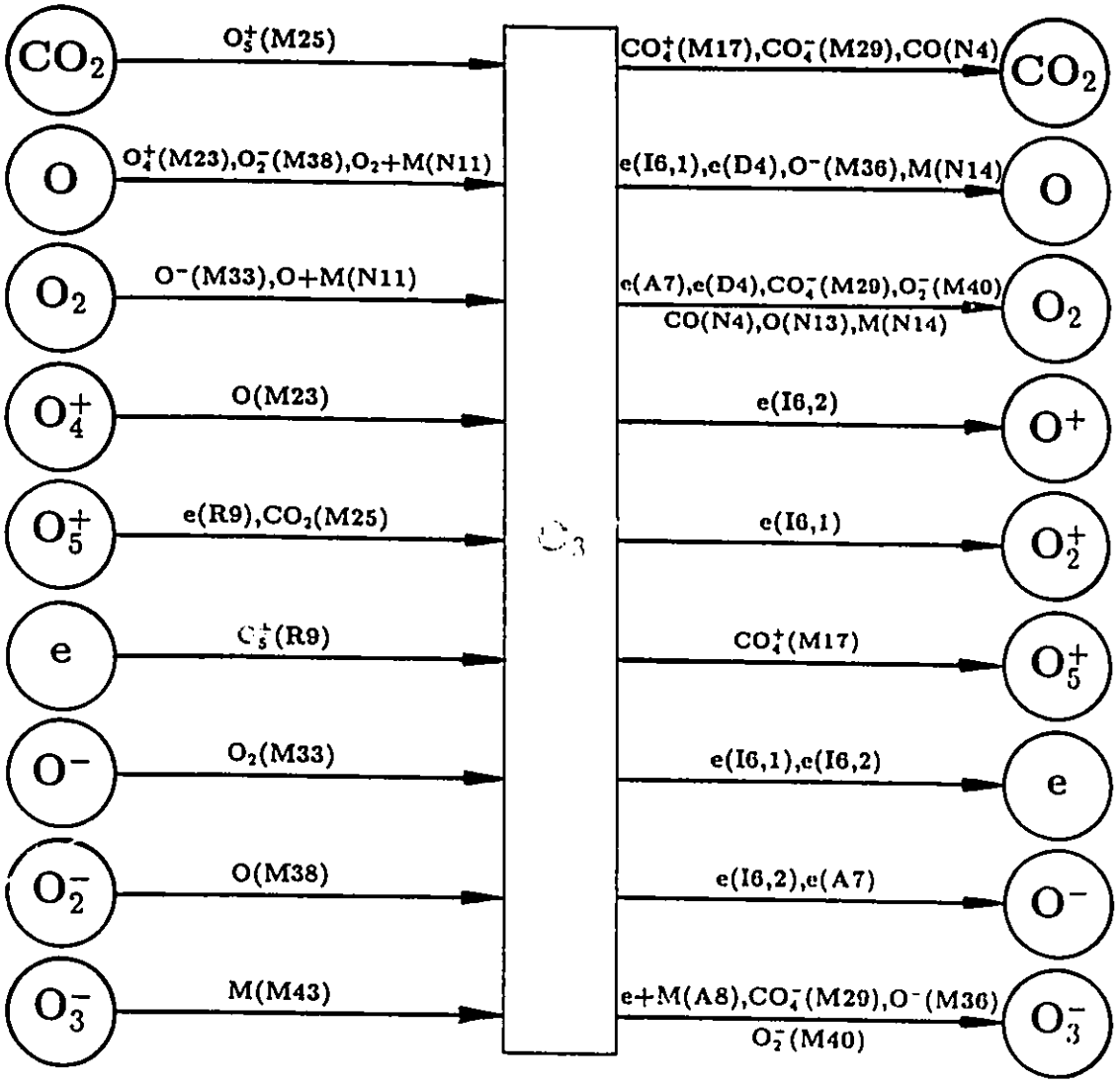

Figure A.9: Sources and sinks of O_3 included in the chemical kinetic Ar-CO_2 thermal plasma model.

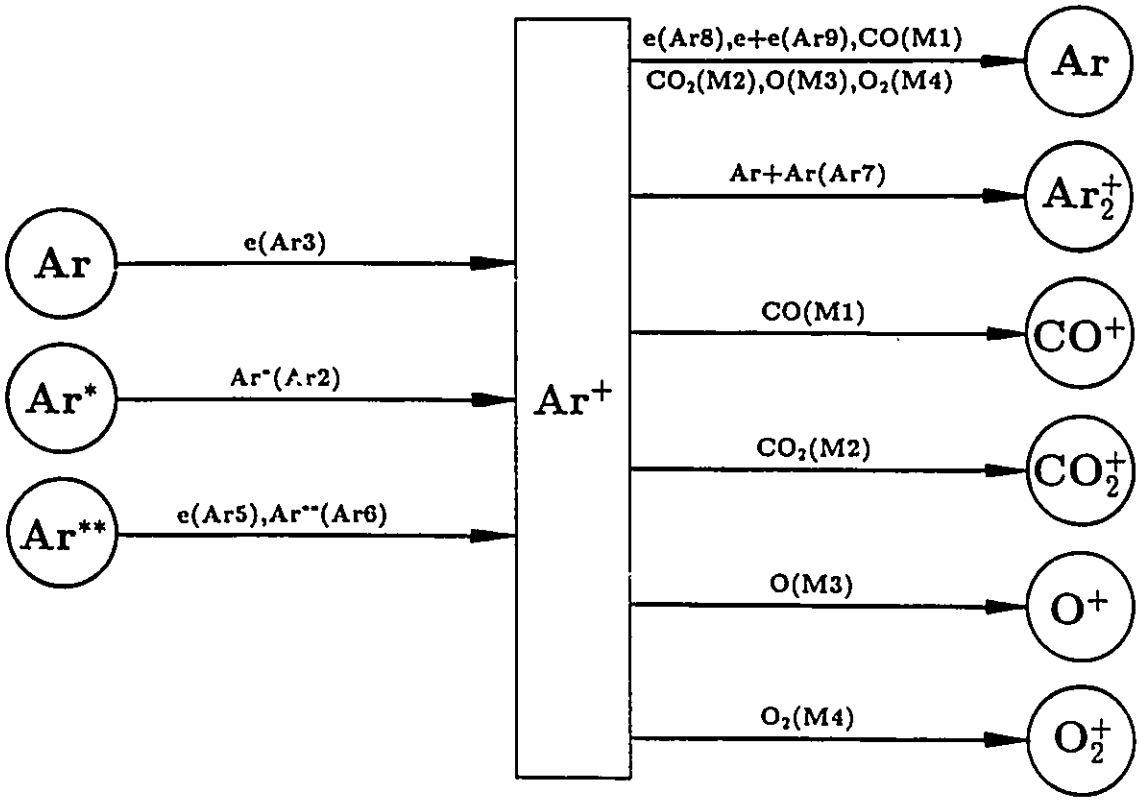

Figure A.10: Sources and sinks of Ar^+ included in the chemical kinetic Ar-CO_2 thermal plasma model.

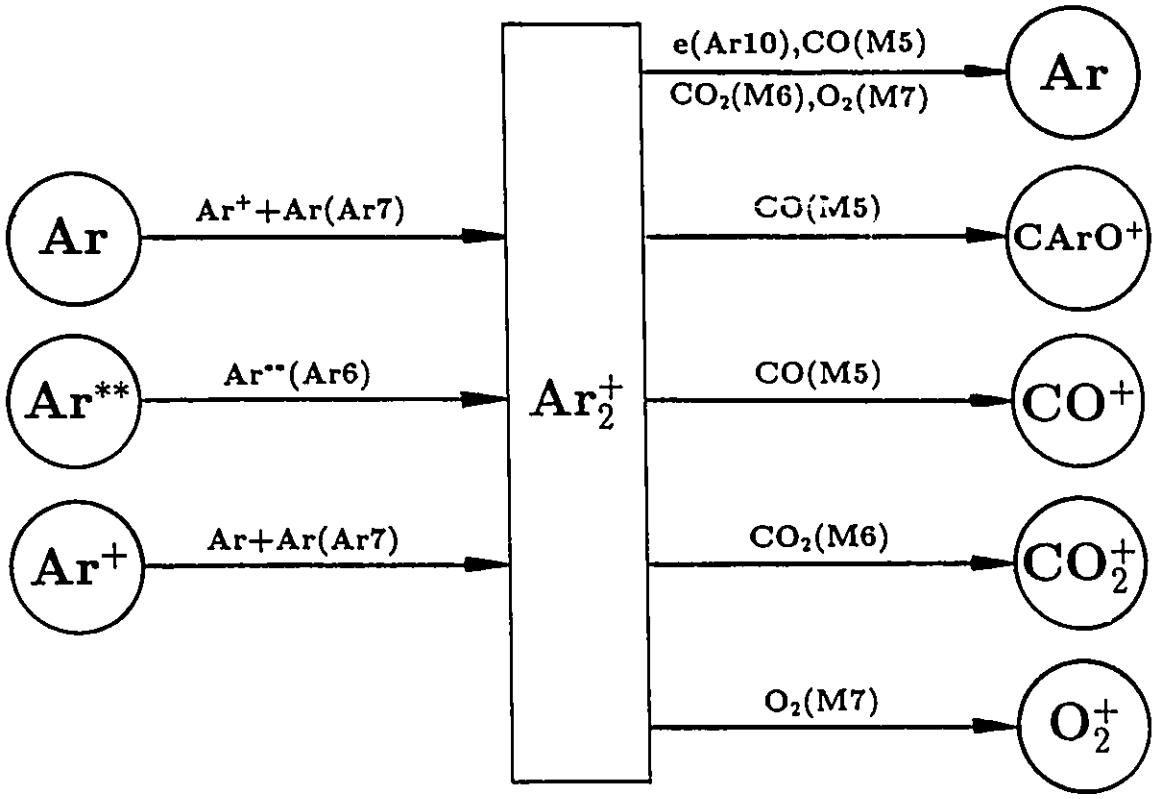

Figure A.11: Sources and sinks of Ar_2^+ included in the chemical kinetic Ar-CO_2 thermal plasma model.

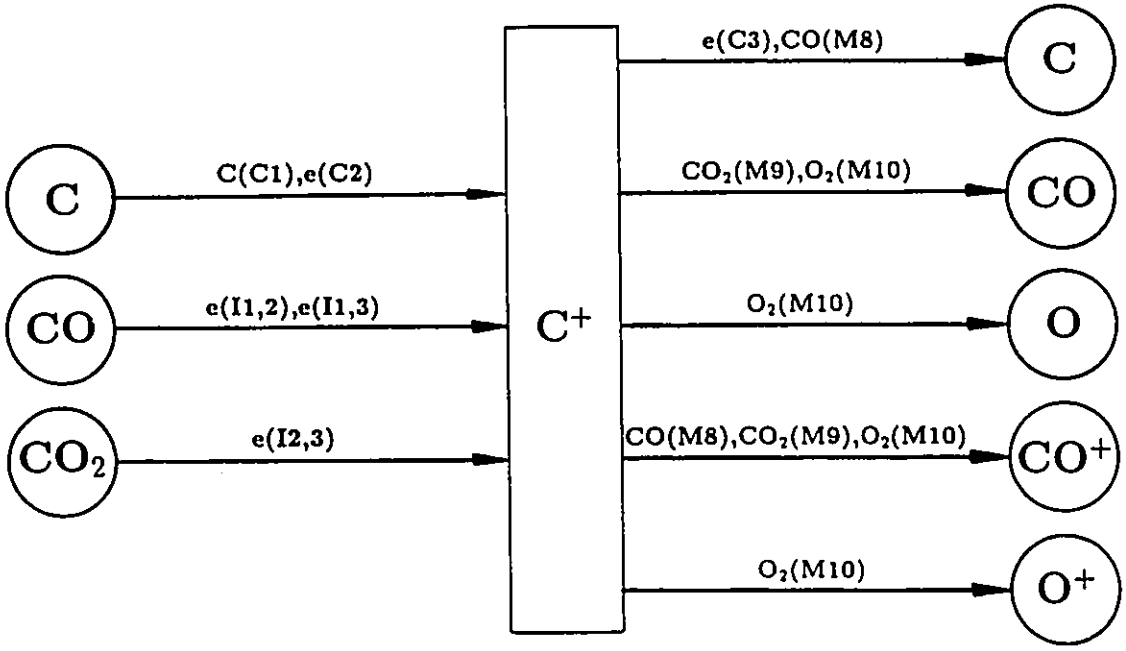

Figure A.12: Sources and sinks of C^+ included in the chemical kinetic Ar-CO_2 thermal plasma model.

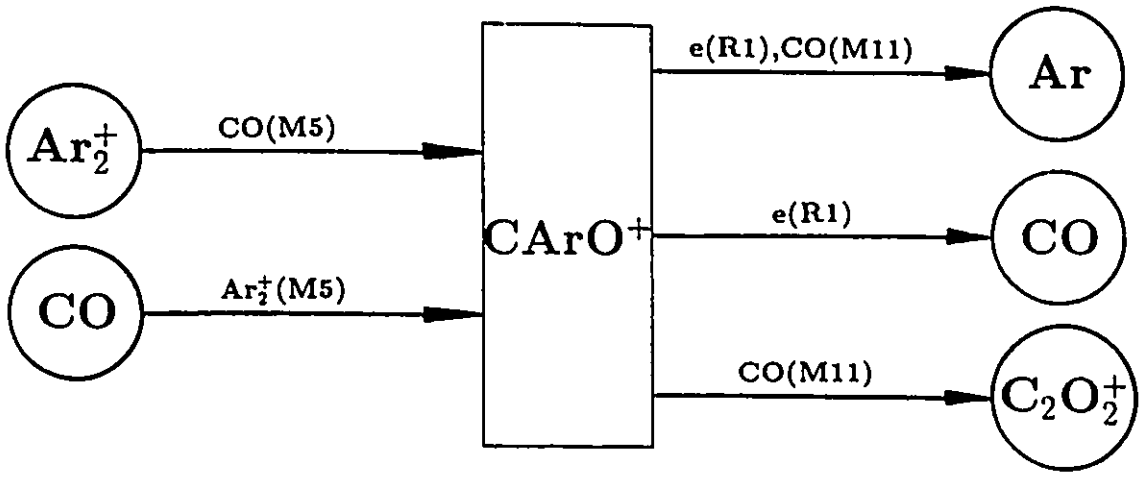

Figure A.13: Sources and sinks of $CArO^+$ included in the chemical kinetic Ar-CO_2 thermal plasma model.

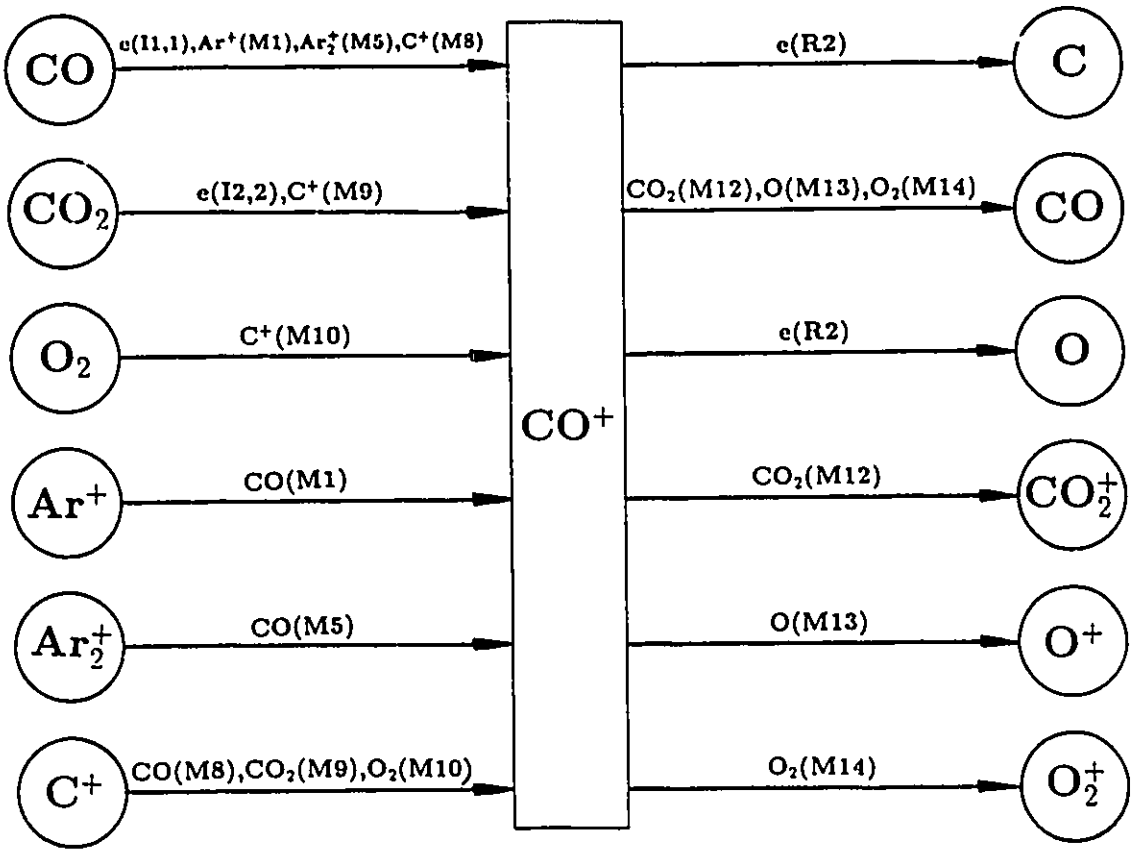

Figure A.14: Sources and sinks of CO^+ included in the chemical kinetic Ar-CO_2 thermal plasma model.

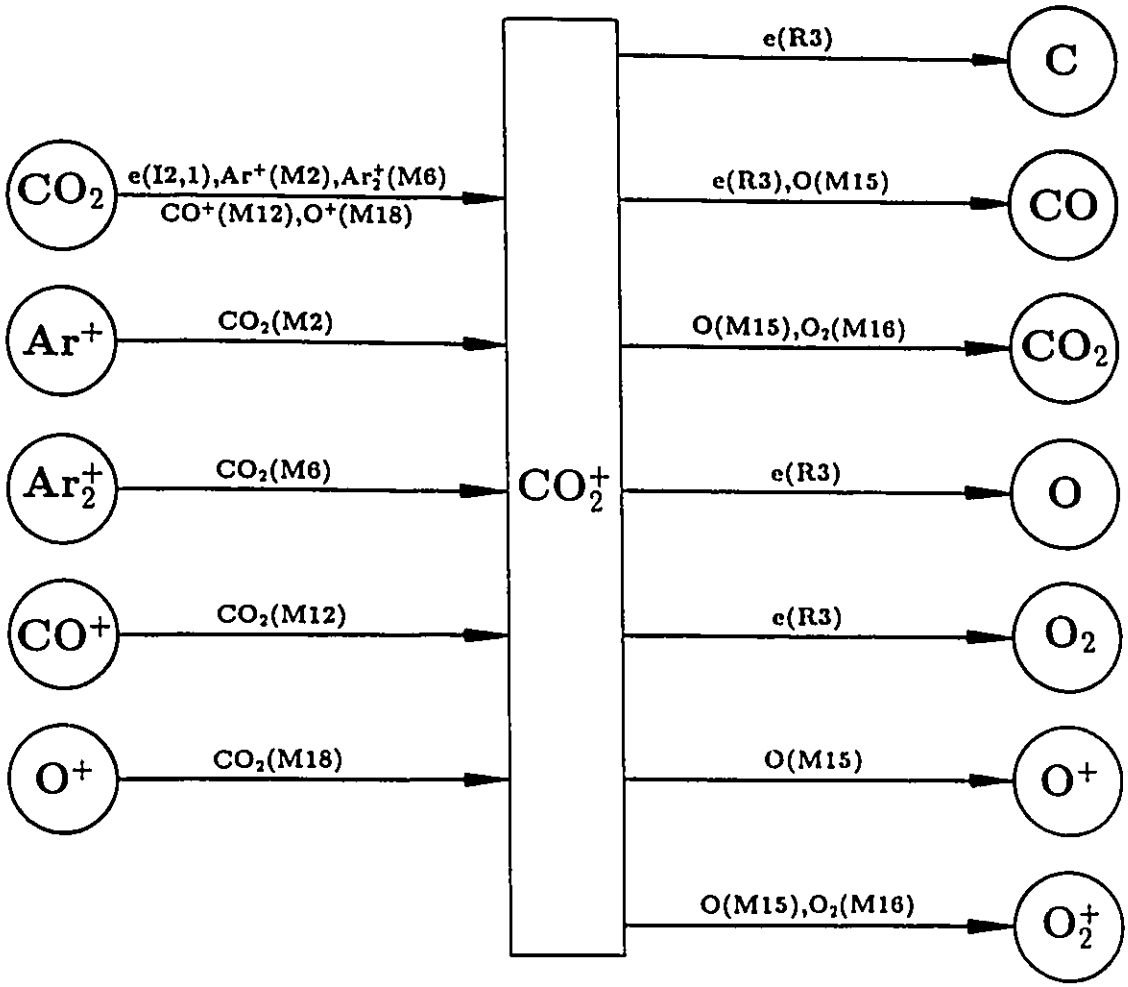

Figure A.15: Sources and sinks of CO_2^+ included in the chemical kinetic Ar-CO_2 thermal plasma model.

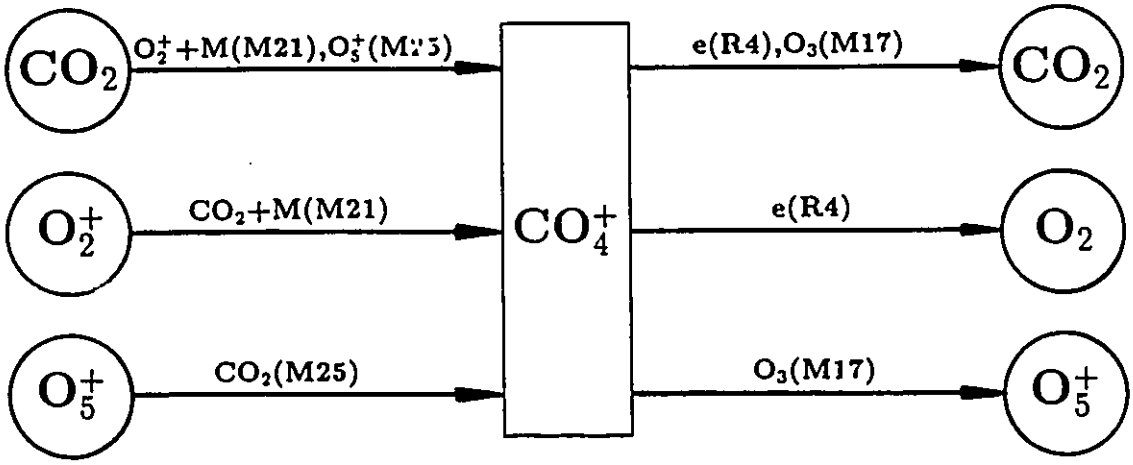

Figure A.16: Sources and sinks of CO_4^+ included in the chemical kinetic Ar-CO_2 thermal plasma model.

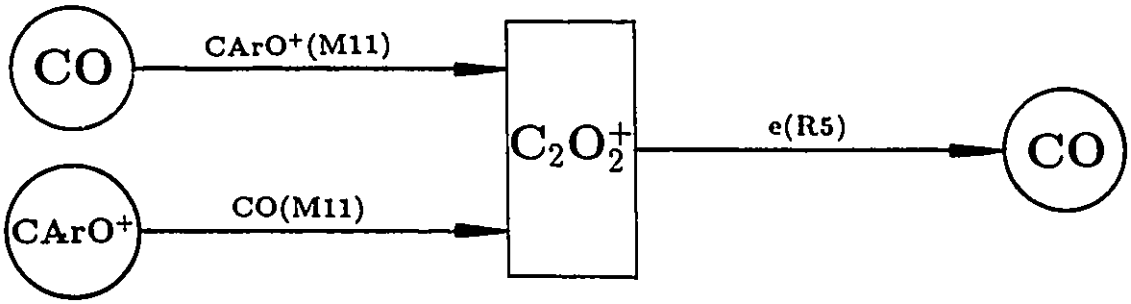

Figure A.17: Sources and sinks of $C_2O_2^+$ included in the chemical kinetic Ar-CO_2 thermal plasma model.

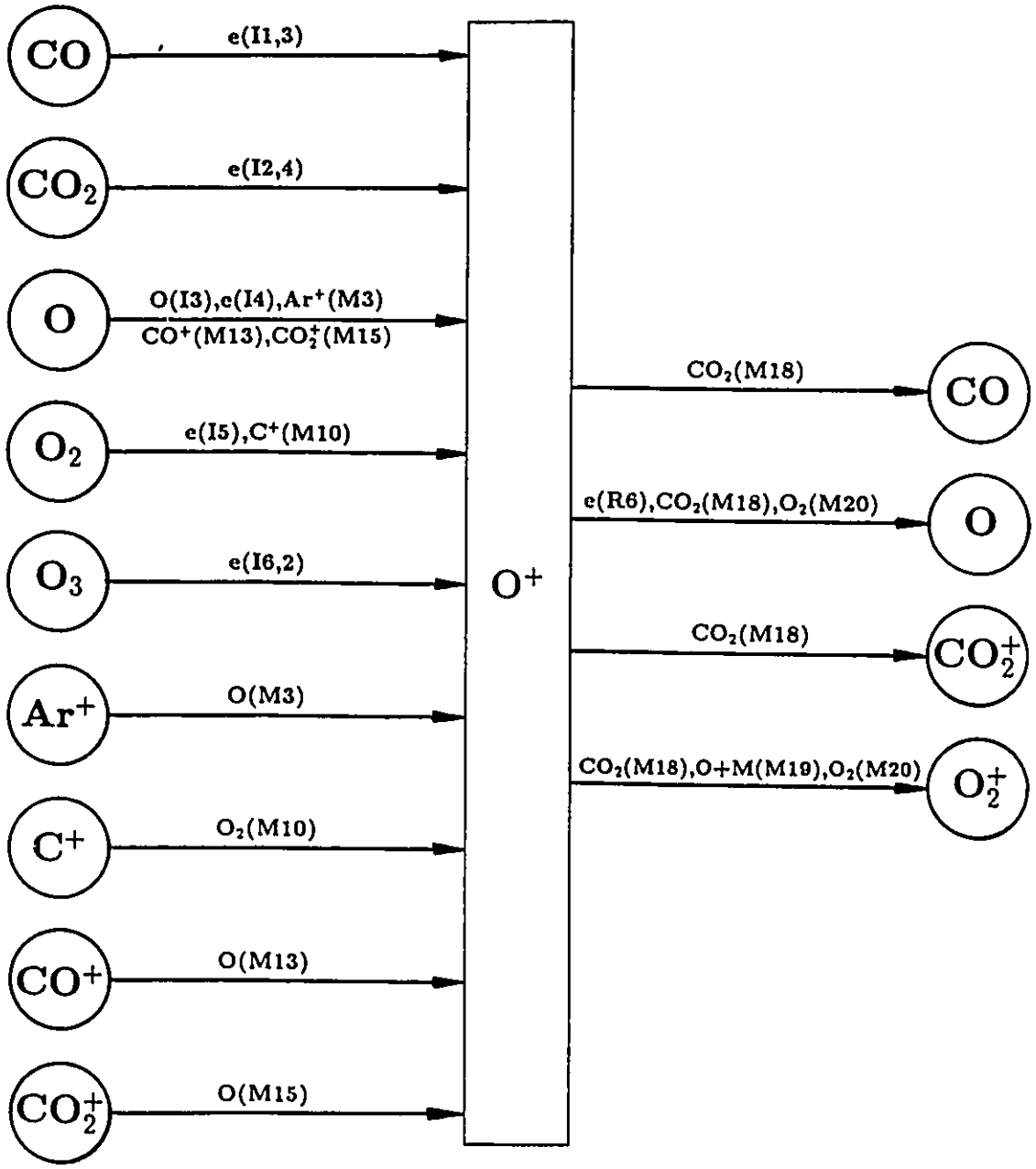

Figure A.18: Sources and sinks of O^+ included in the chemical kinetic Ar-CO_2 thermal plasma model.

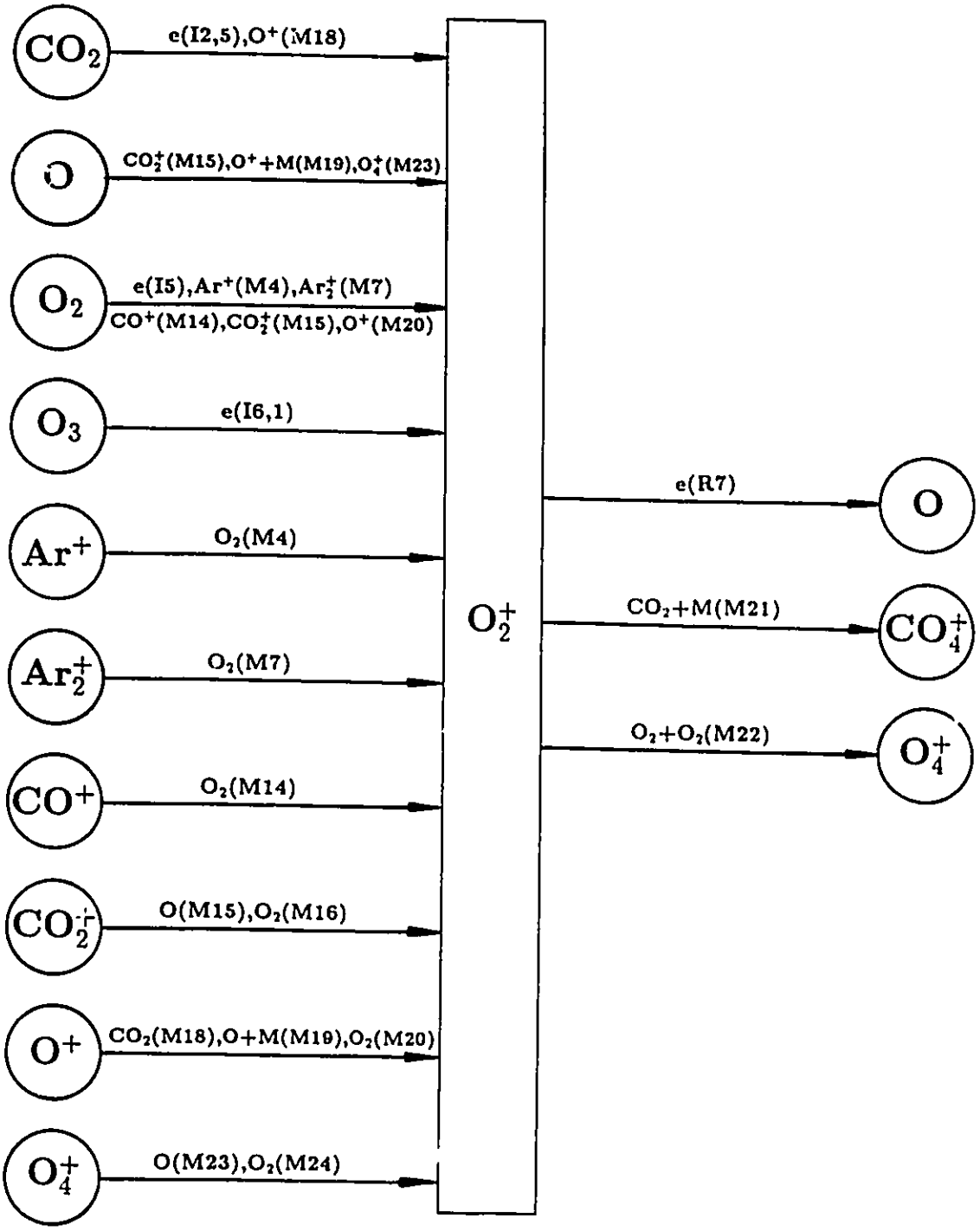

Figure A.19: Sources and sinks of O_2^+ included in the chemical kinetic Ar-CO_2 thermal plasma model.

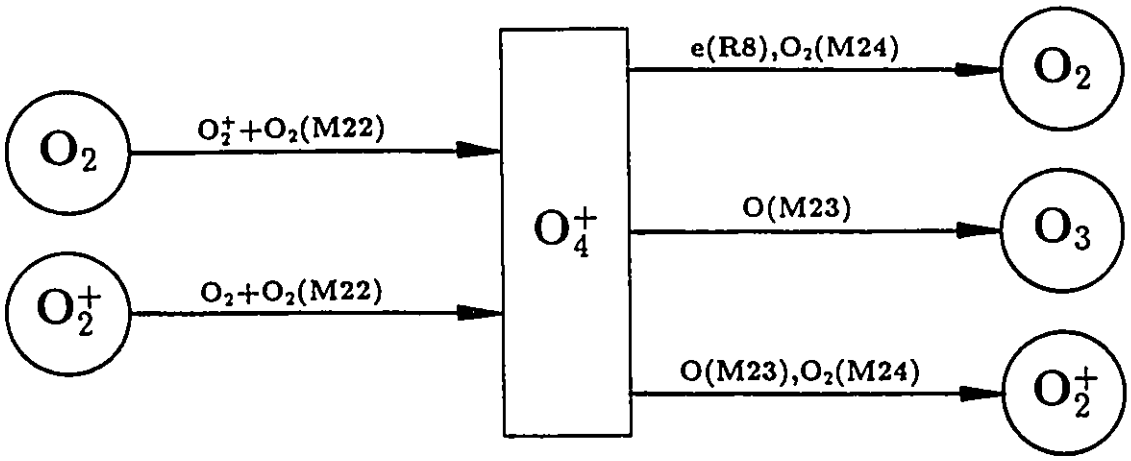

Figure A.20: Sources and sinks of O_4^+ included in the chemical kinetic Ar-CO_2 thermal plasma model.

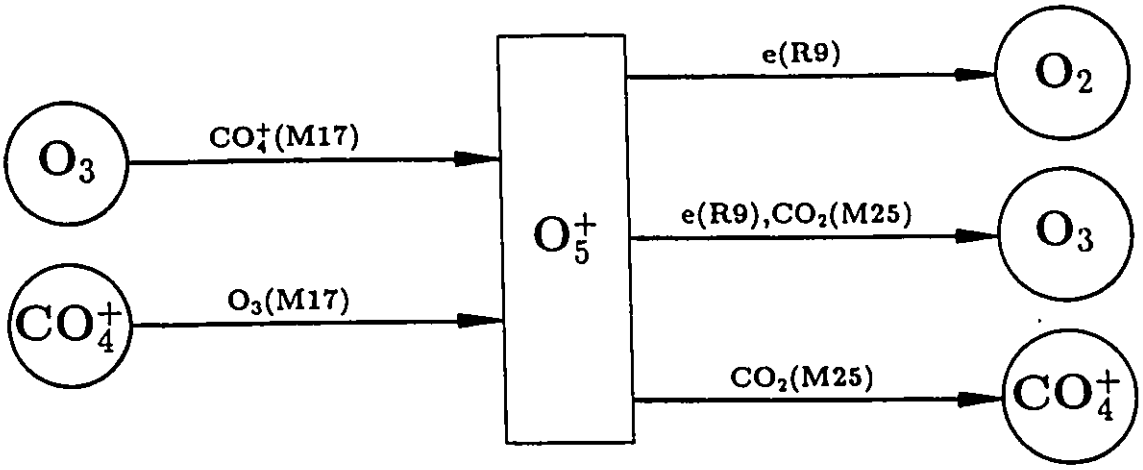

Figure A.21: Sources and sinks of O_5^+ included in the chemical kinetic Ar-CO_2 thermal plasma model.

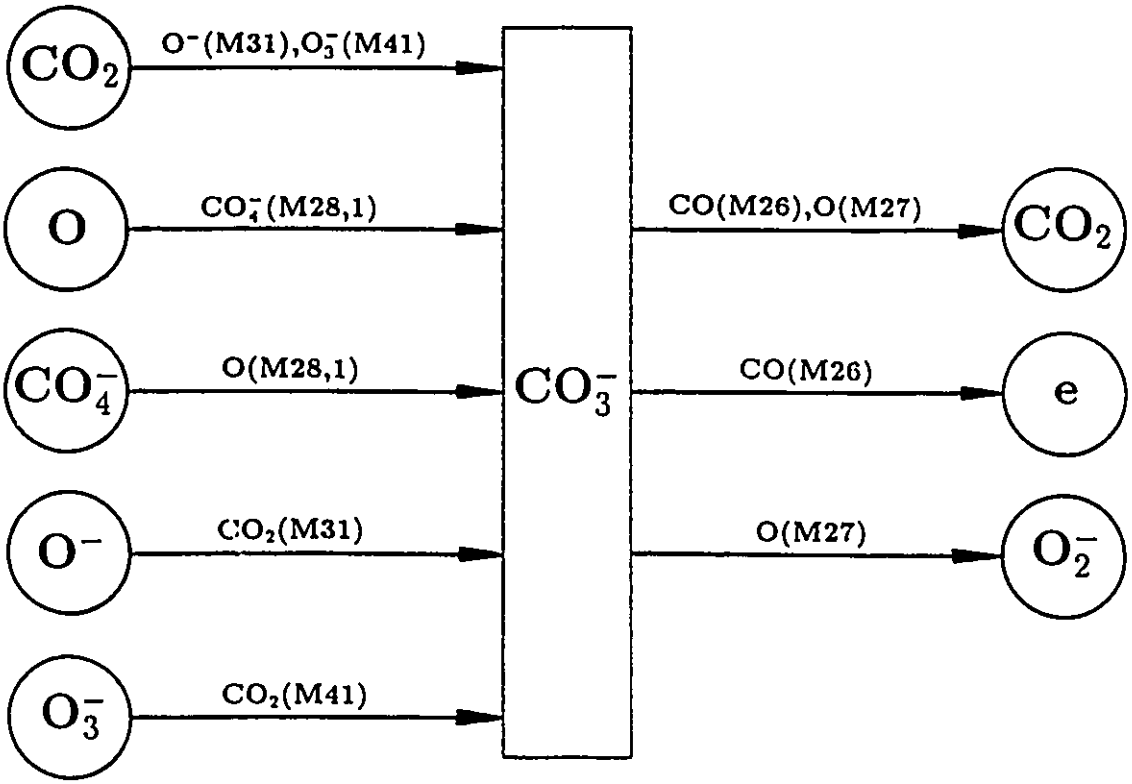

Figure A.22: Sources and sinks of CO_3^- included in the chemical kinetic Ar-CO_2 thermal plasma model.

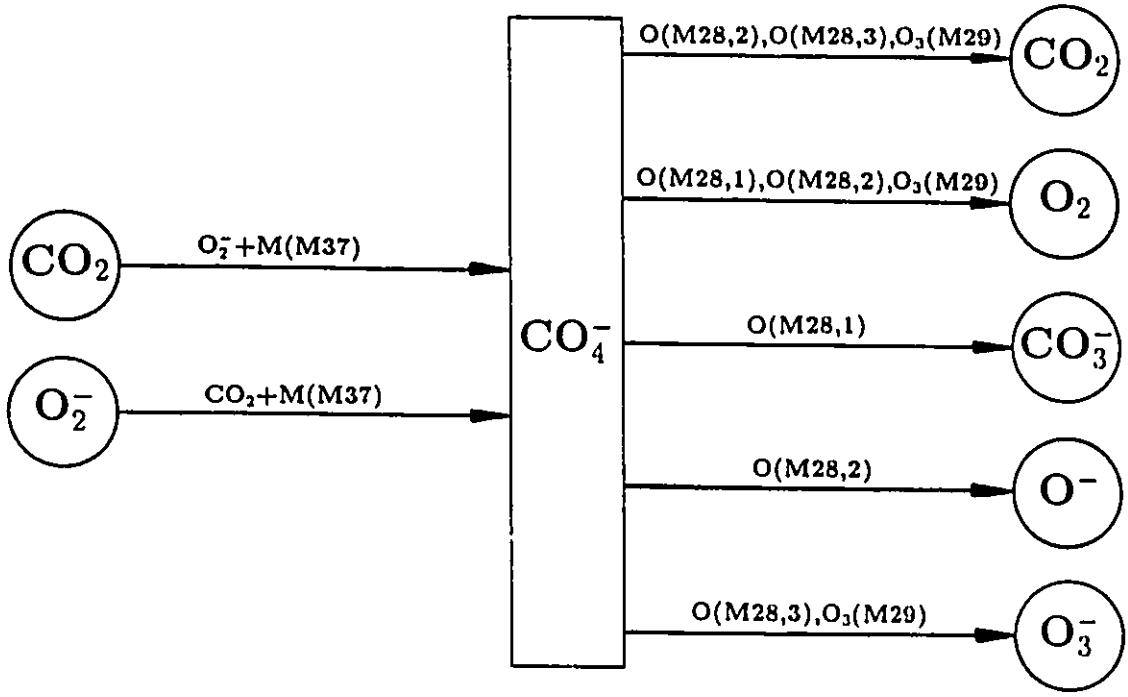

Figure A.23: Sources and sinks of CO_4^- included in the chemical kinetic Ar-CO_2 thermal plasma model.

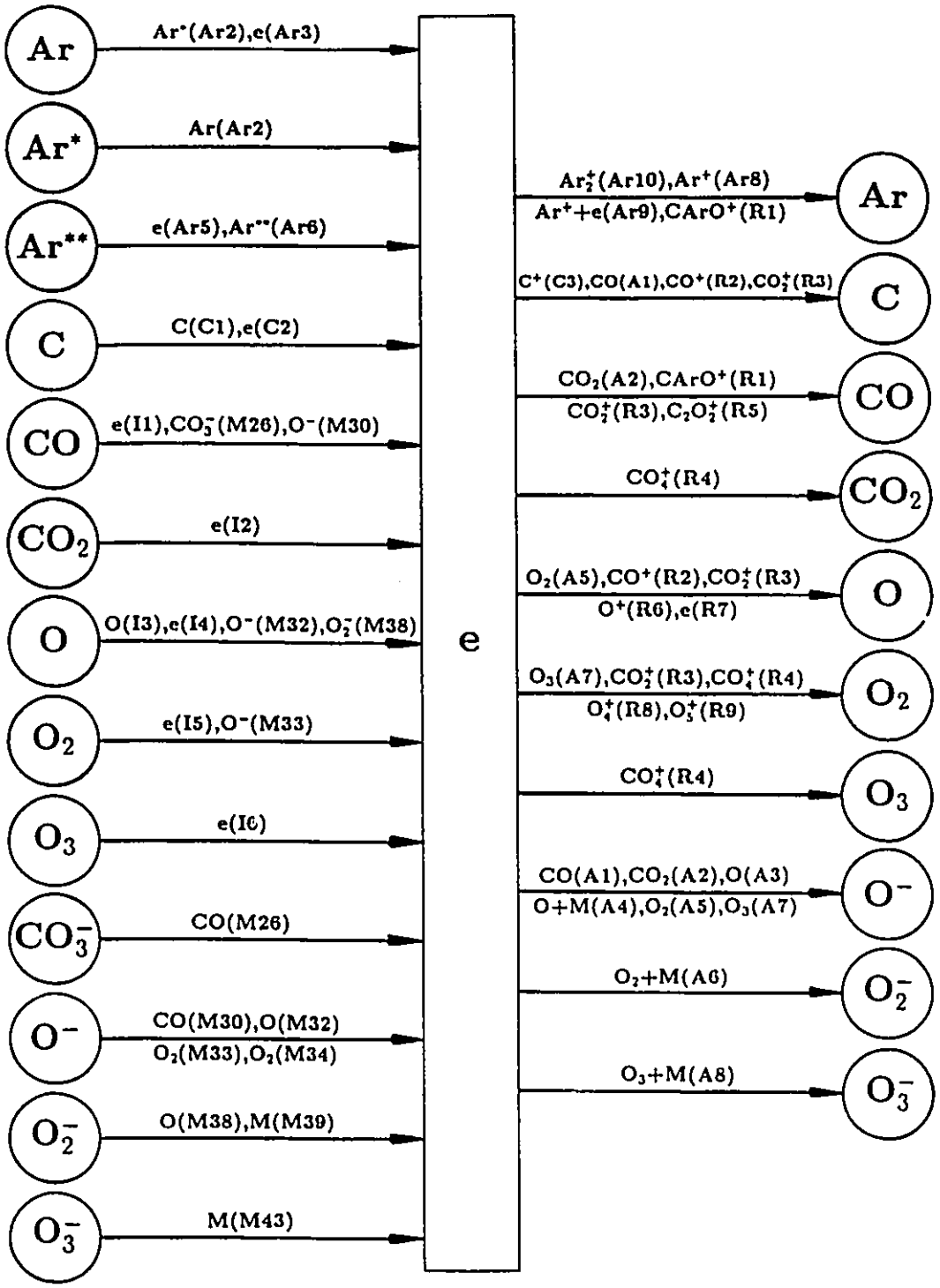

Figure A.24: Sources and sinks of electrons e included in the chemical kinetic Ar-CO_2 thermal plasma model.

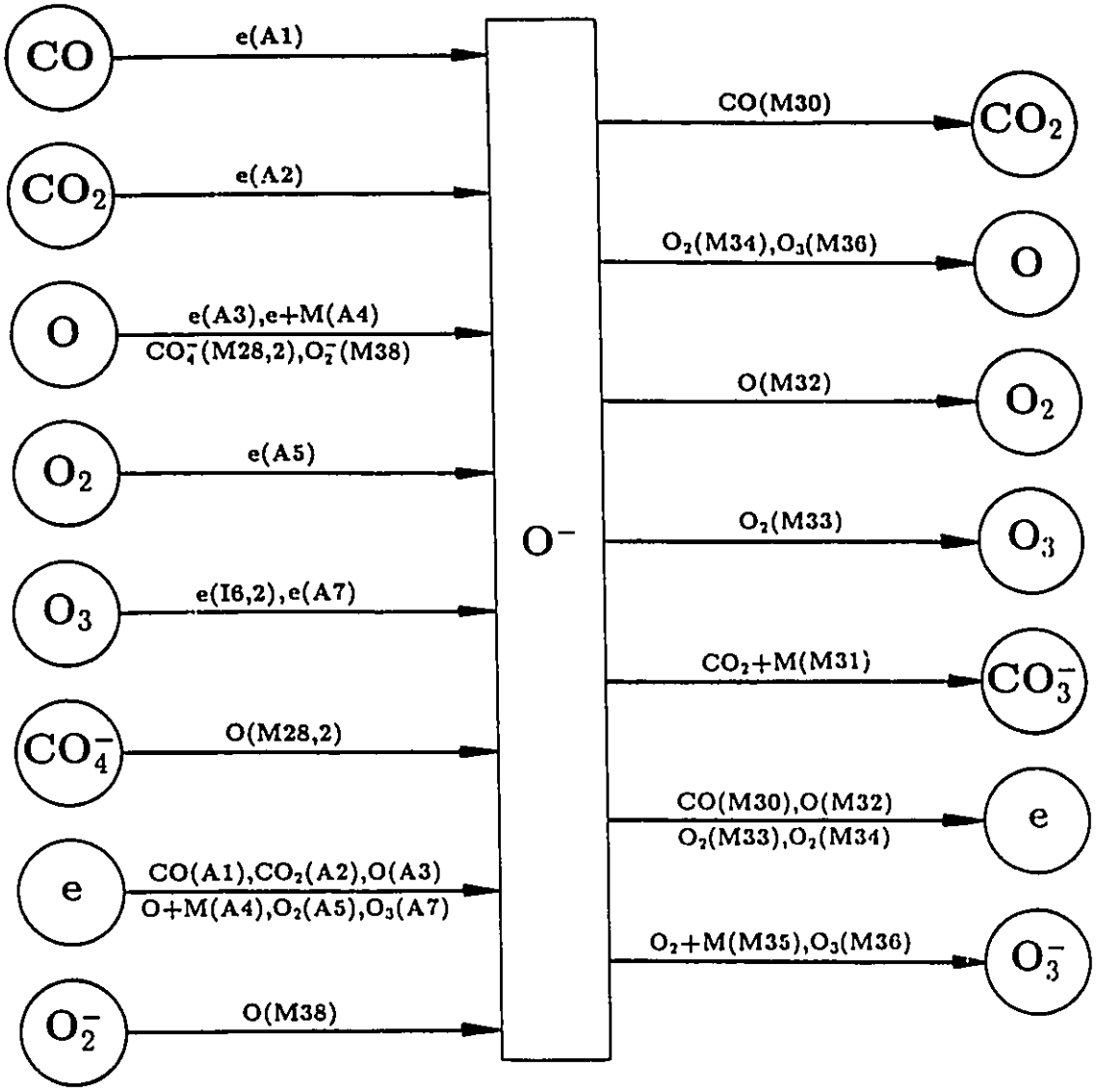

Figure A.25: Sources and sinks of O^- included in the chemical kinetic Ar-CO_2 thermal plasma model.

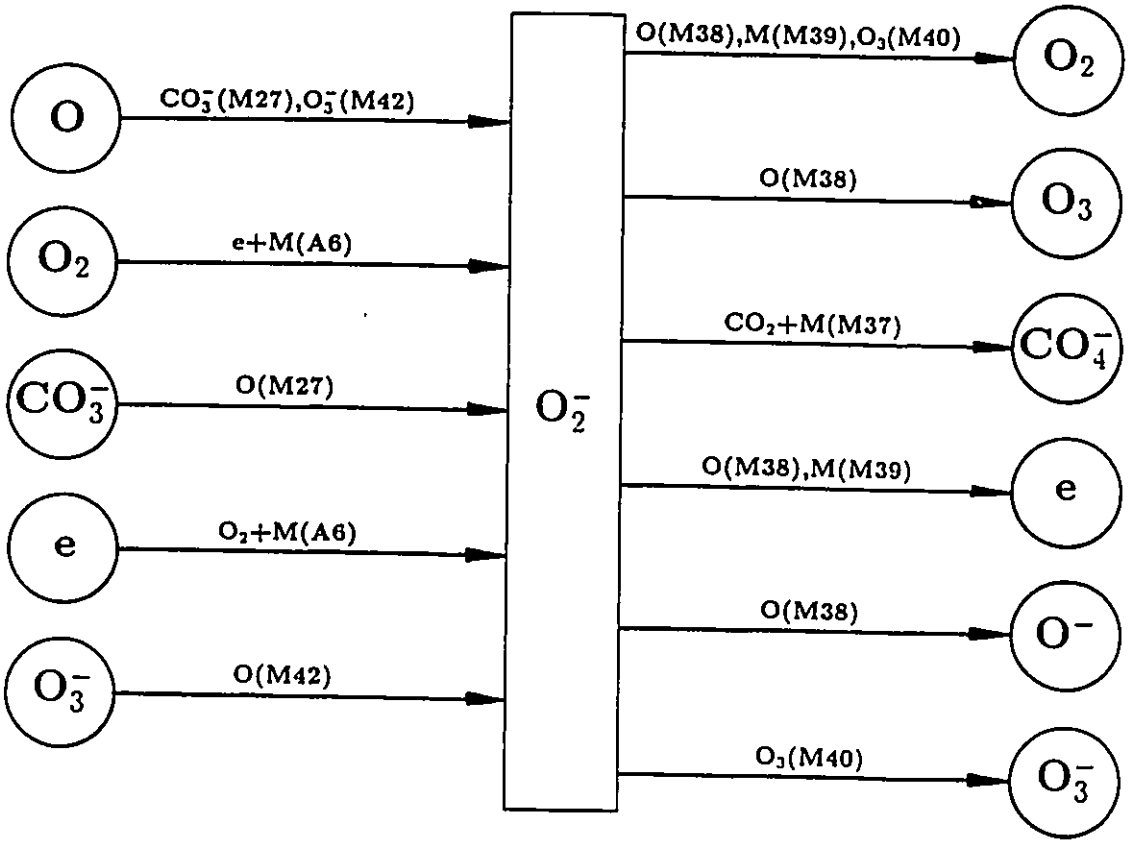

Figure A.26: Sources and sinks of O_2^- included in the chemical kinetic Ar-CO_2 thermal plasma model.

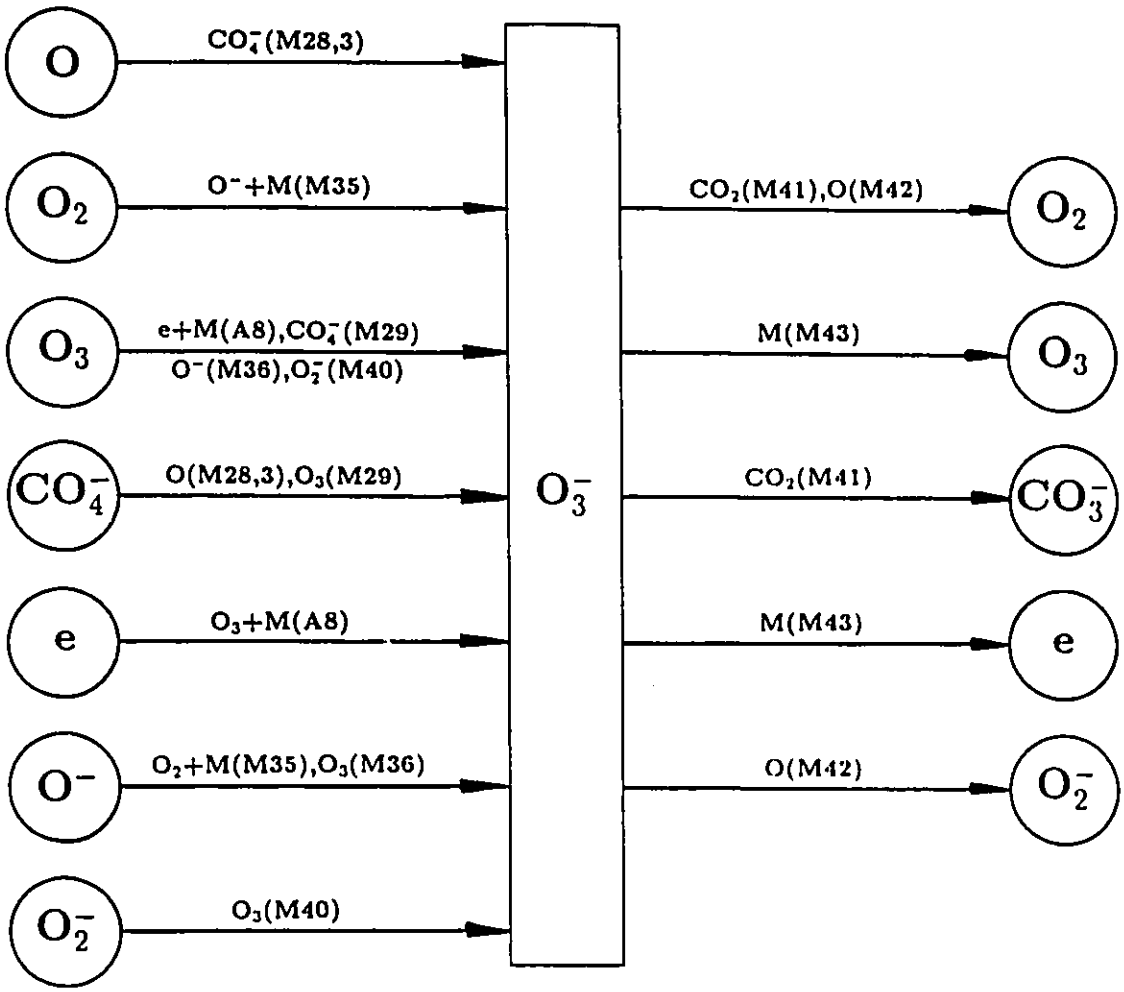

Figure A.27: Sources and sinks of O_3^- included in the chemical kinetic Ar-CO_2 thermal plasma model.

Appendix B

Rate Equations for Ar-CO_2 Thermal Plasma

The coupled rate equations for the species considered in the Ar-CO_2 chemical kinetic mixture plasma model at the centre of a cylindrical discharge tube have been outlined below. The form of the nomenclature the choice of radii follow that used in equations 4.1–4.4. The diffusion coefficients used in the model are listed in Tables 4.2, 5.2 and 6.11.

$$\frac{d[Ar^*]}{dt} = k_{Ar1}[Ar]^2 - k_{Ar2}[Ar][Ar^*] - \frac{q^2 D_{Ar^*-Ar}[Ar^*]}{R^2} \tag{B.1}$$

$$\frac{d[Ar^{**}]}{dt} = k_{Ar4}[Ar][e] - k_{Ar5}[e][Ar^{**}] - 2k_{Ar6}[Ar^{**}]^2 - \frac{q^2 D_{Ar^{**}-Ar}[Ar^{**}]}{R^2}$$

$$\begin{aligned}\frac{d[C]}{dt} = {} & k_{C3}[e][C^+] + f_{I2,5}k_{I2}[e][CO_2] + k_{A1}[e][CO] + k_{D1}[e][CO] \\ & + k_{R2}[e][CO^+] + (1 - f_{R3})k_{R3}[e][CO_2^+] + k_{M8}[C^+][CO] \\ & + k_{N5}[Ar][CO] + \frac{q^2 D_{C^+-Ar}[C^+]}{R^2} \\ & - k_{C1}[C]^2 - k_{C2}[e][C] - k_{N6}[C][CO_2] - k_{N9}[Ar][C][O]\end{aligned} \tag{B.2}$$

$$\begin{aligned}\frac{d[CO]}{dt} = {} & f_{I2,4}k_{I2}[e][CO_2] + k_{A2}[e][CO_2] + k_{D2}[e][CO_2] + k_{R1}[e][CArO^+] \\ & + f_{R3}k_{R3}[e][CO_2^+] + 2k_{R5}[e][C_2O_2^+] + k_{M9}[C^+][CO_2] \\ & + f_{M10}k_{M10}[C^+][O_2] + k_{M12}[CO^+][CO_2] + k_{M13}[CO^+][O]\end{aligned} \tag{B.3}$$

$$
\begin{aligned}
&+k_{M14}[CO^+][O_2] + f_{M15}k_{M15}[O][CO_2^+] + f_{M18}k_{M18}[O^+][CO_2] \\
&+2k_{N6}[C][CO_2] + k_{N7}[O][CO_2] + k_{N8}[Ar][CO_2] \\
&+k_{N9}[Ar][C][O] + \frac{q^2 D_{CArO^+-Ar}[CArO^+]}{R^2} + \frac{q^2 D_{CO^+-Ar}[CO^+]}{R^2} \\
&+\frac{2q^2 D_{C_2O_2^+-Ar}[C_2O_2^+]}{R^2} + \frac{q^2 D_{CO_3^--Ar}[CO_3^-]}{R^2} \\
&-k_{I1}[e][CO] - k_{A1}[e][CO] - k_{D1}[e][CO] - k_{M1}[Ar^+][CO] \\
&-k_{M5}[Ar_2^+][CO] - k_{M8}[C^+][CO] - k_{M11}[CO][CArO^+] \\
&-k_{M26}[CO][CO_3^-] - k_{M30}[CO][O^-] - k_{N1}[CO][O] \\
&-k_{N2}[Ar][CO][O] - k_{N3}[CO][O_2] - k_{N4}[CO][O_3] - k_{N5}[Ar][CO]
\end{aligned}
$$

$$
\begin{aligned}
\frac{d[CO_2]}{dt} \;=\; & k_{R4}[e][CO_4^+] + (1 - f_{M15})k_{M15}[O][CO_2^+] + k_{M16}[CO_2^+][O_2] \\
&+k_{M17}[O_3][CO_4^+] + 2k_{M26}[CO][CO_3^-] + k_{M27}[O][CO_3^-] \\
&+f_{M28,2}k_{M28}[O][CO_4^-] + f_{M28,3}k_{M28}[O][CO_4^-] + k_{M29}[O_3][CO_4^-] \\
&+k_{M30}[CO][O^-] + k_{N1}[CO][O] + k_{N2}[Ar][CO][O] \\
&+k_{N3}[CO][O_2] + k_{N4}[CO][O_3] + \frac{q^2 D_{CO_2^+-Ar}[CO_2^+]}{R^2} \\
&+\frac{q^2 D_{CO_4^+-Ar}[CO_4^+]}{R^2} + \frac{q^2 D_{CO_4^--Ar}[CO_4^-]}{R^2} \\
&-k_{I2}[e][CO_2] - k_{A2}[e][CO_2] - k_{D2}[e][CO_2] \\
&-k_{M2}[Ar^+][CO_2] - k_{M6}[Ar_2^+][CO_2] - k_{M9}[C^+][CO_2] \\
&-k_{M12}[CO^+][CO_2] - k_{M18}[O^+][CO_2] - k_{M21}[Ar][CO_2][O_2^+] \\
&-k_{M25}[CO_2][O_5^+] - k_{M31}[CO_2][O_2][O^-] - k_{M37}[CO_2][O_2][O_2^-] \\
&-k_{M41}[CO_2][O_3^-] - k_{N6}[C][CO_2] - k_{N7}[O][CO_2] - k_{N8}[Ar][CO_2]
\end{aligned} \tag{B.4}
$$

$$
\begin{aligned}
\frac{d[O]}{dt} \;=\; & f_{I1,2}k_{I1}[e][CO] + f_{I2,2}k_{I2}[e][CO_2] + (1 - f_{I5})k_{I5}[e][O_2] \\
&+(k_{I6,1} + k_{I6,2})[e][O_3] + k_{A5}[e][O_2] + k_{D1}[e][CO] + k_{D2}[e][CO_2] \\
&+2k_{D3}[e][O_2] + k_{D4}[e][O_3] + k_{R2}[e][CO^+] + f_{R3}k_{R3}[e][CO_2^+] \\
&+k_{R6}[e][O^+] + 2k_{R7}[e][O_2^+] + (1 - f_{M10})k_{M10}[C^+][O_2] \\
&+(1 - f_{M18})k_{M18}[O^+][CO_2] + k_{M20}[O^+][O_2] + k_{M34}[O_2][O^-] \\
&+k_{M36}[O_3][O^-] + k_{N3}[CO][O_2] + k_{N5}[Ar][CO] + k_{N8}[Ar][CO_2]
\end{aligned} \tag{B.5}
$$

$$
\begin{aligned}
&+2k_{N12}[Ar][O_2] + k_{N14}[Ar][O_3] + \frac{q^2 D_{O^+-Ar}[O^+]}{R^2} \\
&+\frac{q^2 D_{O_5^+-Ar}[O_5^+]}{R^2} + \frac{q^2 D_{O^--Ar}[O^-]}{R^2} + \frac{q^2 D_{O_3^--Ar}[O_3^-]}{R^2} \\
&-k_{I3}[O]^2 - k_{I4}[e][O] - k_{A3}[e][O] - k_{A4}[e][O][O_2] \\
&-k_{M3}[Ar^+][O] - k_{M13}[CO^+][O] - k_{M15}[O][CO_2^+] \\
&-k_{M19}[O][O^+][O_2] - k_{M23}[O][O_4^+] - k_{M27}[O][CO_3^-] \\
&-k_{M28}[O][CO_4^-] - k_{M32}[O][O^-] - k_{M35}[O][O_2^-] \\
&-k_{M42}[O][O_3^-] - k_{N1}[CO][O] - k_{N2}[Ar][CO][O] \\
&-k_{N7}[O][CO_2] - k_{N9}[Ar][C][O] - 2k_{N10}[Ar][O]^2 \\
&-k_{N11}[Ar][O][O_2] - k_{N13}[O][O_3]
\end{aligned}
$$

$$
\begin{aligned}
\frac{d[O_2]}{dt} \;=\; & f_{I2,3}k_{I2}[e][CO_2] + k_{A7}[e][O_3] + k_{D4}[e][O_3] \\
&+(1-f_{R3})k_{R3}[e][CO_2^+] + k_{R4}[e][CO_4^+] + 2k_{R8}[e][O_4^+] \\
&+k_{R9}[e][O_5^+] + k_{M24}[O_2][O_4^+] + f_{M28,1}k_{M28}[O][CO_4^-] \\
&+f_{M28,2}k_{M28}[O][CO_4^-] + k_{M29}[O_3][CO_4^-] + k_{M32}[O][O^-] \\
&+(1-f_{M38})k_{M38}[O][O_2^-] + k_{M39}[O_2][O_2^-] + k_{M40}[O_3][O_2^-] \\
&+k_{M41}[CO_2][O_3^-] + k_{M42}[O][O_3^-] + k_{N4}[CO][O_3] \\
&+k_{N7}[O][CO_2] + k_{N10}[Ar][O]^2 + 2k_{N13}[O][O_3] + k_{N14}[Ar][O_3] \\
&+\frac{q^2 D_{CO_4^+-Ar}[CO_4^+]}{R^2} + \frac{q^2 D_{O_2^+-Ar}[O_2^+]}{R^2} + \frac{2q^2 D_{O_4^+-Ar}[O_4^+]}{R^2} \\
&+\frac{2q^2 D_{O_5^+-Ar}[O_5^+]}{R^2} + \frac{q^2 D_{CO_3^--Ar}[CO_3^-]}{R^2} + \frac{q^2 D_{CO_4^--Ar}[CO_4^-]}{R^2} \\
&+\frac{q^2 D_{O_3^--Ar}[O_3^-]}{R^2} \\
&-k_{I5}[e][O_2] - k_{A5}[e][O_2] - k_{A6}[e][O_2]^2 \\
&-k_{D3}[e][O_2] - k_{M4}[Ar^+][O_2] - k_{M7}[Ar_2^+][O_2] \\
&-k_{M10}[C^+][O_2] - k_{M14}[CO^+][O_2] - k_{M16}[CO_2^+][O_2] \\
&-k_{M20}[O^+][O_2] - k_{M22}[O_2]^2[O_2^+] - k_{M33}[O_2][O^-] \\
&-k_{M35}[O_2]^2[O^-] - k_{N3}[CO][O_2] - k_{N11}[Ar][O][O_2] - k_{N12}[Ar][O_2]
\end{aligned}
\tag{B.6}
$$

$$\begin{aligned}\frac{d[O_3]}{dt} &= k_{R9}[e][O_5^+] + k_{M23}[O][O_4^+] + k_{M25}[CO_2][O_5^+] + k_{M33}[O_2][O^-] \\ &+ f_{M38}k_{M38}[O][O_2^-] + k_{M43}[O_2][O_3^-] + k_{N11}[Ar][O][O_2] \\ &- k_{I6,1}[e][O_3] - k_{I6,2}[e][O_3] - k_{A7}[e][O_3] \\ &- k_{A8}[e][O_2][O_3] - k_{D4}[e][O_3] - k_{M17}[O_3][CO_4^+] \\ &- k_{M29}[O_3][CO_4^-] - k_{M36}[O_3][O^-] - k_{M40}[O_3][O_2^-] \\ &- k_{N4}[CO][O_3] - k_{N13}[O][O_3] - k_{N14}[Ar][O_3]\end{aligned} \tag{B.7}$$

$$\begin{aligned}\frac{d[Ar^+]}{dt} &= k_{Ar2}[Ar][Ar^*] + k_{Ar3}[Ar][e] + k_{Ar5}[e][Ar^{**}] + f_{Ar6}k_{Ar6}[Ar^{**}]^2 \\ &- k_{Ar7}[Ar]^2[Ar^+] - k_{Ar8}[Ar^+][e] - k_{Ar9}[Ar^+][e]^2 \\ &- k_{M1}[Ar^+][CO] - k_{M2}[Ar^+][CO_2] - k_{M3}[Ar^+][O] \\ &- k_{M4}[Ar^+][O_2] - \frac{q^2 D_{Ar^+-Ar}[Ar^+]}{R^2}\end{aligned} \tag{B.8}$$

$$\begin{aligned}\frac{d[Ar_2^+]}{dt} &= (1 - f_{Ar6})k_{Ar6}[Ar^{**}]^2 + k_{Ar7}[Ar]^2[Ar^+] \\ &- k_{Ar10}[e][Ar_2^+] - k_{M5}[Ar_2^+][CO] - k_{M6}[Ar_2^+][CO_2] \\ &- k_{M7}[Ar_2^+][O_2] - \frac{q^2 D_{Ar_2^+-Ar}[Ar_2^+]}{R^2}\end{aligned}$$

$$\begin{aligned}\frac{d[C^+]}{dt} &= k_{C1}[C]^2 + k_{C2}[e][C] + f_{I1,2}k_{I1}[e][CO] \\ &+ f_{I1,3}k_{I1}[e][CO] + f_{I2,3}k_{I2}[e][CO_2] \\ &- k_{C3}[e][C^+] - k_{M8}[C^+][CO] - k_{M9}[C^+][CO_2] \\ &- k_{M10}[C^+][O_2] - \frac{q^2 D_{C^+-Ar}[C^+]}{R^2}\end{aligned} \tag{B.9}$$

$$\begin{aligned}\frac{d[CArO^+]}{dt} &= (1 - f_{M5})k_{M5}[Ar_2^+][CO] \\ &- k_{R1}[e][CArO^+] - k_{M11}[CO][CArO^+] - \frac{q^2 D_{CArO^+-Ar}[CArO^+]}{R^2}\end{aligned} \tag{B.10}$$

$$\begin{aligned}\frac{d[CO^+]}{dt} &= f_{I1,1}k_{I1}[e][CO] + f_{I2,2}k_{I2}[e][CO_2] \\ &+ k_{M1}[Ar^+][CO] + f_{M5}k_{M5}[Ar_2^+][CO] + k_{M8}[C^+][CO] \\ &+ k_{M9}[C^+][CO_2] + (1 - f_{M10})k_{M10}[C^+][O_2] \\ &- k_{R2}[e][CO^+] - k_{M12}[CO^+][CO_2] - k_{M13}[CO^+][O]\end{aligned} \tag{B.11}$$

$$-k_{M14}[CO^+][O_2] - \frac{q^2 D_{CO^+-Ar}[CO^+]}{R^2}$$

$$\frac{d[CO_2^+]}{dt} = f_{I2,1}k_{I2}[e][CO_2] + k_{M2}[Ar^+][CO_2] + k_{M6}[Ar_2^+][CO_2] \quad \text{(B.12)}$$
$$+k_{M12}[CO^+][CO_2] + (1 - f_{M18})k_{M18}[O^+][CO_2]$$
$$-k_{R3}[e][CO_2^+] - k_{M15}[O][CO_2^+] - k_{M16}[CO_2^+][O_2]$$
$$-\frac{q^2 D_{CO_2^+-Ar}[CO_2^+]}{R^2}$$

$$\frac{d[CO_4^+]}{dt} = k_{M21}[Ar][CO_2][O_2^+] + k_{M25}[CO_2][O_5^+] \quad \text{(B.13)}$$
$$-k_{R4}[e][CO_4^+] - k_{M17}[O_3][CO_4^+] - \frac{q^2 D_{CO_4^+-Ar}[CO_4^+]}{R^2}$$

$$\frac{d[C_2O_2^+]}{dt} = k_{M11}[CO][CArO^+] \quad \text{(B.14)}$$
$$-k_{R5}[e][C_2O_2^+] - \frac{q^2 D_{C_2O_2^+-Ar}[C_2O_2^+]}{R^2}$$

$$\frac{d[O^+]}{dt} = f_{I1,3}k_{I1}[e][CO] + f_{I2,4}k_{I2}[e][CO_2] + k_{I3}[O]^2 + k_{I4}[e][O] \quad \text{(B.15)}$$
$$+(1 - f_{I5})k_{I5}[e][O_2] + k_{I6,2}[O_3][e] + k_{M3}[Ar^+][O]$$
$$+f_{M10}k_{M10}[C^+][O_2] + k_{M13}[CO^+][O] + (1 - f_{M15})k_{M15}[O][CO_2^+]$$
$$-k_{R6}[e][O^+] - k_{M18}[O^+][CO_2] - k_{M19}[O][O^+][O_2]$$
$$-k_{M20}[O^+][O_2] - \frac{q^2 D_{O^+-Ar}[O^+]}{R^2}$$

$$\frac{d[O_2^+]}{dt} = f_{I2,5}k_{I2}[e][CO_2] + f_{I5}k_{I5}[e][O_2] + k_{I6,1}[e][O_3] \quad \text{(B.16)}$$
$$+k_{M4}[Ar^+][O_2] + k_{M7}[Ar_2^+][O_2] + k_{M14}[CO^+][O_2]$$
$$+f_{M15}k_{M15}[O][CO_2^+] + k_{M16}[CO_2^+][O_2] + f_{M18}k_{M18}[O^+][CO_2]$$
$$+k_{M19}[O][O^+][O_2] + k_{M20}[O^+][O_2] + k_{M23}[O][O_4^+]$$
$$+k_{M24}[O_2][O_4^+] - k_{R7}[e][O_2^+] - k_{M21}[Ar][CO_2][O_2^+]$$
$$-k_{M22}[O_2]^2[O_2^+] - \frac{q^2 D_{O_2^+-Ar}[O_2^+]}{R^2}$$

$$\frac{d[O_4^+]}{dt} = k_{M22}[O_2]^2[O_2^+] \quad \text{(B.17)}$$
$$-k_{R8}[e][O_4^+] - k_{M23}[O][O_4^+] - k_{M24}[O_2][O_4^+]$$

$$-\frac{q^2 D_{O_4^+-Ar}[O_4^+]}{R^2}$$

$$\frac{d[O_5^+]}{dt} = k_{M17}[O_3][CO_4^+] \quad \text{(B.18)}$$
$$-k_{R9}[e][O_5^+] - k_{M25}[CO_2][O_5^+] - \frac{q^2 D_{O_5^+-Ar}[O_5^+]}{R^2}$$

$$\frac{d[CO_3^-]}{dt} = f_{M28,1}k_{M28}[O][CO_4^-] + k_{M31}[CO_2][O_2][O^-] + k_{M41}[CO_2][O_3^-] \quad \text{(B.19)}$$
$$-k_{M26}[CO][CO_3^-] - k_{M27}[O][CO_3^-] - \frac{q^2 D_{CO_3^--Ar}[CO_3^-]}{R^2}$$

$$\frac{d[CO_4^-]}{dt} = k_{M37}[CO_2][O_2][O_2^-] \quad \text{(B.20)}$$
$$-k_{M28}[O][CO_4^-] - k_{M29}[O_3][CO_4^-] - \frac{q^2 D_{CO_4^--Ar}[CO_4^-]}{R^2}$$

$$\frac{d[O^-]}{dt} = k_{I6,2}[O_3][e] + k_{A1}[e][CO] + k_{A2}[e][CO_2] + k_{A3}[e][O] \quad \text{(B.21)}$$
$$+k_{A4}[e][O][O_2] + k_{A5}[e][O_2] + k_{A7}[e][O_3]$$
$$+f_{M28}k_{M28}[O][CO_4^-] + (1 - f_{M38})k_{M38}[O][O_2^-]$$
$$-k_{M30}[CO][O^-] - k_{M31}[CO_2][O_2][O^-] - k_{M32}[O][O^-]$$
$$-k_{M33}[O_2][O^-] - k_{M34}[O_2][O^-] - k_{M35}[O_2]^2[O^-]$$
$$-k_{M36}[O_3][O^-] - \frac{q^2 D_{O^--Ar}[O^-]}{R^2}$$

$$\frac{d[O_2^-]}{dt} = k_{A6}[e][O_2]^2 + k_{M27}[O][CO_3^-] + k_{M42}[O][O_3^-] \quad \text{(B.22)}$$
$$-k_{M37}[CO_2][O_2][O_2^-] - k_{M38}[O][O_2^-] - k_{M39}[O_2][O_2^-]$$
$$-k_{M40}[O_3][O_2^-] - \frac{q^2 D_{O_2^--Ar}[O_2^-]}{R^2}$$

$$\frac{d[O_3^-]}{dt} = k_{A8}[e][O_2][O_3] + f_{M28,3}k_{M28}[O][CO_4^-] + k_{M29}[O_3][CO_4^-] \quad \text{(B.23)}$$
$$+k_{M35}[O_2]^2[O^-] + k_{M36}[O_3][O^-] + k_{M40}[O_3][O_2^-]$$
$$-k_{M41}[CO_2][O_3^-] - k_{M42}[O][O_3^-]$$
$$-k_{M43}[O_2][O_3^-] - \frac{q^2 D_{O_3^--Ar}[O_3^-]}{R^2}$$

Appendix C

Collision Cross Sections

As illustrated in Tables 4.1, 5.1, and 6.1–6.7, reaction rates are most often tabulated directly in units of cm^3/s for two-body reactions and in units of cm^6/s for three-body reactions. In some cases however, only collision cross-sections are available for the reactions of interest. In this case, the value of the reaction rate constant can be derived from the collision cross-section as described in Section 3.3. In the present investigation, the reaction rate constants of the following reactions were derived from collision cross sections:

$$Ar + e \xrightarrow{k_{Ar3}} Ar^+ + e + e$$

$$Ar + e \xrightarrow{k_{Ar4}} Ar^{**} + e$$

$$Ar^{**} + e \xrightarrow{k_{Ar5}} Ar^+ + e + e$$

$$C + e \xrightarrow{k_{C2}} C^+ + e + e$$

$$CO + e \xrightarrow{k_{11}} \text{Products}$$

$$CO_2 + e \xrightarrow{k_{12}} \text{Products}$$

$$O + e \xrightarrow{k_{14}} O^+ + e + e$$

$$O_2 + e \xrightarrow{k_{15}} \text{Products}$$

$$O_3 + e \xrightarrow{k_{I6,1}} O_2^+ + O + e + e$$

$$O_3 + e \xrightarrow{k_{I6,2}} O^+ + O^- + O + e + e$$

The collision cross-sections which were used to derive the reaction rate constants k_{Ar3}, k_{Ar4}, k_{Ar5}, k_{C2}, k_{I1}, k_{I2}, k_{I4}, k_{I5}, $k_{I6,1}$, and $k_{I6,2}$, have been illustrated in Figures C.1–C.9 below respectively.

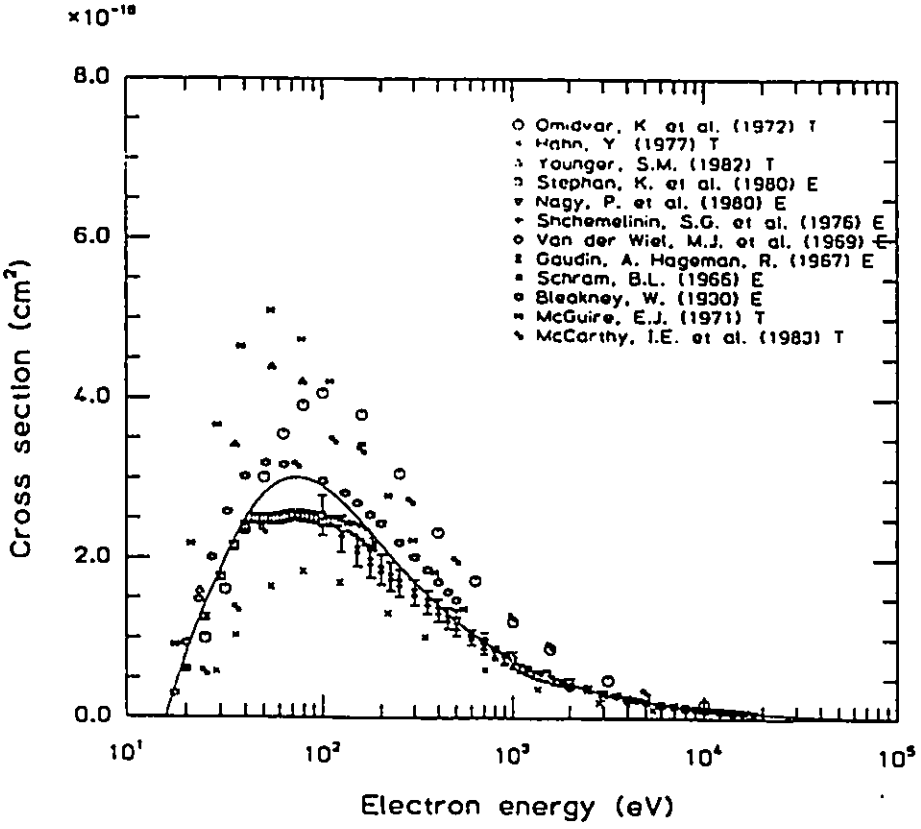

Figure C.1: Collision cross-section for the $Ar + e \xrightarrow{k_{Ar3}} Ar^+ + e + e$ reaction[95].

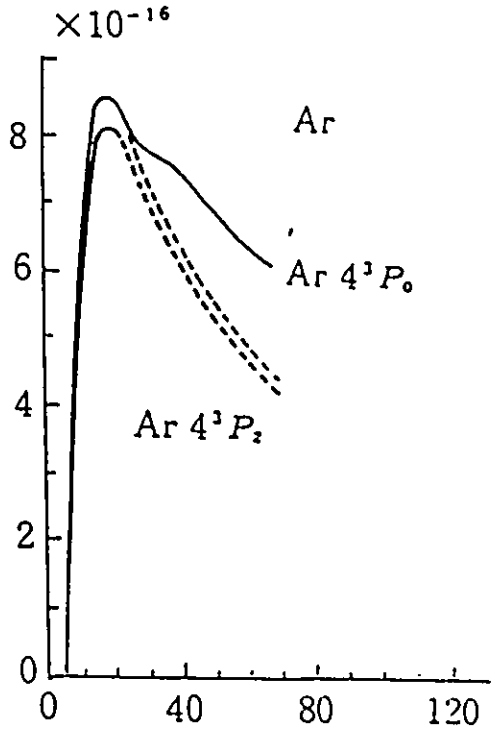

Figure C.2: Collision cross-section for the Ar + e $\xrightarrow{k_{Ar4}}$ Ar** + e reaction[96].

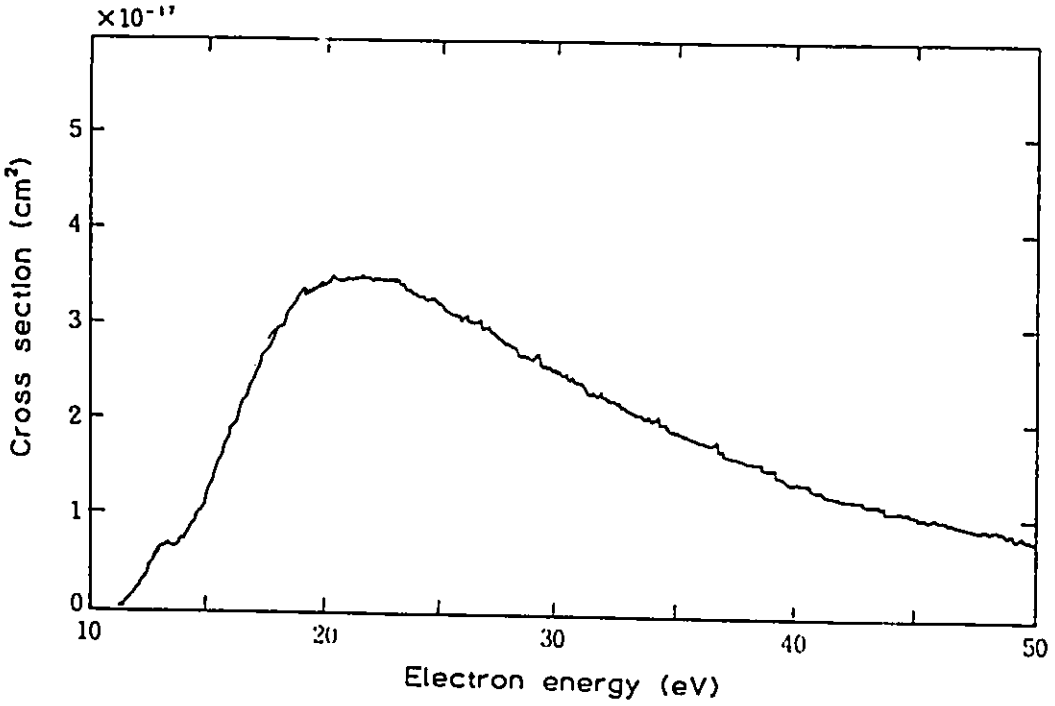

Figure C.3: Collision cross-section for the $Ar^{**} + e \xrightarrow{k_{Ar^{**}}} Ar^{+} + e + e$ reaction[97].

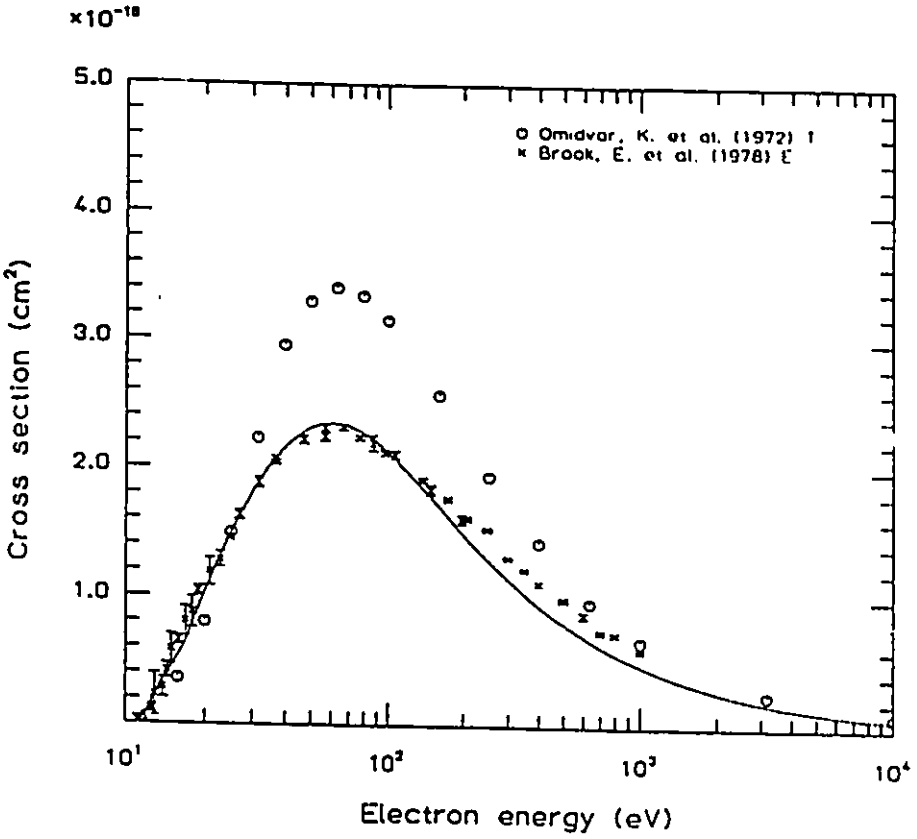

Figure C.4: Collision cross-section for the $C + e \xrightarrow{k_{C2}} C^+ + e + e$ reaction[95].

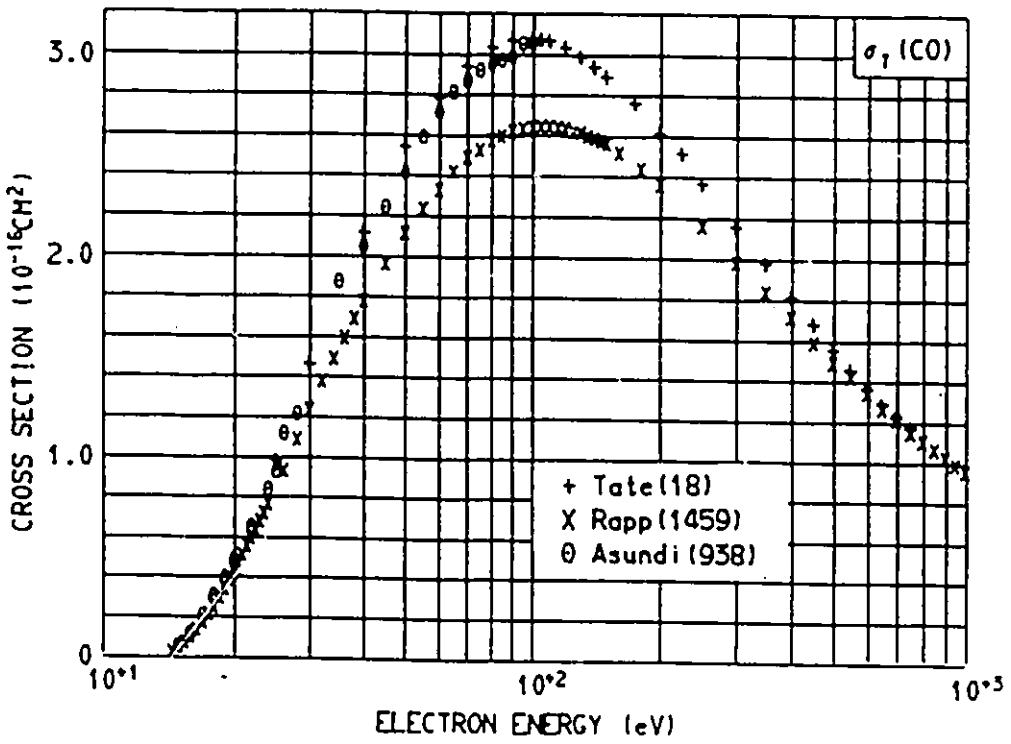

Figure C.5: Collision cross-section for the CO + e $\xrightarrow{k_{11}}$ Products reaction[132].

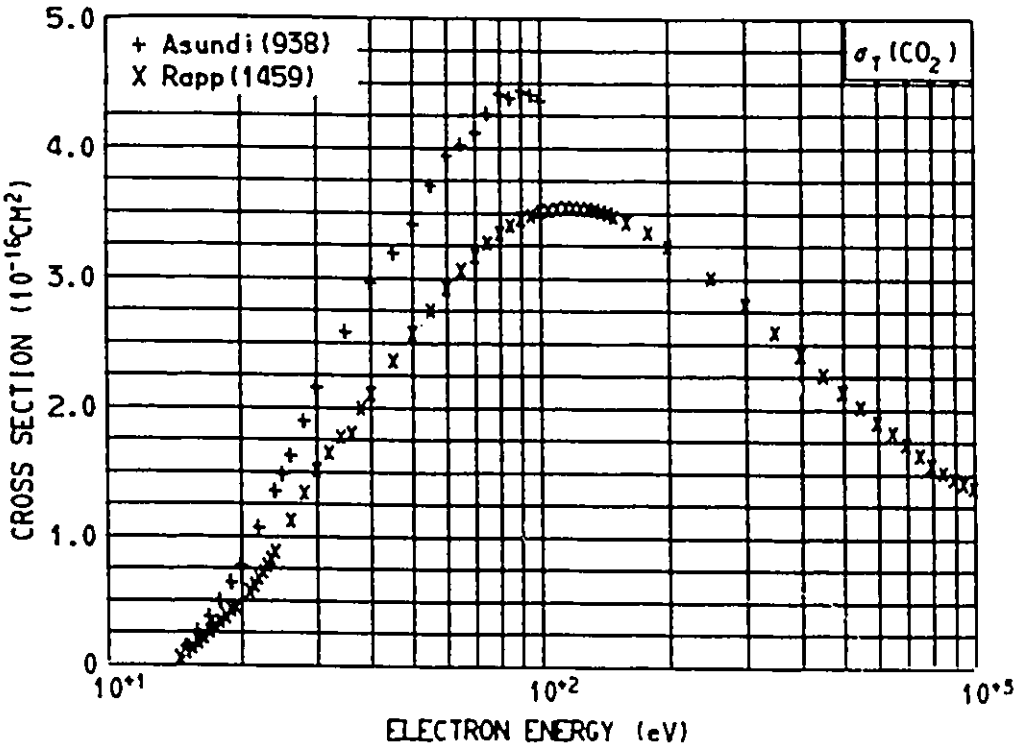

Figure C.6: Collision cross-section for the $CO_2 + e \xrightarrow{k_{12}}$ Products reaction[132].

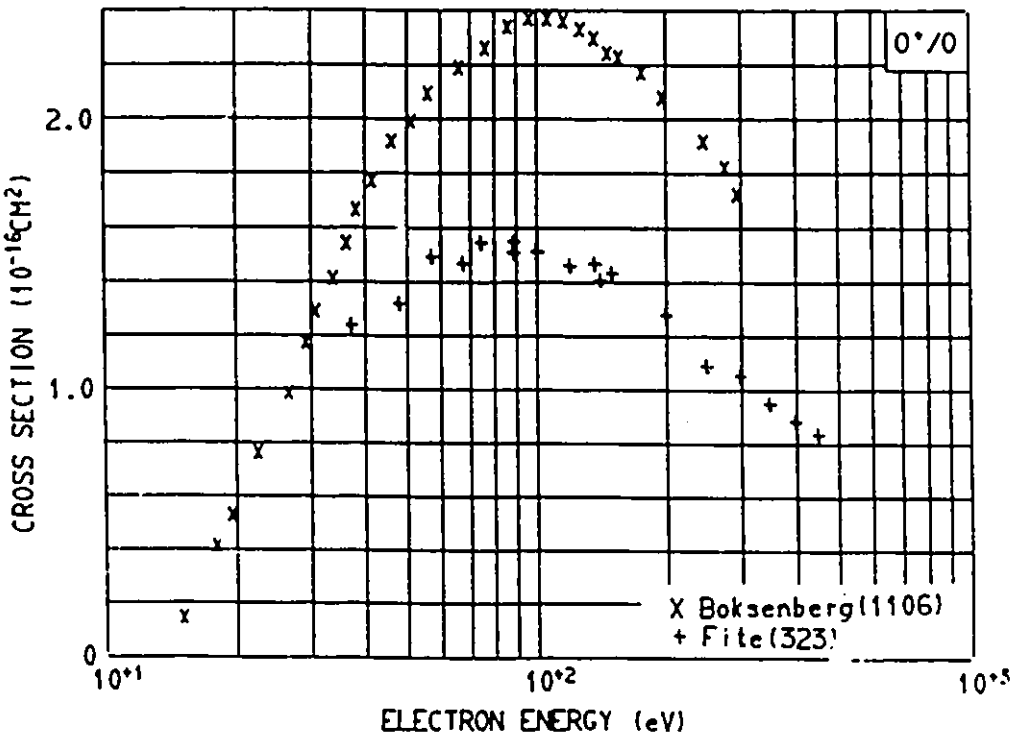

Figure C.7: Collision cross-section for the O + e $\xrightarrow{k_{14}}$ O^+ + e + e reaction[132].

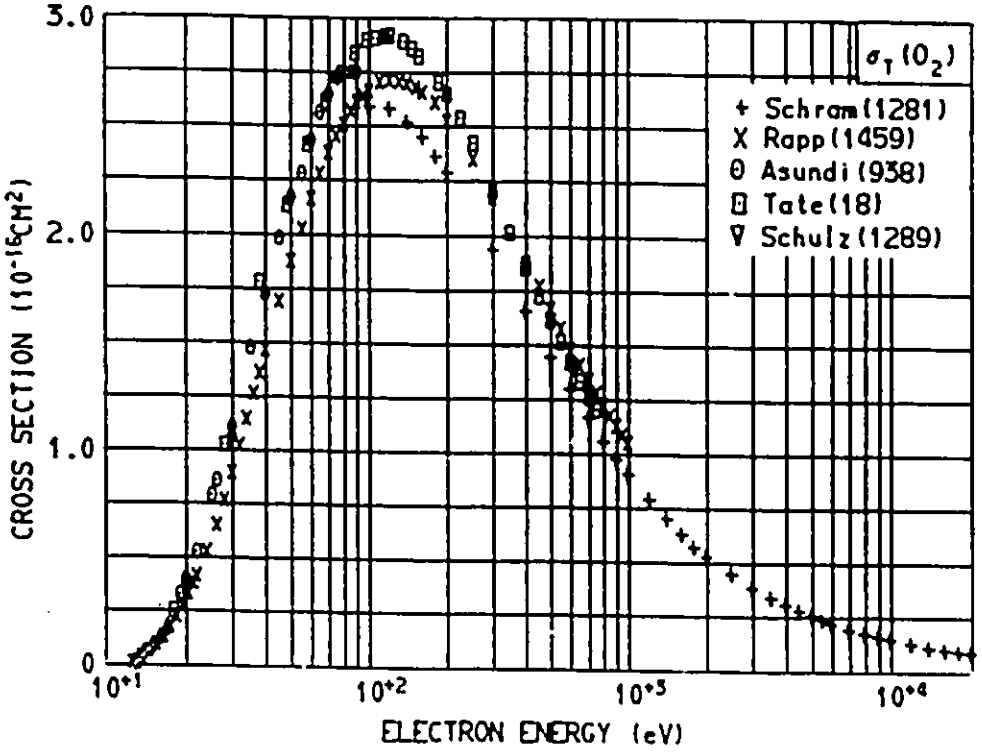

Figure C.8: Collision cross-section for the $O_2 + e \xrightarrow{k_{15}}$ Products reaction[132].

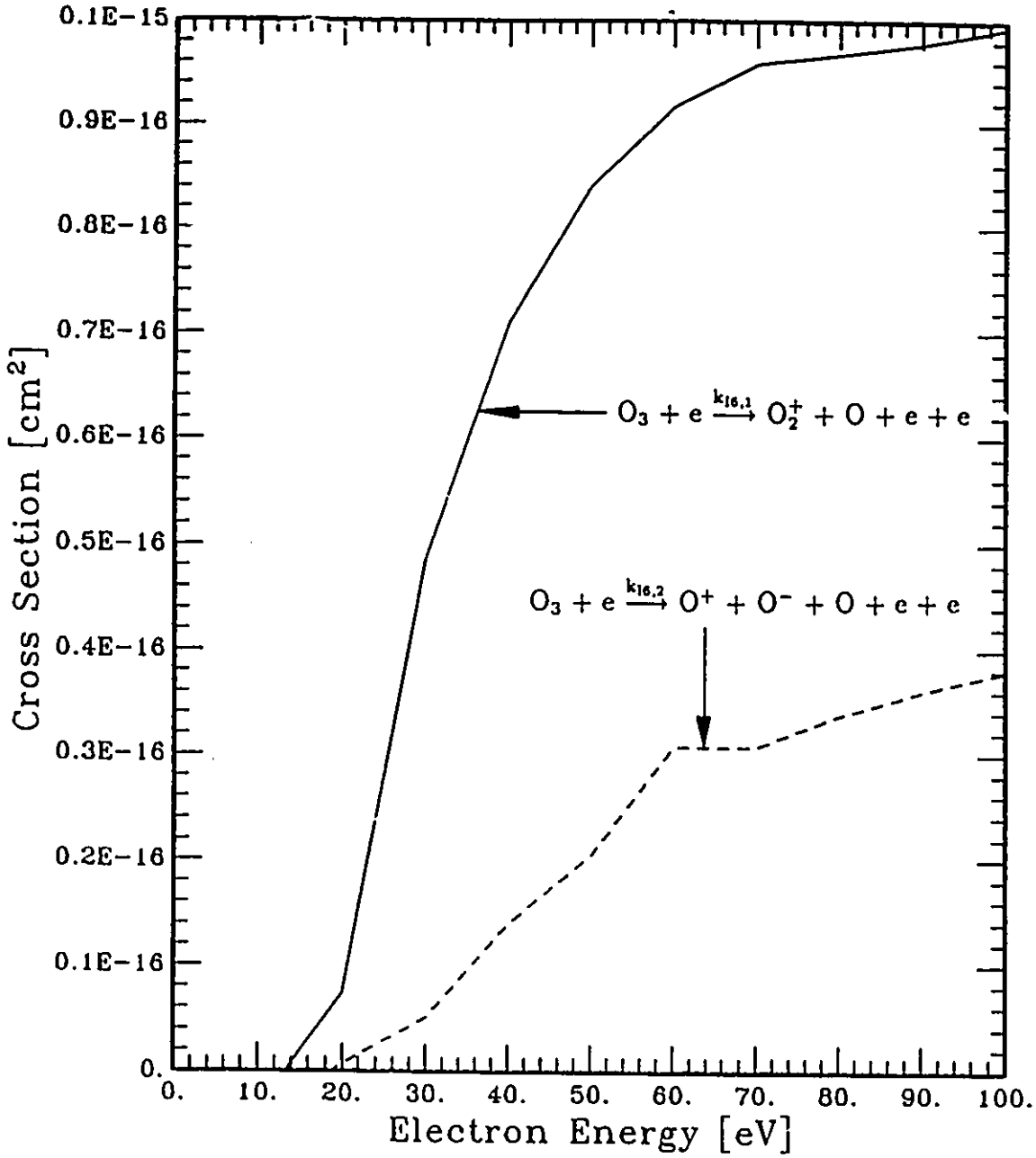

Figure C.9: Collision cross-section for the $O_3 + e \xrightarrow{k_{16,1}} O_2^+ + O + e + e$ and $O_3 + e \xrightarrow{k_{16,2}} O^+ + O^- + O + e + e$ reactions[136].

Appendix D

Program Source Codes

A full listing of the chemical kinetic FORTRAN programs for the pure argon and the argon-carbon thermal plasmas have been included in this appendix. The main programs have been listed in Sections D.1 and D.2 respectively. The subroutines common to both programs have been listed in Section D.3. The Ar-CO_2 chemical kinetic model has not been included due to space limitations.

D.1 Ar Thermal Plasma

```
      PROGRAM ARGON
*
*  THE PURPOSE OF THIS PROGRAM IS TO CALCULATE THE EQUILIBRIUM
*  CONCENTRATIONS OF THE SPECIES FOUND IN AN ARGON THERMAL PLASMA.
*
*
*  VARIABLES
*
*       NAR = CONCENTRATION OF ARGON
*      NARS = CONCENTRATION OF EXCITED ARGON
*     NARSS = CONCENTRATION OF METASTABLE ARGON
*        NE = CONCENTRATION OF ELECTRONS
```

```
*      NARP = CONCENTRATION OF IONIZED ARGON
*     NAR2P = CONCENTRATION OF IONIZED ARGON_2^+
*
      IMPLICIT DOUBLE PRECISION (A-Z)
      INTEGER I,II,NN(50),NLOOP,MAXL,ITER
      REAL ENDE
      PARAMETER (MAXL=2000)
      DOUBLE PRECISION TT(MAXL),N(7,MAXL)
*
*  OPEN THE DATA FILE....
*
      OPEN(1,FILE='DATA.DAT',STATUS='NEW')
*
*  SET CONSTANTS AND COEFFICIENTS
*
*
*  ACCURACY OF ITERATION
*
      EPS=1.0D-8
*
*  THE VALUE OF THE AVOGADRO NUMBER
*
      AVOGAD=6.022045D23
*
*  VALUE OF THE BOLTZMANN CONSTANT IN J/K
*
      KJ=1.380662D-23
*
*  VALUE OF THE BOLTZMANN CONSTANT IN eV/K
*
      KEV=8.6183645D-5
```

```
*
*  THE COEFFICIENT CONTAINING ALL OF THE CONSTANTS
*  FOR THE SAHA EQUATION IN 1/(cm3*K)
*
      ASAHA=2.4146609D+15
*
*  FIRST IONIZATION ENERGY FOR ARGON IN eV
*
      EAR=15.769D0
*
*  THE IDEAL GAS CONSTANT IN (cm^3 atm)/(mole K)
*
      R=82.05D0
*
*  RATE CONSTANTS FOR REACTIONS
*
*       Ar^+  +  Ar + Ar  -> KA1 ->   Ar_2^+  + Ar
*
*       Ar_2^+  +    e    -> KA2 ->   Ar^*  +   Ar
*
*       Ar^+    +    e    -> KA3 ->   Ar    +   h*nu
*
*       Ar      +    Ar   -> KA4 ->   Ar^*  +   Ar
*
*       Ar^*    +    Ar   -> KA5 ->   Ar^+  +   e  + Ar
*
*       Ar^+  +  e  +  e  -> KA6 ->   Ar^*  +   e
*
*       Ar      +    e    -> KA7 ->   Ar^+  +   e  +  e
*
*       Ar      +    e    -> KA8 ->   Ar^*^* +   e
```

```
*
*       Ar^*^*  +    e    -> KA9 ->   Ar^+  +   e  +  e
*
*       Ar^*^*  +  Ar^*^* -> KA10 ->  Ar^+  +   e
*
*       Ar^*^*  +  Ar^*^* -> KA10 ->  Ar_2^+ +  e
*
*
*  NOTE: THE KA1, KA2, KA3, KA4, KA5, KA6, KA7, KA8 AND KA9
*  CONSTANTS ARE FUNCTIONS OF TEMPERATURE AND HAVE BEEN
*  INCLUDED AS FORTRAN FUNCTIONS
*
      KA10=3.06D-10
*
*  THE CONSTANT q SQUARED FOR THE DIFFUSION TERM
*
      Q2=2.53D0*2.53D0
*
*  TEMPERATURE RANGE TO BE CALCULATED
*
      PRINT*,' STARTING (MAXIMUM) GAS TEMPERATURE IN K'
      READ(*,*) TG
*  EQUILIBRIUM CASE
      TE=TG
      PRINT*,' FINAL (MINIMUM) TEMPERATURE IN K'
      READ(*,*) TGFINAL
*
*  PRESSURE IN TORR AND ATMOSPHERES
*
      PRINT*,' SYSTEM PRESSURE IN TORR'
      READ(*,*) PTORR
```

```
      PTORR=760.0D0
      PATM=PTORR/760.0D0
*
*  LOOP AND CHANGE THE TEMPERATURE
*
      I=1
  100 CONTINUE
*
*  TOTAL CONCENTRATION OF THE GAS
*  ACCORDING TO THE IDEAL GAS LAW
*
      TOTNUM=PATM/(R*TG)
*
*  CALCULATE THE CONCENTRATION OF EACH CONSTITUENT IN 1/(cm^3)
*
*
*  ARGON CONCENTRATION
*
      NAR=TOTNUM*AVOGAD
*
*  RADIUS SQUARED OF THE SYSTEM (IN CM)
*
      R2=1.0D0**2
*
*  SET THE INITIAL GUESSES FOR THE ITERATION,
*  BUT ONLY THE FIRST TIME AROUND
*
      IF(I.EQ.1) THEN
        NARS=NAR/1.0D10
        NARSS=NAR/1.0D10
        NAR2P=NAR/1.0D10
```

```
        NARP=NAR/1.0D10
      END IF
*
*  ITERATE TO THE SOLUTION
*
      NLOOP=1
*
  200 CONTINUE
*
*  SAVE THE PREVIOUS VALUES FOR COMPARISON
*
      PNARS=NARS
      PNARSS=NARSS
      PNARP=NARP
      PNAR2P=NAR2P
      PNAR=NAR
*
*  Ar^+ CONCENTRATION
*
      NE=NARP+NAR2P
      A=0.0D0
      B=0.0D0
      C=0.0D0
      D=0.0D0
      C=C-(KA1(TG)*NAR)*NAR
      B=B-KA3(TE)
      C=C-KA3(TE)*NAR2P
      D=D+(KA5(TG)*NARS)*NAR
      B=B-KA6(TE,NE)
      C=C-KA6(TE,NE)*NAR2P
      C=C+KA7(TE)*NAR
```

```
      D=D+(KA7(TE)*NAR)*NAR2P
      C=C+KA9(TE)*NARSS
      D=D+(KA9(TE)*NARSS)*NAR2P
      D=D+(KA10*NARSS)*NARSS
      C=C-Q2*DARP(TE,TG,PTORR)/R2
*
      CALL POLY(NARP,A,B,C,D)
*
*  Ar^* CONCENTRATION
*
      NE=NARP+NAR2P
      A=0.0D0
      B=0.0D0
      C=0.0D0
      D=0.0D0
      D=D+(KA4(TG)*NAR)*NAR
      C=C-(KA5(TG)*NAR)
      C=C-Q2*DARSTAR(TE,TG,PTORR)/R2
*
      CALL POLY(NARS,A,B,C,D)
*
*  Ar^*^* CONCENTRATION
*
      NE=NARP+NAR2P
      A=0.0D0
      B=0.0D0
      C=0.0D0
      D=0.0D0
      D=D+(KA8(TE)*NAR)*NE
      C=C-(KA9(TE)*NE)
      B=B-2.0D0*KA10
```

```
      C=C-Q2*DARSS(TE,TG,PTORR)/R2
*
      CALL POLY(NARSS,A,B,C,D)
*
*  Ar_2^+ CONCENTRATION
*
      A=0.0D0
      B=0.0D0
      C=0.0D0
      D=0.0D0
      D=D+((KA1(TG)*NARP)*NAR)*NAR
      C=C-KA2(TG,TE)*NARP
      B=B-KA2(TG,TE)
      D=D+(KA10*NARSS)*NARSS
      C=C-Q2*DAR2P(TE,TG,PTORR)/R2
*
      CALL POLY(NAR2P,A,B,C,D)
*
*  MAKE A MASS BALANCE CORRECTION IN THE CONCENTRATION OF Ar
*  TO CORRECT FOR THE LOSS DUE TO THE GENERATION
*  OF AR^*, Ar^+, AND Ar_2^+ IONS
*  AT HIGHER TEMPERATURES THE MODEL MAY PREDICT A FULLY
*  IONIZED CASE. THIS CONDITION MUST ALSO BE ACCOUNTED FOR.
*
      IF(NARP.GT.NAR) THEN
        NARP=NAR
      ELSE
        NAR=TOTNUM*AVOGAD-NARS-NARSS-NARP-2.0D0*NAR2P
      END IF
*
      IF(NLOOP.LT.1000) THEN
```

```
      IF(ABS(PNARS-NARS).GT.ABS(EPS*NARS)
     +.OR.ABS(PNARSS-NARSS).GT.ABS(EPS*NARSS)
     +.OR.ABS(PNARP-NARP).GT.ABS(EPS*NARP)
     +.OR.ABS(PNAR2P-NAR2P).GT.ABS(EPS*NAR2P)
     +.OR.ABS(PNAR-NAR).GT.ABS(EPS*NAR)
     +.OR.NLOOP.LT.50) THEN
        NLOOP=NLOOP+1
        GO TO 200
      END IF
      END IF
*
*  CALCULATE THE ELECTRON CONCENTRATION
*  AT TEMPERATURE T FOR AN ARGON GAS
*  VIA THE SAHA EQUATION.
*
      NARPSAHA=
     +SQRT(12.D0*NAR*(ASAHA*((TG**1.5)*EXP((-EAR)/(KEV*TG)))))
*
*
      TT(I)=TE
      N(1,I)=MAX(NAR,10.0D0)
      N(2,I)=MAX(NARS,10.0D0)
      N(3,I)=MAX(NARSS,10.0D0)
      NE=NAR2P+NARP
      N(4,I)=MAX(NE,10.0D0)
      N(5,I)=MAX(NARP,10.0D0)
      N(6,I)=MAX(NAR2P,10.0D0)
      N(7,I)=MAX(NARPSAHA,10.0D0)
*
      PRINT*,' I,TE,NLOOP = ',I,TE,NLOOP
*
```

```
      IF(TG.GT.TGFINAL) THEN
        TG=TG-100.0D0
        TE=TG
      ELSE
        ITER=I
      END IF
*
      IF(ITER.GT.MAXL) THEN
        PRINT*,' ITER.GT.MAXL  ITER=',ITER,' MAXL=',MAXL
        PRINT*,' CORRECT AND RE-RUN!!'
        STOP
      END IF
*
      ENDE=99999.0
      DO 300 I=1,7
        DO 400 II=1,ITER
          WRITE(1,1000) TT(II),N(I,II)
 1000     FORMAT(F6.0,1X,E10.4)
  400   CONTINUE
        WRITE(1,*) ENDE,ENDE
  300 CONTINUE
*
      END
```

D.2 Ar-C Thermal Plasma

```
      PROGRAM ARGONCARBON
*
*  THE PURPOSE OF THIS PROGRAM IS TO CALCULATE THE
*  EQUILIBRIUM CONCENTRATIONS OF THE SPECIES FOUND
*  IN AN ARGON-CARBON THERMAL PLASMA.
*
*  VARIABLES
*
*       NAR = CONCENTRATION OF ARGON
*      NARS = CONCENTRATION OF METASTABLE ARGON
*     NARSS = CONCENTRATION OF HIGHLY EXCITED METASTABLE ARGON
*        NE = CONCENTRATION OF ELECTRONS
*      NARP = CONCENTRATION OF IONIZED ARGON
*     NAR2P = CONCENTRATION OF IONIZED ARGON_2^+
*        NC = CONCENTRATION OF CARBON ATOMS
*       NCP = CONCENTRATION OF IONIZED CARBON ATOMS
*
*
*
      IMPLICIT DOUBLE PRECISION (A-Z)
      REAL ENDE
      INTEGER I,II,NTOT,NLOOP,MAXL,TOTREA,TOTSPE,ITER,IRANGE
*  GIVE THE MAXIMUM FOR DIMENSIONING
      PARAMETER (MAXL=2000)
*  NUMBER OF SPECIES INVOLVED (IONIC,GASEOUS,AND ELECTRONS)
      PARAMETER (TOTSPE=10)
*  NUMBER OF REACTION RATES, INCLUDING DIFFUSION
      PARAMETER (TOTREA=19)
      DOUBLE PRECISION TT(MAXL),N(TOTSPE,MAXL)
```

```
*
*  OPEN THE DATA FILE....
*
      OPEN(1,FILE='DATA.DAT',STATUS='NEW')
*
*  SET CONSTANTS AND COEFFICIENTS
*
*  ACCURACY OF ITERATION
*
      EPS=1.0D-8
*
*  THE VALUE OF THE AVOGADRO NUMBER
*
      AVOGAD=6.022045D23
*
*  VALUE OF THE BOLTZMANN CONSTANT IN J/K
*
      KJ=1.380662D-23
*
*  VALUE OF THE BOLTZMANN CONSTANT IN eV/K
*
      KEV=8.6183645D-5
*
*  THE COEFFICIENT CONTAINING ALL OF THE CONSTANTS
*  FOR THE SAHA EQUATION IN 1/(cm3*K)
*
      ASAHA=2.4146609D+15
*
*  FIRST IONIZATION ENERGY FOR ARGON IN eV
*
      EAR=15.769D0
```

```
*
*  FIRST IONIZATION ENERGY FOR CARBON IN eV
*
      EC=11.260D0
*
*  THE IDEAL GAS CONSTANT IN (cm^3 atm)/(mole K)
*
      R=82.05D0
*
*  RATE CONSTANTS FOR REACTIONS
*
*       Ar^+  +  Ar + Ar  -> KA1 ->   Ar_2^+  + Ar
*
*       Ar_2^+  +    e    -> KA2 ->   Ar^*  +   Ar
*
*       Ar^+    +    e    -> KA3 ->   Ar    +   h*nu
*
*       Ar      +    Ar   -> KA4 ->   Ar^*  +   Ar
*
*       Ar^*    +    Ar   -> KA5 ->   Ar^+  +   e  + Ar
*
*       Ar^+  +  e  +  e  -> KA6 ->   Ar^*  +   e
*
*       Ar      +    e    -> KA7 ->   Ar^+  +   e  +  e
*
*       Ar      +    e    -> KA8 ->   Ar^*^* +   e
*
*       Ar^*^*  +    e    -> KA9 ->   Ar^+  +   e  +  e
*
*       Ar^*^*  +  Ar^*^* -> KA10 ->  Ar^+  +   e
*
```

```
*       Ar^*^*  +  Ar^*^* -> KA10 ->  Ar_2^+ +  e
*
*       C       +  C      -> PHIC ->  C^+    +  C  +  e
*
*       C       +  e      -> KC2  ->  C^+    +  e  +  e
*
*       C^+     +  e      -> KC3  ->  C      +  h*nu
*
*
*  NOTE: THE KA1, KA2, KA3, KA4, KA5, KA6, KA7, KA8 AND KA9
*  CONSTANTS ARE FUNCTIONS OF TEMPERATURE AND HAVE BEEN
*  INCLUDED AS FORTRAN FUNCTIONS
*  ALSO, PHIC, KC2, AND KC3 ARE ALSO FUNCTIONS OF TEMPERATURE
*
      KA10=3.06D-10
*
*  THE CONSTANT q SQUARED FOR THE DIFFUSION TERM
*
      Q2=2.53D0*2.53D0
*
*  THE TEMPERATURE RANGE TO BE CALCULATED
*
      PRINT*,' STARTING (MINIMUM) GAS TEMPERATURE IN K'
      READ(*,*) TG
      TE=TG
      PRINT*,' FINAL (MAXIMUM) TEMPERATURE IN K'
      READ(*,*) TGFINAL
*
*  THE SYSTEM PRESSURE IN TORR AND ATMOSPHERES
*
      PRINT*,' SYSTEM PRESSURE IN TORR'
```

```
      READ(*,*) PTORR
      PATM=PTORR/760.0D0
*
*  SET INITIAL IRANGE...
*
      IRANGE=1
*
*  LOOP AND CHANGE THE TEMPERATURE
*
      I=1
  100 CONTINUE
*
*  TOTAL CONCENTRATION OF THE GAS
*  ACCORDING TO THE IDEAL GAS LAW
*
      TOTNUM=PATM/(R*TG)
*
*  THE PERCENTAGE OF CARBON IN THE SYSTEM
*
      PERC=0.010D0
*
*  CALCULATE THE CONCENTRATION OF EACH CONSTITUENT IN 1/(cm^3)
*
*
*  ARGON CONCENTRATION
*
      NAR=TOTNUM*AVOGAD*(1.0DO-PERC)
*
*  CARBON CONCENTRATION
*
      NC=TOTNUM*AVOGAD*(PERC)
```

```
*
*  RADIUS SQUARED OF THE SYSTEM (IN CM)
*
      R2=1.0D0**2
*
*  SET THE INITIAL GUESSES FOR THE ITERATION,
*  BUT ONLY THE FIRST TIME AROUND
*
      IF(I.EQ.1) THEN
        NARS=NAR/1.0D10
        NARSS=NAR/1.0D10
        NAR2P=NAR/1.0D10
        NARP=NAR/1.0D10
      END IF
*
*  ITERATE TO THE SOLUTION
*
      NLOOP=1
*
  200 CONTINUE
*
*  SAVE THE PREVIOUS VALUES FOR COMPARISON
*
      PNARS=NARS
      PNARSS=NARSS
      PNARP=NARP
      PNAR2P=NAR2P
      PNAR=NAR
      PNC=NC
      PNCP=NCP
*
```

```
*  Ar^+ CONCENTRATION
*
      NE=NARP+NAR2P+NCP
      A=0.0D0
      B=0.0D0
      C=0.0D0
      D=0.0D0
      C=C-(KA1(TG)*NAR)*NAR
      B=B-KA3(TE)
      C=C-KA3(TE)*(NAR2P+NCP)
      D=D+(KA5(TG)*NARS)*NAR
      B=B-KA6(TE,NE)
      C=C-KA6(TE,NE)*2.0D0*(NAR2P+NCP)
      D=D-KA6(TE,NE)*(2.0D0*NAR2P*NCP+NAR2P*NAR2P+NCP*NCP)
      C=C+KA7(TE)*NAR
      D=D+(KA7(TE)*NAR)*(NAR2P+NCP)
      C=C+KA9(TE)*NARSS
      D=D+(KA9(TE)*NARSS)*(NAR2P+NCP)
      D=D+(KA10*NARSS)*NARSS
      C=C-Q2*DARP(TE,TG,PTORR)/R2
*
      CALL POLY(NARP,A,B,C,D)
*
*  Ar^* CONCENTRATION
*
      NE=NARP+NAR2P+NCP
      A=0.0D0
      B=0.0D0
      C=0.0D0
      D=0.0D0
      D=D+(KA4(TG)*NAR)*NAR
```

```
      C=C-(KA5(TG)*NAR)
      C=C-Q2*DARSTAR(TE,TG,PTORR)/R2
*
      CALL POLY(NARS,A,B,C,D)
*
*  Ar^*^* CONCENTRATION
*
      NE=NARP+NAR2P+NCP
      A=0.0D0
      B=0.0D0
      C=0.0D0
      D=0.0D0
      D=D+(KA8(TE)*NAR)*NE
      C=C-(KA9(TE)*NE)
      B=B-2.0D0*KA10
      C=C-Q2*DARSS(TE,TG,PTORR)/R2
*
      CALL POLY(NARSS,A,B,C,D)
*
*  Ar_2^+ CONCENTRATION
*
      NE=NARP+NAR2P+NCP
      A=0.0D0
      B=0.0D0
      C=0.0D0
      D=0.0D0
      D=D+((KA1(TG)*NARP)*NAR)*NAR
      C=C-KA2(TG,TE)*(NARP+NCP)
      B=B-KA2(TG,TE)
      D=D+(KA10*NARSS)*NARSS
      C=C-Q2*DAR2P(TE,TG,PTORR)/R2
```

```
*
      CALL POLY(NAR2P,A,B,C,D)
      IF(PRINT1.EQ.1) THEN
        PRINT*,' NAR2P',NAR2P
      END IF
*
*  C^+ CONCENTRATION
*
      NE=NARP+NAR2P+NCP
      A=0.0
      B=0.0
      C=0.0
      D=0.0
      D=D+PHIC(TG,NC,PTORR)
      D=D+(KC2(TE)*NC)*(NARP+NAR2P)
      C=C+KC2(TE)*NC
      C=C-KC3(TE)*(NARP+NAR2P)
      B=B-KC3(TE)
      C=C-Q2*DCP(TE,TG,PTORR)/R2
*
      CALL POLY(TEMPNCP,A,B,C,D)
*
      IF(IRANGE.EQ.1) THEN
        NCP=TEMPNCP
      END IF
*
*  C CONCENTRATION
*
      NE=NARP+NAR2P+NCP
      A=0.0
      B=0.0
```

```
      C=0.0
      D=0.0
      B=B-((PHIC(TG,NC,PTORR)/NC)/NC)
      C=C-(KC2(TE)*NE)
      D=D+((KC3(TE)*NCP)*NE)
*
      CALL POLY(TEMPNC,A,B,C,D)
*
      IF(IRANGE.EQ.2) THEN
        NC=TEMPNC
      END IF
*
*  MAKE A MASS BALANCE CORRECTION IN THE CONCENTRATION OF Ar
*  TO CORRECT FOR THE LOSS DUE TO THE GENERATION
*  OF AR^*, Ar^+, AND Ar_2^+ IONS
*  THE SAME ALSO APPLIES FOR C AND C^+
*  AT HIGHER TEMPERATURES THE MODEL MAY PREDICT A FULLY
*  IONIZED CASE. THIS CONDITION MUST ALSO BE ACCOUNTED FOR.
*
      IF(IRANGE.EQ.1) THEN
        ARGON=NARS+NARSS+NARP+NAR2P
        NAR=((1.0D0-PERC)*(TOTNUM*AVOGAD))-ARGON
        NC=(PERC/(1.0D0-PERC))*(NAR+ARGON)-NCP
      ELSE IF(IRANGE.EQ.2) THEN
        ARGON=NARS+NARSS+NARP+NAR2P
        NAR=((1.0D0-PERC)*(TOTNUM*AVOGAD))-ARGON
        NCP=(PERC/(1.0D0-PERC))*(NAR+ARGON)-NC
      ELSE
        PRINT*,' IRANGE NOT RIGHT =',IRANGE
        STOP
      END IF
```

```
*
      IF(NLOOP.LT.1000) THEN
      IF(ABS(PNARS-NARS).GT.ABS(EPS*NARS)
     +.OR.ABS(PNARSS-NARSS).GT.ABS(EPS*NARSS)
     +.OR.ABS(PNARP-NARP).GT.ABS(EPS*NARP)
     +.OR.ABS(PNAR2P-NAR2P).GT.ABS(EPS*NAR2P)
     +.OR.ABS(PNAR-NAR).GT.ABS(EPS*NAR)
     +.OR.ABS(PNCP-NCP).GT.ABS(EPS*NCP)
     +.OR.ABS(PNC-NC).GT.ABS(EPS*NC)) THEN
        NLOOP=NLOOP+1
        GO TO 200
      END IF
      END IF
*
*  CHANGE IN THE IRANGE NEEDED?
*
      IF(IRANGE.EQ.1) THEN
        IF(NCP.GE.NC) THEN
          PRINT*,' SET IRANGE = 2'
          IRANGE=2
        END IF
      ELSE IF(IRANGE.EQ.2) THEN
      ELSE
        PRINT*,' IRANGE NOT RIGHT =',IRANGE
        STOP
      END IF
*
*  CALCULATE THE ELECTRON CONCENTRATION
*  AT TEMPERATURE T FOR AN ARGON GAS AND A
*  PURE CARBON GAS VIA THE SAHA EQUATION.
*
```

```
      NARSAHA=TOTNUM*AVOGAD*(1.0D0-PERC)
      NARPSAHA=
     +SQRT(2.D0*6.D0*NARSAHA*(ASAHA*((TG**1.5)*EXP((-EAR)/(KEV*TG)))))
*
      NCSAHA=TOTNUM*AVOGAD*(PERC)
      NCPSAHA=
     +SQRT(2.0D0*(6.0D0/9.0D0)*
     +NCSAHA*(ASAHA*((TG**1.5)*EXP((-EC)/(KEV*TG)))))
*
*
      TT(I)=TG
      N(1,I)=MAX(NAR,10.0D0)
      N(2,I)=MAX(NARS,10.0D0)
      N(3,I)=MAX(NARSS,10.0D0)
      NE=NARP+NAR2P+NCP
      N(4,I)=MAX(NE,10.0D0)
      N(5,I)=MAX(NARP,10.0D0)
      N(6,I)=MAX(NAR2P,10.0D0)
      N(7,I)=MAX(NARPSAHA,10.0D0)
      N(8,I)=MAX(NC,10.0D0)
      N(9,I)=MAX(NCP,10.0D0)
      N(10,I)=MAX(NCPSAHA,10.0D0)
*
      PRINT*,' I,TG,NLOOP = ',I,TG,NLOOP
*
      IF(TG.LT.TGFINAL) THEN
        TG=TG+100.0D0
        TE=TG
        I=I+1
        GO TO 100
      ELSE
```

```
        ITER=I
      END IF
*
      IF(ITER.GT.MAXL) THEN
        PRINT*,' ITER.GT.MAXL  ITER=',ITER,' MAXL=',MAXL
        PRINT*,' CORRECT AND RE-RUN!!'
        STOP
      END IF
*
      ENDE=99999.0
      DO 300 I=1,TOTSPE
        DO 400 II=1,ITER,1
          WRITE(1,1000) TT(II),N(I,II)
 1000     FORMAT(F6.0,1X,E10.4)
  400   CONTINUE
        WRITE(1,*) ENDE,ENDE
  300 CONTINUE
*
      END
```

D.3 Common Subroutines

```
      SUBROUTINE POLY(XX,AA,BB,CC,DD)
*
*  THE MOST GENERAL FORM OF THE EQUATION TO BE SOLVED IS
*  AX^3 + BX^2 + CX + D = 0
*  HERE THE NEWTON RAPHSON SCHEME IS USED.
*
*  UNDER THOSE CONDITIONS WHERE THE EQUATION IS A
*  QUADRATIC POLYNOMIAL OR IS LINEAR,
*  THE ANALYTICAL SOLUTION IS USED.
*
      IMPLICIT DOUBLE PRECISION (A-Z)
*
      DOUBLE PRECISION XX,AA,BB,CC,DD
      DOUBLE PRECISION X,A,B,C,D,XPREV,EPS,DIS,X1,X2,AAA,BBB,CCC
      INTEGER CONTROL
*
      EPS=1.0D-4
*
      X=XX
      A=AA
      B=BB
      C=CC
      D=DD
*
*  CHECK FOR TYPE OF EQUATION...
*
      IF(AA.EQ.0.0.AND.BB.EQ.0.0.AND.CC.EQ.0.0) THEN
        PRINT*,' A=B=C=0 ERROR PROGRAM STOP'
        STOP
```

```
      ELSE IF(AA.EQ.0.0.AND.BB.EQ.0.0.AND.CC.EQ.0.0.AND.DD.EQ.0.0)THEN
        PRINT*,' A=B=C=D=0 ERROR PROGRAM STOP'
        STOP
      END IF
*
      IF(AA.EQ.0.0.AND.BB.EQ.0.0) THEN
*
*  WE HAVE A SIMPLE LINEAR EQUATION
*  SOLVE IT DIRECTLY
*
        XX=-D/C
        IF(XX.LT.0.0) THEN
          PRINT*,' #1  XX=',XX,' (NEGATIVE!)'
          STOP 'PROGRAM STOP'
        END IF
        RETURN
      ELSE IF(AA.EQ.0.0) THEN
*
*  THE POLYNOMIAL IS QUADRATIC
*
*  CALCULATE THE DISCRIMINANT
*
        DIS=(C*C)-(4.0D0*B*D)
*
        IF(DIS.GT.0.0D0) THEN
*  TWO REAL SOLUTIONS
*
*  CAREFUL... THERE CAN BE PROBLEMS WITH TWO REAL ROOTS
*  DUE TO AUSLOESCHUNGSFEHLER CAUSED BY THE SUBTRACTION
*  WHICH TAKES PLACE!!! HERE, ONLY CALCULATE THE ROOT
*  IS CALCULATED IN THE TRADITIONAL MANNER.
```

```
*  CALCULATE THE OTHER ROOT IS OBTAINED VIA A METHOD
*  BASED ON THE SIGN OF C AS OUTLINED IN THE THESIS.
*
*  FIRST ROOT...
          IF(C.LE.0.0D0) THEN
            X1=(-C+SQRT(DIS))/(2.0D0*B)
          ELSE
            X1=(-C-SQRT(DIS))/(2.0D0*B)
          END IF
*  SECOND ROOT...
          X2=(D/(B*X1))
*
          IF(X1.LT.0.0D0.AND.X2.LT.0.0D0) THEN
            PRINT*,' #2 DOUBLE NEGATIVE ROOT'
            PRINT*,' X1=',X1,' X2=',X2
            PRINT*,' PROGRAM STOP'
            STOP
          ELSE IF(X1.LT.0.0D0) THEN
            IF(CONTROL.EQ.1) THEN
              PRINT*,' X1=',X1,' X2=',X2
              PRINT*,' #2 POS. & NEG. ROOTS. CHOOSE POS.:',X2
            END IF
            XX=X2
          ELSE IF(X2.LT.0.0D0) THEN
            IF(CONTROL.EQ.1) THEN
              PRINT*,' X1=',X1,' X2=',X2
              PRINT*,' #2 POS. & NEG. ROOTS. CHOOSE POS.:',X1
            END IF
            XX=X1
          ELSE
*  TWO POSITIVE ROOTS. CHOOSE THE LARGEST.
```

```
            PRINT*,' #2 TWO POSITIVE ROOTS'
            PRINT*,'X1=',MAX(X1,X2),' X2=',MIN(X1,X2)
            PRINT*,' CHOOSE THE LARGEST:',MAX(X1,X2)
            XX=MAX(X1,X2)
          END IF
        ELSE IF(DIS.EQ.0.0D0) THEN
*  DOUBLE ROOT SOLUTION
          XX=-C/(2.0D0*B)
        ELSE
*  IMAGINARY SOLUTION
          PRINT*,' #2 IMAGINARY SOLUTION. DISCRIMINANT = ',DIS
          PRINT*,' PROGRAM STOP'
          STOP
        END IF
      ELSE
*
*  WE HAVE A CUBIC POLYNOMIAL. NEED TO ITERATE TO A SOLUTION.
*
  200   XPREV=X
        TEMP=((3.0D0*A*X+2.0D0*B)*X+C)
        X=((2.0D0*A*X+B)/TEMP)*X*X-(D/TEMP)
*        PRINT*,' #3  X=',X
        IF(ABS(XPREV-X).GT.ABS(EPS*X)) GO TO 200
        XX=X
        IF(X.LT.0.0D0) THEN
          PRINT*,' #3  X=',X,' (NEGATIVE)'
          PRINT*,' SEARCHING FOR OTHER ROOTS'
          AAA=A
          BBB=B+AAA*X
          CCC=D/(-X)
*
```

```
*  HAVING FOUND THE FIRST ROOT,
*  THE OTHER TWO CAN BE FOUND ALGEBRAICALLY.
*  THE SAME ROUTINE WAS USED AS ABOVE,
*  WITH THE EXCEPTION VARIATION OF VARIABLE NAMES.
*
*  CALCULATE THE DISCRIMINANT
*
        DIS=(BBB*BBB)-(4.0D0*AAA*CCC)
*
        IF(DIS.GT.0.0D0) THEN
*  TWO REAL SOLUTIONS
*
*  CAREFUL... THERE CAN BE PROBLEMS WITH TWO REAL ROOTS
*  DUE TO AUSLOESCHUNGSFEHLER CAUSED BY THE SUBTRACTION
*  WHICH TAKES PLACE!!! HERE, ONLY CALCULATE THE ROOT
*  IS CALCULATED IN THE TRADITIONAL MANNER.
*  CALCULATE THE OTHER ROOT IS OBTAINED VIA A METHOD
*  BASED ON THE SIGN OF C AS OUTLINED IN THE THESIS.
*
*  FIRST ROOT...
          IF(BBB.LE.0.0D0) THEN
            X1=(-BBB+SQRT(DIS))/(2.0D0*AAA)
          ELSE
            X1=(-BBB-SQRT(DIS))/(2.0D0*AAA)
          END IF
*  SECOND ROOT...
          X2=(CCC/(AAA*X1))
*
          IF(X1.LT.0.0D0.AND.X2.LT.0.0D0) THEN
            PRINT*,' #4 TRIPLE NEGATIVE ROOT'
            PRINT*,'X=',X,' X1=',X1,' X2=',X2
```

```
            PRINT*,' PROGRAM STOP'
            STOP
          ELSE IF(X1.LT.0.0D0) THEN
            PRINT*,' 2 NEG. ONE POS. ROOT, CHOOSE POSITIVE.'
            XX=X2
          ELSE IF(X2.LT.0.0D0) THEN
            PRINT*,' 2 NEG. ONE POS. ROOT, CHOOSE POSITIVE'
            XX=X1
          ELSE
*  TWO POSITIVE ROOTS. CHOOSE THE LARGEST.
            PRINT*,' ONE NEG. TWO POS. ROOTS.'
            PRINT*,' CHOOSE LARGEST POSITIVE ROOT.'
            XX=MAX(X1,X2)
          END IF
        ELSE IF(DIS.EQ.0.0D0) THEN
*  DOUBLE ROOT SOLUTION
          XX=-BBB/(2.0D0*AAA)
        ELSE
*  IMAGINARY SOLUTION
          PRINT*,' #4 IMAGINARY SOLUTION. DISCRIMINANT = ',DIS
          PRINT*,' PROGRAM STOP'
          STOP
        END IF
      END IF
    END IF
*
    RETURN
*
    END
    DOUBLE PRECISION FUNCTION KA1(TG)
*
```

```
*  THIS FUNCTION RETURNS THE VALUE OF
*  THE RATE CONSTANT FOR THE REACTION
*
*  Ar^+ + Ar + Ar -> KA1 -> Ar_2^+ + Ar
*
*
      DOUBLE PRECISION TG
*
      KA1=2.3D-31*(TG/300.0)**-0.75
*
      RETURN
*
      END
      DOUBLE PRECISION FUNCTION KA2(TG,TE)
*
*  THIS FUNCTION RETURNS THE VALUE OF
*  THE RATE CONSTANT FOR THE REACTION
*
*  Ar_2^+ + e -> KA2 -> Ar^* + Ar
*
*
      DOUBLE PRECISION TG,TE
*
      IF(TG.LE.670.0D0) THEN
        KA2=7.5D-7*(300.0D0/TE)**0.67
      ELSE IF(TG.GT.670.0.AND.TG.GE.TE) THEN
        KA2=4.38D-7*(300.0D0/TG)**1.5
      ELSE IF(TG.GT.670.0D0.AND.TG.LT.TE) THEN
        KA2=4.38D-7*((300.0D0/TG)**1.5)*((TG/TE)**0.67)
      ELSE
        STOP ' ERROR IN KA2'
```

```
      END IF
*
      RETURN
*
      END
      DOUBLE PRECISION FUNCTION KA3(TE)
*
*  THIS FUNCTION RETURNS THE VALUE OF
*  THE RATE CONSTANT FOR THE REACTION
*
*  Ar^+ + e -> KA3 -> Ar + h*nu
*
*
      DOUBLE PRECISION TE
*
      KA3=6.3D-10*(300.0D0/TE)**0.5
*
      RETURN
*
      END
      DOUBLE PRECISION FUNCTION KA4(TG)
*
*  THIS FUNCTION RETURNS THE VALUE OF
*  THE RATE CONSTANT FOR THE REACTION
*
*  Ar + Ar -> KA4 -> Ar^* + Ar
*
      DOUBLE PRECISION TG
*
      KA4=10.0D0**(-78.66913D0+14.8923D0*LOG10(TG))
*
```

```
      RETURN
*
      END
      DOUBLE PRECISION FUNCTION KA5(TG)
*
*  THIS FUNCTION RETURNS THE VALUE OF
*  THE RATE CONSTANT FOR THE REACTION
*
*  Ar^* + Ar -> KA5 -> Ar^+ e + Ar
*
      DOUBLE PRECISION TG
*
      KA5=10.0D0**(-36.8354D0+6.10771D0*LOG10(TG))
*
      RETURN
*
      END
      DOUBLE PRECISION FUNCTION KA6(TE,NE)
*
*  THIS FUNCTION RETURNS THE VALUE OF
*  THE RATE CONSTANT FOR THE REACTION
*
*  Ar^+ + e + e -> KA6 -> Ar^* + e
*
      IMPLICIT DOUBLE PRECISION (A-Z)
      INTEGER I,J
      DOUBLE PRECISION TE,NE,A00,TEMP,A(0:3,0:2),T1,T2
*
      A(0,0)=-13.319D0
      A(0,1)=3.9654D0
      A(0,2)=-0.054716D0
```

```
      A(1,0)=-0.30894D0
      A(1,1)=1.4089D0
      A(1,2)=-0.24503D0
      A(2,0)=-0.10322D0
      A(2,1)=0.73602D0
      A(2,2)=-0.58010D0
      A(3,0)=0.028512D0
      A(3,1)=-0.1206D0
      A(3,2)=0.085961D0
*
      IF(NE.LE.0.0D0) THEN
        KA6=0.0D0
        PRINT*,' NE.LE.0.0 = ',NE,' SET KA6=0'
        RETURN
      END IF
      T1=LOG10(NE/1.0D12)
      T2=1000.0D0/TE
      TEMP=0.0D0
      TEMP=TEMP+A(0,0)
      TEMP=TEMP+A(0,1)*SQRT(T2)
      TEMP=TEMP+A(0,2)*T2
      TEMP=TEMP+A(1,0)*T1
      TEMP=TEMP+A(1,1)*T1*SQRT(T2)
      TEMP=TEMP+A(1,2)*T1*T2
      TEMP=TEMP+A(2,0)*T1*T1
      TEMP=TEMP+A(2,1)*T1*T1*SQRT(T2)
      TEMP=TEMP+A(2,2)*T1*T1*T2
      TEMP=TEMP+A(3,0)*T1*T1*T1
      TEMP=TEMP+A(3,1)*T1*T1*T1*SQRT(T2)
      TEMP=TEMP+A(3,2)*T1*T1*T1*T2
*
```

```
      KA6=10.0D0**(TEMP)
*
      RETURN
*
      END
      DOUBLE PRECISION FUNCTION KA7(TE)
*
*  THIS FUNCTION RETURNS THE VALUE OF
*  THE RATE CONSTANT FOR THE REACTION
*
*  Ar + e -> KA7 -> Ar^+ + e + e
*
      DOUBLE PRECISION TE
      DOUBLE PRECISION PI,KEV,EAR,C,ME,E,TT
*
*  THE VALUE OF PI
*
      PI=4.0D0*ATAN(1.0D0)
*
*  VALUE OF THE BOLTZMANN CONSTANT IN eV/K
*
      KEV=8.6183645D-5
*
*  FIRST IONIZATION ENERGY FOR ARGON IN eV
*
      EAR=15.769D0
*
*  THE CONSTANT C
*
      C=2.0D-17*100.0D0
*
```

```
*  THE ELECTRON MASS IN [KG]
*
      ME=9.1D-31
*
*  THE ELECTRON CHARGE IN [C]
*
      E=1.602D-19
*
*  THE REACTION RATE
*
      TT=KEV*TE/EAR
*
      KA7=( C * (((8.0D0*E)/(PI*ME))**0.5) ) * ((EAR)**1.5)
     +     * (TT**0.5) * (1.0D0 + 2.0D0*TT) * EXP(-1.0D0/TT)
*
      RETURN
*
      END
      DOUBLE PRECISION FUNCTION KA8(TE)
*
*  THIS FUNCTION RETURNS THE VALUE OF
*  THE RATE CONSTANT FOR THE REACTION
*
*  Ar + e -> KA8 -> Ar^* + e
*
      DOUBLE PRECISION TE
      DOUBLE PRECISION PI,KEV,EAR,C,ME,E,TT
*
*  THE VALUE OF PI
*
      PI=4.0D0*ATAN(1.0D0)
```

```
*
*  VALUE OF THE BOLTZMANN CONSTANT IN eV/K
*
      KEV=8.6183645D-5
*
*  ENERGY NEEDED TO BUMP UP TO METASTABLE LEVEL FOR ARGON IN eV
*
      EAR=11.78D0
*
*  THE CONSTANT C IN [CM^2/S]
*
      C=4.5247983D-18*100.0D0
*
*  THE ELECTRON MASS IN [KG]
*
      ME=9.1D-31
*
*  THE ELECTRON CHARGE IN [C]
*
      E=1.602D-19
*
*  THE REACTION RATE
*
      TT=KEV*TE/EAR
*
      KA8=( C * (((8.0D0*E)/(PI*ME))**0.5) ) * ((EAR)**1.5)
     +     * (TT**0.5) * (1.0D0 + 2.0D0*TT) * EXP(-1.0D0/TT)
*
      RETURN
*
      END
```

```
      DOUBLE PRECISION FUNCTION KA9(TE)
*
*  THIS FUNCTION RETURNS THE VALUE OF
*  THE RATE CONSTANT FOR THE REACTION
*
*  Ar^* + e -> KA9 -> Ar^+ + e + e
*
      DOUBLE PRECISION TE
      DOUBLE PRECISION PI,KEV,EAR,C,ME,E,TT
*
*  THE VALUE OF PI
*
      PI=4.0D0*ATAN(1.0D0)
*
*  VALUE OF THE BOLTZMANN CONSTANT IN eV/K
*
      KEV=8.6183645D-5
*
*  ENERGY NEEDED TO BUMP THE METASTABLE LEVEL
*  TO IONIZATION FOR ARGON IN eV
*
      EAR=3.8357D0
*
*  THE CONSTANT C IN [CM^2/S]
*
      C=1.2392860D-16*100.0D0
*
*  THE ELECTRON MASS IN [KG]
*
      ME=9.1D-31
*
```

```
*  THE ELECTRON CHARGE IN [C]
*
      E=1.602D-19
*
*  THE REACTION RATE
*
      TT=KEV*TE/EAR
*
      KA9=( C * (((8.0D0*E)/(PI*ME))**0.5) ) * ((EAR)**1.5)
     +     * (TT**0.5) * (1.0D0 + 2.0D0*TT) * EXP(-1.0D0/TT)
*
      RETURN
*
      END
      DOUBLE PRECISION FUNCTION PHIC(TG,NC,PTORR)
*
*  THIS FUNCTION RETURNS THE
*  GENERATION RATE OF C+ IONS VIA THE REACTION
*
*     C + C -> PHIC -> C^+ + C + e
*
      IMPLICIT DOUBLE PRECISION (A-Z)
*
*  THE VALUE OF PI
*
      PI=4.0D0*ATAN(1.0D0)
*
*  VALUE OF THE BOLTZMANN CONSTANT IN J/K
*
      KJ=1.380662D-23
*
```

```
*  VALUE OF THE BOLTZMANN CONSTANT IN eV/K
*
      KEV=8.6183645D-5
*
*  FIRST IONIZATION ENERGY FOR CARBON IN eV
*
      EC=11.260D0
*
*  F CONSTANT
*
      F=5.0D-4
*
*  MEAN FREE PATH AT THIS PRESSURE...
*
      LAMBDA=5.0D-5/PTORR
*
*  THE MASS OF A SINGLE CARBON ATOM IN [KG]
*
      MC=1.99D-26
*
      AAA=EC/(KEV*TG)
*
      PHIC=((F*NC)/LAMBDA)*SQRT((2.0D0*KJ*TG)/(PI*MC))
     +     *EXP(-1.0D0*AAA)*(AAA+1.0D0)
*
      RETURN
*
      END
      DOUBLE PRECISION FUNCTION KC2(TE)
*
*  THIS FUNCTION RETURNS THE VALUE OF
```

```
*  THE RATE CONSTANT FOR THE REACTION
*
*  C + e -> KC2 -> C^+ + e + e
*
      DOUBLE PRECISION TE
      DOUBLE PRECISION PI,KEV,EAR,C,ME,E,TT
*
*  THE VALUE OF PI
*
      PI=4.0D0*ATAN(1.0D0)
*
*  VALUE OF THE BOLTZMANN CONSTANT IN eV/K
*
      KEV=8.6183645D-5
*
*  FIRST IONIZATION ENERGY FOR ARGON IN eV
*
      EC=11.26D0
*
*  THE CONSTANT C
*
      C=5.89D-18*100.0D0
*
*  THE ELECTRON MASS IN [KG]
*
      ME=9.1D-31
*
*  THE ELECTRON CHARGE IN [C]
*
      E=1.602D-19
*
```

```
*  THE REACTION RATE
*
      TT=KEV*TE/EC
*
      KC2=( C * (((8.0D0*E)/(PI*ME))**0.5) ) * ((EC)**1.5)
     +     * (TT**0.5) * (1.0D0 + 2.0D0*TT) * EXP(-1.0D0/TT)
*
      RETURN
*
      END
      DOUBLE PRECISION FUNCTION KC3(TE)
*
*  THIS FUNCTION RETURNS THE VALUE OF
*  THE RATE CONSTANT FOR THE REACTION
*
*  C^+ + e -> KC3 -> C + h*nu
*
*
      DOUBLE PRECISION TE
*
      KC3=6.3D-10*(300.0D0/TE)**0.7
*
      RETURN
*
      END
      DOUBLE PRECISION FUNCTION DARSTAR(TE,TG,PTORR)
*
*  THIS FUNCTION RETURNS
*  THE DIFFUSION COEFFICIENT OF AR^* IN CM^2/SEC
*
      DOUBLE PRECISION TE,TG,PTORR
```

```
*
      DARSTAR=49.0D0*((TG/300.0D0)**0.5)/PTORR
*
      RETURN
*
      END
      DOUBLE PRECISION FUNCTION DARSS(TE,TG,PTORR)
*
*  THIS FUNCTION RETURNS
*  THE DIFFUSION COEFFICIENT OF AR^*^* IN CM^2/SEC
*
      DOUBLE PRECISION TE,TG,PTORR
*
      DARSS=49.0D0*((TG/300.0D0)**0.5)/PTORR
*
      RETURN
*
      END
      DOUBLE PRECISION FUNCTION DARP(TE,TG,PTORR)
*
*  THIS FUNCTION RETURNS
*  THE DIFFUSION COEFFICIENT OF AR^+ IN CM^2/SEC
*
      DOUBLE PRECISION TE,TG,PTORR,DI
*
      DI=(75.0D0/PTORR)*(TG/300.0D0)**0.5
      DARP=DI*(1.0D0+TE/TG)
*
      RETURN
*
      END
```

```
      DOUBLE PRECISION FUNCTION DAR2P(TE,TG,PTORR)
*
*  THIS FUNCTION RETURNS
*  THE DIFFUSION COEFFICIENT OF AR_2^+ IN CM^2/SEC
*
      DOUBLE PRECISION TE,TG,PTORR
*
      DI=(34.5D0/PTORR)*(TG/300.0D0)**0.5
      DAR2P=DI*(1.0D0+TE/TG)
*
      RETURN
*
      END
      DOUBLE PRECISION FUNCTION DCP(TE,TG,PTORR)
*
*  THIS FUNCTION RETURNS
*  THE DIFFUSION COEFFICIENT OF C ^+ IN CM^2/SEC
*
      DOUBLE PRECISION TE,TG,PTORR
*
      DI=(100.0D0/PTORR)*(TG/300.0D0)**0.5
      DCP=DI*(1.0D0+TE/TG)
*
      RETURN
*
      END
```